MAGNETOHYDRODYNAMIC WAVES IN STRUCTURED ATMOSPHERES

Patricia M. Edwin

A Thesis Submitted for the Degree of PhD
at the
University of St. Andrews

1985

Magnetohydrodynamic Waves in Structured Atmospheres

P. M. Edwin

A thesis submitted for the Degree of Doctor of Philosophy at the University of St Andrews

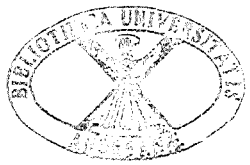

Abstract

The effect of structuring, in the form of magnetic or density inhomogeneities, on the magnetohydrodynamic (mhd) waves of an infinite plasma is investigated. The appropriate dispersion formulae, in both Cartesian and cylindrical polar coordinate geometries, are derived. The main properties of the allowable modes in structured plasmas are described, particularly those featuring in a slender inhomogeneity.

The inclusion of non-adiabatic effects is examined, specifically for a thermally dissipative, unstratified, finite structure and for a slender inhomogeneity in a stratified medium. The dissipative time scales of slender structures are shown to have a dependence on the Péclet number. Growth factors appropriate to these time scales for the overstable motions of a thermally dissipative, Boussinesq fluid are derived.

For the linear analysis of a slender structure it is shown that the dispersive nature of the waves is deducible from the simplified one-dimensional equations. The analysis is extended, for slender structures, to nonlinear motions and the governing equation representing an effective balance between nonlinear, dispersive and dissipative effects, the Benjamin-Ono-Burgers equation, is established. The solutions of this equation are considered and, for weakly-dissipative systems, are shown to be slowly decaying solitons.

The importance, in the context of group velocity, of the dispersive nature of waves in ducted structures is discussed and analogies are made with other ducted waves, for example, the Love waves of seismology. It is suggested that the behaviour of such waves, following an impulse, may account for the range of oscillatory behaviour, the quasi-periodic and short time scales, observed in both the solar corona and Earth's magnetosphere.

Density variations across a structure and the structure's curvature, with possible applications to coronal loops, are also considered.

Further suggestions for possibly identifying some of the theoretical results with observed behaviour in sunspots, chromospheric fibrils and spicules are also made.

I Patricia Mary Edwin hereby certify that this thesis has been written by me, that it is the record of work carried out by me, and that it has not been submitted in any previous application for a higher degree.

Signature of Candidate [redacted]

Date 20th August 1984

I hereby certify that the candidate has fulfilled the conditions of the Resolution and Regulations appropriate to the degree of Doctor of Philosophy of the University of St Andrews and that she is qualified to submit this thesis in application for that degree.

Signature of Supervisor ... [redacted] ...

Date ..... 20 August 1984 .....

I was admitted as a research student under Ordinance No 12 in October, 1979 and as a candidate for the degree of Ph.D. in October, 1980; the higher study for which this is a record was carried out in the University of St Andrews between 1979 and 1984.

Signature of Candidate [redacted]

Date 20th August 1984

Acknowledgements

I am especially grateful to my supervisor, Dr Bernard Roberts, for his unfailing help, advice and encouragement during an extended and sometimes erratic period of study. I should also like to thank Prof Eric Priest and past and present members of his Solar Physics group in St Andrews for many useful discussions.

I am grateful to The Open University for financial support and to my colleagues there for their understanding, encouragement and assistance, especially during periods of study leave.

My family, for their tolerance and sacrifices, I cannot thank enough.

The presentation of this thesis would not be possible without the help of Miss Shiela Wilson in typing the script. I am very grateful to her for her careful work.

Contents

Chapter 1 Introduction : Aspects of Structuring

'Within wave science as a whole, the nature of waves in fluids is characterised especially by their ability to interact with complex ... fields.'

Sir James Lighthill 'Waves in Fluids'

1.1 Waves in Plasmas

A region of plasma such as the solar atmosphere or the Earth's magnetosphere can conceivably support several different types of wave. There are acoustic waves inherent in the medium because of the competing effects of compressibility and the plasma's own inertia. The latter may also form an effective balance with magnetic or buoyancy forces resulting in compressible and shear Alfvén waves, or internal gravity waves, respectively. In a magnetic, compressible and stratified medium these restoring forces may combine in such a way as to support magnetoacoustic-gravity waves, most of the other types of wave being deducible as special cases of this more general class of waves. (Inertial waves due to the Coriolis force in a rotating plasma are not considered here.) For an unbounded, uniform medium the theory of such waves, especially in the gravity-free case, is well-known (e.g., Landau and Lifshitz, 1960; Cowling, 1976; Lighthill, 1978; Priest, 1982). Small perturbations about an equilibrium state mean that the basic equations may be linearized. If the disturbance is assumed to vary in the z-direction, say, with wavenumber k according to e^{ikz} and in time t with frequency ω

according to $e^{i\omega t}$, then, for a uniform medium, ω and k may be related by an algebraic dispersion relation. This relationship determines the phase-speed, ω/k, the group velocity, $\partial\omega/\partial k$, at which the energy is transmitted, and the dispersive properties of the wave. This theory, for a uniform medium, is valid if the wavelength $2\pi/k$ is much smaller than the length scale ℓ of the medium. Priest (1982) summarizes the properties of magnetoacoustic-gravity waves for a uniform plasma and points out the limitations of uniformity assumptions for the solar photosphere where the length scale (the scale-height) may only be a few hundred kilometres.

The emphasis here will be on the non-uniformity of the plasma, specifically inhomogeneities of the medium resulting from magnetic field (or density or temperature) structuring and, to a limited extent, gravitational effects. If the medium is structured in the x-direction, say, then the disturbance may no longer have a Fourier form in this direction; instead the governing linear equations reduce to ordinary differential equations in x. The dispersion relation relating ω and k then results from the condition that these equations and their boundary conditions have a solution. In general the dispersion relation no longer has a simple algebraic form but possesses a complicated spectrum of modes. Thus the Alfvén and fast and slow magnetoacoustic modes of a gravity-free, uniform medium no longer emerge in a simple way from the dispersion relation and the aim in this thesis, having derived the appropriate dispersion formulae, is to examine how the structuring of the medium modifies

these modes and to discover what other new modes, if any, are present. In general the fact that there are now discontinuities in the basic state, due to the inhomogeneities, leads to the existence of *surface* waves and the uniform medium waves are modified in the form of *body* waves (terms to be defined in Chapter 2; see also Roberts, 1981 a,b). Having determined which modes the structured plasma can support, the results are compared with observational data of oscillatory behaviour in the Sun's atmosphere and Earth's magnetosphere to see whether explanations of such phenomena can be offered.

1.2 Outline of Thesis

The remainder of this chapter reviews what is known of the inhomogeneities, and their wave-like properties, in two structured plasmas, the solar atmosphere and the Earth's magnetosphere. It concludes with a summary of the equations which will be used.

In Chapters 2 and 3 the dispersion relations for structures modelled in both Cartesian and cylindrical coordinate geometries are derived and their modes are examined both analytically and numerically. In particular the relationship of these modes to those of the uniform, unbounded medium is shown. Attention is concentrated on the free modes of oscillation, those whose energy is confined to the inhomogeneity, so that the latter acts as a duct guiding the

modes along the structure. The main properties of the allowable modes in structured plasmas are described and the more important modes, in particular those featuring in a *slender* inhomogeneity, which has length scale small compared with the wavelength along the structure, are discussed in detail. In general the waves are dispersive and their existence is shown to depend on the form of the structuring.

For example, if the plasma of the Sun's corona is considered, two widely separated classes of free oscillation are possible, one on an acoustic, the other on an Alfvénic time scale. The acoustic-type oscillations always exist but the shorter period, Alfvénic-type oscillations occur only in high density (low Alfvén velocity) structures. The latter waves are highly dispersive and are analogous to ducted waves occurring in several other branches of physics, in particular the Love waves of seismology (Love, 1911). The behaviour of such ducted, dispersive waves following an impulse has been described by Pekeris (1948) in oceanographic studies. The fact that the phase- and group speeds of waves in structured plasmas have similar properties is used in Chapter 4 to explain the range of oscillatory behaviour observed in the solar corona, in particular the quasi-periodic nature of some of the observations and their extremely short time scales. Moreover the ducts formed by such density inhomogeneities need not be uniform. It is shown in Chapter 4 also that the structure may comprise a continuously-varying density inhomogeneity and still exhibit the appropriate

periodic/quasi-periodic behaviour.

The form of the structuring need not necessarily be one due to a density inhomogeneity. As a result of the investigations of Chapters 2 and 3 it is shown that similar ducted magnetoacoustic modes may occur in, say, the antiparallel magnetic field situations of the plasma sheet of the Earth's magnetotail (described in Subsection 1.3.2) or a coronal neutral sheet. Similar ideas to those of Chapter 4 are thus employed in a different context in Chapter 7 to explain the variety of time scales and the wave-packet behaviour of magnetospheric observations. The deductions may also offer an alternative explanation for some of the coronal observations.

The Alfvén and fast and slow magnetoacoustic modes of an unbounded, uniform medium arise from consideration of an ideal medium. When the medium is both dissipative and structured these modes are modified in a complicated way. In Chapter 5 the effects of thermal dissipation on the modes of a structured plasma are examined, particularly with applications to the solar photosphere in mind. In this region of the solar atmosphere gravitational effects, too, cannot really be ignored and so they are also included in the analysis. If dissipation is present then for real k, ω need no longer be real and the possibility occurs of overstability, that is of there being oscillatory modes whose amplitude increases in time. The applications of these results are discussed in Chapter 7.

From the discussion of Chapters 5 and 6 it is apparent that it is the elasticity of the environment of the structure that gives

rise to the dispersion, that is it is due to the inertia and magnetic nature of the surrounding plasma. The importance of the dispersive nature of the waves in the context of group velocity is discussed in Chapter 4. For non-dispersive waves the idea of how linear theory can become inappropriate and waves steepen into shock waves is well established (see, e.g., Whitham, 1974; Lighthill, 1978; Priest, 1982). However if the waves are dispersive then it is possible for the dispersive effects to counteract the steepening and a *soliton* or solitary wave results (see, e.g., Karpman, 1975). Further, if the dissipative effects also contribute to the effective balance then solitary waves with slowly decaying amplitude may result (see review by Kadomtsev and Karpman, 1970). In Chapter 6 the governing equation representing an effective balance between nonlinear, dispersive and dissipative effects is deduced and its solutions are shown to be solitary waves of slowly decaying amplitude. The possibility of such solutions describing spicular behaviour (see Subsection 1.3.1) or being applicable to the corona is discussed in Chapter 7.

1.3 Structured Plasmas

This work began with the intention of examining waves in the vast plasma comprising three sections of the solar atmosphere, the photosphere, the chromosphere and the corona and this remains the main theme. However as the study progressed it became apparent that,

because of the mathematical analogies involved, waves occurring in other structured media, both in plasmas, such as the Earth's magnetosphere, and those in optical fibres, for example, could not be ignored. In turn ideas from the fields of oceanography, seismology and fibre optics contributed to the examination of magnetohydrodynamic (mhd) waves in structured plasmas.

1.3.1 The solar atmosphere As far as the photosphere is concerned one of its most obvious features, the *sunspot*, has been known to be associated with magnetic field structuring since Hale's (1908) discovery of its kilogauss fields but even now some of its properties, for example its depth and stability, and how a sunspot is formed, are not fully understood. However, there is general agreement on some aspects. A sunspot is dark, has magnetic fields of ~ 3kG and diameters of ~ 4000km (see reviews by Parker, 1979a; Zwaan, 1981). Generally diameters are less than 3×10^4km (Parker, 1979a). Temperatures are typically in the range 4000 ± 100 K but why these temperatures are so much lower (~ 2000K cooler) than those of the surrounding photosphere is not fully explained. One school of thought believes that convection of the sub-photospheric layers is suppressed by the strong magnetic fields of the spot and that the heat which would have emerged through the sunspot region is spread over a vast area. Starting with Biermann's first suggestion of this idea in 1941, Cowling (1976) summarizes how the idea has progressed. Spruit and Roberts (1983) give a more recent review. Alternatively, it has been suggested (Parker, 1974a,b, 1979b; Roberts, 1976) that there is actually enhanced motion within the

spot and that it is cooled by overstable waves.

The sunspot does not present a homogeneous picture to the observer. Sunspots generally exhibit an irregular pattern of bright points, called *'umbral dots'* (see reviews by Moore, 1981a,b), some 150 km in diameter, with a brightness similar to that of the surrounding photosphere and which have lifetimes of ~ 1500 s. It is suspected that magnetic fields are smaller in these dots. Beckers (1981) has pointed out that there are no detectable intensity oscillations at periods of 1 to 300s as might associate mhd waves with these dots though 180s and 300s oscillations are associated with the sunspot umbra in general; periods of from 60 to 500s have been observed as well. For example, Lites *et al.* (1982) found evidence of 130 and 170s periods in sunspot oscillations which they suggested might be connected with magnetoacoustic waves. Athay (1981a) has summarized the Hα (chromospheric) observations of sunspot oscillations. Briefly, there are thought to be vertical oscillations within the umbra with periods ranging from 145s - 185s and horizontal penumbral waves running outwards at speeds of 10 - 20 $km\,s^{-1}$ and periods of 210s, 270s or 300s. In his reviews Moore (1981a,b) quotes a range of 120 - 500s for umbral oscillations.

Sunspots apart, the rest of the photosphere is far from homogeneous. Indeed Stenflo (1976) and Spruit (1981a) have described sunspots as being the largest members of a general class of *magnetic flux tubes*, there being a spectrum of such magnetic flux elements from the small (< 1″ ~ 725 km) bright network elements (~ 1500 G) to the large, dark sunspots. Zwaan (1981) has described this hierarchy

of elements in detail, from sunspots, through *pores* (~ 2 kG, 10^3km diameter), *knots* (1.5 kG, 500 km diameter) down to the small (~ 100 km, 1500 G) concentrations of flux called variously flux elements, magnetic elements or simply flux tubes. Indeed it is now generally accepted that the magnetic field over most of the solar surface is concentrated into regions of magnetic flux (see, e.g., Frazier, 1976; Stenflo, 1976) and that this accounts for over 90% of the flux seen by magnetographs.

Thus the sunspot may be considered as a large flux tube, or, as Parker (1974a, 1979c) has suggested it may be regarded as a cluster of flux tubes which perhaps separates into individual tubes at depths of 1000 km. A general overview of Parker's model is given in the books by Noyes (1982) and Priest (1982). Intense tubes (knots of 1500 G) may assemble to form a sunspot from diffuse magnetic fields. The latter are swept into the boundaries or corners of supergranules by the strong downdrafts (~ 1 km s^{-1}) depending on whether there is predominantly downflow, in which case the tube of field cools and the field strength increases and suppresses motion. If there is upflow the field weakens and disperses. The flux bundle idea is consistent with the umbral fields being nearly vertical (to within 10°) but becoming nearly horizontal at the outer boundary of the penumbra (Zwaan, 1981).

Later in this thesis (Chapter 7) models of the isolated flux tube and sunspot will be considered with a view to deciding just which mhd waves they can support. This problem has already been discussed to some extent by several authors (e.g., Defouw, 1976;

Roberts and Webb, 1978; Wilson, 1979; Roberts, 1981a,b; Spruit, 1982). Here it will be considered in the more general context of a structured plasma.

Of course, isolated flux tubes are at the limit of telescopic resolution so it is extremely difficult to detect oscillatory behaviour within them. Athay (1981a) in discussing acoustic waves in the non-magnetic part of the photosphere/chromosphere points out the observational difficulties of distinguishing between waves, laminar flow and turbulent eddies, all of which would yield Doppler shifts. Giovanelli and Brown (1977) made the first observations of axial velocity fluctuations in gases in photospheric magnetic flux tubes and using the same observational technique Giovanelli *et al.* (1978) provided further stimulating observations of such oscillations. Further observations, however, are very much needed but may have to await developments from space observatories (e.g., the planned Solar Optical Telescope experiment).

It has been suggested that flux tubes may act as a duct mechanism whereby wave information is transmitted from the Sun's interior into the higher solar atmosphere (see summary in Orrall, 1981). Stenflo (1976) stated as one of his main points that magnetic flux concentrations appeared to be cospatial with the photospheric and chromospheric network, that is 'pictures' of the Sun as seen from magnetograph observations seemed to fit those seen in Hα (6536 Å) and CaII H and K light. More recently the EUV (extreme ultraviolet) and the UV (MgII h and k) observations have provided a

much better picture of chromospheric features. Also it is generally agreed (e.g., Beckers, 1976, 1981; Harvey, 1977; Ramsey *et al.*, 1977; Athay, 1981b; Sheeley, 1981; Noyes, 1982) though evidence is incomplete, that the boundaries of supergranule convection cells correlate with the bright photospheric network and the chromospheric network (faculae and network clusters, and within them, filigree; see Dunn and Zirker, 1973).

In turn, *spicules*, radial jets of gas, are seen to shoot upwards with average velocities of 20 $km\,s^{-1}$ from the chromospheric network along the magnetic field lines (Beckers, 1972; Athay, 1981a). Spicules have lifetimes of 5 ~ 10 mins , lengths some 15-20 $\times 10^3$km (several times the thickness of the chromosphere) and diameters typically 1″ (725 km). It is estimated (Athay, 1981b) that at any one time 1 to 2% of the solar surface has spicules, but that these are confined to the network, 'grouped like hedgerows' along the boundaries of supergranule cells (Noyes, 1982). Attempts have been made to explain spicular behaviour by the buffeting of granule or supergranule cells on magnetic flux tubes thus causing waves (Parker, 1974c; Roberts, 1979; Hollweg, 1982; Roberts and Mangeney, 1982). One of the models, regarding a spicule as a soliton, is considered in Chapter 7.

Apart from these vertical features of the chromosphere there are also horizontal (< 3000 km above limb) features, the *fibrils*. These, too, appear to outline magnetic flux tubes but tend to join areas of opposite polarity. Athay (1981b) has discussed fibrils at length, using the term to describe the dark, elongated features seen

in the Hα photosphere of active regions as well as the bright and dark fine-scale mottles of the chromospheric network. He lists their properties; they have diameters of 1-2″, lengths typically 10-15″, lifetimes 15-30 mins and exhibit a range of velocities up to 50 km s^{-1}. Marsh (1976) suggested that structural features such as spicules and fibrils carry (low temperature) matter along their lengths into regions where the ambient temperature is much higher. A canopy of spicule and fibril structure has been suggested (Giovanelli, 1980; Athay, 1981b; Giovanelli and Jones, 1982).

There are many questions to be resolved concerning the chromosphere and the transition region. It is thought that the low chromosphere is affected by photospheric and sub-photospheric layers, but that probably the upper chromosphere and transition region are heated by conduction and convection from the corona and possibly by other processes (Hollweg, 1981). It is not clear however whether it is the magnetic field structure or the temperature structure which "calls the tune".

Observations of chromospheric oscillations are limited (Liu, 1974; Beckers and Artzner, 1974; Giovanelli, 1975; White and Athay, 1979; Athay and White, 1979; Giovanelli and Beckers, 1983). Periods in the range 100-500s are quoted, sometimes down to 30s. Often reference is made to "the 5 min photospheric and the 3 min chromospheric" oscillations (Leibacher and Stein, 1981). (As far as the photosphere is concerned these 300s oscillations have been identified as an evanescent response to acoustic standing waves trapped in the

resonant subphotospheric cavity.) Waves are thought to be upwardly propagating with velocity amplitudes 1-3 $km\,s^{-1}$ and phase-speeds on the order of the sound speed (~ 7.5 $km\,s^{-1}$) (Athay, 1981a). Giovanelli (1975) has described the propagation of waves in chromospheric fibrils. A suggested explanation of these fibril waves is given in Chapter 7.

As a result of increased coronal knowledge, especially via the EUV and soft X-ray observations of the Skylab mission, epithets relating to this part of the solar atmosphere abound - magnetically dominated, paramountly inhomogeneous, inherently structured, highly conducting, arch-like, extremely hot - and from this list a picture has emerged that is one of a highly inhomogeneous medium structured almost entirely by *loops*. Webb, D.F. (1981) has drawn the distinction between the flux loops (isolated tubes of magnetic field surrounded by a relatively field-free medium discussed above) and the plasma loops of the corona, the observed emitting structures which seem to act as coronal magnetic field tracers.

There are loops large and small. Even the tiny X-ray bright points of ephemeral regions which have time scales of the order of $\frac{1}{3}$ day are thought to be small loop structures (Noyes, 1982). This is in contrast to the huge solar prominences (filaments when seen on the disk) supported by magnetic field lines and extending some 5×10^4km above the limb. Like vertical blades they last from days to months and are dense and cool compared with the surrounding coronal gas. They, too, appear to have their own thread-like structure. Some of the loops are 'closed' being anchored by

magnetically opposite footpoints in the denser chromosphere and photosphere, and some appear to be hot and dense themselves, observable because of their X-ray emission (Webb, D.F., 1981; Zirker, 1981). These closed loops, on average, extend no higher than half a solar radius ($R_\odot = 6.96 \times 10^5$km). Other loop structures may be 'open', fading high in the corona. They may emanate from coronal holes, which (at a height of about $1R_\odot$) are the cooler (1.5×10^5K rather than 2×10^6K) and less dense (~ 7% of the $5 \times 10^{14}m^{-3}$ 'normal' particle density at this height) regions of the corona, or they may form part of the 'helmet streamers' (see Figure 1.1 and descriptions in Spicer and Brown, 1981; Priest, 1982). Following a sunspot maximum these streamers have been seen to extend as far as $12R_\odot$ from the Sun (Noyes, 1982).

Because of the large variation in size and type of loop their properties vary considerably. An attempt has been made at a classification into 'hot' and 'cool' loops (Orrall, 1981). Webb, D.F. (1981) quotes field strengths of 300G and suggests that brightness variations over the loop imply density variations. Wentzel (1981) gives a value of 100G for small, compact loops, and a typical Alfvén speed of 3×10^3km s^{-1}. He suggests that loops are not homogeneous but that they may be composed of several flux tubes with different gas pressures. Suggestions have been made that some loops have cool cores (Foukal, 1975, 1976; Jordan, 1975; see also Levine, 1981). The particle density appears to vary according to the model but values ranging from ~ $1.6 \times 10^{16}m^{-3}$ on the axis of the loop to ~ $2 \times 10^{15}m^{-3}$ at its outer surface have been given in the

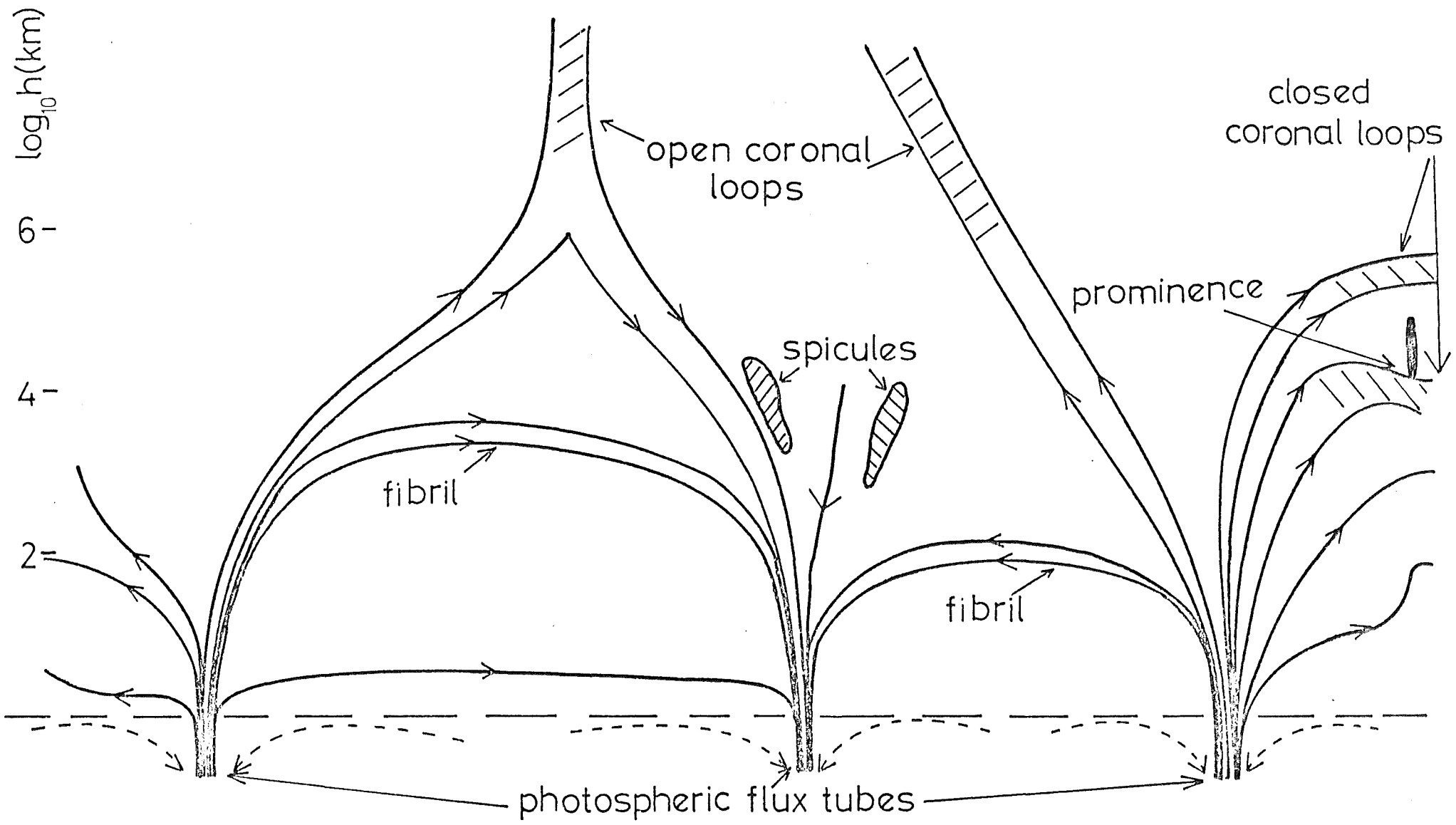

Figure 1.1 A schematic picture, varying logarithmically with height h (km) showing solar atmospheric features. Compiled from similar diagrams in Stenflo (1976), Withbroe and Noyes (1977), Parker (1979a), Spicer and Brown (1981), Noyes (1982) and Spruit (1983).

review by Jordan (1975). Pick *et al.* (1979) analysing a coronal structure overlying an active region estimated it to be about 10 times as dense as the background corona and Spruit (1981a) suggests the coronal tube density may be higher than its environment by a factor of 3-10. These values usually refer to loops in active regions being the easier ones to observe. In Chapter 4 an attempt to model such inhomogeneity will be made by considering loops having transverse density variations. It must be added that loops are often observed to be twisted. The stresses and instabilities resulting from twisting motions are often essential ingredients of theories for coronal heating. Here, however, loops will be assumed to be free of twist; wave-like behaviour, rather than instabilities, will be investigated. Some of these coronal loops are more evident shortly after a solar flare: the 'post-flare' coronal loops.

Information concerning the oscillatory behaviour of the plasma following a flare comes from radio wave data (Krüger, 1979) and more recently from the hard X-ray data of the HXRBS (Hard X-ray Burst Spectrometer) of the Solar Maximum Mission satellite (e.g., Kiplinger, 1983a,b). There is also some coronagraph evidence of oscillations (e.g., Koutchmy *et al.*, 1983; Pasachoff and Landman, 1984). The radio wave data has a complicated categorization (see review by Rosenberg, 1976 and Figure 1.2). Briefly, the Type I and IV data is thought to originate within the region of the explosion itself, as a result of interacting energetic matter and the magnetic fields, the Type III bursts being rapidly upward-propagating emission. Type II emission is associated with shock waves and will

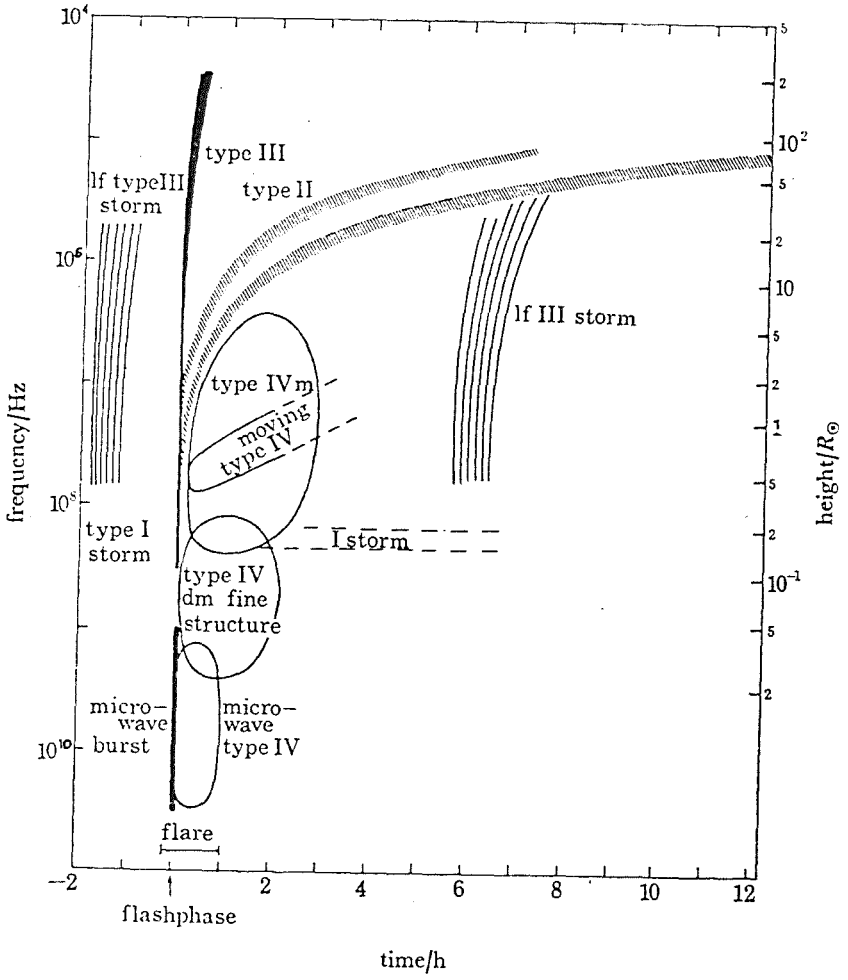

Figure 1.2 Schematic representation of the radiospectrum after Rosenberg (1976). The Type I and ℓf (low frequency) Type III storms are not necessarily flare-related.

not be considered here. In Chapters 4 and 7 models of both open and closed coronal loops will be considered in an attempt to explain the diversity of periodicities, from seconds to minutes, especially the shorter ~ 1s periods observed in the corona. Most oscillatory behaviour appears to be impulsively generated but it is not necessarily associated with flares (Tapping, 1978; Gaizauskas and Tapping, 1980).

As a result, then, of information gained over the past decade or so, particularly from Skylab, a picture of the solar atmosphere has evolved (Parker, 1979a; Noyes, 1982; Spruit, 1983) that more or less represents current thinking as to the atmosphere's structure (Figure 1.1). Photospheric flux tubes are imagined to fan out so that their outer boundaries become more horizontal and tubes merge (e.g., Parker, 1979a; Sheeley, 1981) the coronal tubes (loops) possibly being related to flux tubes as shown in Figure 1.1. At what height this occurs is subject to debate. Spruit (1981a) suggested that the 'interface' between the photospheric flux tube regime and that of the coronal field occurs at about 1500 km in a quiet region and at about 750 km in an active region, whereas Giovanelli (1980) proposed that the chromosphere/corona transition region probably penetrates below 600 km. In a later paper (Giovanelli and Jones, 1982) the canopy height was estimated to be even lower, ~ 300 to 400 km, certainly much lower than the static (potential field) model of Anzer and Galloway (1983) predicts.

In the 1960's the chromosphere was modelled as a plane, stratified atmosphere and much attention was concentrated (and is even now) on producing a model atmosphere which correctly represents the temperature, pressure and density variation with increasing distance outwards from the solar limb (a horizontally-averaged, radial structure). However, as Figure 1.1 shows, an atmosphere which faithfully represents behaviour along a radius at the location of say, a flux tube, may not bear too much resemblance to one

displaced laterally some hundreds of kilometres originating, say, in the quiet photosphere and following the line of a coronal streamer. In order to relate the magnetic inhomogeneities with the emission inhomogeneities (those due to differences in temperature, say) Spruit (1981a) and Zwaan (1981) amongst others, have described the idea of a *filling factor*, f(h), which gives the fraction of the horizontal plane at height h above the solar limb that is occupied by emitting gas. For example, Spruit gives $f(h) \simeq 0.03$ at the photosphere increasing to 0.2 at h = 1500 km for an active region 50G field.

It must be noted that though the overall features of the Sun's atmosphere are often described in terms of the plasma β, the ratio of gas to magnetic pressures, this can often be misleading. In the corona, which is magnetically dominated, it is generally accepted that $\beta << 1$ and the 'cold plasma' approximation, or neglect of sound as compared to Alfvén speed, is an acceptable simplification there. (Spruit (1981a) suggests $\beta \sim 10^{-4} - 10^{-1}$ in the lower solar corona.) However, as Figure 1.1 shows, a description of the photosphere may vary from $\beta \simeq 1$, in the vicinity of an isolated flux tube or sunspot say, to $\beta >> 1$, in a relatively field-free region.

Here attempts will be made to describe some solar features, for example, flux tubes, fibrils and coronal loops by their (lateral) structuring relative to the surrounding medium. One property common to this variety of solar phenomena which is evident from the foregoing descriptions, and which can often be exploited mathematically, is that transverse dimensions are much smaller than longitudinal ones.

This idea will be used extensively, but especially in Chapter 6. It is perhaps a weakness of the modelling that no attempt is made to impose boundary conditions at the 'ends' of these structures and thus relate the various levels of the solar atmosphere. However as regards the coronal oscillations discussed in Chapters 4 and 7, an initial value problem is discussed and conditions on transverse boundaries become less relevant.

As far as the photosphere is concerned the inhomogeneities will be assumed to be those due to magnetic structuring (flux tubes, sunspots), whilst structures in coronal regions will primarily be thought of as density inhomogeneities - though apart from a brief section of Chapter 4, which deals specifically with density variations these are just differences in Alfvén speed and could incorporate structuring due to pressure, or temperature, or magnetic field strength as well.

Thermal conduction effects are considered in Chapter 5 with the magnetically structured inhomogeneities of the photosphere in mind. Spruit (1977) has argued that thermal conductivity in the environment of a sunspot is very large so that the missing flux is spread out over an area several hundred thousand kilometres in diameter. An attempt is made in Chapter 5 to include two important photospheric features in the flux tube models, those of (constant) thermal dissipation and gravity.

The major current problems of coronal heating and mass and energy transport (see reviews by Withbroe and Noyes, 1977; Vaiana and Rosner, 1978; Kuperus *et al.*, 1981; see also Jordan, S., 1981) are not

considered here. The possible waves inherent in the solar atmosphere have proved to be a topic enough in itself; waves may or may not be contributory factors in heating and acceleration mechanisms associated with magnetic fields (see summary by Hollweg, 1981). However it must be emphasized that considerations of mhd waves, coupled with the fact that the corona is highly structured magnetically have led to a resurgence of interest in coronal heating mechanisms. Several ideas have been proposed. Ionson (1978) suggested exploiting a resonance mechanism (see Section 2.1) to produce so called 'dissipationless' damping and this was further investigated by Rae and Roberts (1981, 1982). The idea of enhancing dissipation (and thus heating) by phase mixing of shear Alfvén waves has been proposed by Heyvaerts and Priest (1983) and followed up in more detail by Browning and Priest (1984) and Nocera *et al.* (1984). This work concentrates on the dissipation mechanism due to Alfvén velocity gradients within the corona. Hollweg (1984), on the other hand, concentrates on how energy can be carried from the convection zone to the corona, by waves, and considers a coronal loop as acting as a leaky resonant cavity. Ideas based on wave transport mechanisms have been extended to include not just the corona but the solar wind as well (e.g., Hollweg, 1978, 1983; Habbal and Leer, 1982).

The emphasis in this thesis will be quite different from this current coronal heating work in two respects: the lateral boundaries of a structure (explicitly ignored in some of the above work) will feature much more prominently, and as a result the slow and fast mhd waves (as modified by these boundaries) will therefore assume the dominant role, as opposed to the non-compressive Alfvén waves of the aforementioned work.

1.3.2 The Earth's magnetosphere Another instance where structuring in a plasma is of importance is that of the Earth's magnetosphere. Excellent descriptions and summaries of current thinking regarding the magnetosphere's structure have been given by Vasyliunas (1983) and those features relevant to the discussion here are illustrated in Figures 1.3a and 1.3b. Near the Earth and on its daytime side the structure is thought to be very complicated, a bow shock and magnetospheric boundary layers forming where the solar wind interacts with the Earth's magnetic field, the boundary layers funnelling down towards the earth in the form of polar cusps and relating to the auroral zones.

Two parts of the magnetosphere morphology are, however, well defined. The first is the magnetopause surface 'separating' the magnetosphere itself from the magnetosheath. It is some tens of Earth radii ($Re \simeq 6 \times 10^3 km$) in extent and encompasses the region of both closed and open magnetospheres, some field lines of the latter being able to form the connection between the Earth and the solar wind (Figure 1.3). The second well-defined region is the magnetotail or geomagnetic tail lying downstream (in the solar wind sense) of the closed magnetosphere, being a region of reversed magnetic field between the extended field lines from the northern and southern hemispheres of the Earth. McKenzie (1970) modelled the magnetotail as a cylindrical tube some 20Re in radius ($\sim 2 \times 10^5 km$ diameter).

Extending earthward through the centre of the magnetotail lies the hot plasma sheet. In turn, through its centre lies the neutral or current sheet. There are two ideas regarding the current sheet.

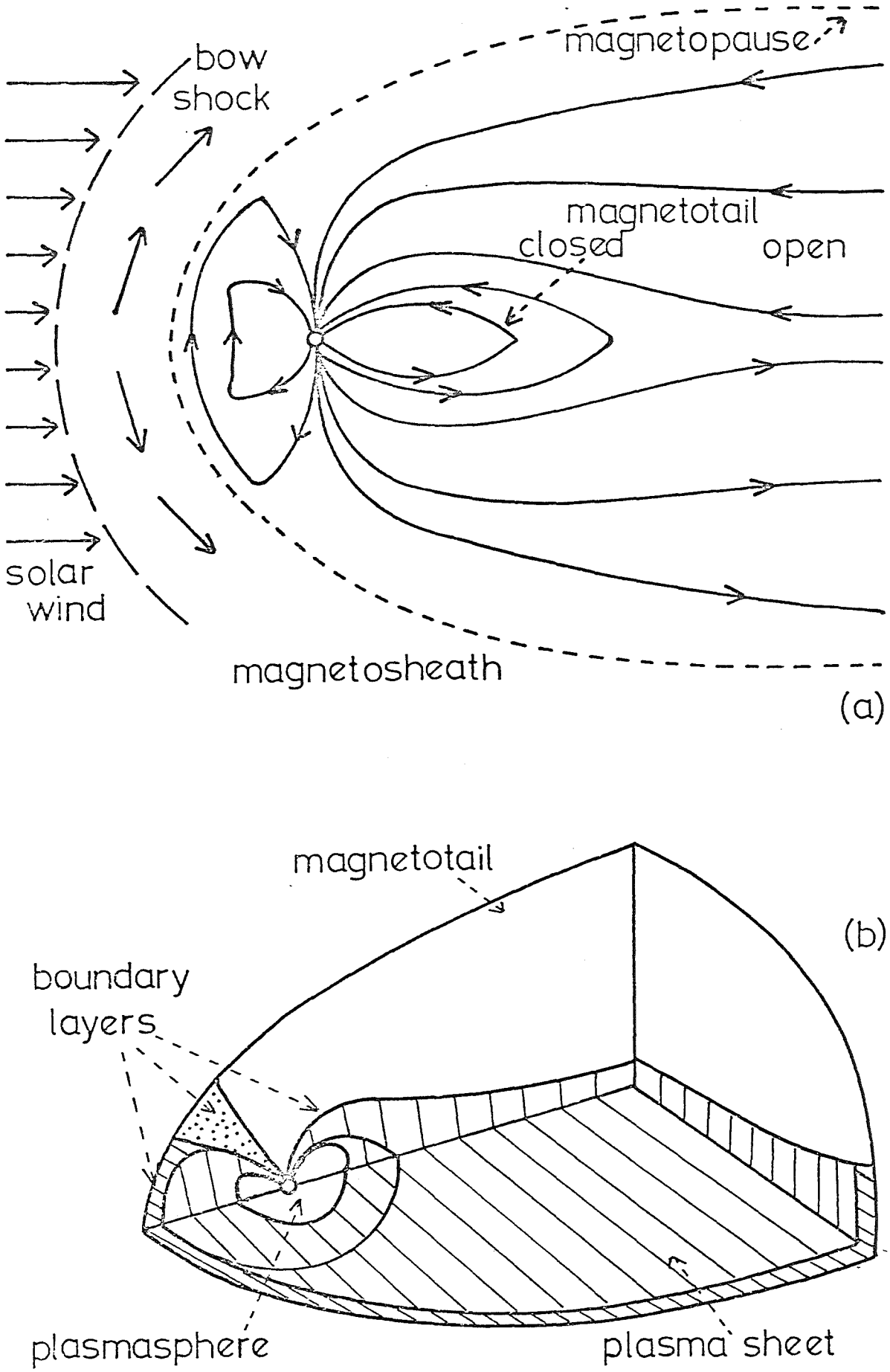

Figure 1.3 Following Vasyliunas (1983) schematic views of (a) the magnetic field line and plasma flow configuration of the magnetosphere and (b) the main regions (cut away) of the magnetosphere such as the plasma sheet and the plasmasphere (with its boundary the plasmapause).

One is that it is a thin structure, forming a core of the plasma sheet, or, alternatively, that together with the plasma sheet it extends across the magnetotail in the form of a slab. McKenzie (1970) adopted this latter view and it is one of the models which will be considered in Chapter 7. Galeev (1982) takes the half-width of the plasma sheet to be just 1 Re. On the other hand, Patel (1968a,b) modelled the magnetic tail as both a cylindrical (radius ~ 7Re) hydromagnetic waveguide and resonator neglecting the plasma sheet which he supposed to be of thickness 4 ~ 6Re. Contrast the lengths used by Patel (~ 25, 40, 50 and 100Re) with that of 220Re being used some 20 years later by Hones *et al.* (1984) who are investigating satellite measurements in the plasma sheet at such a distance from the Earth.

In Chapter 7 the plasma sheet will be considered as a hot plasma slab with half-thickness some few Re and infinitely broader and longer than its thickness.

The magnetopause, the plasma sheet and the flow pattern within it have all been observed to exhibit systematic temporal variations (see reviews by Hughes, 1983; Southwood and Hughes, 1983). Evidence comes from both ground-based and rocket and satellite observations (e.g., Mihalov *et al.*, 1970; Lepping and Burlaga, 1979; Hones *et al.*, 1983). The study of small amplitude oscillations in the strength and direction of the Earth's magnetic field, having periods of seconds to minutes, has traditionally been carried out using ground-based magnetometers, and geomagnetic pulsations have been thought for many years to be related to solar activity via the solar wind. Lanzerotti

and Southwood (1979) mention in particular the observations of Stewart in 1859 following a large magnetic storm and of Carrington in the 1850's following a large solar disruption. Hughes (1983) describes geomagnetic pulsations as being the 'ground signature of hydromagnetic waves in the atmosphere'. However there are difficulties of interpretation of magnetometer data because of the effect of the ionosphere, which, if it is assumed to be a finitely conducting horizontal layer between the magnetosphere (where mhd solutions pertain) and the Earth's insulating atmosphere, probably reflects waves from its upper surface, the magnetic field observed on the ground being due to the ionospheric Hall current (Walker *et al.*, 1979; Hughes, 1983; Southwood and Hughes, 1983). In the former reference, and also in Greenwald *et al.* (1981), these conclusions result from attempts to correlate the STARE (Scandinavian twin auroral radar experiment) auroral radar data with both GEOS2 (a geostationary satellite) data and geomagnetic pulsations from ground-based magnetometers. The arguments in these papers are based on models of field line resonances (Chen and Hasegawa, 1974a; Southwood, 1974; see also Section 2.1) illustrated in Figure 1.4, in which the Earth's (dipole) magnetic field is anchored in the ionosphere and standing waves are set up on the finite length field lines. However such models usually assume that the plasma is cold which, as Lanzerotti and Southwood (1979) and Hughes (1983) point out, is perhaps not the best approximation, since compressional hydromagnetic waves have recently been observed in the magnetosphere (Hones *et al.*, 1983). Hughes suggests that these waves may be due to the structure

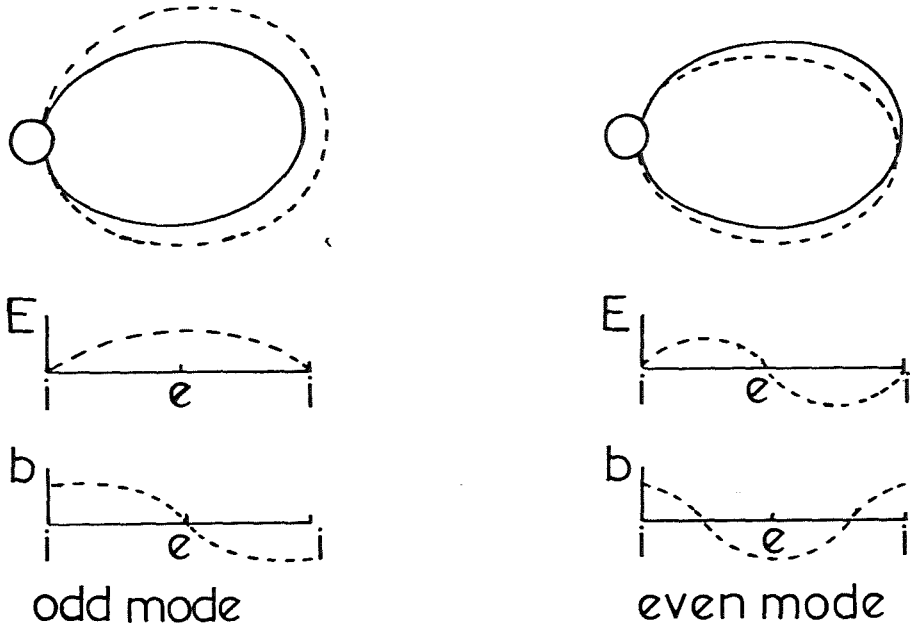

Figure 1.4 Following Southwood and Kivelson (1981) an idealized picture of geomagnetic field line oscillations assuming a perfectly conducting ionosphere (i). e : equator; — : unperturbed field; --- : perturbed field; E : electric field; b : magnetic field perturbation.

of the magnetosphere forming some sort of duct. He hints that surface waves are important. Such waves are described in Chapter 2 and used in magnetospheric models in Chapter 7.

The origin of oscillatory behaviour is open to much speculation. Shawhan (1979) tabulates possibilities and Southwood and Hughes (1983) give a detailed discussion in their review. There appear to be two main ideas. First the motion could be caused by an Alfvénic pulse produced, at the ionosphere, by a sudden change in conductivity. The more popular view, however, suggests that the solar wind is the ultimate source, affecting the magnetosphere either externally in the

form of a Kelvin-Helmholtz instability generated at the magnetopause, or in the form of waves entering the magnetosphere directly at the bow shock or from the turbulent magnetosheath or more subtly via various plasma instabilities in the form of sharp spatial gradients, temperature anistropies, etc. The literature seems almost purposefully vague! Chen and Hasegawa (1974b) refer to pulsations being excited by 'sudden commencements and sudden impulses near to the magnetopause' and Lanzerotti *et al.* (1973) refer to unknown impulse sources which excite mhd surface waves at the plasmapause.

In an attempt to represent the effects of the solar wind on the magnetotail, another series of models was developed (Siscoe, 1969; McKenzie, 1971) which considered a geometry as shown in Figure 1.5, with the solar wind being represented as a (usually sinusoidal) driving force acting on the magnetopause $x = \pm d$. Of course these models presume the magnetotail and its embedded plasma sheet to have almost constant thickness. However analyses of satellite data and related theories (e.g., Mihalov *et al.*, 1970; Forbes and Priest, 1982; Hones *et al.*, 1984) suggest variations in sheet thickness as plasmoids are formed and spontaneously released near the Earth, possibly as a result of magnetic reconnection.

In Chapter 7 two structured plasma models of the magnetosphere will be considered. Both will assume that the magnetic field lines form ducts, in one case the whole magnetotail, in the other the plasma sheet, so that the boundaries of the structure move in such a way that the magnetic field lines are always tangential to the boundaries and the total pressure across the boundaries is in balance. Thus

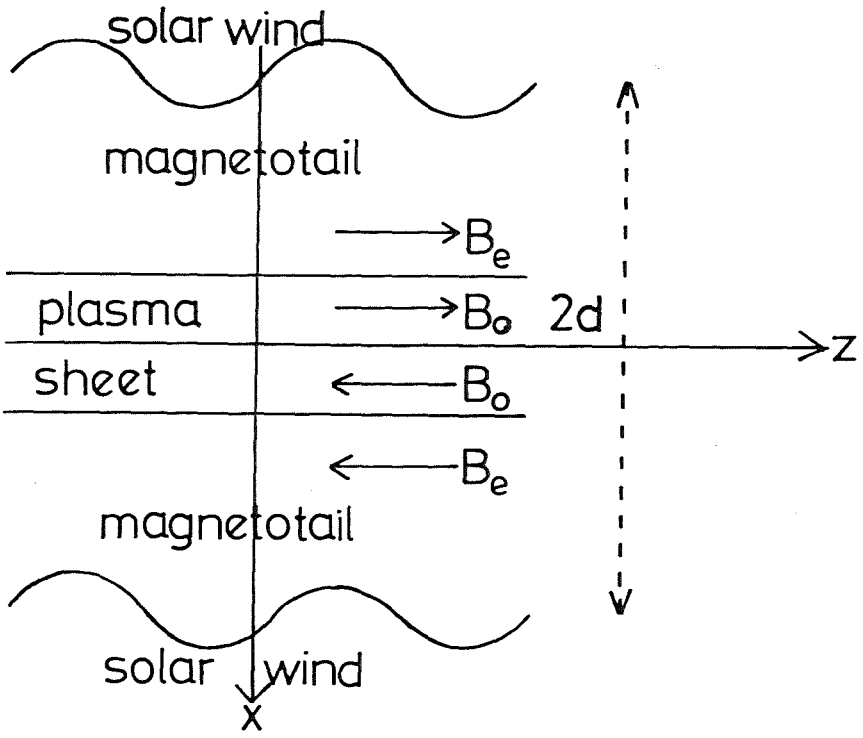

Figure 1.5 The magnetotail geometry of Siscoe's (1969) and McKenzie's (1971) models.

basically the models are similar to those considered by McKenzie (1970). However one feature of oscillatory behaviour occurring in observations, from both space and ground-based stations, is the apparent wave-packet structure (Mier-Jedrzejowicz and Hughes, 1980) or 'decay' of a train of oscillations (Walker *et al.*, 1978). The discussion of Chapter 7 will offer an explanation of these finite wave trains as well as reproduce McKenzie's results as special cases. The analogy between these magnetospheric structures and high density loops of the Sun's corona will be made apparent.

1.4 The Plasma Description : Assumptions and Equations

Reference has been made many times already to the 'plasma' of the solar atmosphere and the magnetosphere without qualification. Similarly mhd waves have been mentioned without any reference to what is meant by an mhd model. Here Goedbloed's (1983) attitude is adopted, of postulating the equations of mhd for a hypothetical medium, 'a plasma', to describe the interaction of a perfectly conducting fluid with a magnetic field. Whilst recognizing that the area of validity of such a model is limited (for example, Wentzel (1981) has warned about inappropriate models for coronal heating theories and Southwood and Hughes (1983) stress the limitations for the magnetospheric problem) it seems only sensible to proceed with the universal idea of a continuum description that is so well-known and well-used (e.g., Landau and Lifshitz, 1960; Roberts, P.H., 1967; Cowling, 1976; Parker, 1979a; Priest, 1982; Goedbloed, 1983).

S.I. (rationalized MKS) units will be used throughout except for brief comparisons with observations in Chapters 4 and 7. The symbols used in the following for the plasma's scalar and vector fields are $\bar{\rho}$ density, $\bar{p}$ pressure, $\bar{T}$ temperature, $\underline{v}$ velocity and $\underline{\bar{B}}$ magnetic induction. t is the time variable.

It will be assumed that the medium under consideration is a perfect (electrical) conductor so that Maxwell's equations may be combined to give the mhd induction equation,

$$\frac{\partial \underline{\bar{B}}}{\partial t} = \underline{\mathrm{curl}}(\underline{v} \times \underline{\bar{B}}). \qquad (1.1)$$

Using one of Maxwell's equations,

$$\operatorname{div} \bar{\underline{B}} = 0, \tag{1.2}$$

and the divergence theorem, the mhd analogue of Helmholtz's theorem, namely

$$\int_S \bar{\underline{B}} \cdot d\underline{S} = \text{constant}, \tag{1.3}$$

where S is a flux tube cross-section, may be derived. This, of course, states the 'frozen-in' condition for perfect conductors.

Other mhd equations which will be referred to throughout this thesis are listed below.

The equation of continuity (conservation of mass) is

$$\frac{d\bar{\rho}}{dt} + \bar{\rho} \operatorname{div} \underline{v} = 0, \tag{1.4}$$

where $\frac{d}{dt} \equiv \frac{\partial}{\partial t} + \underline{v} \cdot \underline{\text{grad}}$ is the (total) Lagrangian differential operator, and the equation of motion (conservation of linear momentum) is

$$\bar{\rho} \frac{d\underline{v}}{dt} = -\nabla \bar{p} + \frac{1}{\mu_0} (\nabla \times \bar{\underline{B}}) \times \bar{\underline{B}} + \bar{\rho} \underline{g}, \tag{1.5}$$

where $\underline{g}$ is the gravitational acceleration (of magnitude $2.74 \times 10^2 \text{ms}^{-2}$). Here isotropic constitutive equations have been assumed in order to combine Maxwell's equations and μ_0 is the magnetic permeability of the plasma, taken equal to the constant value of that of free space ($\mu_0 = 4\pi \times 10^{-7}$ henry m^{-1}).

Neglecting the rate of heat generation internal to the fluid and assuming the heat transfer coefficient, Q (joule $m^{-1}s^{-1}K^{-1}$) is constant, the thermodynamic equation takes the form

$$\bar{\rho} c_p \frac{d\bar{T}}{dt} - \frac{d\bar{p}}{dt} = Q\nabla^2\bar{T} - \mathcal{R} \tag{1.6}$$

where c_p is the specific heat at constant pressure per unit mass, and the radiative loss term, $\mathcal{R}$, will be assumed to obey Newton's law of cooling (see Spiegel, 1957; Bray and Loughhead, 1974) and have the form

$$\mathcal{R} = \frac{\bar{\rho} c_v}{\tau_R} (\bar{T} - T_0). \tag{1.7}$$

Here T_0 is the ambient temperature of the plasma, c_v the specific heat at constant volume (per unit mass) and τ_R is the radiative relaxation (decay) time which will be assumed known from tables such as those in Bray and Loughhead (1974), Spruit (1974) and Giovanelli (1978).

If the plasma is assumed to be a perfect gas, then

$$\bar{p} = R\bar{\rho}\bar{T}, \tag{1.8}$$

where R is a constant for the gas (equal to $c_p - c_v$ or $k_B/\bar{m}$ where k_B is Boltzmann's constant and $\bar{m}$ the average molecular mass). For example in the solar atmosphere R has the value $8.3 \times 10^3/0.6 = 13.8 \times 10^3 m^2 s^{-2} K^{-1}$.

In much of the thesis only the linearized version of the above equations will be used. It will be assumed that there is an equilibrium state ($\underline{v} = \underline{0}$) in which variables have the values ρ_0, p_0, T_0 and $\underline{B}_0$ and all derivatives with respect to time are zero. In this equilibrium state Equation (1.8) becomes

$$p_0 = R\rho_0 T_0, \tag{1.9}$$

and (1.6) gives

$$\nabla^2 T_0 = 0, \tag{1.10}$$

while (1.2) gives

$$\underline{\nabla}.\underline{B}_0 = 0. \tag{1.11}$$

If $\mathfrak{T}$ and $\mathfrak{L}$ are typical time and length scales for the system under consideration then $\tau_\kappa = \mathfrak{L}^2/\kappa$ is a typical diffusion time. Here

$$\kappa = Q/c_p\rho_0$$

is the (constant) thermometric conductivity or thermal diffusivity (m^2s^{-1}). If $\mathfrak{T} << \tau_\kappa, \tau_R$ then the terms on the right-hand side of (1.6) may be neglected and the resulting equation describes adiabatic (isentropic) flow. For adiabatic flow, using (1.8), Equation (1.6) reduces to

$$\frac{d\bar{p}}{dt} = \frac{\gamma\bar{p}}{\bar{\rho}} \frac{d\bar{\rho}}{dt}, \tag{1.12}$$

where $\gamma = c_p/c_v$.

If the gravitational force $\underline{g}$ and the equilibrium magnetic field $\underline{B}_0$ are assumed to act in the $\mp z$ directions respectively (for the Cartesian and cylindrical polar coordinate systems used in this thesis), then the transverse component of the equation of motion (1.5) in the $\underline{n}_s$ direction (where $\underline{n}_s$ is $\hat{\underline{x}}$ or $\hat{\underline{y}}$ or $\hat{\underline{r}}$, a unit vector orthogonal to the z direction) implies that

$$\frac{\partial}{\partial n_s}\left(p_0 + \frac{B_0^2}{2\mu_0}\right) = 0, \tag{1.13}$$

whilst the vertical component gives

$$\frac{dp_0}{dz} = -g\rho_0. \tag{1.14}$$

If ρ, p, $\underline{b}$ and $\underline{v}$ are the (small) perturbations in density, pressure, magnetic induction and velocity fields, respectively, about corresponding equilibrium values, so that $\bar{p} = p_0 + p$, etc., and $c_0^2 = \gamma p_0/\rho_0$ is the speed of sound in the basic state, then Equations (1.1) and (1.11) give

$$\frac{\partial \underline{b}}{\partial t} = \underline{\mathrm{curl}}(\underline{v} \times \underline{B}_0) = (\underline{B}_0.\underline{\nabla})\underline{v} - (\underline{v}.\underline{\nabla})\underline{B}_0 - \underline{B}_0 \,\mathrm{div}\,\underline{v} \tag{1.15}$$

and (1.4), (1.5) and (1.12) become,

$$\frac{\partial \rho}{\partial t} + \mathrm{div}(\rho_0 \underline{v}) = 0, \tag{1.16}$$

$$\rho_0 \frac{\partial \underline{v}}{\partial t} = -\underline{\nabla}\left(p + \frac{1}{\mu_0}\underline{B}_0.\underline{b}\right) + \frac{1}{\mu_0}(\underline{B}_0.\underline{\nabla})\underline{b} + \frac{1}{\mu_0}(\underline{b}.\underline{\nabla})\underline{B}_0 + \rho\underline{g} \tag{1.17}$$

and

$$\frac{\partial p}{\partial t} + (\underline{v}.\underline{\nabla})p_0 = c_0^2\left(\frac{\partial \rho}{\partial t} + (\underline{v}.\underline{\nabla})\rho_0\right). \qquad (1.18)$$

Generally gravitational effects will be ignored ($\underline{g} = \underline{0}$) except for Chapter 5 when this term will be retained to provide a better model of the lower solar atmosphere.

The boundary conditions across a surface of discontinuity, which may be derived by integrating (1.4), (1.5) and (1.6) across the surface (see, e.g., Roberts, P.H., 1967) or in the case of (1.20) by examining perturbations of the transverse momentum equation about the basic state (Roberts and Webb, 1978) and which will be used throughout are that:

$$\text{the transverse (normal) component of velocity is continuous,} \qquad (1.19)$$

$$\text{the total perturbed pressure, } p_T = p + \frac{B_0 b_z}{\mu_0} \text{ is continuous,} \qquad (1.20)$$

$$\text{the transverse heat flux } \kappa \frac{\partial T}{\partial n_s} \text{ is continuous} \qquad (1.21)$$

and

$$\text{the temperature perturbation T is continuous.} \qquad (1.22)$$

The next two chapters concentrate on basic theory, some of which is developed further and applied to the corona in Chapter 4. Further mathematics of waves is discussed in Chapters 5 and 6 and applied, mainly to the photosphere and magnetosphere, in the last chapter.

Chapter 2 Structuring in a Cartesian Geometry

'With a name like yours, you might be any shape, almost.'

Lewis Carroll 'Through the Looking Glass'

2.1 Introduction

In order to examine structuring in the plasma it will be assumed first that the structure can be considered in a Cartesian geometry which has infinite extent in the z-direction (of a Cartesian coordinate system xyz). The effects of stratification due to gravity will be ignored. In the equilibrium state it is supposed that the plasma pressure p_0, density ρ_0 and magnetic field $B_0\hat{z}$ are x-dependent.

Linear, isentropic perturbations about the basic state then obey equations (1.15) to (1.18) with $\underline{g} = \underline{0}$. Following Lighthill (1960), it is convenient to introduce the variables $\Delta = \text{div}\,\underline{v}$, $\Gamma = \partial v_z/\partial z$ and $p_T = p + \frac{B_0}{\mu_0} b_z$, where $\underline{v} = (v_x, v_y, v_z)$ and $\underline{b} = (b_x, b_y, b_z)$. The perturbation equations, (1.15), (1.16) and (1.18), may then be written:

$$\frac{\partial p}{\partial t} = -\rho_0 c_0^2 \Delta - v_x \frac{dp_0}{dx}, \tag{2.1}$$

$$\frac{\partial b_x}{\partial t} = B_0 \frac{\partial v_x}{\partial z}, \tag{2.2a}$$

$$\frac{\partial b_y}{\partial t} = B_0 \frac{\partial v_y}{\partial z}, \tag{2.2b}$$

$$\frac{\partial b_z}{\partial t} = B_0(\Gamma - \Delta) - v_x\left(\frac{dB_0}{dx}\right) \tag{2.2c}$$

and

$$\frac{\partial p_T}{\partial t} = \rho_0 v_A^2 \Gamma - \rho_0 (c_0^2 + v_A^2)\Delta, \tag{2.3}$$

where, in (2.3), the fact that there is total pressure (gas plus magnetic) balance in the basic state (see Equation (1.13)) has been used, that is

$$\frac{d}{dx}\left(p_0 + \frac{B_0^2}{2\mu_0}\right) = 0. \tag{2.4}$$

Here $v_A(x) = (B_0^2/\mu_0\rho_0)^{\frac{1}{2}}$ is the Alfvén speed and $c_0(x) = (\gamma p_0/\rho_0)^{\frac{1}{2}}$ the sound speed.

The equation of motion (Equation (1.17)) may be differentiated partially with respect to time and variables other than $\underline{v}$ eliminated to give (see Roberts, 1981a)

$$\rho_0\left(\frac{\partial^2}{\partial t^2} - v_A^2\frac{\partial^2}{\partial z^2}\right)v_x = \frac{\partial}{\partial x}\left[\rho_0(c_0^2 + v_A^2)\Delta - \rho_0 v_A^2\Gamma\right], \tag{2.5}$$

$$\rho_0\left(\frac{\partial^2}{\partial t^2} - v_A^2\frac{\partial^2}{\partial z^2}\right)v_y = \frac{\partial}{\partial y}\left[\rho_0(c_0^2 + v_A^2)\Delta - \rho_0 v_A^2\Gamma\right] \tag{2.6}$$

and

$$\frac{\partial^2 v_z}{\partial t^2} = c_0^2\frac{\partial \Delta}{\partial z}. \tag{2.7}$$

Equations (2.1) through (2.7) may now be Fourier analysed by writing the variables in the form

$$v_x = \hat{v}_x(x)e^{i(\omega t+\ell y+kz)}, \quad p_T = \hat{p}_T(x)e^{i(\omega t+\ell y+kz)}, \text{ etc.}, \tag{2.8}$$

and after some manipulation it is found that the x-dependent amplitudes of the perturbations, $\hat{v}_x$ and $\hat{p}_T$, satisfy the ordinary differential

equations

$$\frac{d\hat{p}_T}{dx} = \frac{i\rho_0(x)(k^2v_A^2(x) - \omega^2)\hat{v}_x}{\omega} \tag{2.9}$$

and

$$\frac{d\hat{v}_x}{dx} = \frac{\omega[(k^2v_A^2(x)-\omega^2)(k^2c_0^2(x)-\omega^2) + \ell^2(k^2c_T^2(x)-\omega^2)(c_0^2(x) + v_A^2(x))]\hat{p}_T}{i\rho_0(x)(k^2v_A^2(x)-\omega^2)(k^2c_T^2(x)-\omega^2)(c_0^2(x) + v_A^2(x))}, \tag{2.10}$$

where

$$c_T^2(x) = \frac{c_0^2(x)v_A^2(x)}{c_0^2(x) + v_A^2(x)}. \tag{2.11}$$

Equations (2.9) and (2.10) may be combined to give

$$\frac{d}{dx}\left\{\frac{\rho_0(x)(k^2v_A^2(x) - \omega^2)}{m_0^2(x) + \ell^2}\frac{d\hat{v}_x}{dx}\right\} - \rho_0(x)[k^2v_A^2(x) - \omega^2]\hat{v}_x = 0, \tag{2.12}$$

where

$$m_0^2(x) = \frac{(k^2c_0^2(x) - \omega^2)(k^2v_A^2(x) - \omega^2)}{(c_0^2(x) + v_A^2(x))(k^2c_T^2(x) - \omega^2)}. \tag{2.13}$$

Equation (2.12) is the Cartesian equivalent of the Hain-Lüst equation (Hain and Lüst, 1958), arising in a cylindrical geometry, which is discussed in Chapter 3. It has been obtained by, for example, Goedbloed (1971), Chen and Hasegawa (1974b), Wentzel (1979a) and Roberts (1981a).

If there is no structuring of the medium, so that coefficients in (2.12) are independent of x, then this equation simplifies to

$$(k^2v_A^2 - \omega^2)\left[\frac{d^2\hat{v}_x}{dx^2} - (m_0^2 + \ell^2)\hat{v}_x\right] = 0, \tag{2.14}$$

which, for an x-dependence of the form $e^{ik_x x}$, gives

$$(k^2 v_A^2 - \omega^2)(\ell^2 + k_x^2 + m_0^2) = 0. \tag{2.15}$$

The assumptions made in deriving (2.15) mean that a uniform, infinite medium is being modelled. Rewriting (2.15) by substituting for m_0^2 shows that its roots are the well-known Alfvén modes

$$\omega^2 = k^2 v_A^2, \tag{2.16}$$

and magnetoacoustic modes,

$$\omega^2 = \tfrac{1}{2}(k_x^2 + \ell^2 + k^2)(c_0^2 + v_A^2)\left[1 \pm \sqrt{1 - \frac{4k^2 v_A^2 c_0^2}{(k_x^2 + \ell^2 + k^2)(c_0^2 + v_A^2)^2}}\right], \tag{2.17}$$

of a uniform medium (e.g., Cowling, 1976). The aim in this chapter is to investigate how these modes are modified by the x-dependence introduced by the structuring of the medium. If the structuring is weak, in the sense that the factors in (2.12) vary only slightly with x, then a local approximation may be made, with (2.16) and (2.17) giving the appropriate modes.

If the medium is considered both uniform and finite, by the introduction of rigid boundaries, say, at $x = \pm x_0$, then the wavenumber k_x (for ℓ and k fixed) is quantized by being an integer, s times $\pi/2x_0$, where s relates to the number of nodes of the eigenfunction v_x (the transverse velocity). Goedbloed (1983) points out that such a labelling of the discrete eigenvalues still makes sense in an inhomogeneous medium when the equilibrium quantities vary in the x-direction. To demonstrate his idea he considers the limit $k_x \to \infty$

($s \to \infty$) in Equations (2.16) and (2.17) and lists the essential features of the spectra of eigenvalues, ω^2, resulting from this limit, as being:

(i) the infinitely degenerate point eigenvalue, $\omega^2 = k^2 v_A^2$,

(ii) the cluster (or accumulation) point, $\omega^2 \to k^2 c_0^2 v_A^2/(c_0^2 + v_A^2)$,

and (iii) the cluster point, $\omega^2 \to \infty$.

Goedbloed goes on to show that these three facts facilitate a division of the inhomogeneous case, with its associated singularities, as is discussed below.

The singularities of Equation (2.12), in both Cartesian and cylindrical geometries, have been the subject of much discussion, since at these points it is known that in the presence of dissipation the plasma can absorb energy from some external forcing mechanism and cause resonant heating (see, for example, Southwood, 1974; Hasegawa and Chen, 1974, 1976). Most of the discussion in the literature has concentrated on the incompressible ($m_0^2(x) \to k^2$), two-dimensional ($\ell = 0$) form of (2.12), in which the resonance occurs at the singularity $\omega^2 = k^2 v_A^2(x)$, when the external forcing wave matches the local Alfvén speed, $v_A(x)$. Sedláček (1971) attempted to reconcile the different mathematical behaviour resulting from a continuous $v_A(x)$ profile, which gives a continuous spectrum of modes, and that resulting in discrete modes which arise when the medium is uniform and thus the factor $(k^2 v_A^2 - \omega^2)$ is removable from (2.12). Lee (1980) and Rae and Roberts (1981) pointed out, however, that Sedláček's results have been wrongly interpreted by Ionson (1978) and Wentzel (1979b) as being a dissipative process in an *ideal*,

incompressible medium.

Extending consideration of singularities of (2.12) to a compressible medium, Rae and Roberts (1982) have shown that as well as the Alfvén singularity there is the important cusp singularity where $\omega^2 = k^2 c_T^2(x)$. (See also fact (ii) of Goedbloed's classification above.) As Appert *et al.* (1974) have pointed out, in their discussion of a cylindrical geometry, these singularities are more evident from the first-order equations (2.9) and (2.10). Goedbloed (1983) has helped clarify the nature of the differential equation (2.12) by expressing the first term as

$$\frac{d}{dx}\left[\frac{\rho_0(x)\,(c_0^2(x)+v_A^2(x))\,(k^2c_T^2(x)-\omega^2)\,(k^2v_A^2(x)-\omega^2)}{(\omega_1^2-\omega^2)\;(\omega_2^2-\omega^2)}\,\frac{d\hat{v}_x}{dx}\right],$$

where

$$(\omega_1^2-\omega^2)(\omega_2^2-\omega^2) = (k^2c_0^2(x)-\omega^2)(k^2v_A^2(x)-\omega^2) + \ell^2(c_0^2(x)+v_A^2(x))(k^2c_T^2(x)-\omega^2).$$

The structure of (2.12) is then illustrated, following Goedbloed (1975, 1983), in Figure 2.1. Goedbloed has emphasized that $\{\omega_1^2\}$ and

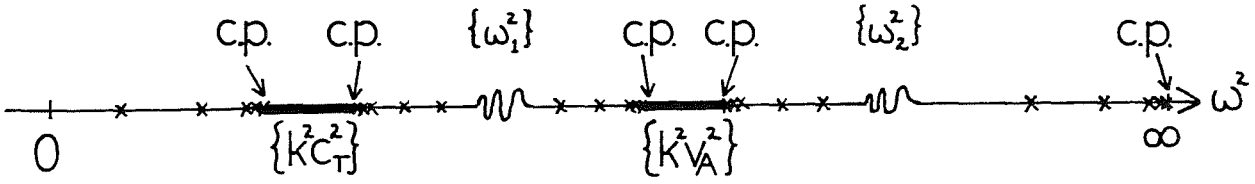

Figure 2.1 Schematic representation of the singularities of Equations (2.12), after Goedbloed (1975, 1983)

∿∿ : spectrum 'separators'; x : discrete modes;

— : continuous spectrum; c.p. : cluster points.

$\{\omega_2^2\}$ are *not* part of the spectrum (note that they are the roots (2.17) in a *uniform* medium). They act as kind of separators of the three subspectra. Separation only obtains if the inhomogeneity is weak. However, a detailed analysis, such as Sedláček's, of the behaviour of the compressible modes near these singularities, where the transition from discrete to continuous spectra takes place, has not been carried out.

Discussion of (2.12) in its general form is, unfortunately, a difficult task and though x-variation will be considered to some extent in Chapter 4, here it will be assumed that the non-uniformity of the medium takes the form of a uniform slab of discontinuity (say a magnetic field or density rapidly varying in the x-direction) which is infinite in the y-direction, so that $\hat{v}_y$ and ℓ are set equal to 0. Of course, as Parker (1979a) has pointed out, such a slab geometry (especially if of infinite extent in the y-direction) will offer much more resistance to any changes in the slab exterior than, for example, an inhomogeneity (such as an intense magnetic flux tube) represented by a cylindrical structure. However, in order to try to elucidate the behaviour in a structured situation, it was decided to examine the simpler Cartesian geometry first. A cylindrical geometry is investigated in the next chapter and compared and contrasted with the results presented below.

2.2 The Uniform Slab

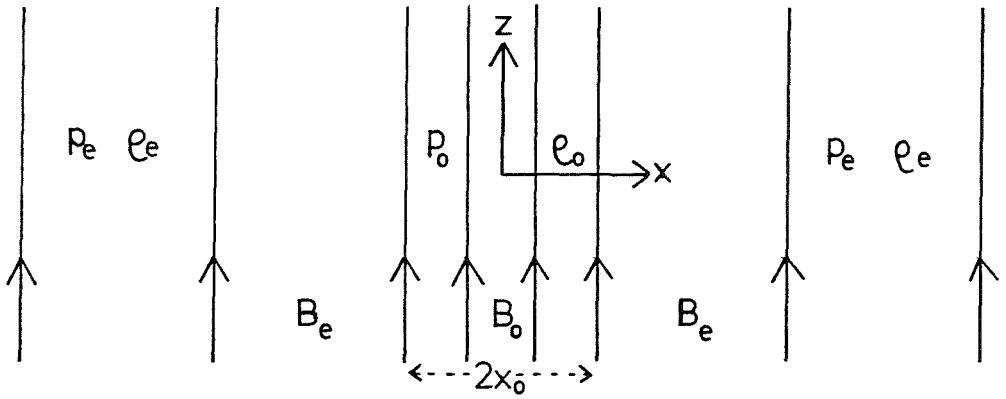

Figure 2.2 The equilibrium configuration

In Figure 2.2 the basic state of the plasma is one in which the pressure, density and magnetic fields are uniform inside a slab of width $2x_0$ and also have uniform (but not necessarily the same) values in the slab's environment. Thus, in the equilibrium state,

$$p_0(x),\ \rho_0(x),\ B_0(x) = \begin{cases} p_0, \rho_0, B_0, & |x| < x_0, \\ p_e, \rho_e, B_e, & |x| > x_0, \end{cases} \tag{2.18}$$

and Equation (2.4) shows in this case that

$$p_0 + \frac{B_0^2}{2\mu_0} = p_e + \frac{B_e^2}{2\mu_0} . \tag{2.19}$$

Using expressions for the sound and Alfvén speeds in the slab's environment ($|x| > x_0$) $c_e^2 = \gamma p_e/\rho_e$ and $v_{Ae}^2 = B_e^2/\mu_0\rho_e$, respectively, together with the equivalent ones for c_0^2 and v_A^2, Equation (2.19) may be expressed in the alternative form

$$\frac{\rho_e}{\rho_0} = \frac{(2c_0^2 + \gamma v_A^2)}{(2c_e^2 + \gamma v_{Ae}^2)} . \tag{2.20}$$

Since the plasma has now effectively been split into two uniform media, the slab interior ($|x| < x_0$) and its environment ($|x| > x_0$), perturbations about the equilibrium (2.18) to (2.20) are described, for the transverse velocity amplitude, by Equation (2.12), where the coefficients are now constants for each region. Inside the slab,

$$\frac{d^2\hat{v}_x}{dx^2} - m_0^2\hat{v}_x = 0 \tag{2.21}$$

where

$$m_0^2 = \frac{(k^2v_A^2 - \omega^2)(k^2c_0^2 - \omega^2)}{(c_0^2 + v_A^2)(k^2c_T^2 - \omega^2)} . \tag{2.22}$$

Also, for $\ell = 0$ and $\hat{v}_y = 0$ (so that there is no variation in the y-direction) Equation (2.10) gives

$$\hat{p}_T = \frac{i\rho_0(c_0^2 + v_A^2)}{\omega} \frac{(k^2c_T^2 - \omega^2)}{(k^2c_0^2 - \omega^2)} \frac{d\hat{v}_x}{dx} , \tag{2.23}$$

and Fourier analysis of Equation (2.7) shows that

$$\hat{v}_z = \frac{ikc_0^2}{(k^2c_0^2 - \omega^2)} \frac{d\hat{v}_x}{dx} . \tag{2.24}$$

Now observations of oscillations in structured plasmas are limited, but there is evidence, for example in the case of chromospheric fibrils (Giovanelli, 1975) and the magnetospheric plasma sheet (McKenzie, 1970) that oscillations are confined mainly to the inhomogeneity. In other words, the inhomogeneity appears to act as a waveguide. It will therefore be assumed that in the

slab's exterior, $|x| > x_0$, disturbances are laterally evanescent so that $\hat{v}_x \to 0$ as $|x| \to \infty$. A brief discussion outlining the nature of solutions which result when this assumption is not made is deferred until Chapter 3 (Section 3.5).

In this case the appropriate solutions of Equation (2.21) in the slab and its exterior can be described by:

$$\hat{v}_x(x) = \begin{cases} \alpha_e e^{-m_e(x-x_0)}, & x > x_0, \\ \alpha_0 \cosh m_0 x + \beta_0 \sinh m_0 x, & |x| < x_0, \\ \beta_e e^{m_e(x+x_0)}, & x < -x_0, \end{cases} \tag{2.25}$$

where α_0, β_0, α_e and β_e are arbitrary constants and m_e is given by

$$m_e^2 = \frac{(k^2c_e^2 - \omega^2)(k^2v_{Ae}^2 - \omega^2)}{(c_e^2 + v_{Ae}^2)(k^2c_{Te}^2 - \omega^2)}, \qquad c_{Te}^2 = \frac{c_e^2 v_{Ae}^2}{(c_e^2 + v_{Ae}^2)}. \tag{2.26}$$

The assumption of lateral evanescence restricts m_e to be positive.

The four constants in (2.25) are evaluated by invoking the boundary conditions, Equations (1.19) and (1.20). These establish continuity across the two boundaries, $x = \pm x_0$, of the slab of the transverse (normal) velocity $\hat{v}_x(x)$ and the total pressure perturbation $\hat{p}_T(x)$. For a non-trivial solution under these conditions ω and k are related by the *dispersion relation:*

$$\rho_e(k^2v_{Ae}^2 - \omega^2)\, m_0 \begin{Bmatrix} \tanh \\ \coth \end{Bmatrix} m_0 x_0 + \rho_0(k^2v_A^2 - \omega^2)m_e = 0, \tag{2.27}$$

where the tanh/coth terms correspond to the sinh/cosh solutions in (2.25).

2.3 General Discussion of Dispersion Relation

For evanescent solutions in the slab's exterior $m_e > 0$ and then there are no unstable ($\omega^2 < 0$) modes of (2.27). This is apparent from physical considerations (only free modes are being considered) but mathematically it can be seen from Equation (2.27). If ω^2 is supposed < 0, then both m_e and m_0 are > 0 and (for $x_0 > 0$) either there are no solutions for ω^2 (a contradiction) or both terms are identically zero and $\omega^2 > 0$ (again a contradiction).

The transcendental equation (2.27) was the basis for discussion in Edwin and Roberts (1982) where an attempt was made to analyse its rich spectrum of solutions, subject to $m_e > 0$, and to categorize the modes, specifically with solar physics applications in mind. Several authors had derived (2.27) earlier but then only subjected the dispersion relation to partial scrutiny as they pursued the problem in hand. For example, McKenzie (1970) derived a slightly more general form of (2.27) (including a bulk velocity of the medium in the basic state) but then immediately simplified the relation in order to model the plasma sheet of the magnetosphere. He considered a non-magnetic slab surrounded by a cold plasma ($B_0 = 0$, $p_e = 0$ here) so that his analysis of inherent modes was limited to a special case (Figure 2.11 later). Similarly, Chakraborty (1968) also included a velocity shear in his examination of a two-dimensional compressional jet, but after deriving a generalized (2.27) pursued a stability analysis which is not relevant here. Special forms of (2.27) have also been derived by Cram and Wilson (1975) and Wilson (1978), for an interface, and a slab in a non-magnetic isothermal exterior; by

Wentzel (1979a), for an interface; and by Roberts (1981 a,b) for an interface and a slab in a non-magnetic exterior.

It is probably appropriate at this stage to define the terminology which is used here in the classification of modes of Equation (2.27) and throughout this thesis, since there is some confusion in the literature. Following Roberts (1981a), solutions of (2.27) with $m_0^2 > 0$ will be referred to as *surface waves* and those with $m_0^2 < 0$ as *body waves*. Thus the distinction pertains only to their spatial behaviour within the inhomogeneity (Figure 2.3). Both these categories are often termed 'surface waves' (Wentzel, 1979a

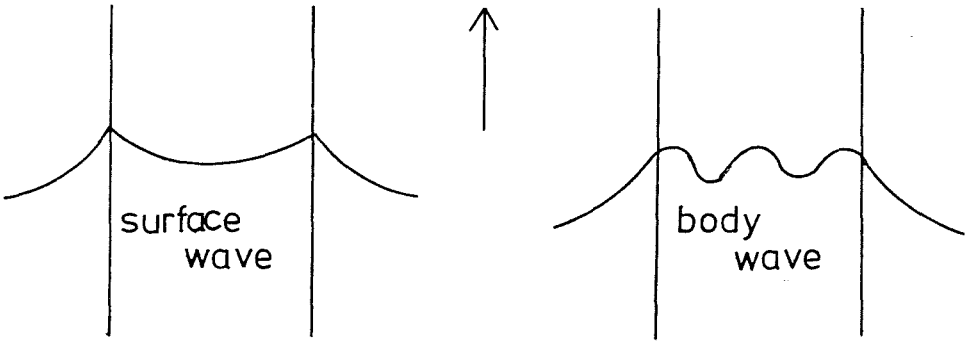

Figure 2.3. Wave classification

and a review by Moisan *et al.*, 1982) probably because they refer to modes confined to the neighbourhood of the slab (the surface discontinuities).

A further categorization arises from the even and odd (coth and tanh) solutions of (2.27). The former describe the 'wiggling snake' motion of the slab and are referred to as the *kink* (or asymmetric or taut-wire) modes whilst those for which the centre of

the slab is not disturbed (corresponding to the sinh $m_0 x$ solutions for $\hat{v}_x$) are called the *sausage* (or symmetric or pulsation) modes (Figure 2.4).

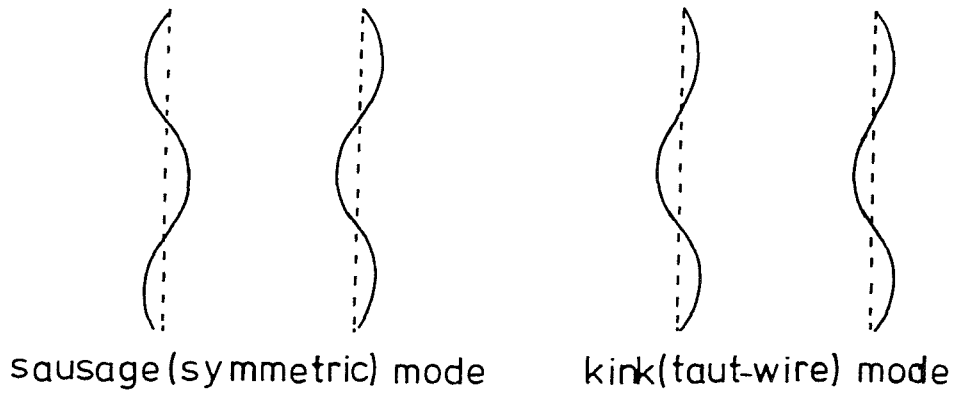

Figure 2.4 Modes of oscillation

There are a number of immediate deductions from (2.26) and (2.27). For example, with $m_e > 0$, surface waves ($m_0^2 > 0$) can only arise if the longitudinal phase-speed ω/k lies between the two Alfvén speeds, that is

$$\min(v_A, v_{Ae}) < \omega/k < \max(v_A, v_{Ae}), \tag{2.28}$$

because only then do the terms in (2.27) have opposite signs and thus the possibility of roots arises. Much the same feature is apparent for a single magnetic interface (Wentzel, 1979a). Also, from (2.26), it is apparent that (2.27) possesses solutions only for

$$\omega < kc_{Te} \quad \text{or} \quad \min(kv_{Ae}, kc_e) < \omega < \max(kv_{Ae}, kc_e). \tag{2.29}$$

Furthermore it is observed from the factors of (2.27) that $\omega/k = \pm v_{Ae}$ and $\omega/k = \pm v_A$ are solutions. However, as Roberts (1981b) has pointed out, consideration of the degenerate form of (2.21) when

$m_0 = 0$ (or $m_e = 0$ in the exterior) reveals that $\omega^2 = k^2 v_A^2$ or $k^2 c_0^2$ lead to zero eigenvectors. Other degenerate cases are those of $c_e = c_0$ when pure sound waves may propagate without disturbing the magnetic field and the incompressible Alfvén waves when $v_A = v_{Ae}$.

Roberts (1981b) examined the problem of a magnetic slab in a field-free exterior. This corresponds here to the case of $B_e = 0$ for which (2.27) reduces to the equation

$$(k^2 v_A^2 - \omega^2) m_e = (\rho_e/\rho_0)\omega^2 m_0 \begin{Bmatrix} \tanh \\ \coth \end{Bmatrix} m_0 x_0 . \qquad (2.30)$$

Roberts showed that (2.30) permits slow magnetoacoustic surface waves which propagate with longitudinal phase-speed below c_T. If, however, there is an external magnetic field present, so that (2.27) above applies, waves with phase-speeds below c_T arise only if $v_{Ae} < c_T$ because, by definition, $c_T < v_A$ and so unless v_{Ae} is less than c_T condition (2.28) is violated. Even the possibility of phase-speeds below c_T is ruled out if both v_{Ae} and c_e are less than c_T because, from (2.29) there are no solutions for $\omega > \max (kc_e, kv_{Ae})$. Thus there are a number of important modifications to be made to the dispersion diagrams given in Roberts (1981b) describing a slab in a field-free environment. This is included in the general discussion and classification of the modes of (2.27), the subject of Edwin and Roberts (1982) and the remainder of this chapter.

In order to embark on this task various methods of examining the dispersion relation were employed including graphical methods,

which indicated the possible solution sets of (2.27) given that, for a general structuring, v_A, v_{Ae}, c_0, c_e could vary relatively in size, subject to (2.20) and to the phase-speeds being constrained by (2.28) and (2.29). Also a number of special cases were investigated and these are discussed below.

One method of simplifying the dispersion relation is to consider it as applying to a *slender* or *wide* inhomogeneity. Of course these terms are relative to the wavelength of the oscillations under consideration. *Slender* slabs will be defined as those for which the wavelength in the dispersion relation of the disturbance is much greater than the lateral dimension of the inhomogeneity, that is, the longitudinal wave number k and the slab half-width satisfy $|k|x_0 << 1$. Correspondingly, a *wide* slab will be one for which $|k|x_0 >> 1$.

2.4 Incompressible Modes

For an incompressible fluid, corresponding to $\gamma \to \infty$, both m_0 and m_e tend to $|k|$ and (2.27) takes the explicit form

$$\omega^2/k^2 = \frac{\rho_0 v_A^2 + \rho_e v_{Ae}^2 \left\{\begin{matrix}\tanh\\ \coth\end{matrix}\right\} |k|x_0}{\rho_0 + \rho_e \left\{\begin{matrix}\tanh\\ \coth\end{matrix}\right\} |k|x_0}, \qquad (2.31)$$

a relation first obtained by Kruskal and Schwarzschild (1954).

The solutions of (2.31) are the phase-speeds of Alfvénic surface waves (since $m_0^2 > 0$). These surface waves owe their existence to the presence of the boundary and have wave amplitudes which take maximum values on

the slab boundaries and decline on either side of $x = \pm x_0$. In the unstructured medium the only solutions of (2.14) with $\ell = 0$ and $m_0^2 = k^2$ are $\omega^2 = k^2 v_A^2$ and, for $\hat{v}_x$ finite at $x = \pm\infty$, the trivial one, $\hat{v}_x = 0$. In this case (2.15) shows that linear disturbances in an incompressible unbounded plasma are Alfvén waves with $\omega^2 = k^2 v_A^2$. This point is made by Parker (1974b) in his direct study of an incompressible fluid.

For long wavelength disturbances in a slender inhomogeneity so that $|k|x_0 \ll 1$, (2.31) reduces, for a (symmetric) sausage disturbance to

$$\omega^2 \simeq k^2 v_A^2 \{1 + \rho_e/\rho_0 (v_{Ae}^2/v_A^2 - 1)|k|x_0\}, \tag{2.32a}$$

and for a kink disturbance to

$$\omega^2 \simeq k^2 v_{Ae}^2 \{1 + \rho_0/\rho_e (v_A^2/v_{Ae}^2 - 1)|k|x_0\}. \tag{2.32b}$$

In a wide slab $|k|x_0 \gg 1$, both modes have phase-speeds given by

$$\frac{\omega^2}{k^2} \simeq \frac{\rho_e v_{Ae}^2 + \rho_0 v_A^2}{\rho_e + \rho_0} \tag{2.33}$$

which is the result, as expected, for a single magnetic interface obtained originally by Kruskal and Schwarzschild (1954).

It is clear from the preceding formulae that the general behaviour of the phase-speeds of the sausage and kink modes interchanges accordingly as v_{Ae} is greater or less than v_A. The phase-speed as a function of kx_0 (for $k > 0$) is sketched in Figure 2.5 for the cases $v_A > v_{Ae}$ and $v_A < v_{Ae}$, using (2.31). It illustrates the behaviour described by (2.32) and (2.33).

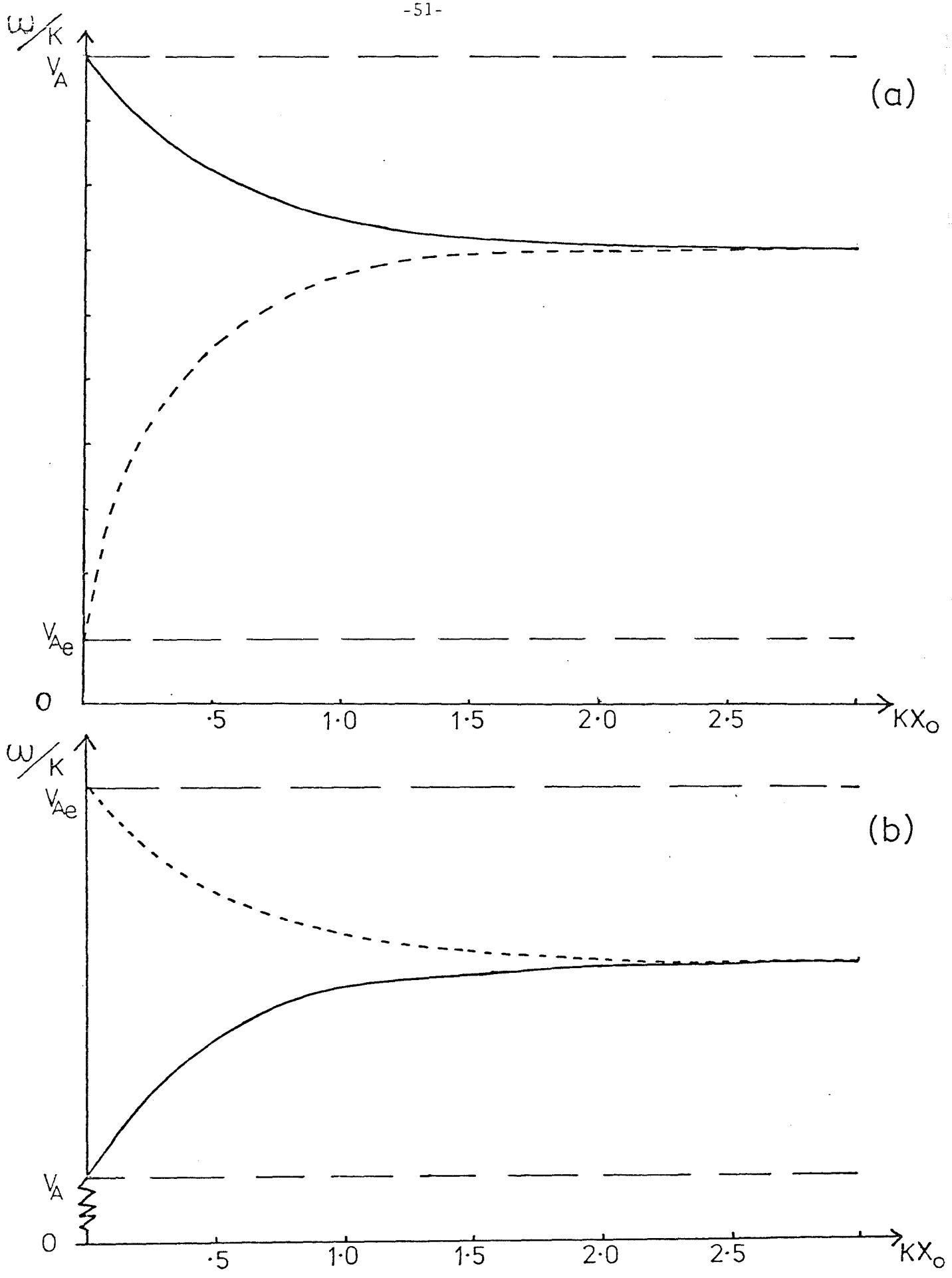

Figure 2.5 The phase-speed as a function of kx_0 ($k > 0$) for Alfvén surface waves in an incompressible plasma. Here $\rho_0 = \rho_e$ and in (a) $v_{Ae} = 0.1v_A$ ($v_{Ae} < v_A$) and in (b) $v_{Ae} = 1.5v_A$ ($v_{Ae} > v_A$). ——: sausage mode; --- : kink mode.

2.5 Compressible Modes

The above procedure of considering modal behaviour in first a slender and then a wide inhomogeneity may be applied to the general dispersion relation (2.27). However the treatment of compressible modes is more difficult because, unlike (2.31), (2.27) is a transcendental equation with m_0 and m_e functions of ω. Having first examined (2.27) analytically, in the slender and wide limits, to gain some insight of the modes, a computer solution of (2.27) was then sought which helped to complete the picture. The results are described below.

2.5.1 Surface modes of a slender slab

To consider the reduction of (2.27) for the tanh function (symmetric modes) in the slender ($|k|x_0 \ll 1$) limit it was supposed that $m_0 x_0 \to 0$ as $|k|x_0 \to 0$ so that $\tanh m_0 x_0 \simeq m_0 x_0$. The results were then checked *a posteriori* to ensure that this assumption was indeed valid. (Roberts and Webb (1979) and Wilson (1980) give a discussion of this point.) Under these conditions (2.27) reduces to

$$\rho_0(k^2 v_A^2 - \omega^2)m_e + \rho_e(k^2 v_{Ae}^2 - \omega^2)m_0^2 x_0 = 0 \qquad (2.34)$$

for the sausage mode. Approximate solutions of (2.34), subject to (2.28) and (2.29), are

$$\omega^2 \simeq k^2 c_e^2 \left\{1 + \left(\frac{\rho_e}{\rho_0}\right)^2 \frac{(c_0^2 - c_e^2)^2 (v_{Ae}^2 - c_e^2) c_e^2 (kx_0)^2}{(c_T^2 - c_e^2)^2 (c_0^2 + v_A^2)^2}\right\}, \qquad (2.35a)$$

$$\omega^2 \simeq k^2 c_T^2 \left\{1 + \left(\frac{\rho_e}{\rho_0}\right) \frac{(c_0^2 - c_T^2)(v_{Ae}^2 - c_T^2)^{\frac{1}{2}}(c_e^2 + v_{Ae}^2)^{\frac{1}{2}}(c_{Te}^2 - c_T^2)^{\frac{1}{2}}(|k|x_0)}{(c_e^2 - c_T^2)^{\frac{1}{2}}(c_0^2 + v_A^2)c_T^2}\right\}, \quad c_{Te} > c_T$$

(2.35b)

and

$$\omega^2 \simeq k^2 c_T^2 \left\{1 - \left(\frac{\rho_e}{\rho_0}\right) \frac{(c_0^2 - c_T^2)(c_T^2 - v_{Ae}^2)^{\frac{1}{2}}(c_e^2 + v_{Ae}^2)^{\frac{1}{2}}(c_T^2 - c_{Te}^2)^{\frac{1}{2}}(|k|x_0)}{(c_e^2 - c_T^2)^{\frac{1}{2}}(c_0^2 + v_A^2)c_T^2}\right\},$$

$$c_e > c_T > v_{Ae}. \qquad (2.35c)$$

Equations (2.35) show that the sausage modes in a slender slab are only weakly affected by the magnetic field structuring since these modes are essentially the same as those for a slab in a field-free medium ($v_{Ae} = 0$) (Roberts, 1981b) or for a field-free slab ($v_A = 0$) (McKenzie, 1970, to be discussed later). However, pressure, density or temperature structuring is crucial to the existence of the mode given by (2.35a), as noted by Webb (1980) and Roberts (1981b). Indeed this mode was not apparent in Cram and Wilson's (1975) study of wave propagation because the case of $c_e = c_0$ (see comment following (2.29)) was being considered. Wentzel (1979a) too overlooked this mode in his discussion of the interface problem.

The mode given by (2.35a) is illustrated in Figures 2.6, 2.7 and 2.8 and that of (2.35c) in Figure 2.6. Equation (2.35b) is illustrated later as a special case of a field-free slab (Figure 2.11).

In the limit of $|k|x_0 << 1$, the reduction of (2.27) for the kink mode leads to

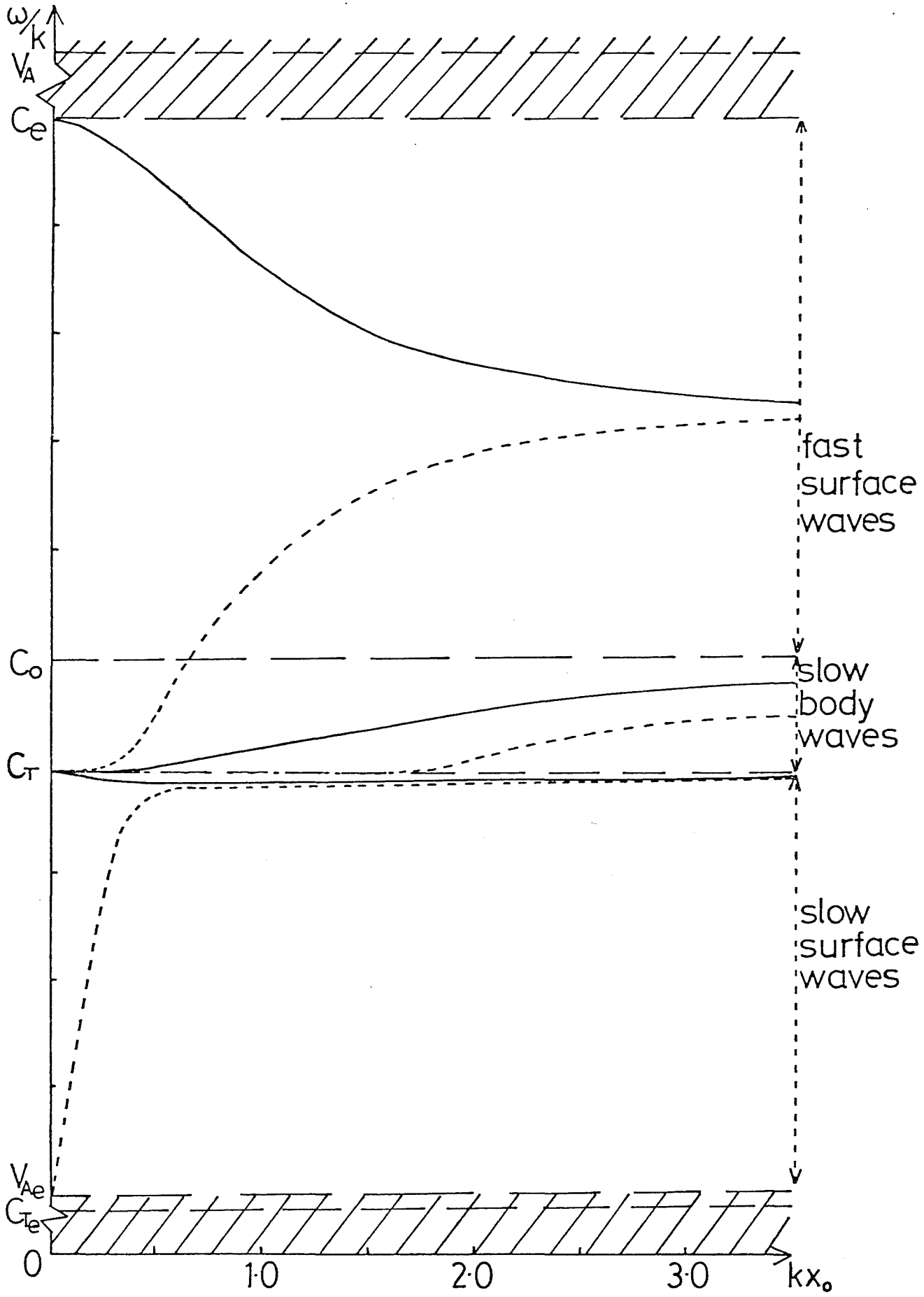

Figure 2.6 The phase-speed as a function of kx_0 ($k > 0$) for $v_A > c_e > c_0 > v_{Ae}$ (e.g. photospheric conditions). Here $v_A = 2.0c_0$, $c_e = 1.5c_0$ and $v_{Ae} = 0.5c_0$. Only two of the infinitely many slow body waves are shown. Hatching indicates regions where free modes (real ω and k) do not occur. ——: sausage mode; --- : kink mode.

$$\rho_e(k^2v_{Ae}^2 - \omega^2) + \rho_0(k^2v_A^2 - \omega^2)m_e x_0 = 0 \qquad (2.36)$$

which may be solved to give two sets of modes,

$$\omega^2 \simeq k^2c_{Te}^2 \left\{1 - \left(\frac{\rho_0}{\rho_e}\right)^2 \frac{(c_{Te}^2 - v_A^2)^2(c_e^2 - c_{Te}^2)(kx_0)^2}{v_{Ae}^4\, c_{Te}^2}\right\}, \quad c_{Te} > v_A, \qquad (2.37)$$

and

$$\omega^2 \simeq k^2v_{Ae}^2 \left\{1 - \left(\frac{\rho_0}{\rho_e}\right)^2 \left[1 - \frac{v_A^2}{v_{Ae}^2}\right]\left[1 - \frac{c_e^2}{v_{Ae}^2}\right](kx_0)^2\right\}, \qquad (2.38)$$

provided v_{Ae}/v_A is not $0(kx_0)$. If v_{Ae}/v_A is $0(kx_0)$, and thus $v_{Ae} \ll v_A$ for $|k|x_0 \ll 1$, then Equations (2.37) and (2.38) do not hold. Instead, solving (2.36) in this limit gives

$$\omega^2 \simeq k^2v_{Ae}^2 \{1 + \rho_0/\rho_e\, v_A^2/v_{Ae}^2\, (|k|x_0)\}, \quad v_{Ae} \to 0. \qquad (2.39)$$

This is the mode described by Roberts (1981b), for $v_{Ae} = 0$, as being the companion kink mode to (2.35c). Roberts notes, however, that for the case of the field-free environment there is no companion kink mode to that described by (2.35a). Here then is seen again the effect of magnetic field structuring. Provided the slab of inhomogeneity (e.g. magnetic field) is sufficiently narrow its behaviour in the kink mode is dictated by the size of the external magnetic field, the narrow (weaker) band of field lines being vibrated by the surrounding structure. If the combined effects of external gas and magnetic pressure

are sufficiently weak so that the slab is the dominant part of the structure and $c_{Te} < v_A$ then (2.37) is inapplicable and only one mode occurs given by (2.38) or (2.39). If the structuring is such that the magnetic field in the exterior is negligible then only the mode (2.39) is pertinent.

Chakraborty (1968) also derived expressions (2.34) to (2.38) but thereafter his analysis was one of stability and further wave structure resulting from (2.27) was not considered.

The behaviour given by expression (2.37) of the phase-speed ω/k is illustrated in Figures 2.7 and 2.8 and that of expression (2.39) in Figure 2.6. Expressions (2.37) and (2.38) are illustrated later (Figure 2.11) for the special case of a field-free slab.

2.5.2 The wide slab More indication of which waves are present in the structured plasma may be gained from consideration of the general dispersion relation (2.27) for a wide ($|k|x_0 >> 1$) slab. If it is supposed that $m_0 x_0 >> 1$ for $|k|x_0 >> 1$, an assumption which must be verified *a posteriori*, then $\tanh m_0 x_0 \to 1$ and for both kink and sausage modes Equation (2.27) reduces to

$$m_0\rho_e(k^2v_{Ae}^2 - \omega^2) + m_e\rho_0(k^2v_A^2 - \omega^2) = 0. \qquad (2.40)$$

Recalling the expressions for m_0 and m_e given by (2.22) and (2.26) respectively, it is seen that (2.40) is a cubic in ω^2 which may be solved for ω/k to determine which phase-speeds are present. (In fact this is how the behaviour of the surface waves at the right-hand sides of Figures 2.6, 2.7 and 2.8, for a wide slab, were predicted

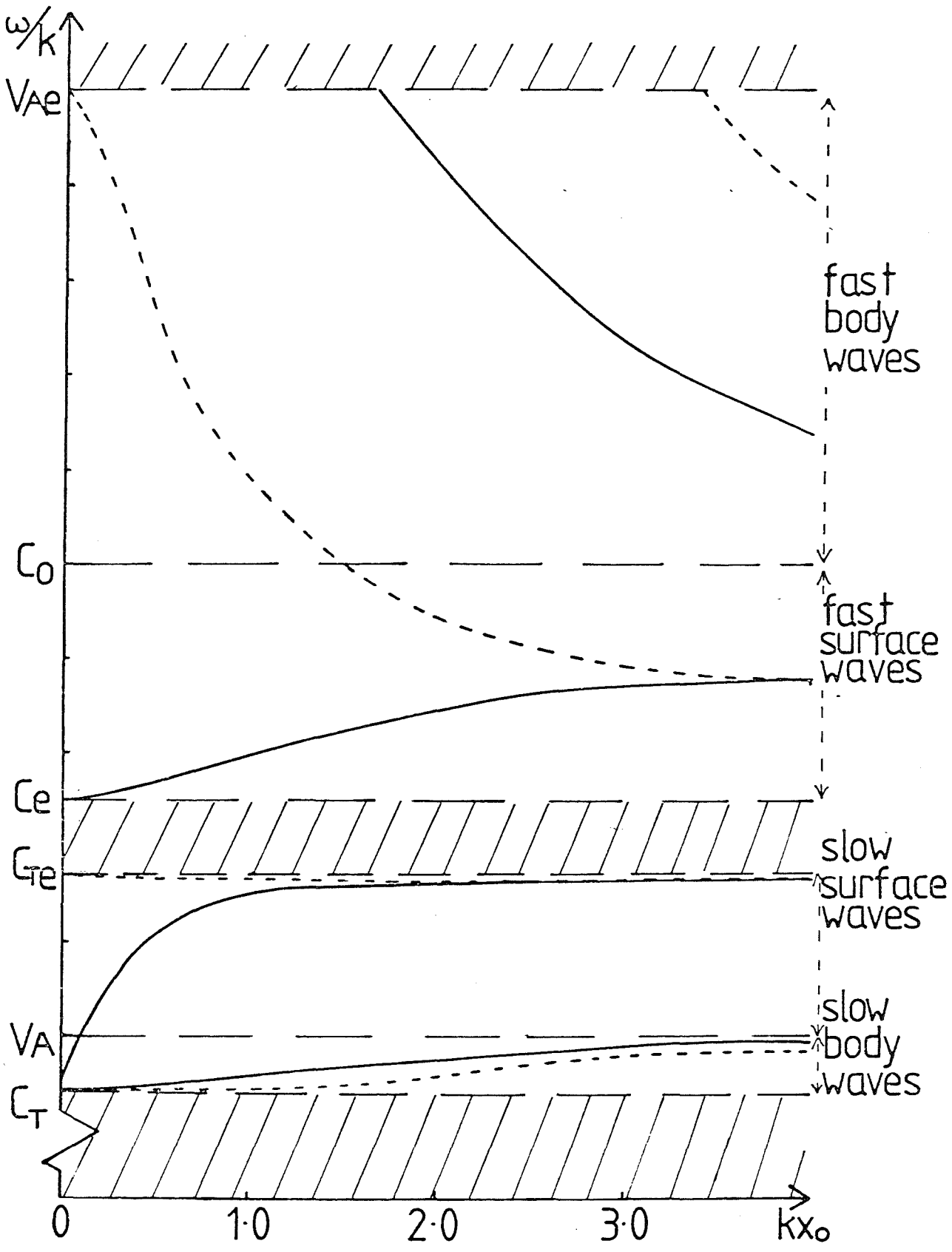

Figure 2.7 The phase-speed as a function of kx_0 ($k > 0$) for $v_{Ae} > c_0 > c_e > v_A$ (e.g. magnetospheric plasma sheet conditions). Here $v_{Ae} = 1.5c_0$, $c_e = 0.75c_0$ and $v_A = 0.5c_0$. Only two of the infinitely many slow body waves are shown. Hatching indicates regions from which free modes are excluded. ——: sausage mode; --- : kink mode.

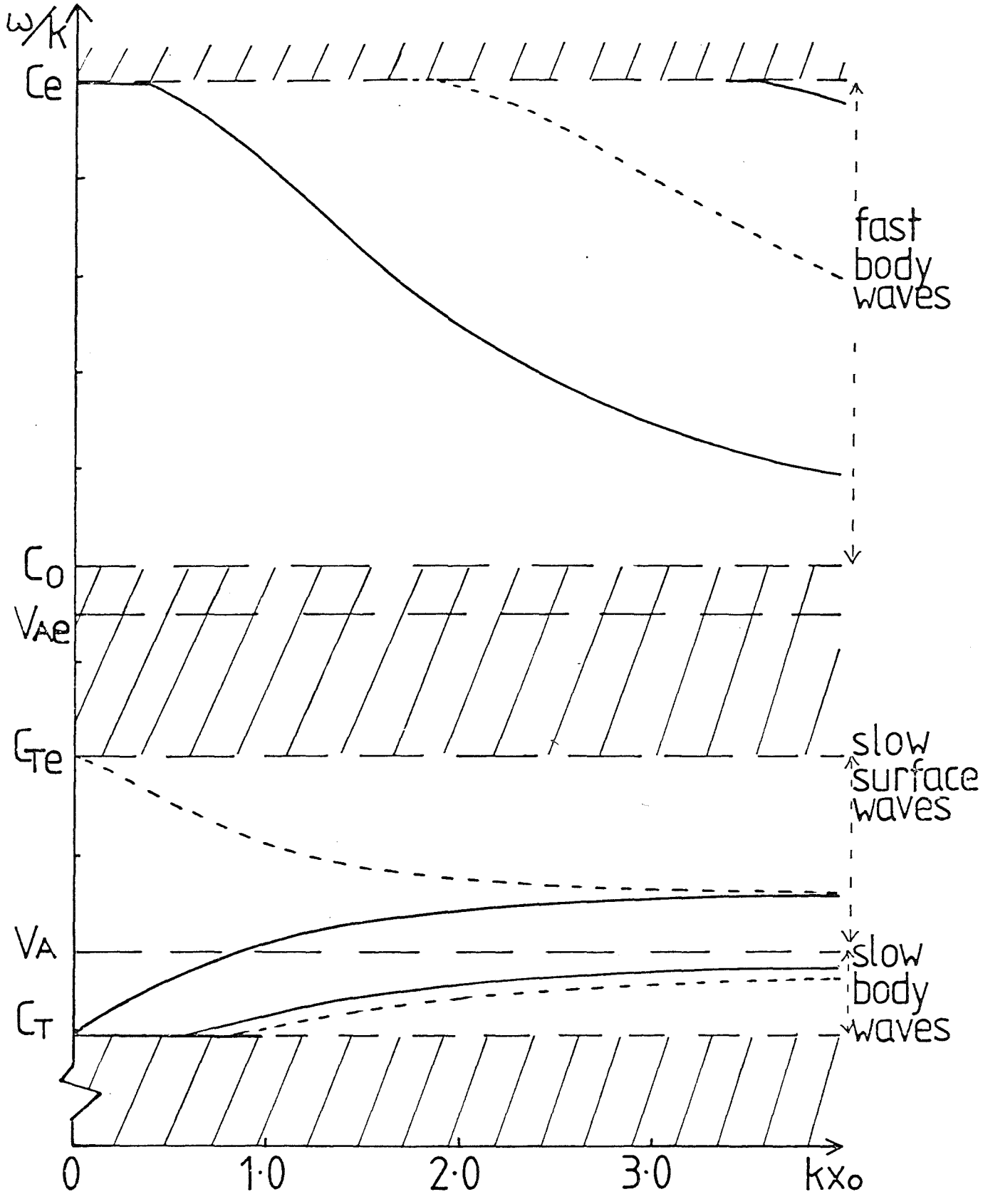

Figure 2.8 The phase-speed as a function of kx_0 ($k > 0$) for $v_{Ae} = 0.95c_0$, $c_e = 1.5c_0$ and $v_A = 0.6c_0$. Only two typical body waves ($m_0^2 < 0$) of the infinite number occurring in $c_T < \omega/k < v_A$ are shown. Hatching indicates regions where free modes do not occur. ——: sausage mode; ---: kink mode.

and a check for consistency made with the computer solutions for these figures.) The dispersion relation (2.40) which governs the behaviour of sausage and kink surface waves is precisely that encountered for surface waves at a single magnetic interface and has been considered by Wentzel (1979a) and Roberts (1981a). Thus propagation of surface waves in a structure having large lateral dimension ($|k|x_0 >> 1$) is essentially the same as that for a single interface. On the other hand, the results for a slender slab, Equations (2.35) to (2.39), are more complicated - it is the structuring which leads to this complication - and the behaviour does not have a direct parallel in the interface problem.

2.5.3 Body waves Now in considering Equation (2.27) it has been implicitly assumed that $m_0^2 > 0$ (though it is observed that Equation (2.36) is independent of m_0 and so the classification into surface or body waves is not obvious). To interpret what the classification $m_0^2 > 0$ (surface waves) and $m_0^2 < 0$ (body waves) means it is instructive to look at an unbounded, unstructured medium. For such a medium (2.15) holds and it is clear that for disturbances of the form (2.8) to be finite at $x = y = \pm\infty$, k_x^2 and ℓ^2 must be positive and so m_0^2 must be negative. From the definition of m_0^2, Equation (2.22), this means that, for $m_0^2 < 0$, ω^2 must lie either in the range

$$k^2c_T^2 < \omega^2 < \min(k^2c_0^2, k^2v_A^2) \tag{2.41}$$

or in

$$\omega^2 > \max(k^2c_0^2,\ k^2v_A^2). \qquad (2.42)$$

These inequalities, for an unbounded medium, define the two sets of waves given by (2.17) as the slow and fast magnetoacoustic waves. (There are also Alfvén waves resulting from (2.16), of course.) So if $m_0^2 < 0$, the modes which are here called body waves are just the manifestations of the usual magnetoacoustic waves of the unbounded medium. In general these body waves oscillate across the width of the inhomogeneity as may be seen from the solution (2.25) with $m_0^2 < 0$. The surface waves, on the other hand, arise from the structuring (Figure 2.3). In keeping with the classification for the unbounded medium (Cowling, 1976), wave modes lying in the range (2.41) will be referred to as the *slow* modes, those satisfying (2.42) will be called the *fast* modes. However, as will be apparent in what follows, the classification is not so straightforward in a structured medium.

Body waves ($m_0^2 < 0$) may be investigated by putting $n_0^2 \equiv -m_0^2$ in Equation (2.27) which then becomes

$$\rho_e(k^2v_{Ae}^2 - \omega^2)n_0 \left\{\begin{matrix}-\tan\\ \cot\end{matrix}\right\}(n_0x_0) + \rho_0(k^2v_A^2 - \omega^2)m_e = 0. \qquad (2.43)$$

Equation (2.43) is valid for $m_e > 0$ and $n_0 > 0$. A scrutiny of the general dispersion relation (2.27) in the special case $v_{Ae} = 0$ (see Roberts and Webb, 1979; Roberts, 1981b) revealed that there are solutions with m_0x_0 remaining bounded (but not necessarily tending to zero) as $|k|x_0 \to 0$, but that these only occur for $m_0^2 < 0$. Here, too, it was found that such modes exist, and that (2.43), rather than (2.27) is the most appropriate form of dispersion relation for these

particular modes. If $n_0 x_0 \neq 0$ as $|k|x_0 \to 0$ then it would appear that $n_0^2 \to \infty$ and this will occur if $\omega^2 \to k^2 c_T^2$ (see Equation (2.22)). This possibility was examined by assuming a solution of the form

$$\omega^2 \simeq k^2 c_T^2 \{1 + \nu(kx_0)^2\}, \quad \nu > 0, \tag{2.44}$$

in (2.43), where ν is to be determined; thus $\omega^2 \to k^2 c_T^2$ as $|k|x_0 \to 0$. Then, from (2.22), $n_0^2 \to \infty$ as $|k|x_0 \to 0$ but for meaningful solutions of (2.43), of the form (2.44), $n_0 x_0$ must remain finite and non-zero.

Considering the sausage mode solution of (2.43), for $n_0 \tan(n_0 x_0)$ to remain finite whilst $n_0^2 \to \infty$ it is necessary that $\tan(n_0 x_0) = 0$ so that

$$n_0 x_0 \to \pi q \text{ for positive integers } q.$$

Hence,

$$n_0^2 x_0^2 \simeq \frac{(c_0^2 - c_T^2)(v_A^2 - c_T^2)}{(c_0^2 + v_A^2) c_T^2 \nu} = \pi^2 q^2, \tag{2.45}$$

so that $\nu = \nu_q$ in (2.44) is determined, resulting in sausage (body) waves in a slender slab of the form

$$\omega_q^2 \simeq k^2 c_T^2 \left\{1 + \frac{(c_0^2 - c_T^2)(v_A^2 - c_T^2)(kx_0)^2}{(c_0^2 + v_A^2) c_T^2 \pi^2 q^2}\right\}, \quad q = 1,2,\ldots, \quad |k|x_0 \ll 1. \tag{2.46}$$

To this order (2.46) is independent of properties of the slab's environment so the waves oscillate back and forth within the slender inhomogeneity unaffected by its exterior. Similarly, consideration of (2.43) for the cot modes shows that the behaviour of kink (body)

waves in a slender slab is of the form

$$\omega^2 \simeq k^2 c_T^2 \left\{1 + \frac{(c_0^2 - c_T^2)(v_A^2 - c_T^2)(kx_0)^2}{(c_0^2 + v_A^2)\, c_T^2 \pi^2 (q - \tfrac{1}{2})^2}\right\}, \quad q = 1,2,\ldots, \ |k|x_0 << 1. \quad (2.47)$$

These waves therefore propagate slightly faster than their symmetric counterparts. These slow body waves (note $\omega/k > c_T$ in (2.46) and (2.47) and it is presumed initially that $\omega^2 < \min(k^2 c_0^2, k^2 v_A^2)$ so (2.41) is satisfied) are illustrated in Figures 2.6 to 2.10.

The analysis of (2.43) for a wide slab is not so straightforward but it is possible to gain some idea of the behaviour of these slow body waves as $|k|x_0 \to \infty$. Assuming that $n_0 x_0 \neq 0$ but to some finite value as $|k|x_0 \to \infty$ then it would appear that $n_0^2 \to 0$ and this will occur if $\omega^2 \to k^2 v_A^2$ or $\omega^2 \to k^2 c_0^2$ (see Equation (2.22)). For simplicity the analysis will be carried out assuming that $v_A = c_0$ since the essential features of the general case, $v_A > c_0$, $v_A = c_0$, $v_A < c_0$, are not lost by doing this. A fuller description for the case $v_{Ae} = 0$ is given in Roberts (1981b).

A solution of (2.43) of the form

$$\omega^2 \simeq k^2 c_0^2 \left(1 - \frac{A}{|k|x_0}\right) \quad (2.48)$$

is assumed, where A is to be determined, and a minus sign is used to ensure that (2.41) is satisfied, for slow body waves, in the limit $\omega^2 \to k^2 c_0^2$ $(= k^2 v_A^2)$ as $|k|x_0 \to \infty$. Then substitution of (2.48) into (2.43) shows for $n_0 x_0$ to remain finite, equal to ψ, say, that

$$A = \psi$$

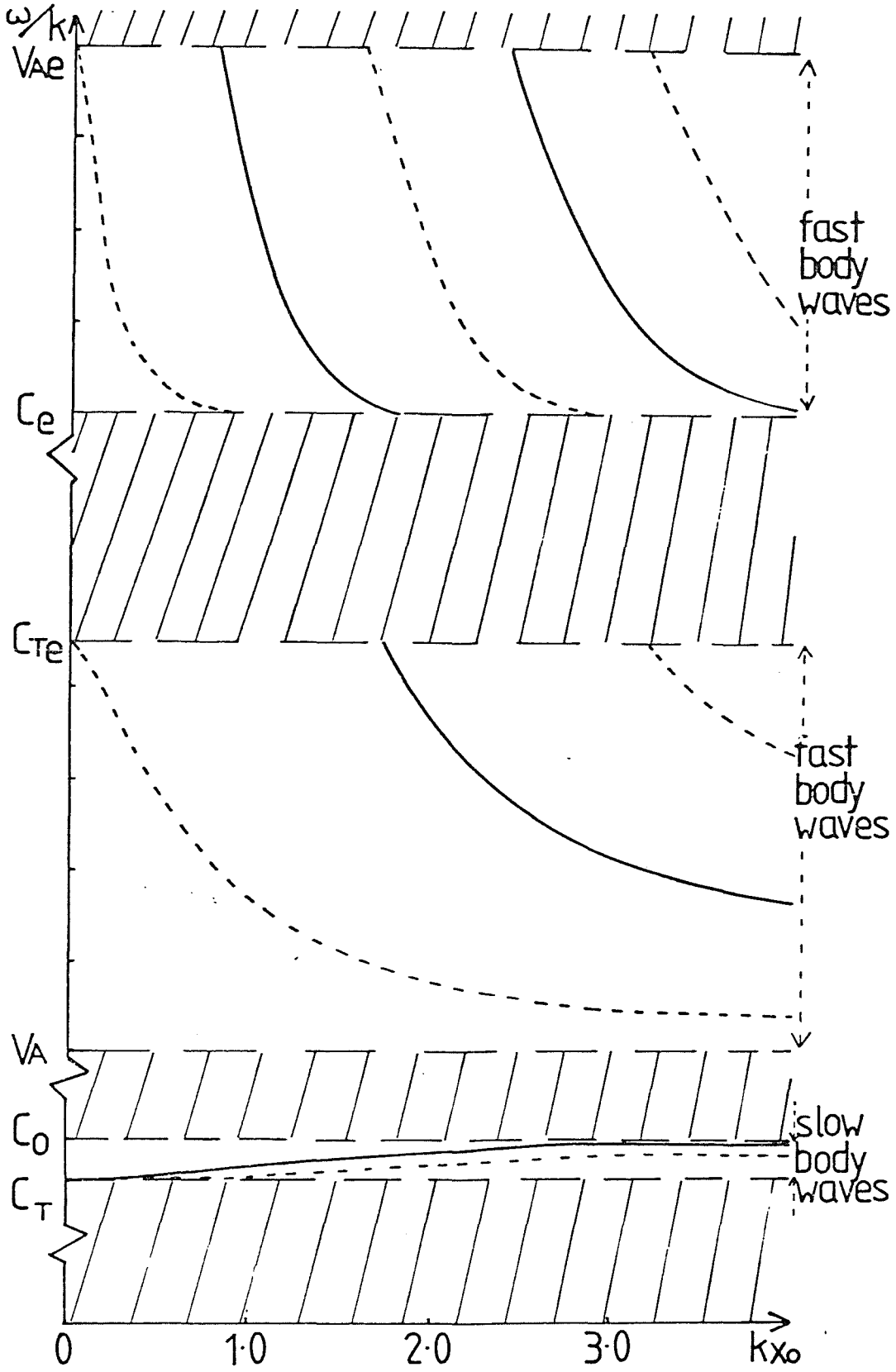

Figure 2.9 The phase-speed as a function of kx_0 ($k > 0$) showing three bands of body ($m_0^2 > 0$) waves. Here $v_{Ae} = 5.0c_0$, $c_e = 4.0c_0$ and $v_A = 2.0c_0$. Only two of the infinitely many slow waves are shown. Hatching indicates regions where free modes do not occur. ——: sausage mode; ---: kink mode.

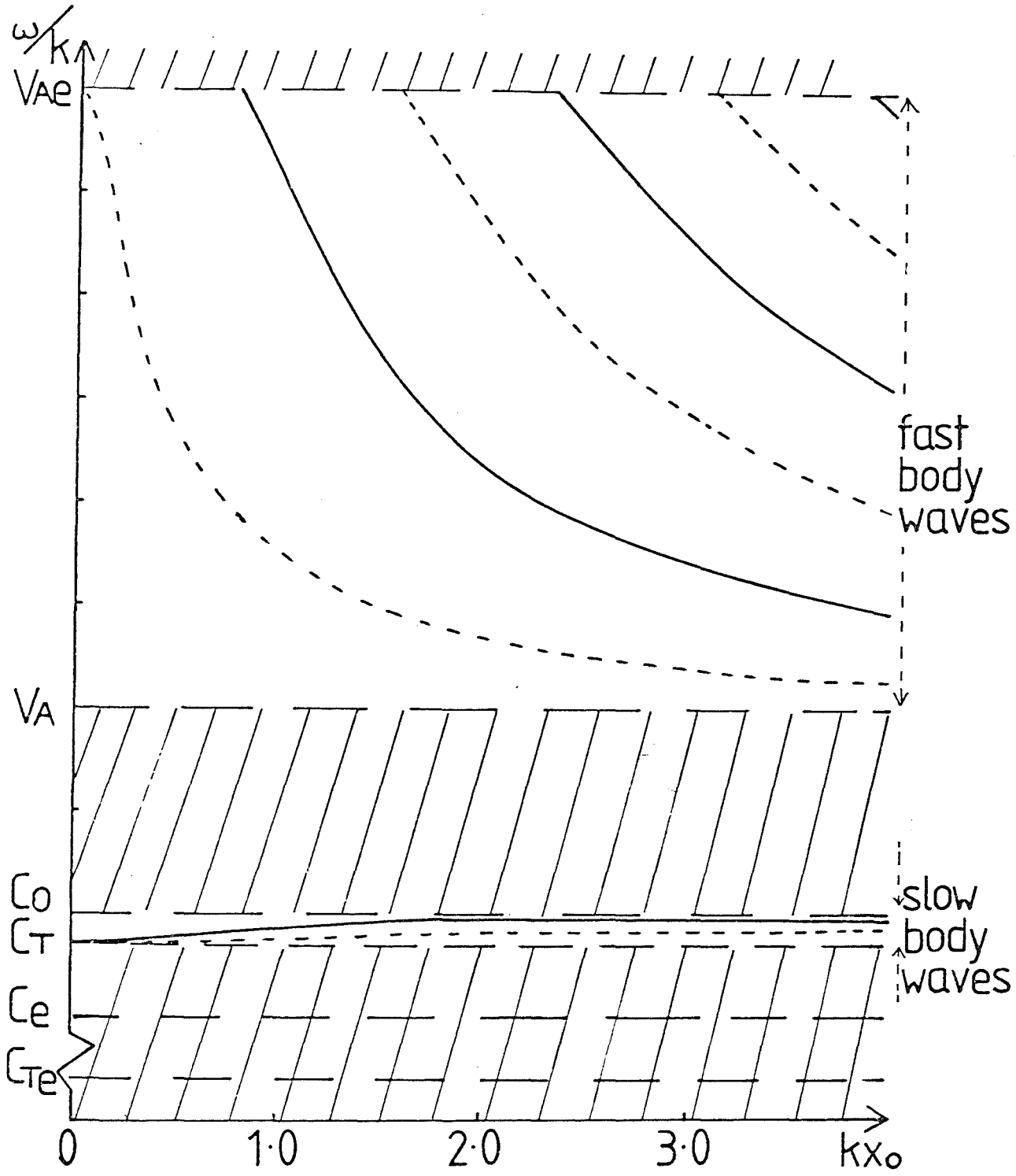

Figure 2.10 The phase-speed as a function of kx_0 ($k > 0$) under conditions representative of the corona. Here $v_{Ae} = 5c_0$, $c_e = 0.5c_0$ and $v_A = 2c_0$. Only two sets of body ($m_0^2 < 0$) waves exist; the slow band contains infinitely many harmonics of which only two are shown. Hatching denotes regions in which there are no free modes. ——: sausage mode; ---: kink mode.

and $\tan\psi$ must take certain values, some of which are given below. It would be tedious to list all the possible cases, so only those relevant to Figures 2.6, 2.9 & 2.10 are presented. Thus for slow, symmetric, body waves with $v_A = c_0$ and $|k|x_0 >> 1$ the harmonics ω_q are given by

$$\omega^2 \simeq k^2 c_0^2 \, (1 - \psi_q/|k|x_0), \quad q = 1,2,..., \tag{2.49}$$

where ψ_q are the positive roots of

$$\left.\begin{aligned}
\tan\psi &= \frac{\rho_0 c_0^2 (c_0^2 - c_e^2)^{\frac{1}{2}}}{\rho_e (v_{Ae}^2 + c_e^2)^{\frac{1}{2}} (c_0^2 - c_{Te}^2)^{\frac{1}{2}} (v_{Ae}^2 - c_0^2)^{\frac{1}{2}}} \quad , \quad c_{Te} < c_e < c_T < \frac{\omega}{k} < c_0 < v_{Ae} \\
&\qquad\qquad \text{(Figure 2.10)}, \\
\tan\psi &= \frac{\rho_0 c_0^2 (c_e^2 - c_0^2)^{\frac{1}{2}}}{\rho_e (v_{Ae}^2 + c_e^2)^{\frac{1}{2}} (c_{Te}^2 - c_0^2)^{\frac{1}{2}} (v_{Ae}^2 - c_0^2)^{\frac{1}{2}}} \quad , \quad c_{Te} > c_0 \\
&\qquad\qquad \text{(Figure 2.9)}, \\
\text{or} \quad \tan\psi &= \frac{-\rho_0 c_0^2 (c_e^2 - c_0^2)^{\frac{1}{2}}}{\rho_e (v_{Ae}^2 + c_e^2)^{\frac{1}{2}} (c_0^2 - c_{Te}^2)^{\frac{1}{2}} (c_0^2 - v_{Ae}^2)^{\frac{1}{2}}} \quad , \quad c_{Te} < v_{Ae} < c_T < \frac{\omega}{k} < c_0 < c_e \\
&\qquad\qquad \text{(Figure 2.6)}.
\end{aligned}\right\} \tag{2.50}$$

The equivalent result for $v_{Ae} = 0$ of Roberts (1981b) is a special case of the last expression in (2.50). An investigation shows that a set of slow kink modes arises in a similar manner. The slow sausage and kink body waves having behaviour described by (2.46), (2.47) and (2.50) (in general $v_A \neq c_0$) are shown in Figures 2.6 to 2.10. Only two waves are shown because there is obviously an infinite set of such waves.

It would seem strange, given the argument that body waves ($m_0^2 < 0$) in a structured medium are the manifestation of the magnetoacoustic

waves in an unbounded medium, if only a set of slow waves such as described above, and no fast body waves, were to be found. Fast harmonics do arise, though a full analytical description is difficult. Roberts (1981b), interested in structuring due to a magnetic field alone, was nevertheless able to demonstrate the existence of fast body waves by considering an infinite field-free region structured instead by a slab of temperature (density) inhomogeneity, so that (2.43) with $v_A = v_{Ae} = 0$ became

$$m_e = \left(\frac{\rho_e}{\rho_0}\right) n_0 \left\{ \begin{matrix} \tan \\ -\cot \end{matrix} \right\} n_0 x_0 \qquad (2.51)$$

where now $n_0^2 = (\omega^2 - k^2 c_0^2)/c_0^2 > 0$. This he investigated graphically to show that waves existed for

$$(0 =) v_A < c_0 < \omega/k < c_e;$$

they were fast body waves, according to (2.42). Diagrams in Roberts (1981b), however, illustrated these fast body waves as emanating from c_e, that is the phase-speeds of these modes, for slender slabs, were essentially equal to c_e but decreased with increasing slab width. The discussion which follows later shows that this is not quite the true picture and indeed it was the 'discovery' of the true nature of these waves which led to much of the work to be described in Chapters 4 and 7.

2.5.4 The field-free slab It must be remembered that the present aim is to examine all possible waves resulting from the general dispersion relation (2.27) subject to their being evanescent away from the region of the inhomogeneity (i.e. subject to $m_e > 0$). Accordingly, using the analysis developed so far as a guide, the computer solutions of (2.27) were sought, at first for the particular case of a field-free region inside the slab. Though this special case is of limited relevance for photospheric applications (except perhaps for field-free regions below umbral dots - see Chapter 7) it is appropriate for the hot plasma sheet of the magnetospheric tail or the neutral sheet above a 'post-flare' loop system. Also the investigation gave insight into the case where the slab inhomogeneity had, not zero, but small Alfvén speed. This was particularly helpful towards consideration of the high density coronal loops of Chapter 4.

Of course taking B_0 equal to zero means that the categorization according to (2.41) and (2.42) is somewhat redundant and instead the relative magnitudes of the sound and Alfvén speeds in the exterior of the slab must feature in a classification of the possible modes. Inequalities (2.29) still hold and the modes are surface or body waves according as $\omega/k < c_0$ or $\omega/k > c_0$ respectively.

	Configuration	Surface Waves: sausage Eqn. (2.52) / kink Eqn. (2.37)	Surface Waves: sausage Eqn. (2.35a) / kink Eqn. (2.38)	Body Waves	
$v_{Ae} > c_e$	$c_0 < c_{Te} < c_e < v_{Ae}$	S (K)		$c_0 < \omega/k < c_{Te}$ ✓	$c_e < \omega/k < v_{Ae}$ ✓
	$c_{Te} < c_0 < c_e < v_{Ae}$	S K			$c_e < \omega/k < v_{Ae}$ ✓
	$c_{Te} < c_e < c_0 < v_{Ae}$	S K	S (K)		$c_0 < \omega/k < v_{Ae}$ ✓
	$c_{Te} < c_e < v_{Ae} < c_0$	S K	S K		
$c_e > v_{Ae}$	$c_0 < c_{Te} < v_{Ae} < c_e$	S (K)		$c_0 < \omega/k < c_{Te}$ ✓	$v_{Ae} < \omega/k < c_e$ ✓
	$c_{Te} < c_0 < v_{Ae} < c_e$	S K			$v_{Ae} < \omega/k < c_e$ ✓
	$c_{Te} < v_{Ae} < c_0 < c_e$	S K			$c_0 < \omega/k < c_e$ ✓
	$c_{Te} < v_{Ae} < c_e < c_0$	S K			

Table 2.1 The possible wave modes in a field-free slab. Circles indicate that these are body waves in a slender tube but surface waves in a wider structure - see Equation (2.62) and comments thereabouts.

S : sausage; K : kink; ✓ : body waves occur in region indicated.

The results for $B_0 = 0$ are summarized in Table 2.1. Note that for $v_A = 0$ Equation (2.35b) becomes

$$\omega^2 \simeq k^2 \left(\frac{\rho e}{\rho_0}\right) v_{Ae}^2 (|k|x_0). \tag{2.52}$$

If c_e is also zero then (2.52) describes the only sausage waves in a slender tube and the only kink mode is (2.37) with $c_{Te} = v_{Ae}$.

The surface waves are most easily explained by their slender tube behaviour, $\omega/k \to 0$ for the sausage mode and $\omega/k \sim c_{Te}$ for the kink. For surface waves the only asymmetry in the table appears in the form of two additional sets of waves for entries 3 and 4, sausage waves ($\omega/k \sim c_e$) and kink waves ($\omega/k \sim v_{Ae}$). This arises because of the constraint $m_e > 0$. Otherwise, m_e and m_0 are symmetric in v_{Ae}, c_e and v_A, c_0 respectively. So the surface waves can readily be explained by the foregoing analysis and, as anticipated, where there is a weak, slender inhomogeneity it is the effect of the surrounding medium which dictates the wave behaviour in the structure. The implication of this will be discussed further in Chapter 6. An example of the two sets of surface waves occurring in this field-free configuration (entry 4 of Table 2.1) is shown in Figure 2.11.

2.5.5 Fast body waves There remains the outstanding problem referred to above of describing the 'fast' body waves ($m_0^2 < 0$). This is further complicated by there sometimes being two sets of these 'faster' waves ($\omega/k > c_0$ for $v_A = 0$) as items 1 and 5 of Table 2.1 and Figure 2.9 show. More generally some description of all the fast body waves in Figures 2.7 to 2.10 is needed and this is best done by

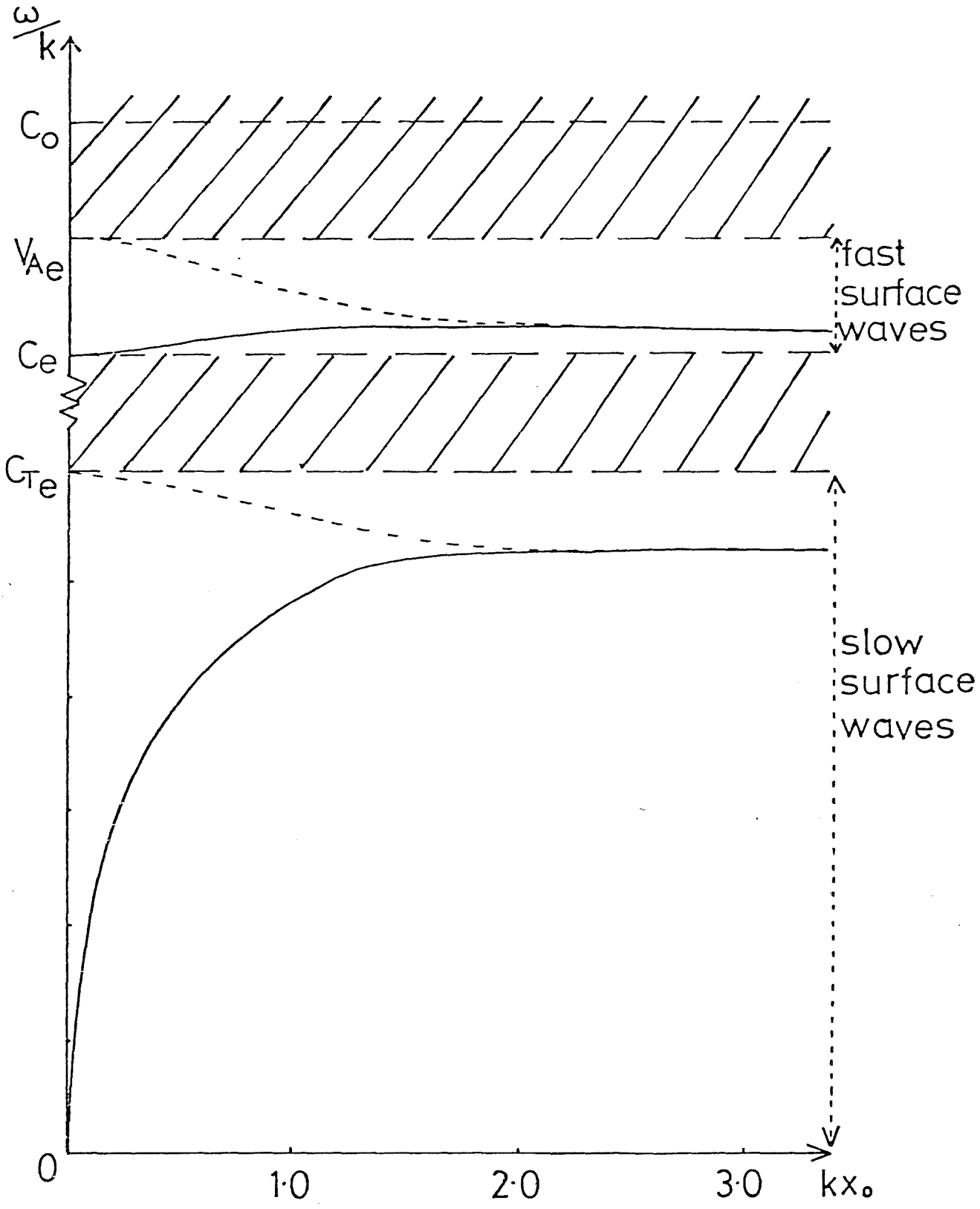

Figure 2.11 The phase-speed as a function of kx_0 ($k > 0$) showing two sets of surface ($m_0^2 > 0$) waves for a field-free slab. Here $v_{Ae} = 0.9c_0$ and $c_e = 0.8c_0$. Hatching indicates regions where free modes (real ω and k) do not occur. ——: sausage mode; --- : kink mode.

looking at Equation (2.43) in special cases.

(i) The cold plasma approximation $c_e = c_0 = 0$. Here the structuring is due either to the magnetic field, a strongly magnetic region surrounding a weak inhomogeneity, or the density, possibly for example a coronal loop, where a region of relatively uniform magnetic field is structured by a slab of higher density. In this case, setting $c_e = c_0$ would eliminate for example, the narrow band of body waves in Figure 2.10. Equation (2.43) describes the remaining fast body waves. With $c_e = c_0 = 0$, Equations (2.22) and (2.26), respectively, become $-m_0^2 = n_0^2 = \left(\frac{\omega}{v_A}\right)^2 - k^2$ and $m_e^2 = k^2 - \left(\frac{\omega}{v_{Ae}}\right)^2$, and Equation (2.43) reduces to

$$\rho_e \frac{(k^2 v_{Ae}^2 - \omega^2)^{\frac{1}{2}}}{v_A} \left\{ \begin{matrix} -\tan \\ \cot \end{matrix} \right\} (n_0 x_0) - \rho_0 \frac{(\omega^2 - k^2 v_A^2)^{\frac{1}{2}}}{v_{Ae}} = 0, \qquad (2.53)$$

with

$$\frac{\rho_e}{\rho_0} = \frac{v_A^2}{v_{Ae}^2}, \qquad (2.54)$$

from Equation (2.20).

Equation (2.53) may be rewritten as

$$\tan(n_0 x_0) = -\frac{n_0}{m_e} \qquad (2.55)$$

for the fast sausage modes, and as

$$\tan(n_0 x_0) = \frac{m_e}{n_0} \qquad (2.56)$$

for the kink modes. Equation (2.56) is Love's equation (Love, 1911; see also Ewing *et al.*, 1957; Kennet, 1983) which was studied early this century by Love in his investigation of waves in another structured medium, the elastic layers of the Earth's crust. Equation (2.55) also arises in seismological and oceanographic studies and has been considered at length by Pekeris (1948). The behaviour of the fast body waves with their sharp cut-offs (e.g., at $\omega/k = v_{Ae}$ in Figure 2.10) was confirmed in diagrams given by Pekeris (1948), Ewing *et al.* (1957), Tolstoy (1973), and others. These authors' investigations and results suggested an important new aspect to the problem in the solar physics context: this is described fully in Chapters 4 and 7.

McKenzie (1970) was aware of these fast body waves in his analysis of the magnetospheric plasma sheet, though he did not categorize them as such, or identify them as Love and Pekeris waves. Instead he referred to them as 'bouncing waves'. Also his diagram showed the spurious root behaviour present also in some diagrams given in Edwin and Roberts (1982); these diagrams were subsequently corrected in Edwin and Roberts (1983).

(ii) No magnetic structuring, $v_A = v_{Ae} = 0$. This case (for example Figure 2.8 with the lower half ignored, or item 7 of Table 2.1), in which (2.43) reduces to (2.51) has already been mentioned. If Equation (2.20) is used to substitute for the density ratio ρ_e/ρ_0 (presumed $\neq 1$ so that there is some density or temperature structuring of the medium) Equation (2.51) reduces to

$$\tan(n_0 x_0) = \left(\frac{c_e^2}{c_0^2}\right) \frac{m_e}{n_0} \qquad (2.57)$$

for the sausage modes, and

$$\tan(n_0 x_0) = -\left(\frac{c_0^2}{c_e^2}\right)\frac{n_0}{m_e} \tag{2.58}$$

for the kink modes. Here $n_0^2 = \left(\frac{\omega}{c_0}\right)^2 - k^2$ and $m_e^2 = k^2 - \left(\frac{\omega}{c_e}\right)^2$ and both are positive because $c_0 < \omega/k < c_e$. Equations (2.57) and (2.58) are again seen to be the Love and Pekeris equations.

(iii) The cold slab $c_0 = 0$. In a similar manner one of the set of fast body waves in Figure 2.9 may be better understood by putting $v_{Ae} = c_e$ and eliminating the faster band. Again Equation (2.43) gives Love and Pekeris equations in the form

$$\left\{\begin{matrix}-\tan \\ \cot\end{matrix}\right\}(n_0 x_0) = \frac{n_0}{q_e}\left(\frac{2+\gamma}{\gamma}\right), \tag{2.59}$$

where $q_e = (k^2 - 2\omega^2/c_e^2)^{\frac{1}{2}}$, for modes satisfying $v_A < \omega/k < c_{Te}$.

It is slightly more complicated to demonstrate the nature of the second band of waves with phase-speeds $c_e < \omega/k < v_{Ae}$, since putting $c_{Te} = v_A = 0$ to eliminate the waves given by (2.59) would imply $c_e = 0$ and the analogy is lost. However it is clear from the above examples that in the general case $v_A < c_{Te} < c_e < v_{Ae}$ these body waves will satisfy a modified Love/Pekeris equation, as indeed the form of curves in Figure 2.9 shows.

(iv) Cut-offs. The sharp cut-offs possessed by fast body waves (made particularly evident in the above special cases) mean that only certain frequencies may propagate. This fact is important in

formulating a theory of coronal oscillations (Chapter 4). The cut-offs may easily be calculated, and this serves as a check on the computer solutions for the figures. For sausage waves the general dispersion relation (2.43) may be written

$$\tan(n_0 x_0) = - \frac{\rho_0(\omega^2 - k^2 v_A^2) m_e}{\rho_e (k^2 v_{Ae}^2 - \omega^2) n_0} . \qquad (2.60)$$

At cut-off, in Figure 2.10, $\omega/k \to v_{Ae}$ so $\tan(n_0 x_0) \to \infty$ and $n_0 x_0 \to \frac{(2n-1)\pi}{2}$, $n = 1,2,\ldots$. Also, from (2.22), $n_0 \to \frac{(v_{Ae}^2 - c_0^2)^{\frac{1}{2}}(v_{Ae}^2 - v_A^2)^{\frac{1}{2}} k}{(v_{Ae}^2 - c_T^2)^{\frac{1}{2}}(c_0^2 + v_A^2)^{\frac{1}{2}}}$, so the cut-offs are given by

$$k x_0 \simeq \frac{(2n-1)\pi}{2} \frac{(v_{Ae}^2 - c_T^2)^{\frac{1}{2}}(c_0^2 + v_A^2)^{\frac{1}{2}}}{(v_{Ae}^2 - c_0^2)^{\frac{1}{2}}(v_{Ae}^2 - v_A^2)^{\frac{1}{2}}} . \qquad (2.61)$$

With the values of v_{Ae}, v_A and c_e appropriate for Figure 2.10 (namely, $5c_0$, $2c_0$ and $0.5c_0$) substituted in (2.61), the cut-offs are found to occur at

$$k x_0 \simeq 0.77, 2.31, 3.85, \ldots .$$

Similarly, the cut-offs for the kink modes are given by

$$k x_0 \simeq n\pi \frac{(v_{Ae}^2 - c_T^2)^{\frac{1}{2}}(c_0^2 + v_A^2)^{\frac{1}{2}}}{(v_{Ae}^2 - c_0^2)^{\frac{1}{2}}(v_{Ae}^2 - v_A^2)^{\frac{1}{2}}}, \quad n = 0,1,2,\ldots .$$

For the data of Figure 2.10 (namely, $v_{Ae} = 5c_0$, $v_A = 2c_0$ and $c_e = 0.5c_0$), the kink cut-offs are

$$k x_0 = 0, 1.53, 3.08, \ldots .$$

2.6 Detailed Nature of the Modes

One small problem remains. In Figure 2.6 the fast kink mode appears to change in character from a body to a surface wave as the phase-speed passes through the slab's sound speed. This behaviour is apparent also in Figure 2.8 (the slow sausage mode passing through $\omega/k = v_A$) and Figure 2.7 (the fast kink mode). Consider the latter figure. The transition appears to take place for a value of $|k|x_0 \simeq 1.5$. When the form of the transverse velocity component $\hat{v}_x$ (for the fast kink wave of Figure 2.7) was plotted against the slab's transverse coordinate (Figure 2.12) its profile was found to be approximately uniform across the slab for both body and surface waves in the transition region, $\omega/k \simeq c_0$. Of course, for $\omega/k = c_0$ (see the remark in the paragraph following Equation (2.29)) the problem has only the trivial eigenvector solution. So the sinusoidal behaviour of the body wave for $\omega/k \lesssim c_0$ is weak (Figure 2.12) and it bears a resemblance to the surface wave ($\omega/k \gtrsim c_0$) into which it 'evolves'. Of course the slender slab approximation does not predict this fast kink surface wave, which has a phase-speed equal to the sound speed at an *intermediate* value of $|k|x_0$. In fact this fast kink surface mode, arising from a body wave, does not appear in Figure 1b of Roberts (1981b) (which describes a similar case to that of Figure 2.6 but for $v_{Ae} = 0$) and was in fact overlooked. To illustrate that this transition occurs at an intermediate value of kx_0, consider Roberts' case of zero external field. Then putting

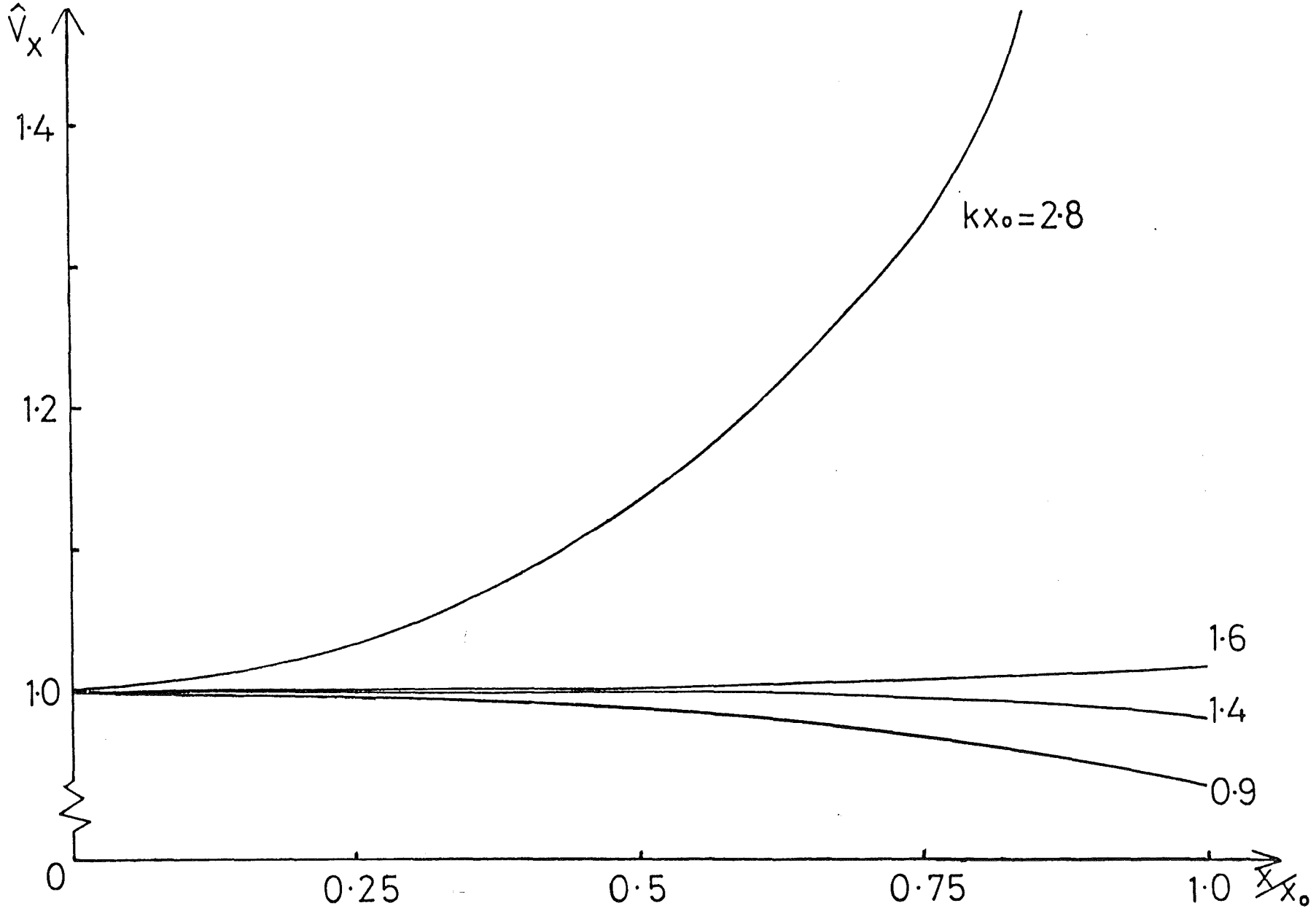

Figure 2.12 The form of the velocity component $\hat{v}_x$ for the fast kink wave of Figure 2.7 in a finite slab. The results illustrate the almost uniform profiles for both body ($m_0^2 < 0$) and surface ($m_0^2 > 0$) waves in the vicinity of $kx_0 = 1.5$.

$v_{Ae} = 0$ in dispersion equation (2.27) and knowing that the transition takes place when

$$\frac{\omega^2}{k^2} \simeq c_0^2 + \varepsilon, \quad \text{where} \quad \frac{\varepsilon}{c_0^2} << 1,$$

substitution of this approximation into (2.27) shows that ε satisfies

$$A_1(1 - \varepsilon/\alpha_1)(1 - \varepsilon/\beta_1) = (c_0^2 + \varepsilon)\varepsilon^{\frac{1}{2}}(1 - \varepsilon/\gamma_1)\coth u_1,$$

where

$$u_1 = B_1(|k|x_0)\varepsilon^{\frac{1}{2}}(1 - \varepsilon/\alpha_1)(1 - \varepsilon/\gamma_1),$$

$$A_1 = (v_A^2 - c_0^2)^{\frac{1}{2}}(c_0^2 + v_A^2)^{\frac{1}{2}}(c_0^2 - c_T^2)^{\frac{1}{2}}(c_e^2 - c_0^2)^{\frac{1}{2}}\rho_0/\rho_e c_e,$$

$$B_1 = (v_A^2 - c_0^2)^{\frac{1}{2}}/\{(c_0^2 + v_A^2)^{\frac{1}{2}}(c_0^2 - c_T^2)^{\frac{1}{2}}\}, \quad \alpha_1 = 2(v_A^2 - c_0^2),$$

$$\beta_1 = 2(c_e^2 - c_0^2) \quad \text{and} \quad \gamma_1 = 2(c_0^2 - c_T^2).$$

To order $\varepsilon^{\frac{1}{2}}$, it may then be shown that at a slab width of

$$kx_0 \simeq \frac{(c_0^2 + \gamma v_A^2/2)c_0^2}{(v_A^2 - c_0^2)(c_e^2 - c_0^2)^{\frac{1}{2}}c_e} \tag{2.62}$$

the change from body to surface waves occurs. For the parameter values of Figure 2.6 ($v_{Ae} \neq 0$) this is at $kx_0 = 0.86$. Similar arguments apply, for example, to Figures 2.7 and 2.8 or indeed wherever there is a change in character between surface and body mode.

Inevitably, most of this chapter has been concerned with the solutions of the dispersion relation (2.27). Solutions of the form (2.8) were assumed for the velocity and pressure fields. It is thus

possible to show what form the transverse and longitudinal velocity amplitudes would take if the modes of the foregoing discussion were present in a structure. The transverse velocity amplitude is given by (2.25) (with the appropriate change from hyperbolic to trigonometric functions if $m_0^2 = -n_0^2 < 0$) and Equation (2.24) gives the longitudinal velocity amplitude.

Considering Figure 2.7, there is a fast kink body wave which has a phase-speed $\omega/k \simeq v_{Ae}$ for a slender slab. Examination of the cosine and sine terms for this situation shows, as expected, that the cosine term dominates and so $\hat{v}_z$ is negligibly small. So for this mode in a slender slab the motion is principally transverse, in the x-direction. Also, again for a slender slab, there is a fast surface wave which has a phase-speed close to c_e. This time $\hat{v}_x$ is small for this sausage mode (~ sinh) but $\hat{v}_z$ is large. So for this mode the motion is principally longitudinal. Similarly the slow sausage mode, with phase speed ~ c_T, and the slow kink mode of Figure 2.7 are principally longitudinal ($\hat{v}_x$ small) and transverse ($\hat{v}_x$ large), respectively. This confirms the descriptions 'sausage' and 'kink' assigned to the motions initially.

Finally the forms of the velocity components $\hat{v}_x$ and $\hat{v}_z$ for the slow surface wave (sausage mode) in a finite field-free slab (Figure 2.11) are sketched in Figure 2.13. The results are illustrated for $c_0 = c_e = v_{Ae}$ and show that for a slender slab ($|k|x_0 << 1$), $|\hat{v}_x| << |\hat{v}_z|$. Equations (2.23) and (2.24) show that the variation in $\hat{v}_z$ also gives an indication of the total (gas plus magnetic) pressure variation across the slab. From Figure 2.13 (see also

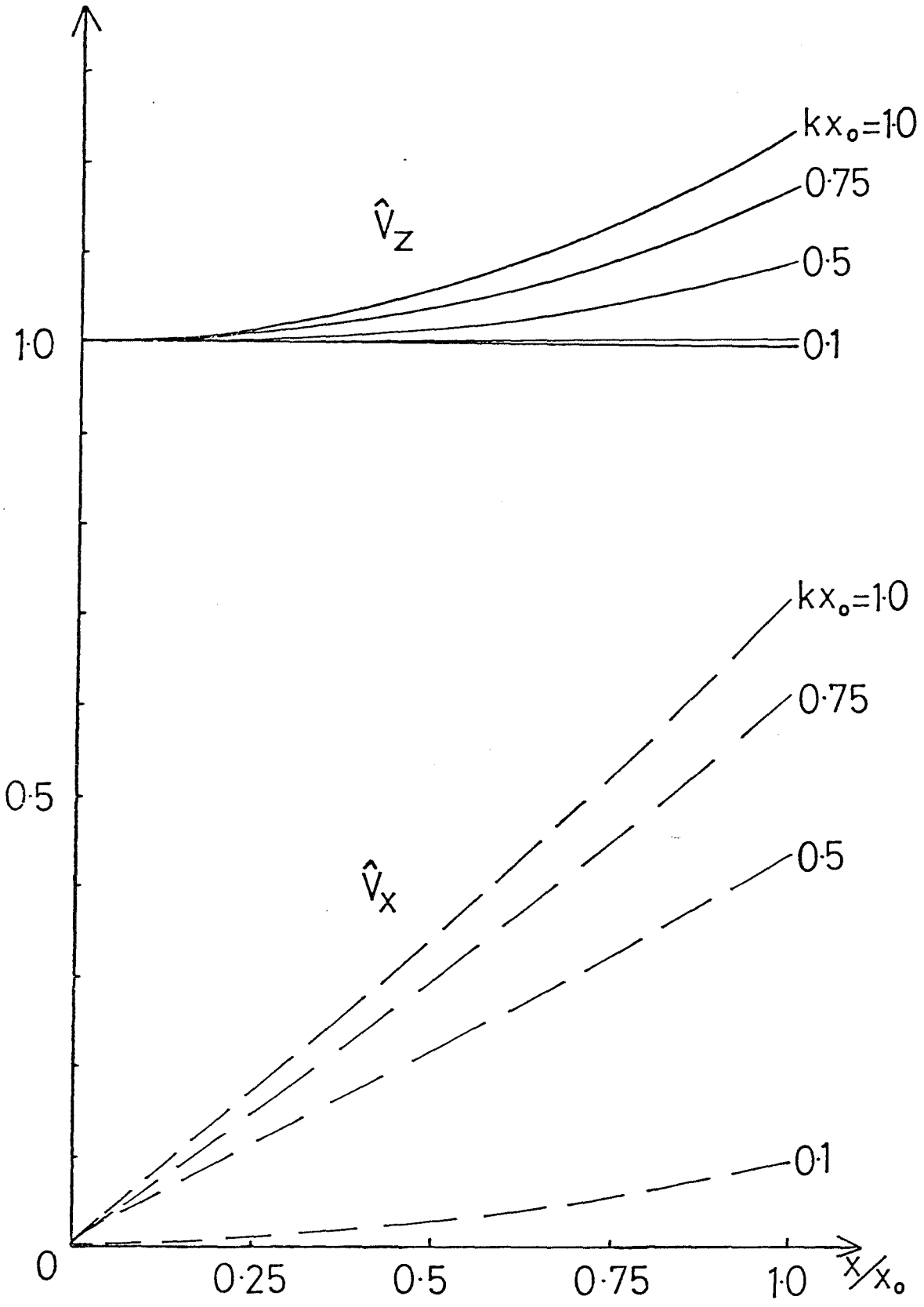

Figure 2.13 The form of the velocity components $\hat{v}_x$(--) and $\hat{v}_z$(—) for the slow surface wave (sausage mode) in a finite field-free slab. The results (illustrated for $c_0 = v_{Ae} = c_e$) show that for a slender slab ($|k|x_0 << 1$) $|\hat{v}_x| << |\hat{v}_z|$ and $\hat{v}_z(x)$ is approximately uniform across the slab.

Figure 2 of Roberts (1981b)) it is seen that for a slender tube, $kx_0 = 0.1$, say, $\hat{v}_z$ is approximately uniform across the slab. This result will be exploited later in Chapters 5 and 6.

2.7 Summary

Of course to illustrate the modal behaviour of a structured medium for all the various combinations of the set of parameters $\{c_T, c_0, v_A, c_{Te}, c_e, v_{Ae}\}$ in Equation (2.27), which describes the slab inhomogeneity subject to evanescent exterior modes, would result in many diagrams and tables. In an attempt to provide examples pertinent to both solar and magnetospheric physics to be discussed in later chapters, a few particular cases have been shown in Figures 2.6 to 2.11, but to describe the overall pattern a general summary is given in Table 2.2 ($v_A \neq 0$). This must be read in conjunction with Table 2.1 ($v_A = 0$), since, as was pointed out in the discussion of the $B_0 = 0$ case, the classification 'slow' (waves satisfying (2.41)) becomes meaningless in the case where the slab inhomogeneity is environment dominated. Examples of the interpretation of these tables will be given later in Chapters 4 and 7.

The possible normal modes of vibration of a uniform slab of inhomogeneity embedded in a uniform atmosphere are thus many and varied. As a result of categorizing them into slow and fast, body and surface waves it is seen that for certain configurations, for example, $v_{Ae} > c_0 > c_e > v_A$ (Figure 2.7), it is possible for all

Type of Wave		slender slab	(i) $v_{Ae} < c_e$, $v_A < c_0$	(ii) $v_{Ae} < c_e$, $v_A > c_0$	(iii) $v_{Ae} > c_e$, $v_A < c_0$	(iv) $v_{Ae} > c_e$, $v_A > c_0$
Body Waves	slow < $\min(c_0, v_A)$	c_T sausage $v_{\prime\prime}$	← ✓ except when $\max(v_{Ae}, c_e) < c_T$ →			
			Figs. 2.6 & 2.8		Figs. 2.7, 2.9, 2.10	
	fast > $\max(c_0, v_A)$	v_{Ae} kink $v_\perp$	—	—	✓ for $\max(v_A, c_0) < v_{Ae}$ Figs. 2.7, 2.9, 2.10	
		c_e sausage $v_{\prime\prime}$	✓ for $\max(v_A, c_0) < c_e$ Fig. 2.8		—	—
		c_{Te} kink $v_\perp$	← ✓ only for $c_{Te} > \max(v_A, c_0)$ →			
			Fig. 2.9			
Surface Waves	slow < $\min(c_0, v_A)$	v_{Ae} kink $v_\perp$	✓ for $v_{Ae} < c_T$ Fig. 2.6		—	—
		c_{Te} kink $v_\perp$	✓ for $c_0 > c_e > v_{Ae} > v_A$ (or c_0 & c_e interchanged) Fig. 2.8	—	✓ for $v_{Ae} > c_0 > c_e > v_A$ (or c_e & c_0 interchanged) Fig. 2.7	—
		c_T sausage $v_{\prime\prime}$	✓ for $v_{Ae} < c_T < c_e$ Fig. 2.6		—	—
	fast > $\max(c_0, v_A)$	v_{Ae} kink $v_\perp$	—	✓ for $c_e > v_A > v_{Ae} > c_0$ & $v_A > c_e > v_{Ae} > c_0$	✓ for $c_0 > v_{Ae} > c_e > v_A$ & $c_0 > v_{Ae} > v_A > c_e$ (or v_A & v_{Ae} interchanged)	—
		c_e sausage $v_{\prime\prime}$	$c_0 > v_A > c_e > v_{Ae}$	$v_A > c_e > v_{Ae} > c_0$ $v_A > c_e > c_0 > v_{Ae}$ (or c_e & c_0 interchanged) Fig. 2.6	$c_0 > v_{Ae} > c_e > v_A$ $c_0 > v_A > v_{Ae} > c_e$ $v_{Ae} > c_0 > c_e > v_A$ Fig. 2.7	—

Table 2.2 The four types of wave which may be present for the configurations (i) to (iv) in a slab structure.

✓ (followed by a qualifying statement): indicates the type of mode (described at left) for the configuration (head of column). Figures referred to give a general illustration of the wave. Entries for surface waves which 'originate' as body waves in a slender (long wavelength) regime are excluded from the table.

— : indicates no waves are possible; $v_\perp$, $v_{\prime\prime}$ resp. : motion is principally transverse to or along magnetic field direction.

four classes of waves to occur in a structure. No simple description of the allowable ($m_e > 0$) modes seems possible, each case requiring investigation in its own right. However the figures and tables presented here give a guide to the possible wave structures. The effect of the assumptions made here (the nature of the inhomogeneity i.e. a slab or a cylinder, uniform structure, linear approximation, adiabatic assumptions, etc.) on this wave structure will be examined in subsequent chapters.

Chapter 3 Structuring in a Cylindrical Geometry

'A flux tube limited to a finite cross-section, in place of the infinitely broad slab, is not so heavily burdened by the external fluid!

E.N. Parker 'Cosmical Magnetic Fields'

3.1 Cylindrical Structuring

In the above quotation Parker's comment is directed to the kink mode in an incompressible, slender flux tube. If the analogy with waving strings and sheets of paper around in the air is used then certainly his statement and the result of the ensuing calculation seem intuitively obvious. Here the wave modes of the previous chapter are examined in the physically-more-realistic cylindrical geometry to see if the 'intuitively obvious' in fact holds. Modelling a structure in a cylindrical geometry is certainly more appropriate for many applications in solar physics, for example, for photospheric flux tubes and coronal loops, and for the geomagnetic tail where transverse dimensions are roughly of the same order and less than longitudinal ones (see Chapter 1). But there are other examples of structured media, for example the plasma sheet within the geomagnetic tail (see Chapter 1), which are perhaps better modelled in a Cartesian geometry, since the thickness of the sheet, compared with its width and length, is small. Thus the aim of this chapter is to extend the analysis of Chapter 2 to cylindrical structures, and to compare and contrast the results of structuring in the two geometries.

The cylindrical geometry has received considerable attention in the past, not so much from the point of view of possible wave

motions but from the stability aspect. In the 1950's and 1960's particular interest was directed towards the plasma confinement problem and associated controlled thermonuclear reactions. In solar physics, too, there have been several treatments of cylindrically structured plasmas (notably, Roberts and Webb, 1978, 1979; Wilson, 1979; Parker, 1979a; Wentzel, 1979c; Webb, 1980; Spruit, 1981 a,b, 1982) but nevertheless these analyses provided only a partial view of the complex array of free modes in such media. Several aspects of the work presented in this chapter have been described in condensed form in Edwin and Roberts (1983) which aimed to complement and extend the work of other authors.

The discussion will parallel that of the previous chapter but will be in cylindrical polar coordinates, r, θ and z. Again, the effects of stratification due to gravity will be ignored. In the equilibrium state it is assumed that the pressure p_0, the density ρ_0 and the magnetic field $B_0\hat{z}$ are dependent only on r, satisfying the condition of transverse pressure balance (see Equation (1.13))

$$\frac{d}{dr}\left(p_0 + \frac{B_0^2}{2\mu_0}\right) = 0.$$

The relevant equations are those for linear perturbations about this equilibrium, namely Equations (1.15) to (1.18) with $\underline{g} = \underline{0}$, which, for perturbations of the form $\underline{v} = (v_r, v_\theta, v_z)$ and $\underline{b} = (b_r, b_\theta, b_z)$, may be reduced, as in the previous chapter, to give:

$$\frac{\partial b_r}{\partial t} = B_0 \frac{\partial v_r}{\partial z}, \tag{3.1a}$$

$$\frac{\partial b_\theta}{\partial t} = B_0 \frac{\partial v_\theta}{\partial z}, \tag{3.1b}$$

$$\frac{\partial b_z}{\partial t} = -v_r \frac{dB_0}{dr} - B_0\left(\frac{1}{r}\frac{\partial}{\partial r}(rv_r) + \frac{1}{r}\frac{\partial v_\theta}{\partial \theta}\right), \tag{3.1c}$$

$$\frac{\partial \rho}{\partial t} + \rho_0\left[\frac{1}{r}\frac{\partial}{\partial r}(rv_r) + \frac{1}{r}\frac{\partial v_\theta}{\partial \theta} + \frac{\partial v_z}{\partial z}\right] + v_r \frac{d\rho_0}{dr} = 0, \tag{3.1d}$$

$$\frac{\partial p_T}{\partial t} = \rho_0 v_A^2 \frac{\partial v_z}{\partial z} - \rho_0(c_0^2 + v_A^2)\Delta, \tag{3.1e}$$

$$\frac{\partial^2 v_z}{\partial t^2} = c_0^2 \frac{\partial \Delta}{\partial z}, \tag{3.1f}$$

$$\rho_0\left(\frac{\partial^2}{\partial t^2} - v_A^2 \frac{\partial^2}{\partial z^2}\right)v_r = \frac{\partial}{\partial r}\left[\rho_0(c_0^2 + v_A^2)\Delta - \rho_0 v_A^2 \frac{\partial v_z}{\partial z}\right] \tag{3.1g}$$

and

$$\rho_0\left(\frac{\partial^2}{\partial t^2} - v_A^2 \frac{\partial^2}{\partial z^2}\right)v_\theta = \frac{1}{r}\frac{\partial}{\partial \theta}\left[\rho_0(c_0^2 + v_A^2)\Delta - \rho_0 v_A^2 \frac{\partial v_z}{\partial z}\right]. \tag{3.1h}$$

Here p_T is the total pressure perturbation $p + \frac{1}{\mu_0} B_0 b_z$, and Δ is the divergence of $\underline{v}$ in cylindrical polars, $\frac{1}{r}\frac{\partial}{\partial r}(rv_r) + \frac{1}{r}\frac{\partial v_\theta}{\partial \theta} + \frac{\partial v_z}{\partial z}$.

The sound and Alfvén speeds, $c_0 = (\gamma p_0/\rho_0)^{\frac{1}{2}}$ and $v_A = (B_0^2/\mu_0\rho_0)^{\frac{1}{2}}$, respectively, are functions of r.

Assuming that the variables in Equations (3.1) have a Fourier form, for example,

$$v_r = \hat{v}_r(r)\exp i(\omega t + n\theta + kz), \tag{3.2}$$

Equations (3.1e) to (3.1h) may be used to relate the velocity and total pressure perturbations according to

$$\hat{v}_\theta = \frac{n\omega\hat{p}_T}{r\rho_0(k^2v_A^2 - \omega^2)} \tag{3.3}$$

and

$$\hat{v}_z = \frac{-\omega\hat{p}_T}{k\rho_0(k^2v_A^2 - \omega^2)c_0^2}\left[(k^2v_A^2 - \omega^2) + \frac{n^2}{r^2}(c_0^2 + v_A^2)\right] - \frac{(c_0^2 + v_A^2)}{ikc_0^2 r}\frac{d(r\hat{v}_r)}{dr}. \tag{3.4}$$

The components $\hat{v}_r$ and $\hat{p}_T$ satisfy the pair of first-order differential equations

$$\hat{v}_r = \frac{-i\omega}{\rho_0(k^2v_A^2 - \omega^2)}\frac{d\hat{p}_T}{dr} \tag{3.5}$$

and

$$\frac{i}{r}\frac{d(r\hat{v}_r)}{dr} = \frac{\hat{p}_T\omega}{\rho_0(k^2v_A^2 - \omega^2)}\left(m_0^2 + \frac{n^2}{r^2}\right). \tag{3.6}$$

Here m_0^2 is a function of r given by

$$m_0^2(r) = \frac{(k^2v_A^2(r) - \omega^2)(k^2c_0^2(r) - \omega^2)}{(c_0^2(r) + v_A^2(r))(k^2c_T^2(r) - \omega^2)}, \tag{3.7}$$

where

$$c_T^2(r) = c_0^2(r)v_A^2(r)/(c_0^2(r) + v_A^2(r)).$$

Equation (3.6) may be written in the alternative form,

$$\hat{p}_T = \frac{i\rho_0(k^2v_A^2 - \omega^2)(k^2c_T^2 - \omega^2)(c_0^2 + v_A^2)}{\omega[(k^2v_A^2 - \omega^2)(k^2c_0^2 - \omega^2) + n^2/r^2(c_0^2 + v_A^2)(k^2c_T^2 - \omega^2)]} \frac{1}{r} \frac{d(r\hat{v}_r)}{dr} . \tag{3.8}$$

Equations (3.5) and (3.8) have been presented in the above forms by Appert *et al.* (1974) in order to demonstrate explicitly the singularities which arise when these equations are combined to give the twist-free, Hain-Lüst equation (Hain and Lüst, 1958):

$$\frac{d}{dr}\left\{\frac{\rho_0(k^2v_A^2 - \omega^2)}{(m_0^2 + n^2/r^2)} \frac{1}{r} \frac{d(r\hat{v}_r)}{dr}\right\} - \rho_0(k^2v_A^2 - \omega^2)\hat{v}_r = 0. \tag{3.9}$$

As in the Cartesian case of the previous chapter, singularities are seen to arise (from (3.8)) where $\omega^2 = k^2v_A^2(r)$ and $\omega^2 = k^2c_T^2(r)$ but not, as Goedbloed (1975, 1983) has pointed out, where the quadratic for ω^2 in the denominator of (3.8) or (3.9) has roots. There is, as yet, no coherent picture of the spectrum of modes resulting from (3.9) in its general form. The modes may be grouped, as shown in the previous chapter, according to Goedbloed's résumé (Figure 2.1) but there are no detailed analyses, especially of the compressive problem in the regions of the singularities.

The axisymmetric ($n = 0$) form of Equation (3.9) has been derived by Pneuman (1965) for a specific (parabolic) equilibrium density distribution. In this chapter Equation (3.9) will form the basis for discussion, but in a sharply-structured medium. Conditions will be relaxed somewhat in Chapter 4 when structures having gradual density variations will be considered.

3.2 The Uniform Cylinder

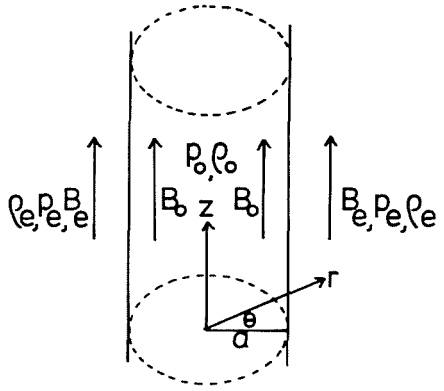

Figure 3.1 The equilibrium configuration of a magnetic cylinder

The starting point is again the equilibrium configuration (Figure 3.1) where now the inhomogeneity is modelled by a cylinder of radius a and the uniform equilibrium magnetic fields, B_0 and B_e, are aligned parallel with the z-axis. The equilibrium pressure p_0 and density ρ_0 (correspondingly p_e and ρ_e outside the cylinder) will also be assumed uniform.

Coefficients in Equation (3.9) are thus independent of r and the equation reduces to a Bessel equation for $\hat{v}_r$:

$$\frac{d}{dr}\left[\frac{1}{r}\frac{d}{dr}(r\hat{v}_r)\right] - \left(m_0^2 + \frac{n^2}{r^2}\right)\hat{v}_r = \frac{d^2\hat{v}_r}{dr^2} + \frac{1}{r}\frac{d\hat{v}_r}{dr} - \left(m_0^2 + \frac{n^2+1}{r^2}\right)\hat{v}_r = 0. \quad (3.10)$$

It is slightly more convenient to use the Bessel equation for the divergence of the velocity vector, Δ, which in Fourier form is

$$\Delta = \hat{R}(r) \exp i(\omega t + n\theta + kz).$$

Then using (3.10), and (3.3) and (3.4), where the coefficients are now independent of r, $\hat{R}$ may be shown to satisfy

$$\frac{d^2\hat{R}}{dr^2} + \frac{1}{r}\frac{d\hat{R}}{dr} - \left(m_0^2 + \frac{n^2}{r^2}\right)\hat{R} = 0, \tag{3.11}$$

where

$$m_0^2 = \frac{(k^2c_0^2 - \omega^2)(k^2v_A^2 - \omega^2)}{(c_0^2 + v_A^2)(k^2c_T^2 - \omega^2)}. \tag{3.12}$$

The amplitudes of the density, pressure, velocity and magnetic fields may be expressed in terms of $\hat{R}$ (see also Webb (1980) for the axisymmetric case), thus:

$$\left.\begin{aligned}
v_r &= -\frac{(c_0^2 + v_A^2)(k^2c_T^2 - \omega^2)}{\omega^2(k^2v_A^2 - \omega^2)}\frac{d\hat{R}}{dr}, & b_r &= -\frac{B_0k(c_0^2 + v_A^2)(k^2c_T^2 - \omega^2)}{\omega^3(k^2v_A^2 - \omega^2)}\frac{d\hat{R}}{dr},\\
v_\theta &= \frac{n(k^2c_0^2 - \omega^2)}{i\omega^2m_0^2}\frac{\hat{R}}{r}, & b_\theta &= \frac{B_0kn(k^2c_0 - \omega^2)}{i\omega^3m_0^2}\frac{\hat{R}}{r},\\
v_z &= (kc_0^2/i\omega^2)\hat{R}, & b_z &= \frac{(k^2c_0^2 - \omega^2)B_0\hat{R}}{i\omega^3},\\
\rho &= -\rho_0\hat{R}/i\omega \quad \text{and} & p &= -c_0^2\rho_0\hat{R}/i\omega.
\end{aligned}\right\} \tag{3.13}$$

In (3.13) the multiplicative factors $\exp i(\omega t + n\theta + kz)$ have been suppressed for simplicity. (For the lowest symmetric mode (n = 0)

there will be no torsional fields.) Again corresponding formulae apply in the cylinder's exterior, with

$$m_e^2 = \frac{(k^2 v_{Ae}^2 - \omega^2)(k^2 c_e^2 - \omega^2)}{(c_e^2 + v_{Ae}^2)(k^2 c_{Te}^2 - \omega^2)} \quad \text{and} \quad c_{Te}^2 = \frac{c_e^2 v_{Ae}^2}{(c_e^2 + v_{Ae}^2)} \; . \tag{3.14}$$

Lateral pressure balance in equilibrium (Equation (1.13)) implies that

$$p_0 + \frac{B_0^2}{2\mu_0} = p_e + \frac{B_e^2}{2\mu_0} , \tag{3.15}$$

so that the ratio of the densities may be expressed as

$$\frac{\rho_e}{\rho_0} = \frac{2c_0^2 + \gamma v_A^2}{2c_e^2 + \gamma v_{Ae}^2} , \tag{3.16}$$

where, as previously, $c_e = (\gamma p_e/\rho_e)^{\frac{1}{2}}$ and v_{Ae} are the sound and Alfvén speeds exterior to the inhomogeneity.

In general Equation (3.11) has solutions of the form

$$\hat{R}(r) = \begin{cases} A_0 I_n(m_0 r) + A_1 K_n(m_0 r), & m_0^2 > 0, \\ A_0 J_n(n_0 r) + A_1 Y_n(n_0 r), & m_0^2 = -n_0^2 < 0, \end{cases} \tag{3.17}$$

where the arbitrary constants A_0, A_1 must be determined for each mode number, n. J_n, I_n, K_n and Y_n denote Bessel functions (Abramowitz and Stegun, 1967). Obviously a similar set of solutions is possible in the cylinder's environment. Solutions appropriate to the problem in hand are

$$\hat{R}(r) = A_0 \begin{cases} I_n(m_0 r), & m_0^2 > 0, \\ J_n(n_0 r), & m_0^2 = -n_0^2 < 0, \end{cases} \quad (r < a) \tag{3.18}$$

and

$$\hat{R}(r) = A_2 K_n(m_e r) \quad (r > a), \tag{3.19}$$

where A_2 is an arbitrary constant. Equations (3.18) have been chosen to ensure that solutions are bounded as $r \to 0$ and so non-physical solutions are not introduced and (3.19) means, as in Chapter 2, that attention is concentrated on solutions evanescent away from the inhomogeneity. This point is discussed further in Section 3.5 of this chapter but essentially it means that radiating (propagating) solutions are ignored, that m_e (Equation (3.14)) is positive and, in turn, that the roots of the dispersion relation, which will follow, are real. The modes are stable.

The boundary conditions ((1.19) and (1.20)) for the transverse velocity v_r and the total pressure $p_T = p + \frac{B_0 b_z}{\mu_0}$ must be obeyed. On using expressions (3.13) for v_r, b_z and p and substituting for $\hat{R}$ from (3.18) and (3.19) the following dispersion relations are obtained:

for surface waves $(m_0^2 > 0)$

$$\rho_0(k^2 v_A^2 - \omega^2) m_e \frac{K_n'(m_e a)}{K_n(m_e a)} = \rho_e(k^2 v_{Ae}^2 - \omega^2) m_0 \frac{I_n'(m_0 a)}{I_n(m_0 a)}, \tag{3.20}$$

and for body waves ($m_0^2 = -n_0^2 < 0$)

$$\rho_0(k^2v_A^2 - \omega^2)m_e \frac{K_n'(m_e a)}{K_n(m_e a)} = \rho_e(k^2v_{Ae}^2 - \omega^2)n_0 \frac{J_n'(n_0 a)}{J_n(n_0 a)} . \qquad (3.21)$$

The dash denotes the derivative of a Bessel function so that, for example, $K_n'(m_e a) \equiv \left(\frac{d}{dx}\right) K_n(x)$ evaluated at $x = m_e a$, etc.

Dispersion relations (3.20) and (3.21) have been obtained previously for a variety of special cases. For example, Kruskal and Schwarzschild (1954) investigated the stability of a cylinder of plasma and obtained a form similar to (3.20) but for a field-free region surrounded by a toroidal magnetic field in a vacuum. Jensen (1957) obtained the special form of (3.9) with k set equal to zero (no z variation) but allowing for radial density variation within the cylinder. He obtained the dispersion relation for such a cylinder in temperature equilibrium with an incompressible, field-free exterior. McKenzie (1970) actually obtained (3.20) but did not investigate its modes; being interested instead in modelling the geomagnetic tail, he considered the special case of a cold magnetic cylinder in a field-free medium. The body wave equation (3.21) was obtained by Meerson *et al.* (1978) but they were interested in non-evanescent modes in the cylinder's exterior and again did not investigate the properties of the dispersion formula. One of the more detailed analyses was carried out by Wilson (1980) but he examined only a magnetic cylinder in a field-free environment which limited his investigation and, as subsequent discussion will show,

not all the possible modes were evident. Though Spruit (1982) included a magnetic environment in his treatment, he overlooked the fast modes and considered only a slender cylinder, concentrating mainly on non-evanescent modes in the cylinder's exterior.

Investigation of the slab structure (Chapter 2) indicated that a complex array of modes could be expected to result in the cylindrical case, too, from (3.20) and (3.21), but earlier analyses did not appear to give a complete picture of them.

3.3 Incompressible Modes

In the incompressible limit ($c_0^2 \to \infty$, $c_e^2 \to \infty$) m_0 and m_e become simply $|k|$ and so m_e is positive and (3.20) is the relevant dispersion relation. This gives

$$\omega^2 = k^2(v_{Ae}^2 - \rho_0/\rho_e \, v_A^2 \, \phi_n)/(1 - \rho_0/\rho_e \, \phi_n), \qquad (3.22)$$

where $\phi_n = I_n(a|k|) \, K_n'(a|k|)/\{I_n'(a|k|) \, K_n(a|k|)\}$. Thus the sausage ($n = 0$) and kink ($n = 1$) modes are given explicitly by (3.22). Surprisingly, this dispersion formula does not, to the author's knowledge, appear to have received much attention in the mhd literature, possibly because most analyses, even of the incompressible case, have been considering a magnetic cylinder in a field-free environment (e.g., Gerwin, 1967; Trehan and Singh, 1978). Uberoi and

Somasundarum (1980) gave a discussion of (3.22) but it must be noted that this paper contains some erroneous ideas, corrected in a later paper, Uberoi and Somasundarum (1982).

Equation (3.22) is interpreted in Figure 3.2 where plots of the phase-speed ω/k as a function of the dimensionless wavenumber ka ($k > 0$) are shown, for the two incompressible situations $v_{Ae} > v_A$ and $v_{Ae} < v_A$. It is interesting to note that, for the former case, the phase-speed for the kink mode is not monotonic as a function of wavenumber (supposed positive in the diagram) but possesses a minimum. Similarly for the latter case ($v_{Ae} < v_A$) the kink mode possesses a maximum, whereas for both cases the sausage mode remains monotonically increasing/decreasing respectively. This feature of a maximum or minimum in the phase-speed of the kink wave is absent in the slab case (Figure 2.5) and so is evidently a reflection of the geometry.

In the slender tube limit ($|k|a \ll 1$) Equation (3.22) yields a phase-speed $c = \omega/k$ given approximately by

$$c = v_A \left[1 - \frac{\rho_e}{\rho_0} \left(1 - \frac{v_{Ae}^2}{v_A^2} \right) \frac{k^2 a^2}{4} K_0(|k|a) \right], \qquad (3.23a)$$

for the sausage mode, and,

$$c = c_k \left[1 - \frac{\rho_e \rho_0}{2(\rho_e + \rho_0)} \frac{(v_{Ae}^2 - v_A^2) k^2 a^2}{(\rho_0 v_A^2 + \rho_e v_{Ae}^2)} K_0(|k|a) \right], \qquad (3.23b)$$

for the kink mode, where $c_k = (\rho_0 v_A^2 + \rho_e v_{Ae}^2)^{\frac{1}{2}} / (\rho_0 + \rho_e)^{\frac{1}{2}}$. If these equations are compared with those for a slender slab in an incompressible

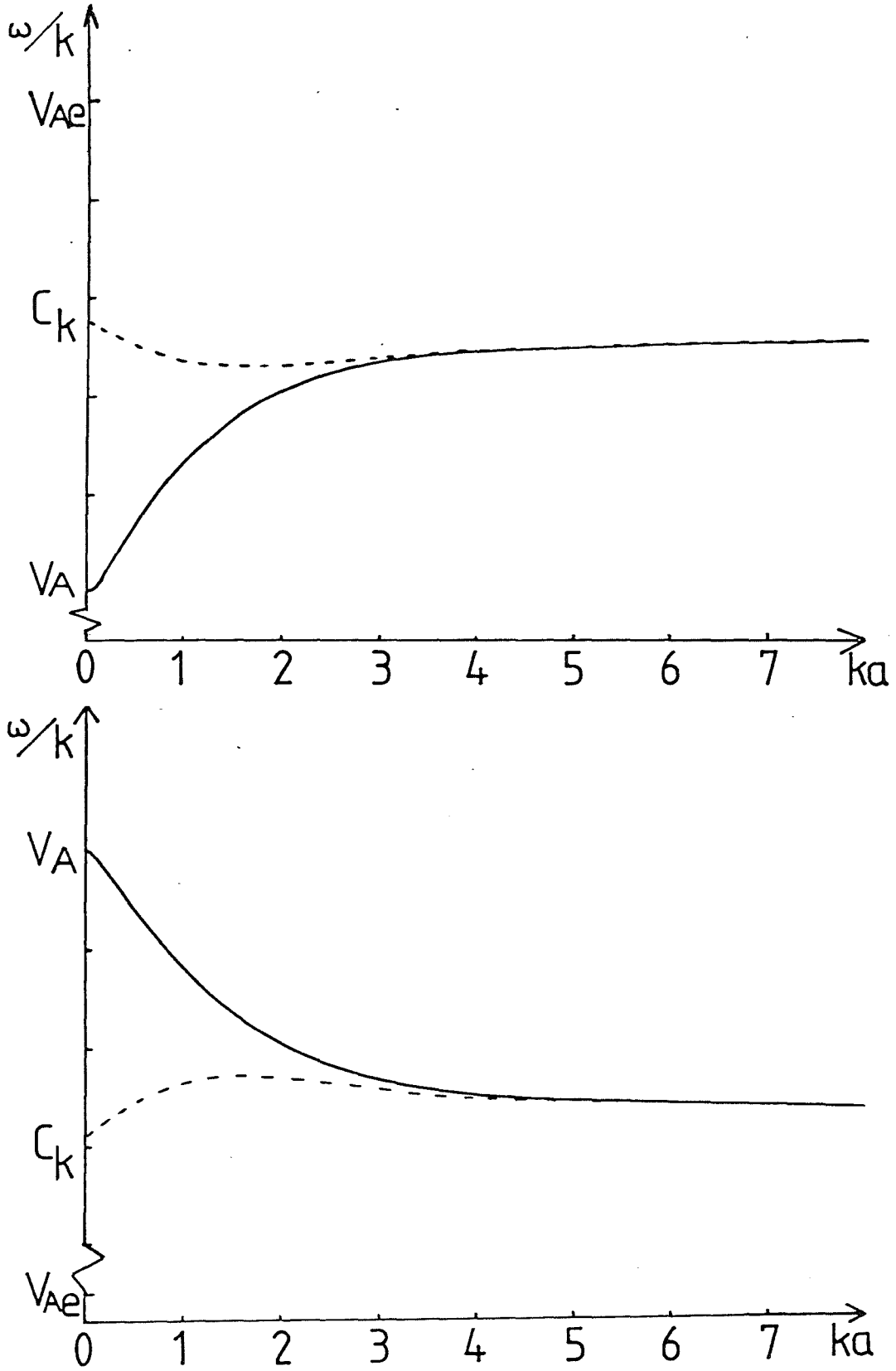

Figure 3.2 The phase-speed ω/k as a function of dimensionless wavenumber ka ($k > 0$) in an incompressible medium, for $v_{Ae} > v_A$ and $v_{Ae} < v_A$ ($\rho_0 = \rho_e$ in both cases).
——: sausage mode; ---: kink mode.

medium (Equations (2.32)) it is seen that whereas the symmetric (sausage wave) behaviour is similar ($\sim v_A$) in both geometries, the kink wave for the slab is determined almost solely by the external field ($\sim v_{Ae}$), whereas in the cylindrical geometry the parameters of the structure in general, ρ_0, ρ_e, v_A and v_{Ae}, determine the behaviour. This is not unexpected on physical grounds, since, as Parker (1979a) noted, the cylinder oscillating transversely displaces less of its surroundings than its counterpart in the magnetic slab. However it is noted that Equation (3.23a) indicates a slower fall-off rate with increasing $|k|a$ ($<< 1$) than occurs in a slab geometry (cf., Equation (2.32a)), since $K_0(|k|a) \sim -\ell n(|k|a)$ as $|k|a \to 0$, as mentioned in Roberts and Webb (1978).

In a cylinder of large radius $|k|a >> 1$, both $n = 0$ and $n = 1$ modes of (3.22) have phase-speeds given by

$$\frac{\omega^2}{k^2} \simeq \frac{\rho_e v_{Ae}^2 + \rho_0 v_A^2}{\rho_e + \rho_0} \quad (\equiv c_k^2), \qquad (3.24)$$

which, of course, is just the result for a wide, incompressible slab (2.33), being the dispersion relation for a single interface between two uniform media.

3.4 Compressible Modes

3.4.1 Surface waves - solutions of Equation (3.20)

Webb (1980) examined this dispersion relation for the case of symmetric

($n = 0$) modes of a magnetic flux tube in a field-free ($v_{Ae} = 0$) environment. His results are generalized below in several ways: (i) the structure is not necessarily slender, (ii) kink as well as sausage modes are considered, and (iii) the structuring is as general as the assumptions of this chapter will allow (i.e., $v_{Ae} \neq 0$, and hence, for example, $\rho_0 > \rho_e$ is possible).

Using the Bessel function relation $K_0' = -K_1$, Equation (3.20) may be rewritten

$$\rho_0(k^2v_A^2 - \omega^2)m_e \frac{K_1(m_e a)}{K_0(m_e a)} = -\rho_e(k^2v_{Ae}^2 - \omega^2)m_0 \frac{I_1(m_0 a)}{I_0(m_0 a)}. \qquad (3.25)$$

For a slender cylinder, $|k|a \to 0$, it is assumed that $m_0 a \to 0$ and $m_e a \to 0$. This will possibly not be the case if either (a) $\omega^2 \simeq k^2c_T^2$ or (b) $\omega^2 \simeq k^2c_{Te}^2$ (from the definitions (3.12) and (3.14), respectively, of m_0 and m_e). It can be shown, *a posteriori*, that though (a) occurs, $m_0 a$ does indeed tend to zero, and that (b) never occurs (essentially K_1 has no roots). Therefore, assuming that $m_0 a$, $m_e a \to 0$ as $|k|a \to 0$, and noting that

$$I_0(m_0 a) \sim 1, \quad I_1(m_0 a) \sim \tfrac{1}{2}m_0 a,$$

$$K_0(m_e a) \sim -\ln(m_e a), \quad K_1(m_e a) \sim (m_e a)^{-1},$$

(3.25) reduces to

$$\frac{\rho_e a^2}{4}(k^2v_{Ae}^2 - \omega^2)(k^2c_0^2 - \omega^2)\ln[m_e^2a^2] = \rho_0(c_0^2 + v_A^2)(k^2c_T^2 - \omega^2). \qquad (3.26)$$

This dispersion relation for a slender, cylindrical inhomogeneity gives two symmetric modes:

$$\omega^2 \simeq k^2 c_T^2 - \frac{\rho_e (v_{Ae}^2 - c_T^2)(c_0^2 - c_T^2) k^4 a^2 \ell n(k^2 a^2)}{4\rho_0 (c_0^2 + v_A^2) c_T^2} \qquad (3.27)$$

and

$$\omega^2 \simeq k^2 c_e^2 - \frac{(c_{Te}^2 - c_e^2)(c_e^2 + v_{Ae}^2)}{a^2 (v_{Ae}^2 - c_e^2)} \exp\left\{ \frac{-4\rho_0 (c_0^2 + v_A^2)(c_e^2 - c_T^2)}{\rho_e k^2 a^2 (c_e^2 - v_{Ae}^2)(c_e^2 - c_0^2)} \right\} \qquad (3.28)$$

for $c_e > c_0$ and $c_e > v_{Ae}$, $c_e < c_T$ and $c_e > v_{Ae}$,

$c_0 > c_e > c_T$ and $v_{Ae} > c_e$.

These agree with Webb's (1980) expressions for $v_{Ae} = 0$. Spruit (1982) recovers the c_T mode but overlooks the one given by (3.28). So, when a plasma's structure has the form of a narrow inhomogeneity, as far as symmetric modes of oscillation are concerned it makes little difference whether this structure is modelled in a Cartesian or cylindrical geometry, since, to first order in ka or kx_0, comparison of Equations (3.27) and (3.28) with Equations (2.35) shows that the slow and fast modes behave as c_T and c_e, respectively. There is no discernible difference, for the symmetric modes, between Figures 3.3 and Figure 2.6 of the previous chapter. However the kink mode presents a different picture.

Equation (3.20) also holds for $n \geqslant 1$. Here only $n = 1$ will be investigated since, in general, it will be the lower order modes $n = 0$ and $n = 1$ which will be excited. For $n = 1$, Equation (3.20) is

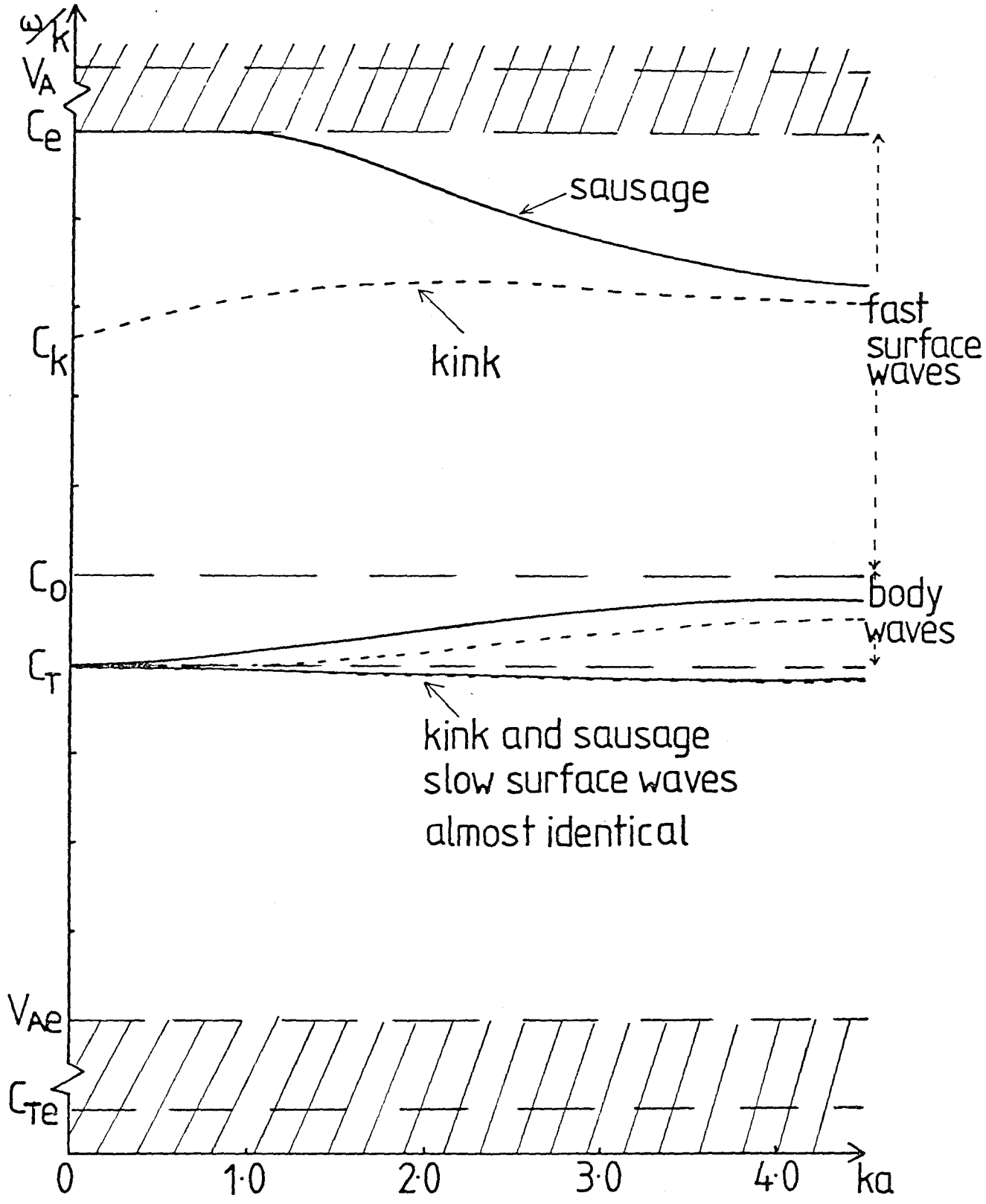

Figure 3.3 The phase-speed (illustrated for $v_A = 2.0c_0$, $c_e = 1.5c_0$, $v_{Ae} = 0.5c_0$ and $k > 0$) under photospheric conditions. Only two of the infinitely many slow body waves are shown. Hatching denotes regions in which there are no free (real ω and k) modes.

$$\rho_0(k^2v_A^2 - \omega^2)m_e \frac{K_1'(m_e a)}{K_1(m_e a)} = \rho_e(k^2v_{Ae}^2 - \omega^2)m_0 \frac{I_1'(m_0 a)}{I_1(m_0 a)} . \qquad (3.29)$$

The existence of *two* kink modes in a cylindrical geometry - aside from the body waves - is suggested by the order of Equation (3.9) and is borne out by the analyses for a slab (for example, Figures 2.6 and 2.11) and for a single interface. The slab geometry yielded a slow kink mode with phase-speed close to c_{Te} in the slender tube limit and a fast kink mode with phase-speed close to v_{Ae} (Equations (2.37) and (2.38) or (2.39)). The available analyses for a slender, cylindrical inhomogeneity in the kink mode (Parker, 1979a; Wilson, 1980; Spruit, 1982) all give possibility (a) below, $\omega/k \simeq c_k$, but none yields the slow kink (or indeed any speed other than c_k).

For a slender cylinder, $|k|a << 1$, there are three possibilities: either

(a) $m_0 a \to 0$ and $m_e a \to 0$,

or (b) $m_0 a \to 0$ but $m_e a \to \mu$, say, some finite value,

or (c) $m_e a \to 0$ but $m_0 a \to \nu$, say, where ν is finite.

Using the standard Bessel function relations (Abramowitz and Stegun, 1967),

$$\frac{K_1'(m_e a)}{K_1(m_e a)} = -\left[\frac{K_0(m_e a)}{K_1(m_e a)} + \frac{1}{m_e a}\right], \quad \frac{I_1'(m_0 a)}{I_1(m_0 a)} = \left[\frac{I_0(m_0 a)}{I_1(m_0 a)} - \frac{1}{m_0 a}\right], \qquad (3.30)$$

the three cases (a), (b) and (c) may be analysed.

(a) $\underline{m_0 a \to 0,\ m_e a \to 0}$. In this limit (3.29) combined with (3.30) reduces to

$$\frac{\omega^2}{k^2} \simeq \frac{\rho_e v_{Ae}^2 + \rho_0 v_A^2}{\rho_e + \rho_0} \equiv c_k^2. \tag{3.31}$$

This is the slender tube behaviour, $\omega/k \simeq c_k$, deduced by Wilson (1980) and Spruit (1982), and, for the case of $v_{Ae} = 0$, $\rho_e = \rho_0$, by Parker (1979a). However, possibilities (b) and (c) have not been considered previously.

(b) $\underline{m_0 a \to 0,\ m_e a \to \mu,\ \text{a finite value}}$. In this limit the terms in Equations (3.30) combine to give

$$m_0 a \frac{I_1'(m_0 a)}{I_1(m_0 a)} \to 1 \quad \text{and} \quad m_e a \frac{K_1'(m_e a)}{K_1(m_e a)} \to -\mu \frac{K_0(\mu)}{K_1(\mu)} - 1,$$

which mean that the dispersion relation (3.29) has the form:

$$-\rho_0 (k^2 v_A^2 - \omega^2) \left[\mu \frac{K_0(\mu)}{K_1(\mu)} + 1\right] = \rho_e (k^2 v_{Ae}^2 - \omega^2). \tag{3.32}$$

Now if $m_e a \to \mu$ as $|k|a \to 0$ an heuristic argument suggests that $m_e^2 \to \infty$, or in other words, (3.14) implies that $\omega \to k c_{Te}$. So μ (> 0) will be a solution of (3.32) in this limit; it will satisfy

$$\mu \frac{K_0(\mu)}{K_1(\mu)} + 1 = \frac{\rho_e (v_{Ae}^2 - c_{Te}^2)}{\rho_0 (c_{Te}^2 - v_A^2)}. \tag{3.33}$$

The left-hand side of this equation is positive so real solutions are only possible if $c_{Te} > v_A$. For example, the parameters used in compiling Figure 2.7 ($v_{Ae} = 1.5 c_0$, $c_e = 0.75 c_0$, $v_A = 0.5 c_0$) mean

that the right-hand side of (3.33) has value 4.45, so there is a value for μ in this case. Examination of solutions of (3.32) near $\omega^2 \sim k^2 c_{Te}^2$ shows that the phase-speed ω/k satisfies

$$\omega^2 \simeq k^2 c_{Te}^2 \left[1 - \frac{c_{Te}^2 (ka)^2}{(c_e^2 + v_{Ae}^2)\mu^2} \right] \tag{3.34}$$

where μ is given by (3.33). This limiting behaviour has not, to the author's knowledge, appeared in the literature before. [Parker (1979a, p.162) gives a formula for a slender flux tube in the incompressible case ($m_e = |k|$), $\rho_e = \rho_0$ and $v_{Ae} = 0$:

$$\frac{\omega^2}{k^2} \simeq \frac{kav_A^2}{(1+ka)} . \tag{3.35}$$

This may easily be deduced from the dispersion relation for a kink mode in a slender *slab* (Equation (2.36)) but not for a cylinder because the right-hand side of (3.33) would then be negative implying no (real) solutions for μ if $c_{Te} < v_A$.]

(c) $m_e a \to 0$ but $m_0 a \to \nu$, a finite value. For this case Equations (3.30) and (3.29) result in

$$m_0 a \frac{I_1'(m_0 a)}{I_1(m_0 a)} \to \nu \frac{I_0(\nu)}{I_1(\nu)} - 1 \quad \text{and} \quad m_e a \frac{K_1'(m_e a)}{K_1(m_e a)} \to -1$$

and

$$-\rho_0 (k^2 v_A^2 - \omega^2) = \rho_e (k^2 v_{Ae}^2 - \omega^2) \left[\nu \frac{I_0(\nu)}{I_1(\nu)} - 1 \right] . \tag{3.36}$$

Again, arguing heuristically, if $m_0 a \to \nu$ as $|k|a \to 0$ then it would appear that $m_0^2 \to \infty$ and this will occur if $\omega^2 \to k^2 c_T^2$. So ν (> 0) exists if there are finite (real) solutions of

$$\frac{\rho_0(v_A^2 - c_T^2)}{\rho_e(c_T^2 - v_{Ae}^2)} = \nu \frac{I_0(\nu)}{I_1(\nu)} - 1. \qquad (3.37)$$

It may be noted that the left-hand side of (3.37) is positive if $c_T > v_{Ae}$. For example, if $v_{Ae} = 0$, (3.37) requires that

$$c_0^2 + \tfrac{1}{2}\gamma v_A^2 < v_A^2\left(\frac{c_e}{c_0}\right)^2.$$

This inequality is satisfied by the parameters ($c_e = 1.5c_0$, $v_{Ae} = 0.5c_0$, $v_A = 2.0c_0$) of Figure 2.6. An expansion around $\omega^2 = k^2c_T^2$ in the dispersion relation (3.36) shows that indeed there is a solution near this value; its form is

$$\omega^2 \simeq k^2 c_T^2 \left[1 - \frac{c_T^2 (ka)^2}{(c_0^2 + v_A^2)\nu^2}\right], \qquad (3.38)$$

where $\nu > 0$ satisfies (3.37). This slow kink wave is illustrated in Figure 3.3, which shows the same structure as Figure 2.6 but modelled by a cylindrical rather than a Cartesian geometry.

So far only a slender cylindrical situation has been discussed. When the radius of the cylinder is large the dispersion relation (3.20) for both sausage ($n = 0$) and kink ($n = 1$) surface waves becomes

$$\rho_0 m_e(k^2 v_A^2 - \omega^2) + \rho_e m_0(k^2 v_{Ae}^2 - \omega^2) = 0, \qquad (3.39)$$

and so the large radius cylinder has the same characteristics as a wide slab (Equation (2.40)) or a single interface (Roberts, 1981a). (This latter analysis, which showed that there were, under certain circumstances, two kink modes for the single interface was a further indicator that two kink modes for the slender cylinder could be expected.) Thus a discussion of the modes given by (3.39) would be identical to that given in Chapter 2 (following Equation (2.40)) for the wide slab and will therefore not be repeated. It may be noted that Wilson (1979) also considered the large radius cylinder, in agreement with the analysis here, but a later paper (1980) incorrectly illustrates this behaviour.

This completes the discussion of the allowable surface ($m_0^2 > 0$) modes in a cylindrically structured medium. Consideration of the similarities and the differences between this model and that in a slab geometry will be given at the end of the chapter, in Section 3.6.

3.4.2 Body waves - solutions of Equation (3.21) The pattern of allowable symmetric modes is very similar to that for the slab structure. For sausage (symmetric) modes, $n = 0$ in Equation (3.21) gives

$$\rho_0(k^2v_A^2 - \omega^2)\, m_e \frac{K_1(m_e a)}{K_0(m_e a)} \cdot \frac{J_0(n_0 a)}{J_1(n_0 a)} = \rho_e(k^2v_{Ae}^2 - \omega^2)n_0. \qquad (3.40)$$

If it is assumed that, as $|k|a \to 0$, $n_0 a \to 0$, then an examination of Equation (3.40) shows that it has no roots. So supposing that

$n_0 a \to \nu$, a non-zero finite value, as $|k|a \to 0$, an argument similar to that in Chapter 2 (which supposes that $n_0^2 \to \infty$ $(\omega^2 \simeq k^2 c_T^2)$ for $|k|a$ small) may be used. For $n_0 a J_1(n_0 a)$ to be finite, $n_0 a$ must tend to the roots of $J_1(n_0 a) = 0$, that is $n_0 a \to j_i^{(1)}$ for $i = 1,2,\ldots$. Hence

$$n_0^2 a^2 \simeq \frac{k^2(c_0^2 - c_T^2)(v_A^2 - c_T^2)a^2}{(c_0^2 + v_A^2)c_T^2 \nu} = j_i^{(1)2}$$

and the modes of (3.40) for $|k|a \ll 1$ are given by

$$\omega^2 = \omega_i^2 \simeq k^2 c_T^2 \left\{1 + \frac{k^2 a^2 c_T^2}{(c_0^2 + v_A^2) j_i^{(1)2}}\right\}, \quad i = 1,2,\ldots . \qquad (3.41)$$

So, as in the slab case, there are an infinite number of modes resulting from (3.41). The existence of these modes, in the $v_{Ae} = 0$ case, was pointed out by Roberts and Webb (1979) and Webb (1980) and Wilson (1980) (though Wilson does not give an explicit form for these modes).

For $n = 1$ Equation (3.21) becomes

$$\rho_0(k^2 v_A^2 - \omega^2)\, m_e \frac{K_1'(m_e a)}{K_1(m_e a)} \cdot \frac{J_1(n_0 a)}{J_1'(n_0 a)} = \rho_e(k^2 v_{Ae}^2 - \omega^2) n_0 . \qquad (3.42)$$

If $|k|a \to 0$ then, as for the surface waves, either (a) $n_0 a \to 0$ and $m_e a \to 0$, or (b) $m_e a \to 0$ but $n_0 a \to$ some finite value, or (c) $n_0 a \to 0$ but $m_e a$ tends to some finite value.

In case (a), when the inhomogeneity is slender, (3.42) reduces to

$$\frac{\omega^2}{k^2} \simeq \frac{\rho_0 v_A^2 + \rho_e v_{Ae}^2}{\rho_0 + \rho_e} \quad (\equiv c_k^2), \tag{3.43}$$

so that, once again, as for the slender slab, this kink mode is a 'combined' mode in the sense that it is indistinguishable as a body or surface wave; it is independent of m_0 (or n_0) to this order. (Equation (2.36) for the slab is independent of m_0.) Once more, as in (3.31), this 'natural' c_k mode occurs. It reflects the combination with the environment, without pressure changes, of a cylindrical structure. The fact that the speed c_k is relevant to both a body and a surface mode, is present in a slender and wide configuration, and is also a 'natural' speed in the incompressible system, has been observed by other authors (Wentzel, 1979a; Wilson, 1980), and its multi-role has probably added to the confusion in descriptions of the allowable modes.

Case (b) follows in a similar manner to the surface modes. Supposing $n_0 a \to \mu$, a non-zero finite constant, as $|k|a \to 0$ then (3.42) yields modes

$$\omega^2 = \omega_i^2 \simeq k^2 c_T^2 \left\{ 1 + \frac{k^2 c_T^2 a^2}{(c_0^2 + v_A^2)\mu_i^{(1)2}} \right\}, i = 1,2,\ldots \tag{3.44}$$

where the $\mu_i^{(1)}$ are the roots of $J_1'(n_0 a) = 0$. So again, as Wilson (1980) pointed out (for the $v_{Ae} = 0$ case), there are an infinite number of modes.

It is possible for case (c) to yield a body wave - a mode $\omega^2 \sim k^2 c_{Te}^2$ - similar to that given by (3.34) subject to (3.33) since

the Bessel functions of the first kind have the same limiting behaviour as their modified counterparts in this case. However this would have to correspond to some very artificial combination of parameters since (3.33) implies both $c_{Te} > v_A$ and

$$\frac{v_{Ae}^2(2c_0^2 + \gamma v_A^2)}{c_e^2(2c_e^2 + \gamma v_{Ae}^2)} > 1, \tag{3.45}$$

because the left-hand side is 1 plus a positive term. What is more c_{Te} must be greater than c_0 if these are to be body and not surface waves. Thus the regime is that of entry 1 of Table 2.1. (The parameters of Figure 2.9, for example, do not satisfy (3.45) so this body wave, for a slender structure, does not occur in the configuration shown there.)

For a cylindrical structure of large radius the relation for symmetric body waves (3.40) becomes

$$\tan(n_0 a - \pi/4) = \frac{\rho_0(k^2 v_A^2 - \omega^2)}{\rho_e(k^2 v_{Ae}^2 - \omega^2)} \cdot \frac{m_e}{n_0}, \tag{3.46}$$

whilst that for kink body waves (3.42) becomes

$$\tan(n_0 a - \pi/4) = -\frac{\rho_e(k^2 v_{Ae}^2 - \omega^2) n_0}{\rho_0(k^2 v_A^2 - \omega^2) m_e}. \tag{3.47}$$

Examples best illustrate these equations. If $c_e = c_0 = 0$, so that the cold plasma approximation is assumed, then

$$\tan(n_0 a - \pi/4) = \begin{cases} -n_0/m_e, & \text{for sausage modes} \\ m_e/n_0, & \text{for kink modes,} \end{cases} \tag{3.48}$$

which evidently are the equivalents of the Pekeris equation (Eqn. (2.55)) and Love equation (Eqn. (2.56)), respectively, phase-shifted by $\pi/4$. These body waves are illustrated in Figure 3.4. Similarly, a temperature or density structuring with $v_A = v_{Ae} = 0$ gives Love's equation (2.57) phase-shifted by $\pi/4$, that is, Equation (3.46) becomes

$$\tan(n_0 a - \pi/4) = \frac{c_e^2}{c_0^2} \frac{m_e}{n_0} . \tag{3.49}$$

So the fast mode, non-slender behaviour in a cylindrical structure is very similar to that in a slab.

3.5 Non-evanescent Modes

In the foregoing discussions of both this and the previous chapter it has been assumed that $m_e > 0$. This means that $m_e^2 > 0$, negative values of m_e being rejected because solutions are required to be finite at large distances from the inhomogeneity (see Equations (2.25) and (3.19)). If m_e^2 is not restricted to be positive then consideration of the allowable modes in this and the previous chapter, complicated as it is, represents just a small

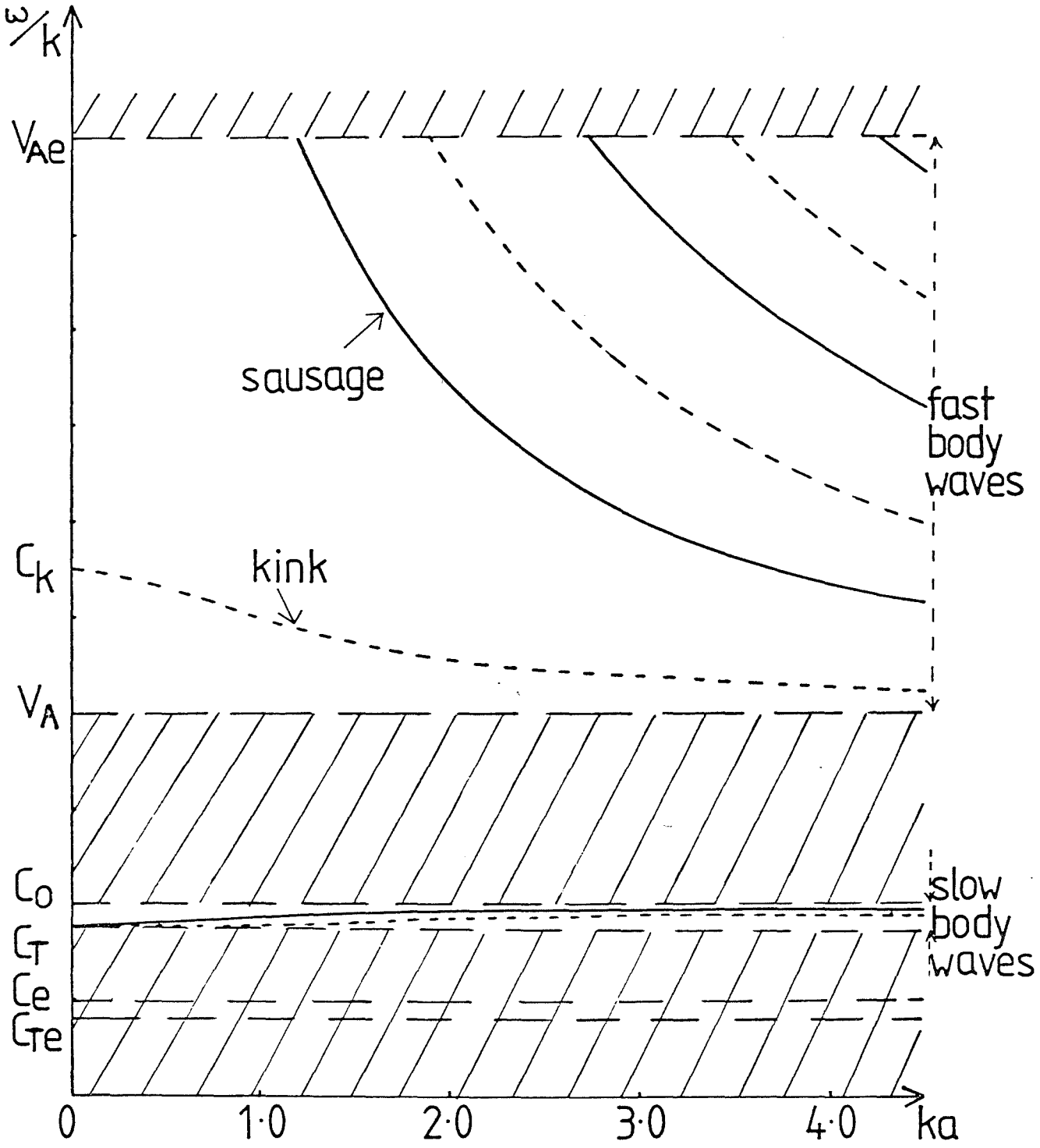

Figure 3.4 The phase-speed (illustrated for $v_{Ae} = 5c_0$, $c_e = 0.5c_0$, $v_A = 2c_0$ and $k > 0$) under coronal conditions. Only two of the infinitely many slow body waves are shown. Hatching denotes regions in which there are no free (real ω and k) modes.

portion of a greater problem in which m_e could be complex. This problem has only been partially examined, mainly for a cylindrical inhomogeneity, and the appropriate dispersion relation produced (see, e.g., Meerson *et al*, 1978; Roberts and Webb, 1979). In the latter paper, which discussed a magnetic cylinder in a field-free environment, two possibilities were considered. If $m_e^2 = -n_e^2 < 0$ and $n_e > 0$ then standing waves in the cylinder's exterior are possible, requiring either a generator of waves at some infinite distance, or a perfect reflector at some finite distance from the cylinder. Wilson (1979) had considered these standing waves too. Though conceivably of interest in the laboratory, as Roberts and Webb (1979) point out such waves are not physically realistic in the solar physics context. The second possibility discussed by Roberts and Webb (1979) is that of n_e being complex. They found that the dispersion relation then implied complex ω (or complex k), the physically realistic interpretation of which is an outgoing propagating wave with $\mathrm{Im}(\omega) > 0$ if k is real. Wilson (1981) and Spruit (1982) have both examined this possibility further. Wilson produced numerical solutions of the dispersion relation for an imposed sinusoidal motion at the cylinder's axis, for kink modes only, whilst Spruit calculated the damping rate based on an expansion in $m_e a$.

Both authors give the asymptotic form of field solutions in the exterior of the cylinder (arising from the Hankel functions in their dispersion relations):

$$r^{-\frac{1}{2}} \exp(-i n_e r) \qquad (r >> a), \tag{3.50}$$

where for an outward propagating wave which is finite at ∞ $\mathrm{Im}(n_e) < 0$, and where r is the cylindrical polar coordinate measuring distance from the cylinder's axis. Moisan *et al.* (1982), in their review of waves along a plasma column, point out the differences between *radiation* (or *space*) waves behaving, at large distances, according to (3.50) and those resulting from (3.19) (or (2.25)), where $m_e > 0$ and solutions have the form (arising from the modified Bessel functions):

$$r^{-\frac{1}{2}} \exp(-m_e r). \tag{3.51}$$

To illustrate the comparison they consider waves emitted from a cylindrical source with energy leaking perpendicular to the axis. This wave energy propagates in all transverse directions and its intensity decreases inversely with distance from the source simply because the energy is being distributed over a larger (cylindrical) surface with increasing distance. In the case of (3.51), however, the field intensities (see expressions (3.13)) are proportional to the expression (3.51) and m_e (> 0) is a measure of the decay. The wave energy flows principally along the cylinder, not transverse to the boundary. This is the characteristic feature which distinguishes the non-radiating ($m_e > 0$) *trapped* (or *truly guided*) waves discussed in this thesis from the radiating waves (sometimes called *partially guided* or *leaky* waves). The latter description is usually reserved for certain cold plasma ($c_e = 0$) situations, and their analogies, (see Chapter 4 for further discussion) when, from (2.26) and (3.14), m_e^2 simplifies to

$$m_e^2 = (k^2 v_{Ae}^2 - \omega^2)/v_{Ae}^2.$$

For example, it is then easy to see that one possibility for $m_e^2 < 0$ is when k is purely imaginary and ω is real, say. In fact, cold plasma body waves (see Figure 3.4 with c_e and c_0 set equal to zero) may be categorized (Olshansky, 1979) for real ω according to

(i) k real and in the range $\omega/v_{Ae} \leq |k| \leq \omega/v_A$ (so $m_e > 0$),

(ii) k real and in the range $0 \leq |k| < \omega/v_{Ae}$,

and (iii) $\mathrm{Im}(k) > 0$ and $0 \leq |\mathrm{Re}(k)| < \omega/v_{Ae}$.

These three classes, for a cold plasma, are illustrated in Figure 3.5 (following Marcuse, 1972).

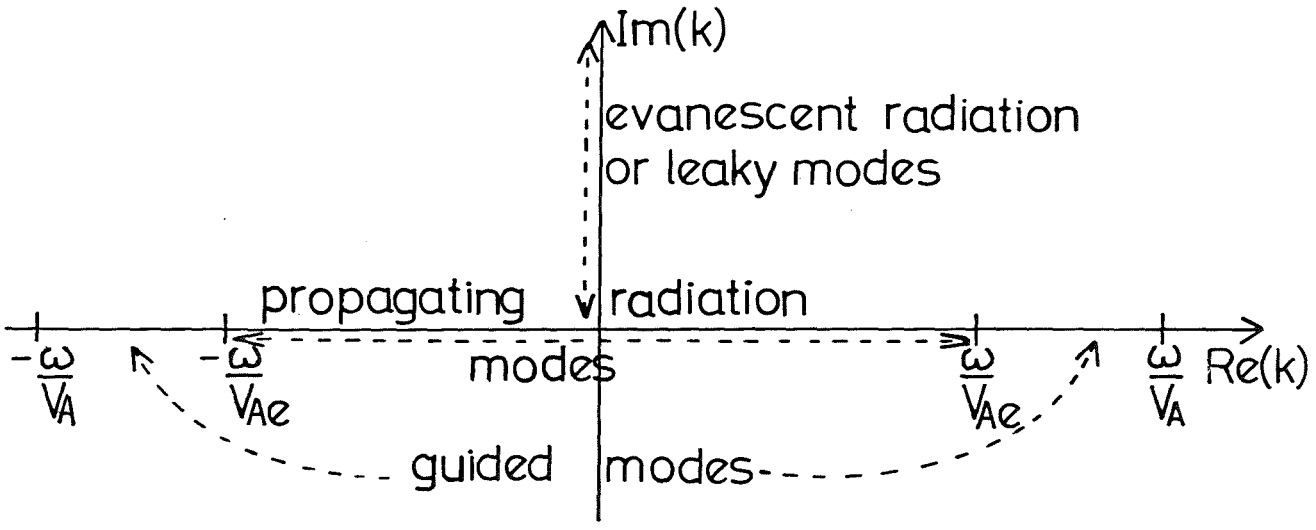

Figure 3.5 Categorization of the modes in a cold plasma for real frequency ω.

In general all types of wave may be excited. In this thesis attention is concentrated on the guided modes, those whose energy is confined predominantly to the duct formed by an inhomogeneity in the structuring.

3.6 A Slab/Cylinder Comparison

It is difficult to present a simple, concise summary comparing the slab and cylindrical models. Much depends on the relative magnitude of the 'natural' speed of the cylindrical model, c_k. For solutions evanescent away from the inhomogeneity m_e is greater than 0 and the allowable phase-speed 'windows' are

$$\text{(a)}\quad 0 \leqslant c_k \leqslant c_{Te}, \quad \text{or} \quad \text{(b)}\quad \min(v_{Ae}, c_e) \leqslant c_k \leqslant \max(v_{Ae}, c_e).$$

For case (a) the slab and cylindrical models are the same, except that slow, slender tube behaviour in a cylinder would be dominated, in the kink mode, by c_k rather than c_{Te}. Figures 2.8, 2.9 and entry 1 of Table 2.1 exemplify this behaviour, though these situations are rather unphysical.

In case (b), again as expected, the slab and cylindrical models would yield similar results except for the kink modes. This time it is the *fast*, slender tube behaviour which is dominated by c_k rather than v_{Ae} (Figures 2.7, 2.10, 2.11), whilst the slow modes are not changed (Figures 2.7, 2.11). The exception is when, for example,

the magnetic inhomogeneity is particularly strong, as in Figure 2.6. Then the slow (kink) mode is characteristically the tube speed c_T rather than v_{Ae}.

Thus with the above provisos, Table 2.1 and Figures 2.6 to 2.11 remain essentially unchanged. However these few detailed changes of the kink mode behaviour, due to geometry, are important in physical interpretation. Accordingly, Figures 2.6 (a typical photospheric situation) and 2.10 (a typical coronal situation) have been redrawn as Figures 3.3 and 3.4, for cylindrically structured media. They will be discussed further in Chapters 4 and 7.

Chapter 4 Oscillations in the Corona : Applications and Analogies

'... nothing but loops, some "closed" in graceful arches, and some "open", extending away from the surface to fade high in the corona. The corona is nothing more, and nothing less, than magnetic loops.'

R.W. Noyes 'The Sun, Our Star'

4.1 An Overview

4.1.1 Observations

Since the end of the 1960's many observations of coronal oscillations have been reported, the bulk of the evidence being provided by radio wave (see review by Krüger, 1979) and hard X-ray (e.g., Kiplinger, 1983 a,b) data, though coronagraph observations have also been reported (e.g., Koutchmy *et al.*, 1983; Pasachoff and Landman, 1984). One of the interesting features of these observations is their splitting into several time scales. There are numerous observations of short period oscillations, with periodicities of around one second (see Table 4.1) but there are also long period (one minute) radio pulsations reported by, for example, Trottet *et al.* (1979). Oscillations on an even longer scale have been observed by, for example, Koutchmy *et al.* (1983), who give evidence of periods of 43s, 80s and 300s, and by Strauss *et al.* (1980) who noted an unusual 5.6 min oscillation in a loop prominence.

A second interesting feature, especially of the short period observations, is the form of the observed signature, the temporal variation. Some examples are shown in Figure 4.1. Short bursts of oscillatory behaviour are seen to occur; the wave-packet or wave

Reference		Time period/scale	E.m. designation	Nature of source
Janssens & White (1969)	P	train (> 9 pulses) of ~ 16s preflare pulse train ~ 23s	UHF, μ	trains during and *before* flare
Parks & Winckler (1969)	Q	~ 5s separated by ~ 15s	X-ray, μ	flare assoc.
Abrami (1970)	Q	1.7 → 3.1 s	VHF	some subflare assoc., Type IV
Rosenberg (1970)	P,Q	~ 1s, subharmonic ~ 3s	VHF	Type IV
McLean *et al.* (1971)	Q	~ 1s, 2.5 → 2.7s between pulses in train of ~ 50	VHF	flare 25 min. earlier, Type IV
Abrami (1972)	Q	trains of sub-sec. pulses, fast spike bursts	VHF	observed in ~ 50% Type IV events
Gotwols (1972)	Q	~ 0.5s	UHF	flare 6-10 min. earlier, Type IV
Janssens *et al.* (1973)	P,Q	4,5,6 spikes separated by 10 → 20s	X-ray, EUV, μ	some flare assoc., Type III
Kai & Takayanagi (1973)	Q	~ 2 → 5s	VHF	double structure, flare assoc. with ⩾ 1 part, Type II, IV
McLean & Sheridan (1973)	P	~ 4s, sudden onset, gradual decay	VHF	subflare earlier
Maxwell & Fitzwilliam (1973)	Q	1 → 200s periods 7 → 15 min durations	μ	Type IV
Achong (1974)	Q	~ 4s	HF	
Kaufmann *et al.* (1977)	Q	4.7 ± 0.9s for > 1 hr	μ	simultaneous solar great burst
Pick & Trottet (1978)	Q	0.37s, trains recurring after 1.7 ± 0.4s	VHF	flare assoc., moving Type IV
Tapping (1978)	Q	trains of ≤ 20 pulses, $0.2s^{-1}$ → $15s^{-1}$ freq.	VHF	no flare
Pračka & Karlický (1979)	Q	bursts of ~ 0.1s	UHF	2-ribbon flare ~ 4hr earlier
Gaizauskas & Tapping (1980)	Q	~ 2.5s, chains of pulsations ~ several min long	μ	no flare, source over plage area
Dennis *et al.* (1981)	Q	≥ 8 peaks ~ 1s separated by 1 → 2s	HXRBS	flare assoc.
Orwig *et al.* (1981)	Q	groups of spikes 7 → 11s between peaks	UVSP, HXIS, HXRBS	flare assoc.
Trottet *et al.* (1981)	Q	1.7 ± 0.5s	VHF	moving Type IV
Kane *et al.* (1983)	Q	7 peaks with 8s separation	X-ray, μ, VHF	flare assoc. source stationary
Kiplinger *et al.* (1983a)	Q	< 1s	HXRBS	flare assoc.
Kiplinger *et al.* (1983b)	Q	recurrent train of 8.2s pulse interval	HXRBS, μ, γ-ray	flare assoc.
Takakura *et al.* (1983)	Q	3 → $4s^{-1}$ freq.	X-ray, EHF	subflare earlier
Benz (private comm., 1983)	Q	1.1s for ~ 29s	UHF	
Pasachoff & Landman (1984)	Q	0.5 → 2.0s	visible	
Zodi & Kaufmann (1984)	Q	1.5s	μ EHF	source stationary

Table 4.1 Examples of fast coronal oscillations. Last column indicates if observations are flare associated and describes radio wave classification, if known.

Q : quasi-periodic; P : periodic (as described by authors)

HF : 3 MHz - 30 MHz; VHF : 30 MHz - 300 MHz; UHF : 300 MHz - 3 GHz; μ : 3 GHz - 30 GHz; EHF : 30 GHz - 300 GHz.

HXRBS, HXIS, UVSP are hard X-ray and UV instruments on the SMM satellite.

train behaviour is described variously as periodic, quasi-periodic or as a sequence of spikes. Indeed Kiplinger (private communication 1984) has pointed out that, of the various criteria that any successful model of these oscillations must meet, one is certainly that the process is not an enduring one. Theory must be able to explain the termination of the pulses. Kiplinger also stresses two other observed features of the hard X-ray (and also microwave and γ-ray) pulse train phenomena; the source appears to be more or less stationary and the oscillations are very irregular. He feels a model must ascribe a time scale of the variations rather than a well-defined period. Indeed the phrase often used by observers to describe one phase of the motion (e.g., Trottet *et al.*, 1981) is *quasi-periodic*.

Are there any other observed features related to these oscillations and which could perhaps explain how they are generated? On this point observations differ. The source is suspected to be impulsive, perhaps a solar flare, as in the examples given by McLean and Sheridan (1973) and Kiplinger *et al.* (1983 a,b), but on the other hand Tapping (1978) and Gaizauskas and Tapping (1980) have reported bursts of oscillations with which there appears to be no associated flare activity. K.T. Tapping (1978; and private communication 1984) has attempted to correlate observed microwave oscillations with known solar activity. Though there appears to be some identification with the trailing part of a plage area, no strong correlations exist. On the contrary, not every flare exhibits oscillatory emission (V. Gaizauskas, private communication 1983).

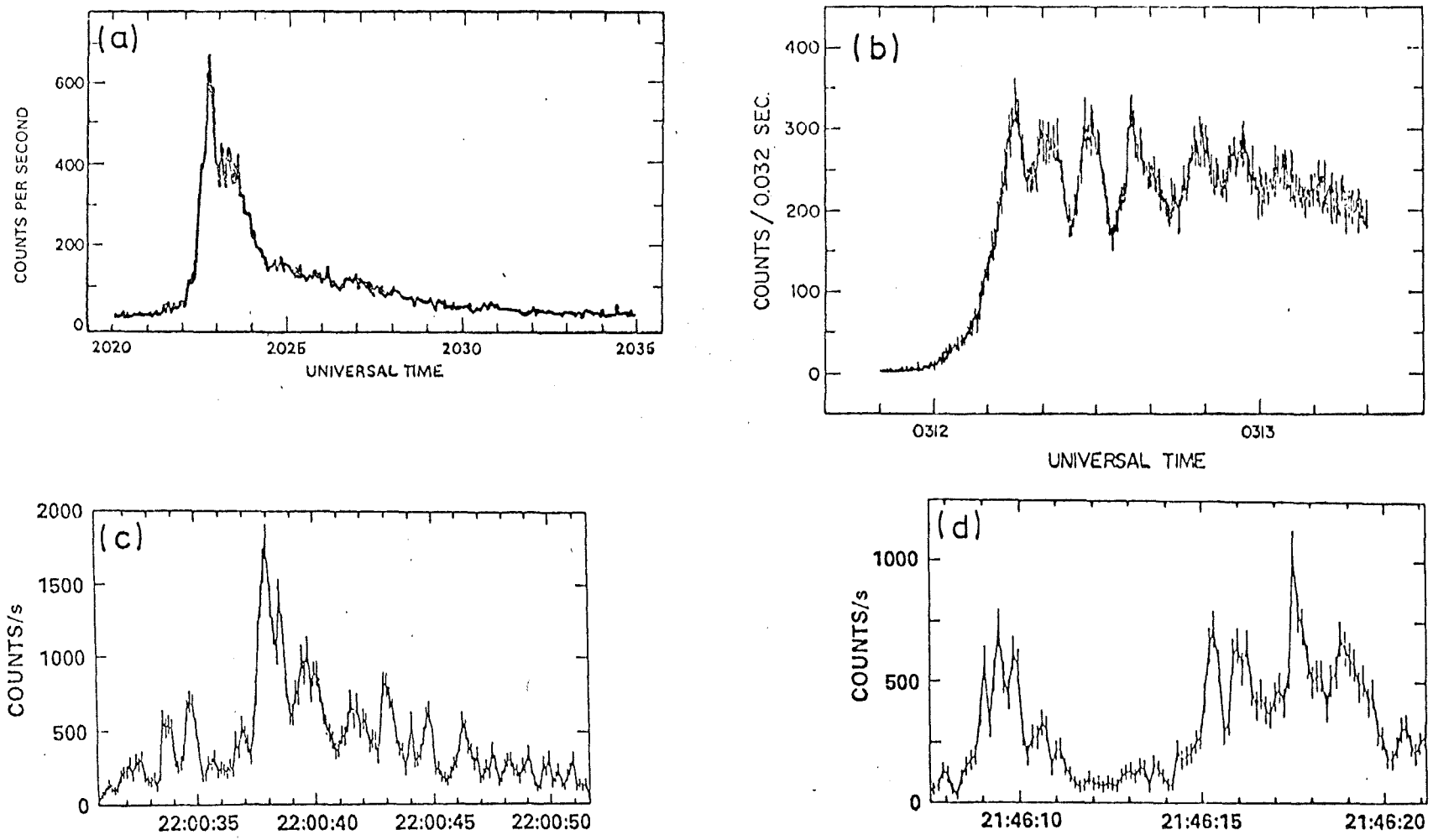

Figure 4.1 Examples of short period coronal oscillations. (a), (b), (c) and (d) show count rates of hard X-rays plotted against time. (a) and (b) are after Orwig *et al.* (1981) and Kane *et al.* (1983) respectively. (c) and (d) are after Kiplinger *et al.* (1983a). (e), (f), (g), (h) and (i) show intensity variation at radio wavelengths plotted against time and are after Pick and Trottet (1978), McLean and Sheridan (1973), McLean *et al.* (1971), Tapping (1978) and Rosenberg (1970), respectively. (Continued on next page.)

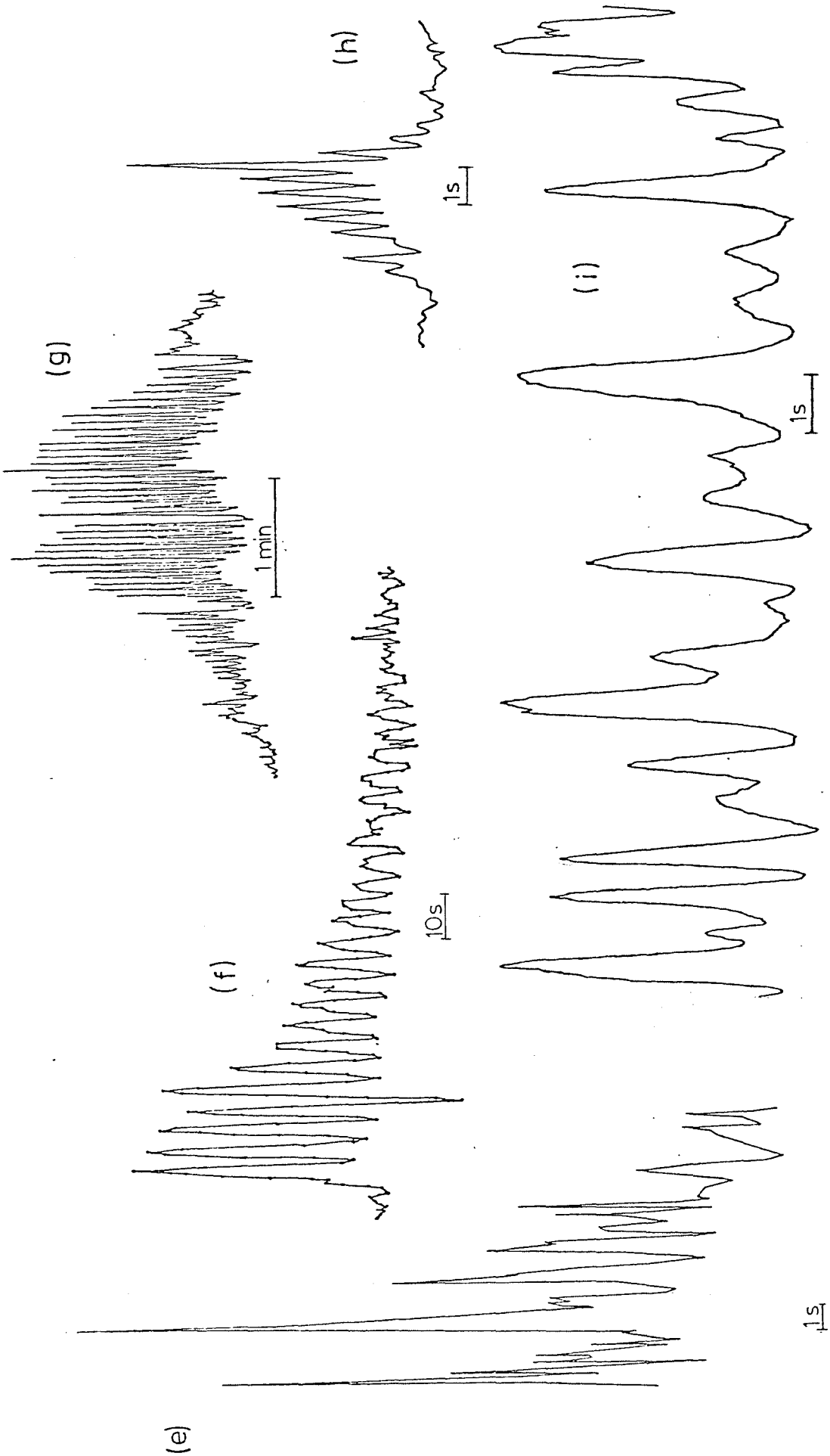

Figure 4.1 (cont.) Examples of short period coronal oscillations

4.1.2 Theories One of the early attempts to link the (then) scant observations with a theory of oscillations was made by Jensen (1957). He had no one particular solar feature in mind but examined 'the radial pulsations of a cylindrical tube of force embedded in stellar material and in temperature equilibrium with its (incompressible) surroundings'. The cylindrical case which Jensen considered corresponds to taking $k = 0$ and the body wave, $J_n(n_0 r)$, solution, in (3.13) and (3.17). In this case, for the lowest order symmetric mode, the radial velocity v_r is given by

$$v_r = \frac{(c_0^2 + v_A^2)}{\omega^2} J_0'(n_0 r) e^{i\omega t} = - \frac{(c_0^2 + v_A^2)}{\omega^2} J_1(n_0 r) e^{i\omega t}, \qquad (4.1)$$

where $n_0^2 = \dfrac{\omega^2}{(c_0^2 + v_A^2)}$, since $k = 0$.

Jensen then argued that for purely radial variation ($\partial/\partial\theta = \partial/\partial z = 0$) and zero pressure perturbation on the boundary with a field-free, incompressible fluid, div $\underline{v}$ would equal zero on that boundary. Using the Bessel function relations he deduced that the appropriate frequencies of such radial oscillations would be given by the zeros of the Bessel function J_0,

$$J_0(n_0 a) = 0,$$

that is, they would satisfy

$$\omega = \frac{(c_0^2 + v_A^2)^{\frac{1}{2}} j_n(0)}{a}, \qquad n = 1,2,3,\ldots . \qquad (4.2a)$$

Interestingly enough Rosenberg (1970) briefly considered a very similar model in a research note in which he reported (~ 1s) pulsations associated with Type IV solar radio emission. He, too, considered only radial pulsations (k = 0) and deduced that a standing wave of the form (4.1) would be produced, that is he considered a magnetic cylinder and neglected its exterior. So Rosenberg derived the equivalent of (4.2a) for $v_r' = 0$ on r = a, that is he considered amplitude maxima given by

$$\omega = \frac{(c_0^2 + v_A^2)^{\frac{1}{2}} j_n^{(1)'}}{a} \qquad n = 1,2,3,\ldots . \tag{4.2b}$$

where $j_n^{(1)'}$ are the zeros of the derivative of the J_1 Bessel function equal to 1.8, 5.3, etc. Assuming a tube radius of several thousand kilometers and field strengths of several to ten Gauss he was able to explain the short periods he had observed (see also Rosenberg, 1972).

In spite of (or perhaps because of!) its simplicity Rosenberg's 'theory' became the generally accepted model for coronal periodic pulsations. Observers believed that the sources of Type IV emissions were the 'magnetic tubes' of the corona and that the radio emission was modulated by the mhd oscillations of Rosenberg's theory. It did not prove to be the panacea for all observers' problems however. Pick and Trottet (1978), for example, found that Rosenberg's theory, if applied to their observations, would result in source sizes which were too large and it was not compatible with the intensity profile which they obtained (see Figure 4.1e).

Meerson *et al.* (1978), concerned that the plasma outside the tube was not taken into account in Rosenberg's model, considered the problem in more detail. Their discussion centred on a dispersion relation similar in form to (3.21) but assuming non-evanescent (radiating) modes in the cylinder's exterior (see Section 3.5). The problem then arose of how to explain the source of excitation of these modes in order to overcome the dissipationless (emissive) damping in the exterior plasma (see Equation (3.50)). Meerson *et al.* also noted that the dispersive effects, arising from the cylinder's environment, would lead to variations in ω, and therefore in the pulse period, and so were reluctant to abandon Rosenberg's theory with ω given by (4.2b) to explain strictly periodic pulsations. However, they did not consider the free modes of oscillation of coronal inhomogeneities given by dispersion relations such as (3.20) and (3.21). It will be shown in this chapter that free modes of oscillation, taking full account of the tube's exterior, can provide a means of explaining observed oscillatory behaviour, so Meerson *et al.'s* grounds for rejecting Rosenberg's theory were in fact false.

A quite different mechanism has been invoked recently to explain finite series of pulses such as those reported by Kiplinger *et al.* (1983 a,b) (see Figure 4.1 c,d). Vorpahl (1976) and Emslie (1981) have suggested that the pulse trains represent the successive firings of adjacent coronal loops, triggered by a propagating disturbance. However there are difficulties with such multi-loop models; they are inconsistent with the source being more or less stationary and they require a specific geometry of loops aligned

parallel to one another, more or less equally spaced, and spanning a north-south neutral line (Kiplinger, 1983b).

The diversity of periodicities, from seconds to minutes, occurring in coronal oscillation data is apparent from the above discussion. A theory which could explain the short ($\sim$ 1s) periods, both periodic and quasi-periodic motions, the finite (sometimes) recurring pulse trains and relatively compact source sizes was needed. As a result of discussions between B. Roberts and A.O. Benz the possibility of explaining these phenomena in terms of mhd coronal flux tube waves became apparent. This is the theme pursued in the following, the main principles of which (see Sections 4.4 and 4.5) have been published as Roberts, Edwin and Benz (1983, 1984).

4.2 The Coronal Loop Model

A description of the corona was given in Chapter 1. A magnetically dominated region, it consists of both 'open' and 'closed' loops of varying sizes which are often twisted and are hot and dense. The loops may have cool cores and it is thought that brightness variations over loops imply density variations. Not all these observed properties can be incorporated into a model which is mathematically simple enough to exhibit the wave-like phenomena associated with the corona. Here the effects of gravity (not so important for a region of scale $\gtrsim 3 \times 10^3$km above the photosphere), curvature (more important for closed loops) and twist (important in knowing if an equilibrium exists) will be neglected, save for a

brief discussion of curvature effects in Section 4.8. Since transverse dimensions are usually much smaller than longitudinal ones, the loop will be modelled by a straight cylinder and the inhomogeneity will be one of either density or temperature. Since the magnetic field dominates, the flow of heat is principally along the field lines and lateral temperature inhomogeneities are readily maintained. Only adiabatic, linear oscillations will be considered. For simplicity of presentation attention will concentrate on a density inhomogeneity, though magnetic field inhomogeneities could equally well be present. Variations in density across the inhomogeneity will be considered later. The case of an open loop containing a neutral sheet above, say, a 'post-flare' loop, will be discussed in Chapter 7.

In the basic state the density inhomogeneity is presumed to take the form of a uniform, magnetic cylinder in an otherwise uniform magnetic environment (see Figure 3.1). Since $\beta << 1$ in the corona, the appropriate picture of wave modes in a cylindrical inhomogeneity is that given by Figure 3.4. To be more precise, and for ease of reference, a diagram with the same qualitative features appears as Figure 4.2. In comparison with Figure 3.4, the sound speeds have been interchanged so that a high density inhomogeneity is represented in Figure 4.2.

It must be emphasized that the only modes considered in Chapters 2 and 3, and therefore those being discussed here, are *free* modes of oscillation. This arises from the insistence that $m_e^2 > 0$ (see Section 3.5) so that only real frequency ω and wavenumber k are

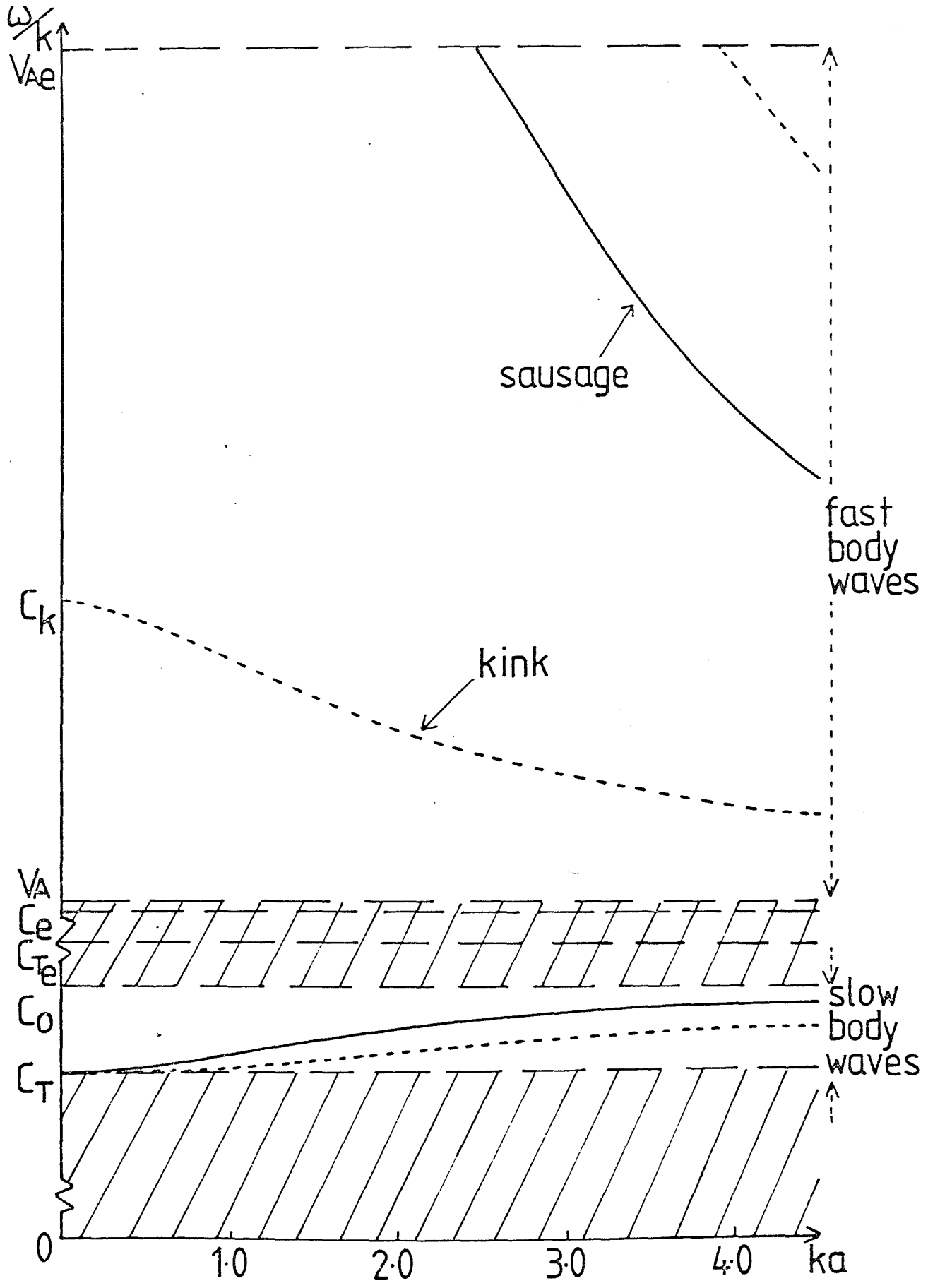

Figure 4.2 The phase-speed as a function of ka ($k > 0$) for the case of a high density coronal loop in a uniform magnetic field ($\rho_0 >> \rho_e$, $B_0 = B_e$). Here $v_{Ae} = 3c_0$, $v_A = 2c_0$ and $c_e = 1.5c_0$. Only two of the infinitely many slow body waves are shown.

considered and there is no radial propagation outside the loop. It can be seen from Table 2.2 that for a low β plasma these modes can only arise for a loop with an Alfvén speed that is *lower* than in its surroundings. If $v_{Ae} < v_A$ the fast waves are necessarily radiative with complex k or ω. So in terms of density it means that only high density loops can oscillate freely (that is, without radiating energy to infinity) in the fast magnetoacoustic mode. Motions in the environment of the coronal loop arise merely as a result of those confined to the loop: the loop acts as a wave duct trapping the fast mhd oscillations, which penetrate only a small distance into the environment. This idea of ducted fast (but non-dispersive) waves was also used in a dipole model by Habbal *et al.* (1979).

4.3 Coronal Body Waves

Figure 4.2 shows that for this density configuration no surface waves occur but that there are two classes of body waves which, because the sound and Alfvén speeds differ by an order of magnitude, have widely separated frequencies. One class of oscillations has slow, acoustic time scales, for both kink and sausage modes, and the waves are only mildly dispersive. In a low β plasma the tube speed c_T is close to the sound speed c_0 so the phase-speeds of both these slow modes are given (to a good approximation, provided ka is not too large) by

$$\frac{\omega}{k} = c_T. \qquad (4.3)$$

On the other hand, the Alfvénic time scales $v_A < \omega/k < v_{Ae}$ of the fast oscillations differ and, especially for a high density, low Alfvén velocity cylinder, the waves are highly dispersive (barring the fundamental kink mode).

Figure 4.2 may be interpreted as a picture of the wave modes in an inhomogeneous corona where regions of low Alfvén speed (*high* density) act as wave ducts and trap the fast magnetoacoustic modes. If this coronal loop is closed so that its footpoints are anchored in the high density chromosphere/photosphere, then standing modes may occur.

On the other hand, propagating waves are possible in both closed and open field regions provided the wavenumber k is larger than its cut-off value. Of the fast waves both sausage and kink modes possess cut-offs, except for the principal kink mode (see Figure 4.2) which has phase-speed (for ka not too large) of

$$\frac{\omega}{k} = c_k, \tag{4.4}$$

where c_k is given by (3.24). Like the c_T modes of Equation (4.3) this oscillation exists for all k.

The cut-offs of the sausage modes are easily determined from Equation (3.40). At cut-off $\omega^2/k_c^2 \simeq v_{Ae}^2$, so that propagation is possible only for wavenumbers $k > k_c$, where

$$\text{sausage:} \qquad k_c = \left[\frac{(c_0^2 + v_A^2)\ (v_{Ae}^2 - c_T^2)}{(v_{Ae}^2 - v_A^2)(v_{Ae}^2 - c_0^2)}\right]^{\frac{1}{2}} \left(\frac{j_s^{(0)}}{a}\right), \quad s = 1,2,3,\ldots . \tag{4.5}$$

and $j_s^{(0)} = (2.40, 5.52, \ldots)$ are the zeros of the Bessel function J_0.

Similarly, the cut-offs of the higher harmonics of the kink modes may be determined from the appropriate dispersion relation (3.42). This time $j_s^{(1)}$, the zeros of the Bessel function J_1, arise; the kink wavenumber cut-offs are given by

$$\text{kink:} \qquad k_c = \left[\frac{(c_0^2 + v_A^2)(v_{Ae}^2 - c_T^2)}{(v_{Ae}^2 - v_A^2)(v_{Ae}^2 - c_0^2)}\right]^{\frac{1}{2}} \left(\frac{j_s^{(1)}}{a}\right), \qquad s = 1,2,3,\ldots . \tag{4.6}$$

The standing waves of closed loop situations will be considered first.

4.4 Standing Waves in a Coronal Loop

For a coronal loop of length L with its footpoints anchored in the dense chromosphere/photosphere both the slow and fast waves may occur as standing modes. Assuming that longitudinal perturbations at the ends of the loop $z = 0$ and $z = L$ are zero, then the wavenumber k is given by

$$k = j\pi/L, \tag{4.7}$$

for integers $j = 1,2,3,\ldots$.

So, using (4.3), the period, $\tau_s \equiv 2\pi/\omega$, of the slow (sausage and kink) mode, which does not exhibit cut-off, is:

$$\tau_s = 2L/jc_T. \tag{4.8}$$

The integer j determines the number of nodes (j-1) in the oscillation along the loop. Generation of a standing mode for a particular j, to the exclusion of all the others, may be difficult in practice. Presumably it will be the lower modes which are the easier to excite. $j = 1$ corresponds to the apex $z = L/2$ of the loop being disturbed. If j were equal to 2 the apex would be a node. Observationally, such details are presently unknown. For coronal conditions in which $v_A >> c_0$, c_T is approximately equal to c_0 and so (4.8) becomes, with $j = 1$;

$$\tau_s = 2L/c_0. \qquad (4.9)$$

For example, with a coronal sound speed of 200 km s^{-1} and a loop length of, say, 2×10^4 - 10^5km, (4.9) yields a period of order 200-1000 s.

Švestka *et al.* (1982) reported a giant magnetic arch having an associated 20 min period but a correspondence with him (supplied directly to B. Roberts) revealed that it was not a loop anchored in the chromosphere (see also Švestka, 1983). The quasi-periodic variations occurred not in the arch but below and above it. Cribbens and Matthews (1969) cite fourteen examples with periods from 10 to 500 s. The resolution of their data was only 2s and evidence of long period waves, rather than wave-packets of shorter periods, is not clear. Tsubaki (1977) reported oscillations in the 5303Å FeXIV coronal line with periods of approximately 300s which he suggested were the well-known 5 min oscillations penetrating into the corona.

Returning now to Figure 4.2, the fast $v_A < \omega/k < v_{Ae}$ modes in a dense loop may also be considered as standing waves. The fundamental kink mode given by (4.4) has a period τ_f (for $j = 1$) of

$$\tau_f = \frac{2L}{c_k} = \frac{2(1 + \rho_e/\rho_0)^{\frac{1}{2}} L}{(v_A^2 + \rho_e/\rho_0 v_{Ae}^2)^{\frac{1}{2}}} , \qquad (4.10)$$

where expression (3.24) for c_k has been used. If the loop is supposed to be very much denser than its surroundings so that $\rho_0/\rho_e >> 1$, and if $B_0 \simeq B_e$ then

$$\tau_f = \sqrt{2}\ L/v_A . \qquad (4.11)$$

For an Alfvén speed of $\sim$ 2000 km s^{-1} and a loop length of $L = 10^5$km this results in a period for the fast kink mode of $\sim$ 70s. There are several examples of observations of periodic pulsations with time periods of this order. Comparisons with them is easier if (4.10) is expressed in terms of electron density, N_0, and in cgs units. From (4.11), for $v_A = B_0(4\pi N_0 m_p)^{-\frac{1}{2}}$, where m_p is the proton mass (1.673×10^{-24}g), the period is

$$\tau_f = 6.5 \times 10^{-12} \frac{L\ N_0^{\frac{1}{2}}}{B_0} . \qquad (4.12)$$

Trottet *et al.* (1979) reported quasi-periodic pulsations at 169 MHz of a double source associated with a Type IV radio burst. The period was of the order of 1 min.

Cliver *et al.* (1976) tabulate examples of quasi-periodic bursts, fifteen of their own observed at 2.8 GHz, plus another twenty-two gathered from the literature. They identify two distinct sub-classes, those with periods of 10-50s and those with periods $\gtrsim$ 180s. However there is doubt as to whether the 2.8 GHz recordings are of true periodic phenomena or, as the authors suggest, they are due to random flaring of several bright points.

Another observational study by Koutchmy *et al.* (1983), in which the green coronal line 5303 Å of Fe XIV was used to search for short period coronal waves, gave evidence of 43, 80 and 300s periods. Using the values $N_0 = 2.5 \times 10^8 cm^{-3}$ and $L = 1.2 \times 10^{10} cm$ (which Koutchmy *et al.* give) in Equation (4.12), results in a period of 80s if $B_0 = 15G$. A similar interpretation but in terms of Alfvén waves has been given by the authors.

A rare (recorded only once in 250 hours of observing) 5.6 minute oscillation in a loop prominence was reported by Strauss *et al.* (1980). If the values of $L = 1.6 \times 10^{10} cm$ and $N_0 = 2 \times 10^{10} cm^{-3}$, which the authors give, are substituted into (4.12), the observed period results for a field of 44 G. Again, a similar explanation in terms of Alfvén waves was given by Strauss *et al.*

A.O. Benz of ETH Zurich supplied Figure 4.3, which is also reproduced in Roberts *et al.* (1984). It shows seven slow, quasi-periodic pulsations separated by about 40s observed in the 400-800 MHz range. Benz points out that the fact that no drifts are observed can be interpreted as a simultaneous oscillation (a free mode) of the whole loop. Presuming a density and length of arch

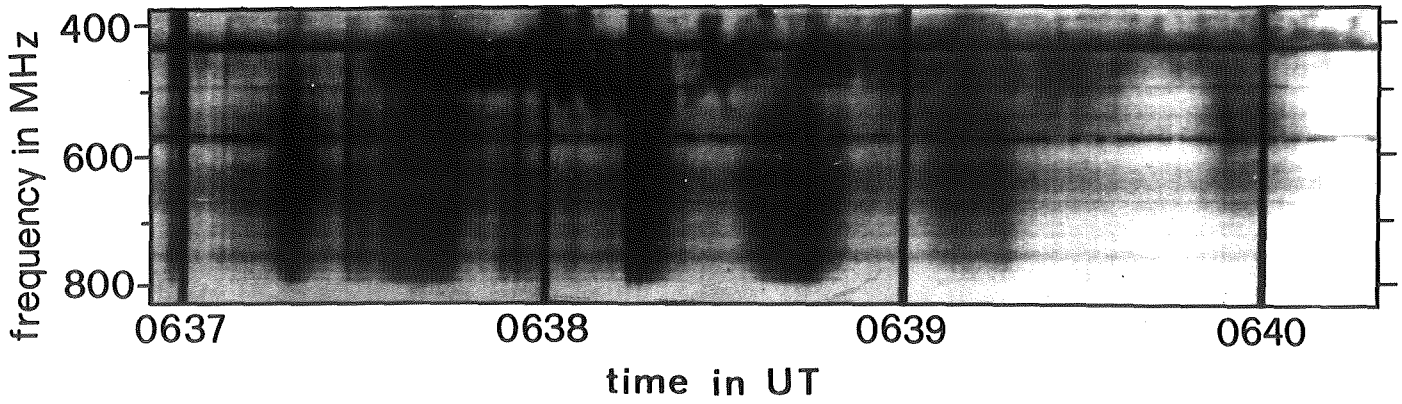

Figure 4.3 Dynamic spectrum of 1980 April 3 from the Daedalus analog spectrograph (courtesy of A.O. Benz). Enhanced radio flux is shown bright. Horizontal lines are caused by terrestrial interference; vertical lines are minute marks. Seven slow, quasi-periodic pulsations separated by about 40s are shown. Short period oscillations are possibly superposed on the long period modulation.

similar to those given by Koutchmy *et al.* (1983), as described above, would yield, from Equation (4.12), the observed period for $B_0 \sim 30G$. (A smaller magnetic field value results if it is assumed that a node occurs at the top of the arch, so that $j = 2$ applies.)

There are of course fast sausage and kink modes other than the fundamental kink mode just discussed; the fast modes possess cut-offs, given by (4.5) and (4.6). It is doubtful if such waves would be excited as standing waves for the following reasons. The period of the lowest fast sausage mode that is first permitted as a free oscillation ($k > k_c$) may be estimated by fixing the frequency, thus:

$$\omega = kc_k. \tag{4.13}$$

(It will not differ too greatly; see Figure 4.2). However, for $ka \sim 1$, (4.7) yields

$$j \sim L/\pi a. \tag{4.14}$$

This mode will therefore only arise if j is sufficiently large. If it were excited it would have a period (from (4.13)) of

$$\tau_f' = \frac{2L}{c_k j} \sim \frac{2\pi a}{c_k} = \frac{2\pi a(1 + \rho_e/\rho_0)^{\frac{1}{2}}}{(v_A^2 + \rho_e/\rho_0\ v_{Ae}^2)^{\frac{1}{2}}}. \tag{4.15}$$

Thus (4.15) is related to (4.10), the expression for τ_f, by a factor $\pi a/L$. For coronal loops with transverse dimensions smaller than longitudinal ones, a/L is of the order of 10^{-2}, say, which means τ_f' is of the order of 1s. Thus $\tau_f' < \tau_f < \tau_s$. Such short period waves

certainly have been observed in the corona, as is shown in Table 4.1. However, it is unlikely that j will satisfy (4.14) (for $a/L \sim 10^{-2}$) to the exclusion of the other lower order modes. An alternative, more plausible mechanism for explaining extremely short period coronal pulsations is by means of propagating rather than standing waves. This will be given next.

4.5 Impulsively Generated Modes

Propagating, rather than standing, waves will result whenever disturbances are initiated impulsively, say, by a solar flare, which may act as a single or multiple source of the disturbance. Alternatively, there may be other less energetic sources generating the waves. The waves may arise either in a closed coronal loop, if the motions have insufficient time to reflect from the far ends of the loop, or in open field regions.

To simplify the discussion and interpretation of these propagating waves, it will be assumed that the plasma is cold. This is reasonable for the low β corona, and involves no loss of essential physics as far as the fast modes are concerned. Mathematically, it means that $c_0 = c_e = 0$ in Figure 4.2 and just the fast band of body waves remains. It was noted earlier (Equations (2.55), (2.56) and (3.48)) that these fast mhd waves are analogous to the Love waves of seismology and the Pekeris waves of oceanography. The fast sausage waves in particular have a dispersion relation given by (3.40) with $c_e = c_0 = 0$, which for a cylindrical structure of large radius

(see (3.48a)) reduces to

$$\tan(n_0 a - \pi/4) = - n_0/m_e, \tag{4.16}$$

where here $n_0 = (\omega^2 - k^2 v_A^2)^{\frac{1}{2}}/v_A$ and $m_e = (k^2 v_{Ae}^2 - \omega^2)^{\frac{1}{2}}/v_{Ae}$. Except for the phase-shift of $\pi/4$, (4.16) is identical to the dispersion relation given by Pekeris (1948) for the propagation of explosive sound in shallow water. (In fact, for the slab case the equations are identical.)

For the highly dispersive fast body waves of Figure 4.2, the dependence of ω on k is significant and is described by the dispersion relation (3.40), with $c_e = c_0 = 0$. If waves are generated impulsively, then the resulting disturbance ϕ may be represented as a Fourier integral over all frequencies ω and wavenumbers k. In general a wavepacket results. For example, if ω is related to k from (4.16) by $\omega = \pm W(k)$, then for an initial impulse of the form $\phi = \phi_0(z)$, $\frac{\partial \phi}{\partial t} = \phi_1(z)$ at $t = 0$, ϕ is given by

$$\phi = \int_{-\infty}^{\infty} F_1(z) e^{ikz - iW(k)t} dk + \int_{-\infty}^{\infty} F_2(z) e^{ikz + iW(k)t} dk, \tag{4.17}$$

where F_1 and F_2 are related to ϕ_1 and ϕ_0 through their Fourier transforms. For example, a delta function impulse $\phi_0 = \delta(z)$, $\phi_1 = 0$ gives $F_1 = F_2 = 1/4\pi$. ϕ is also implicitly a function of r and thus is related to $\hat{R}$ of Equation (3.11), and the other variables of the problem, by the boundary conditions.

Though (4.17) gives the formal Fourier integral solution, in practice the integrations are not possible and detailed physical interpretations of the solutions are difficult. The main features of these dispersive waves, however, may be understood by considering the asymptotic nature of (4.17) for large z and t, say for $t \to \infty$ with z/t held fixed. Integrals of the form (4.17) may then be expressed as

$$\phi(z,t) = \int_{-\infty}^{\infty} F(k) e^{-i\chi t} dk \qquad (4.18)$$

where $\chi(k) = W(k) - kz/t$, and evaluation of the asymptotic behaviour by the method of stationary phase (steepest descents) (e.g., Whitham, 1974; Bender and Orszag, 1978) is then possible. Theory dictates that for large t the main contribution to (4.18) comes from the neighbourhood of stationary points k = K such that

$$\chi'(K) = W'(K) - z/t = 0. \qquad (4.19)$$

Otherwise the contributions oscillate rapidly and make little net contribution. So for stationary points K

$$\phi \sim \sum_{\substack{\text{stationary} \\ \text{points } K}} F(K) \sqrt{\frac{2\pi}{t|W''(K)|}} \exp\left\{iKz - iW(K)t - \frac{i\pi}{4} \operatorname{sgn} W''(K)\right\}, \qquad (4.20)$$

where K(z,t) satisfies (4.19). It must be noted that if $W''(K) \equiv 0$, then W'(K) is constant. In general there are no stationary points

and the whole asymptotic analysis is different. However, as will be seen shortly, $W''(K) \neq 0$ in the case of waves satisfying (3.40), but does equal zero for a stationary point K. Then the correct behaviour of (4.18) is described by taking higher order terms in the Taylor expansion of χ and as a result the main contribution to the integral (see Pekeris, 1948; Whitham, 1974) is

$$\left(\frac{1}{3}\right)!\ 3^{5/6}2^{1/3}\ \frac{F(K)}{(t|W'''(K)|)^{1/3}}\ \exp\{iKz - iW(K)t\}. \qquad (4.21)$$

For a stationary point K, (4.20) may be written in the form

$$\phi \sim A(z,t)e^{i\psi(z,t)} \qquad (4.22)$$

where $A(z,t) = F(K)\sqrt{\frac{2\pi}{t|W''(K)|}}\ e^{-(\pi i/4)\mathrm{sgn}W''(K)}$ and $\psi(z,t) = zK(z,t)$ $- t\omega(z,t)$. Thus (4.22) describes an oscillatory wave train with ψ giving the variation between local maxima and minima. However, since A, K and ω are not constant the wave train is not uniform. The distance and time between successive maxima and the amplitude are not constant.

Since $\omega = \pm W(k)$, (4.19) defines the group velocity $c_g \equiv d\omega/dk$ at $k = K\ (= W'(K))$. It is obvious from (4.20) that extrema, $W'' = 0$, of the group velocity function are important, since then (4.21) must be invoked instead of (4.20).

A typical group velocity plot for the lowest order sausage

mode of dispersion relation (3.40) with $c_e = c_0 = 0$ (essentially (4.16)) is shown in Figure 4.4. Since it has a minimum there is a point where $W''(k) = 0$. Consider the lowest order fast sausage mode of Figure 4.2. If at time $t = 0$ a pulse is generated at a point source $z = 0$, say, then it is composed of all frequencies, and the wave observed at large distance $z = h$ from the source, on the basis of the group velocity curve Figure 4.4, evolves through a sequence of events as follows. Near cut-off the wave has wavenumber k_c given by (4.5) (with $c_e = c_0 = 0$) and so a signal from $z = 0$ arrives at $z = h$ with a frequency

$$\omega_c = k_c v_{Ae}, \tag{4.23}$$

having taken a travel time of $t = h/v_{Ae}$. This marks the start of a *periodic* phase. As time progresses the frequency and amplitude of this nearly sinusoidal wave grow slowly until a time h/v_A when high frequency information arrives from the source. So a new train of high frequency waves, due to the right-hand branch of the group velocity curve, is superimposed on those arriving from the left-hand branch. The result is a strong increase in amplitude and the oscillation becomes quasi-periodic (see (4.22) where the amplitude varies inversely as the square root of the slope of the group velocity curve). During this *quasi-periodic* phase the frequency of the 'v_A' wave decreases and that of the 'v_{Ae}' wave continues to increase (see Figure 4.4) until at a time $t = h/c_g^{min}$, where c_g^{min} is the minimum group velocity, they coincide. The disturbance then consists of the single frequency ω^{min} (see Figure 4.4) and, though the disturbance

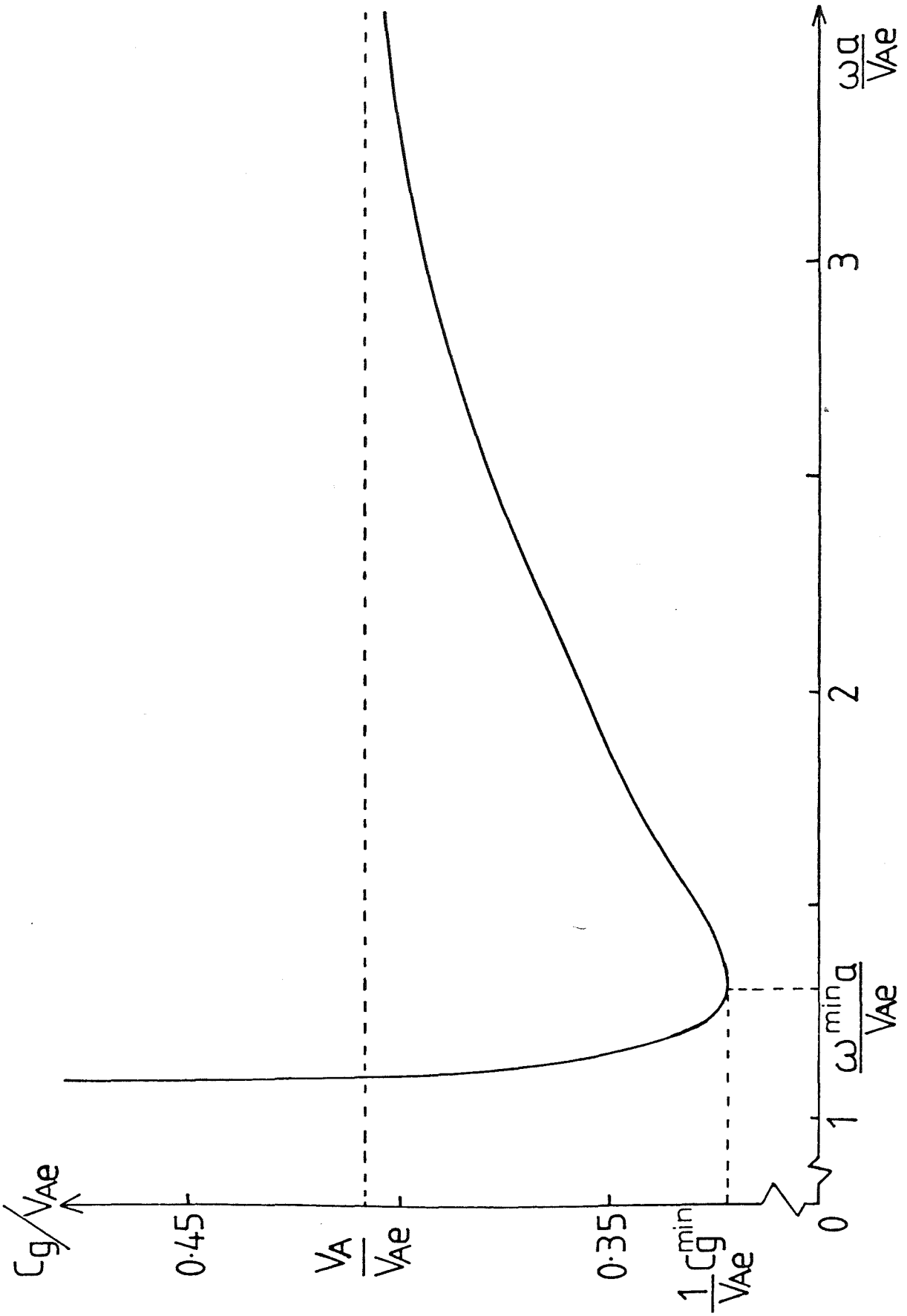

Figure 4.4 The group velocity $c_g = d\omega/dk$ in units of the external Alfvén speed v_{Ae} as a function of dimensionless frequency $\omega a/v_{Ae}$, for the lowest order fast sausage wave of Figure 4.2, in the low β limit. Here $\rho_0/\rho_e = 6$. The occurrence of a minimum in c_g at the dimensionless frequency $\omega^{min} a/v_{Ae}$ is shown.

continues to oscillate with this constant frequency, the amplitude declines rapidly according to (4.21) ($W(K) = \omega^{min}$) in the *Airy* or *decay* phase.

The foregoing description of these distinct phases has been rather heuristic since only the group velocity, c_g, has been calculated to construct Figure 4.4. The group velocity is given explicitly by

$$G = \frac{c_g}{v_{Ae}} = \frac{2D_1V^2K_1J_0 + \hat{W}^2D_3XK_0J_0 - 2D_2VK_0J_1}{\hat{W}[2D_1K_1J_0 + D_3XK_0J_0 - 2D_2VK_0J_1 - \frac{D_1D_2D_3X}{V}K_1J_1]}, \quad (4.24)$$

where $V = \frac{v_A}{v_{Ae}}$, $X = ka$, $\hat{W} = \frac{\omega}{kv_{Ae}}$, $D_1 = (1-\hat{W}^2)^{\frac{1}{2}}$, $D_2 = (\hat{W}^2-V^2)^{\frac{1}{2}}$, $D_3 = (1-V^2)$, and the J and K Bessel functions have arguments n_0a and m_ea, respectively. The higher order derivatives corresponding to dispersion relation (4.16) have been calculated by Pekeris (1948) for oceanographic studies and the corresponding formulae (4.20) and (4.21) evaluated. Thus the behaviour at a location $z = h$ from the source is well-known (Ewing *et al*, 1957; Brekhovskikh, 1960; Tolstoy, 1973; Kennett, 1983) and the sequence of phases described above can be illustrated as in Figure 4.5.

Impulsively generated fast sausage waves, then, exhibit both periodic and quasi-periodic signatures. The evolution of a disturbance generated impulsively, perhaps by a flare, described in Figure 4.5 thus resembles the pulsations recorded in the radio data (see Figure 4.1 and also Table 4.1). This led to the suggestion,

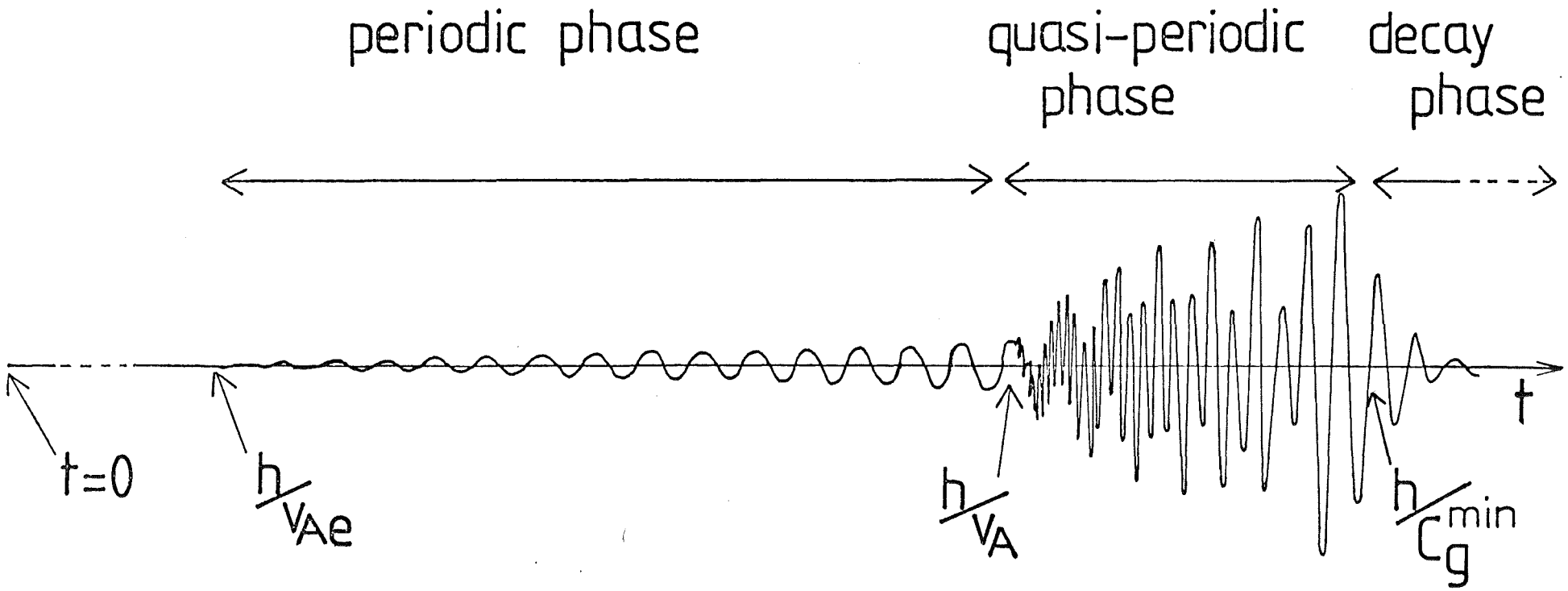

Figure 4.5 A sketch of the evolution of the fast sausage wave in the low β extreme ($c_0, c_e << v_A, v_{Ae}$) showing the various phases in the disturbance as recorded at an observation level z = h away from an impulsive source at z = 0. (A similar sketch has been given by Pekeris (1948) in his discussion of waves in an ocean layer.)

put forward in Roberts *et al*, (1983), that radio pulsations may be produced by fast magnetoacoustic waves propagating in a dense region of the corona. Briefly, the suggested mechanism is as follows. A free mode of oscillation of the (open or closed) loop in which particles are trapped disturbs the equilibrium situation and affects the energy level of the plasma waves. The sausage mode in particular (see Figure 2.4) locally changes the magnetic field strength and thus the orbits of the trapped particles. The mhd oscillation effectively moves the particles in and out of (loss-cone) instability. Kuijpers (1974) has proposed that loss-cone instability of energetic electrons is the origin of plasma waves. In turn, Benz and Tarnstrom (1974) have associated Type IV emission with high frequency plasma waves.

In order to draw comparison with theory the particular frequencies and time scales associated with Figure 4.5 must be identified. The frequency representative of the periodic phase is given by (4.23) by substituting k_c from (4.5) [with $c_0 = c_e = 0$ and $s = 1$ for the lowest order sausage mode]. In terms of period this means that for the periodic oscillations, $\tau_c = 2\pi/\omega_c$ is given by

$$\tau_c = \frac{2\pi a}{j_1^{(0)} v_{Ae}} \left(\frac{\rho_0}{\rho_e} - 1\right)^{\frac{1}{2}} = \frac{2\pi a}{j_1^{(0)} v_A} \left(1 - \frac{\rho_e}{\rho_0}\right)^{\frac{1}{2}}, \qquad (4.25)$$

where the low β version of (3.16) has been used to relate ρ_e and ρ_0 (i.e., $\rho_0 v_A^2 \simeq \rho_e v_{Ae}^2$). For a dense inhomogeneity ($\rho_0 >> \rho_e$),

$$\tau_c \simeq \frac{2\pi a}{\left(j_1^{(0)} v_A\right)} \simeq 2.6\left(\frac{a}{v_A}\right); \qquad (4.26)$$

τ_c is never greater than this value and for typical coronal values of a and v_A, τ_c may be small, perhaps of the order of a second. Coincidentally, Rosenberg's (1970) argument for explaining short period puslations (see Equation (4.2b)) gives periods in agreement with (4.26) . However the theory presented here, unlike Rosenberg's, takes full account of the loop's exterior, and because free modes of oscillation have been considered there is no requirement for an energetic source to maintain radiating waves, as Meerson *et al.* (1978) suggested.

To illustrate (4.26) numerically, taking $N_0 = 10^9 cm^{-3}$, $B_0 = 40G$ and a tube of diameter $2 \times 10^3 km$ gives τ_c as 0.94 s. It must be noted that ω_c, the frequency of the periodic phase, is the smallest frequency in the impulsively generated disturbance and so τ_c is the largest periodicity, small as τ_c may in fact be. Thus many of the reported short period pulsations (Table 4.1) can be explained in terms of an impulsively generated fast sausage wave propagating in a dense coronal inhomogeneity.

The other important frequency is that representative of the quasi-periodic phase. ω^{min}, which characterizes the frequency at the end of the quasi-periodic phase, is sketched in Figure 4.6 as a function of $(\rho_0/\rho_e)^{\frac{1}{2}}$. The associated period, $\tau^{min} \equiv 2\pi/\omega^{min}$, is smaller than τ_c and so rapid oscillations occur during the quasi-

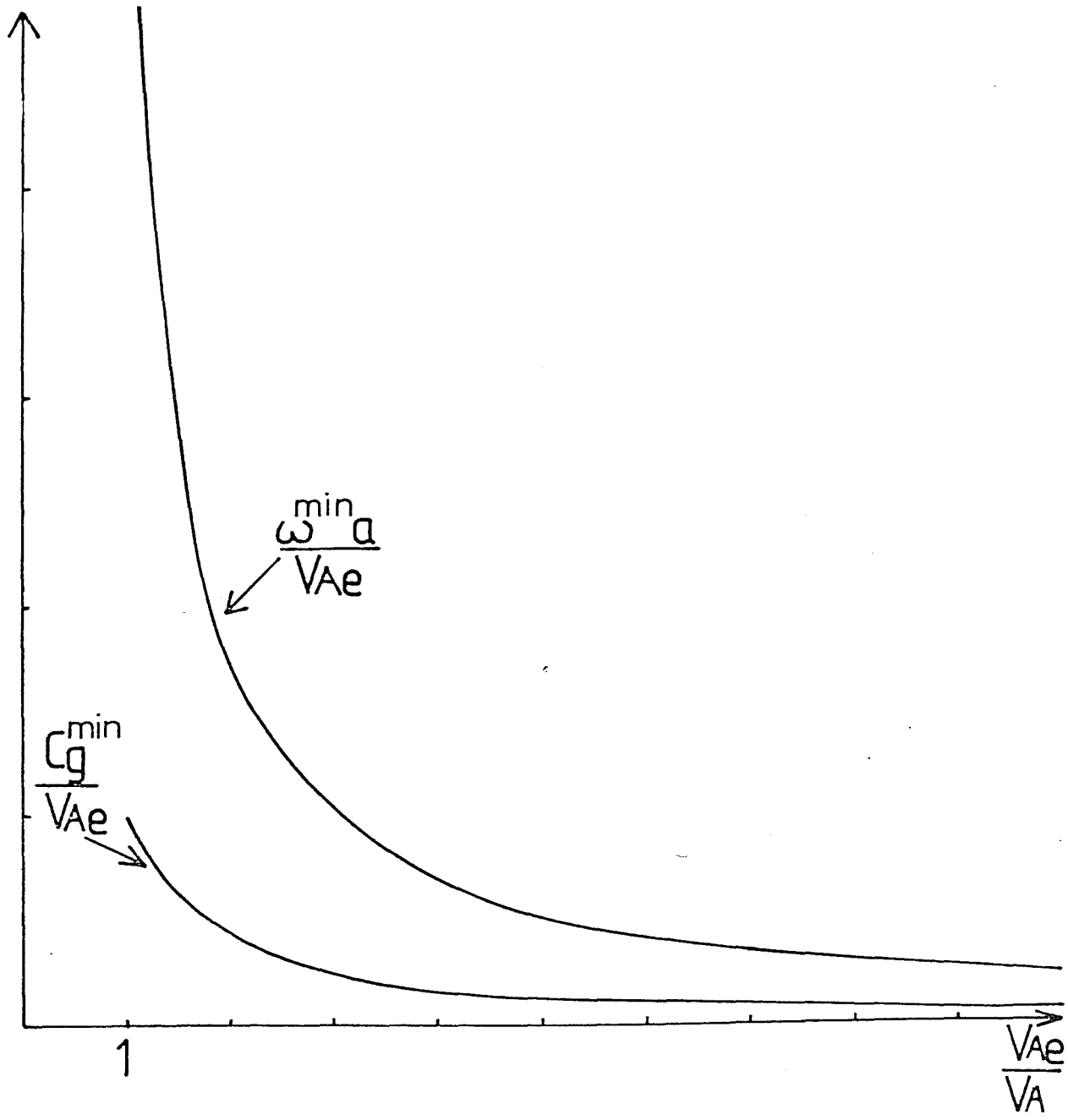

Figure 4.6 The variation of the minimum in the group velocity and the frequency ω^{min} at which it occurs, with $v_{Ae}/v_A = (\rho_0/\rho_e)^{\frac{1}{2}}$. ($c_g^{min}$ is in units of v_{Ae}, ω^{min} is in units of v_{Ae}/a.)

periodic phase, as indeed observational data reveals (see Table 4.1 and Figure 4.1). Figure 4.6 also shows the behaviour of the minimum in the group velocity, c_g^{min}, with the parameter $(\rho_0/\rho_e)^{\frac{1}{2}} = v_{Ae}/v_A$, a measure of the inhomogeneity.

Apart from the periodicities there are the time scales associated with the durations of the periodic and quasi-periodic phases. Observational determination of the onset of the periodic phase is expected to be difficult because the lower amplitude oscillations may be lost in background noise; but the quasi-periodic phase is theoretically distinctive (Figure 4.5) and so comparisons with estimates of its duration and observed signals of similar form should be possible (see Figure 4.1). Figure 4.7 shows a graph of the duration time

$$T_{dur} = h\left[\frac{1}{c_g^{min}} - \frac{1}{v_A}\right] \qquad (4.27)$$

plotted against the frequency ω^{min} attained at the end of the quasi-periodic phase. The duration time of the quasi-periodic phase decreases with increasing frequency (decreasing periodicity). Superimposed on this graph are the results of Tapping (1978) who, coincidentally, plotted duration times against pulse repetition rates (effectively frequency). Figure 4.7 shows good agreement between observation and theory, given the uncertainties in the observational determination of physical parameters (e.g., the distance h). The construction of a log-log plot shows that the variation is

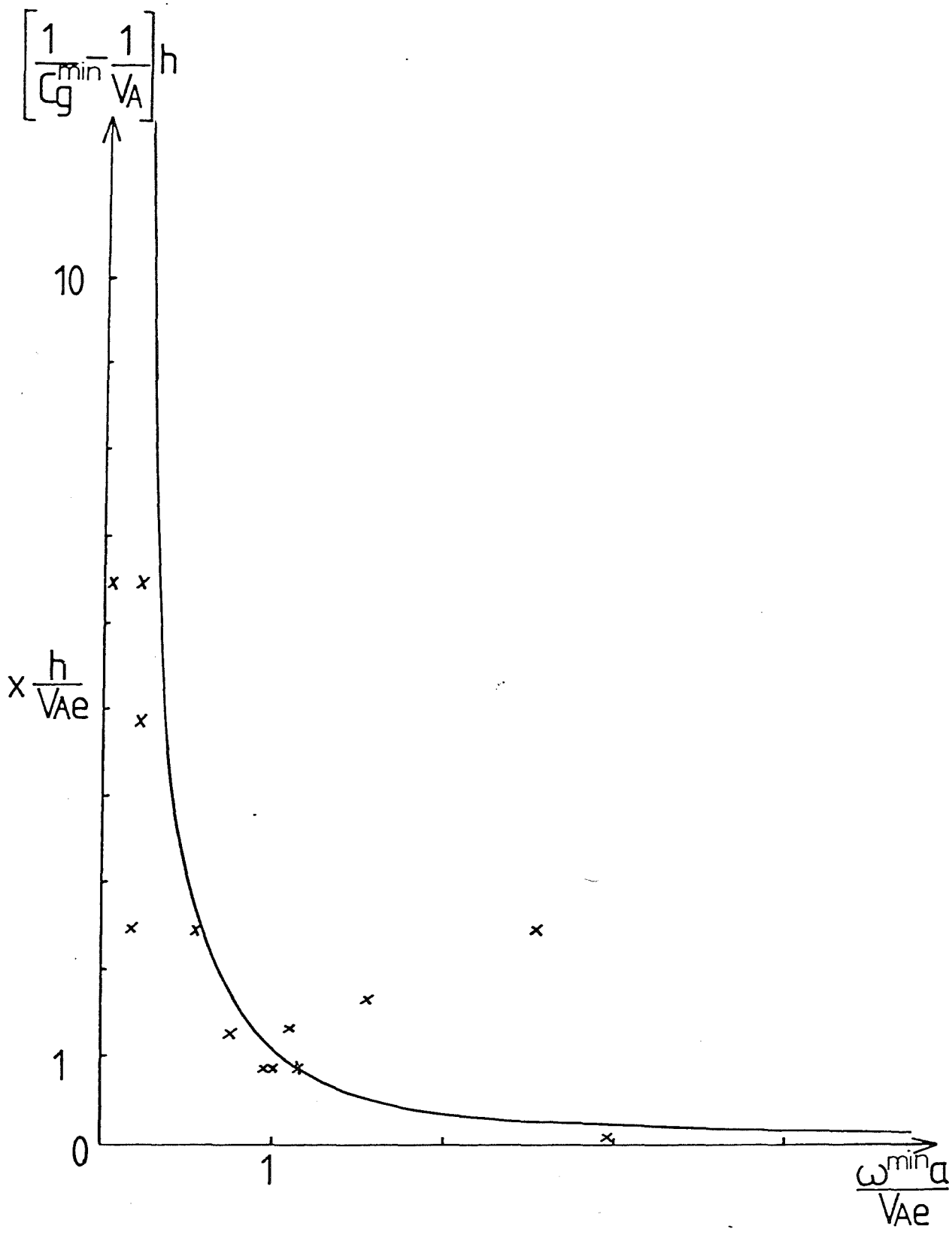

Figure 4.7 The variation of the duration time, $T_{dur} = h(1/c_g^{min} - 1/v_A)$, of the quasi-periodic phase with $\omega^{min}a/v_{Ae}$. The duration time is given in units of h/v_{Ae}, where h is the distance of the observation level from the source. x : data points from Tapping's (1978) record of metre wavelength pulsating bursts during the 1972 May 21 solar noise storm.

of the form $T_{dur} \sim (\omega^{min})^{-1.7}$ for the cylinder ($T_{dur} \sim (\omega^{min})^{-1.4}$ for a slab geometry).

In Roberts *et al.* (1984) the above theory is compared to the observations of McLean *et al.* (1971) (Figure 4.1g and entry 5 of Table 4.1) who recorded a series of about 50 regular pulses, the period of which changed slowly from 2.5s to 2.7s during the 150s of observed pulse train. A large flare was reported some 25 minutes earlier which may have initiated other impulses, say 5 minutes, before the start of the quasi-periodic phase. This would be the time h/v_A of Figure 4.5, which is compatible with $v_A = 1000$ kms^{-1} and $h = 3 \times 10^5$km. Substituting the observed periodicity of 2.5s into (4.25) shows that the observed behaviour is consistent with a cylindrical loop of diameter in excess of 1910 km. It is possible to predict this diameter using Figure 4.8 which shows a plot of the ratio of cylinder radius a to the location height h against the duration time T_{dur} of the quasi-periodic phase. The scales in the figure are determined by the time of onset of the quasi-periodic phase, $\tau_{onset} = h/v_A$, and the pulse periodicity τ^{min}. Reading off the McLean *et al.* duration time of 150 secs gives a diameter of approximately 2250 km.

Figure 4.8 may also be helpful in determining physical conditions in the corona using radio pulsation data. For example, observations will generally have the onset time τ_{onset} and the pulse periodicity τ^{min}. Figure 4.8 will then give the scale of the inhomogeneity a/h. Thence the width of the inhomogeneity and the associated Alfvén speeds may be deduced.

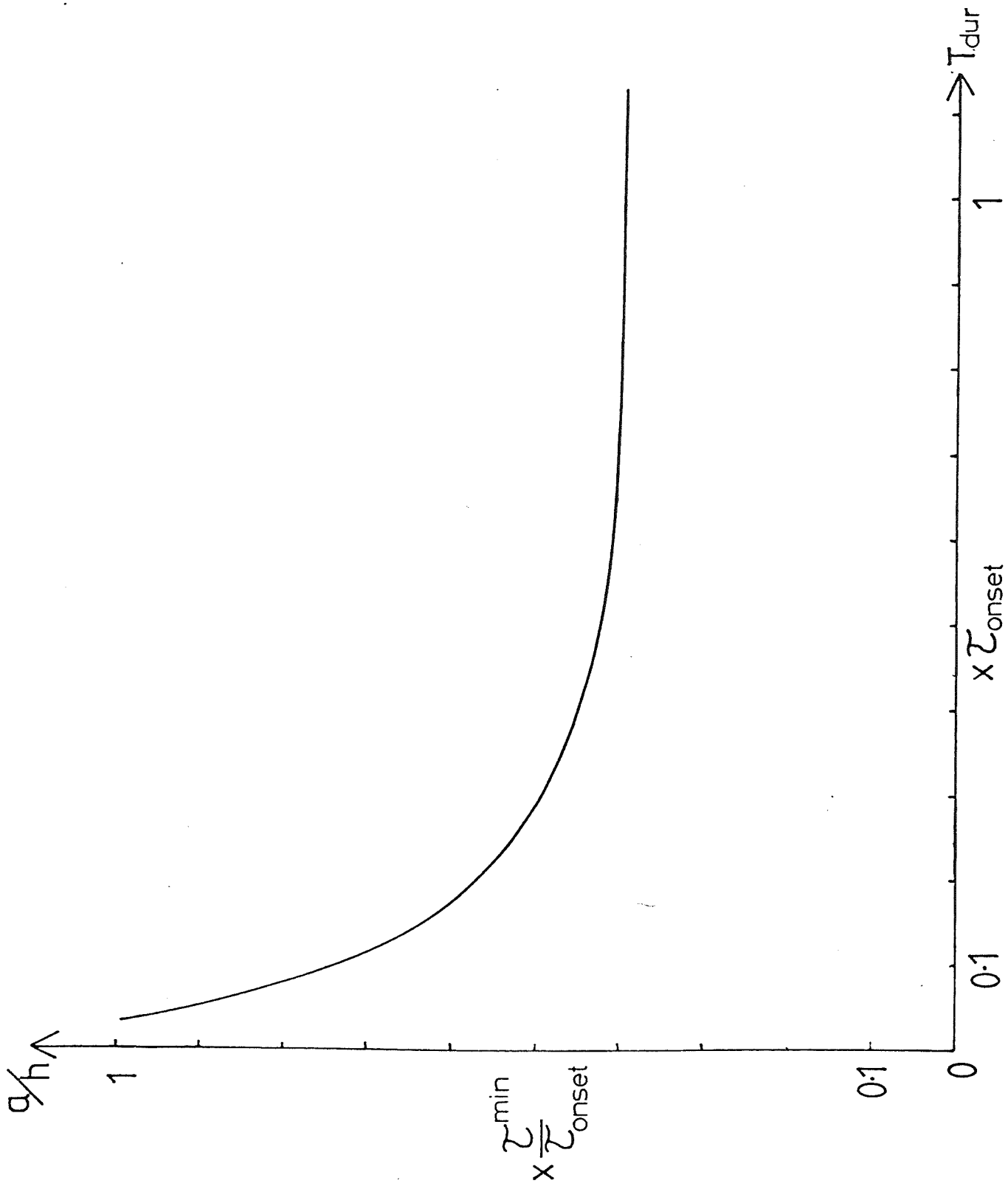

Figure 4.8 A plot of a/h (in units of τ^{min}/τ_{onset}) against T_{dur} (in units of τ_{onset}). Here $\tau_{onset} \equiv h/v_A$ is the time that elapses between the impulsive generation of the disturbance and the onset of the quasi-periodic phase; τ^{min} is the period of the disturbance at the end of the quasi-periodic phase. The figure may be used to deduce the width (diameter) 2a of the inhomogeneity in terms of the recorded values of T_{dur}, τ_{onset}, τ^{min} and h.

The picture presented by Figure 4.5 depends largely on the comparative sizes of v_A, v_{Ae} and c_g^{min}. If the density of the inhomogeneity is not very different to that of its surroundings so that v_A is close to v_{Ae} and the structuring is weak, then the quasi-periodic phase is of fairly short duration because $c_g^{min} \sim v_A$ (see Figure 4.6). Then, especially if the periodic phase is lost in noise, the observed pulse train will start abruptly. Also, it will decay more gradually because the Airy phase is correspondingly extended. (Figure 4.9 shows that the curvature of the group velocity curve at the minimum is not so pronounced for $v_A \sim v_{Ae}$ so $|W'''(K)|$ in (4.21) is smaller.) This theoretical possibility may correspond to the event observed by McLean and Sheridan (1973) (see Figure 4.1f).

Nearly all of the above discussion has concentrated on the behaviour of the lowest order fast sausage mode in a cylindrical inhomogeneity. Higher order modes possess similar features, as do kink disturbances. In general all these modes will be generated by the impulsive source. Most of the foregoing analysis (the group velocity curves, etc.) has also been carried out in both slab and cylinder geometries, and for both sausage and kink modes. The only 'anomaly' is the lowest order kink mode in a cylindrical geometry (the c_k mode) which is only weakly dispersive (cf., Figure 4.2 and Figure 3.4) and so does not therefore possess the Love/Pekeris type features. It is associated instead with, say, standing waves of periods given by (4.10).

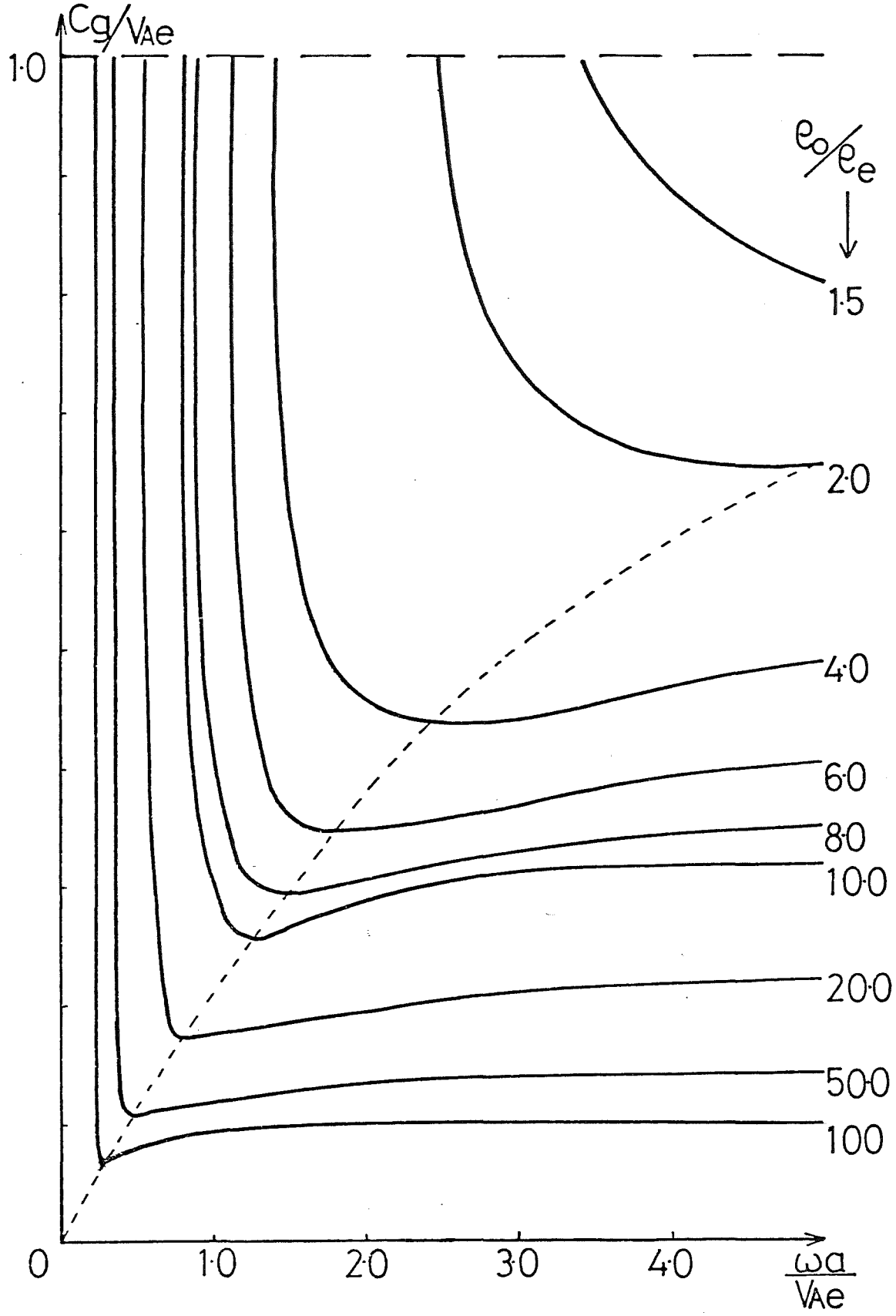

Figure 4.9 The changing curvature of the group velocity curve for various density ratios ρ_0/ρ_e.

The dotted line passes through the minimum of each curve.

The discussion has concentrated on just a single impulse generated at $t = 0$. Disturbances could be generated by a series of impulses at various times, so that a quasi-periodic phase resulting from one disturbance may interact with the periodic phase of a subsequent impulse to give a much more complicated picture than that presented in Figure 4.5. Interactions between impulses and the various combinations of modes could therefore produce a far more distorted signature than that described here for a single mode and a single impulse.

4.6 Analogies

This chapter has so far concentrated on the allowable modes in a uniform, cylindrical inhomogeneity in an otherwise uniform but cold plasma. Figures 2.10, 3.4 and 4.2 show that (ignoring the lowest order, c_k, cylindrical mode) the fast body waves in a cold plasma ($c_e = c_0 = 0$), in either geometry, are just the mathematical analogies of the Love waves of seismology (Equations 2.56 and 3.48b) and the Pekeris waves of oceanography (Equations 2.55 and 3.48a).

These Love and Pekeris dispersion relations resulted from consideration of the governing differential equations (2.21) and (3.11) in a structured (ducted) situation; in the cold plasma approximation they are

$$\text{slab :} \qquad \frac{d^2\hat{v}_x}{dx^2} - \frac{(k^2 v_A^2 - \omega^2)}{v_A^2}\hat{v}_x = 0, \qquad (4.28)$$

and

$$\text{cylinder :} \qquad \frac{d^2\hat{R}}{dr^2} + \frac{1}{r}\frac{d\hat{R}}{dr} - \left\{\frac{(k^2 v_A^2 - \omega^2)}{v_A^2} + \frac{n^2}{r^2}\right\}\hat{R} = 0. \qquad (4.29)$$

Similar equations arise in other ducted situations, some examples of which are given below.

4.6.1 Waves on the lee side of mountains Yih (1965) describes the work of R.S. Scorer and others who have modelled the atmospheric waves in the lee of mountains. The Earth's atmosphere may be stratified by variations in one or some of entropy or temperature or density. Also, stationary waves are observed on the lee side of mountains which have rising and descending air currents above them. This has led to a suggestion of atmospheric ducted waves which are similar to those occurring in a stream of water on the lee side of a barrier or in the shallower waters of the continental shelf, along a coastline (Summerfield, 1972).

A two-dimensional (Cartesian) situation as illustrated in Figure 4.10 is envisaged where the troposphere forms a horizontal layer of depth d underlying the (infinite) stratosphere. In the

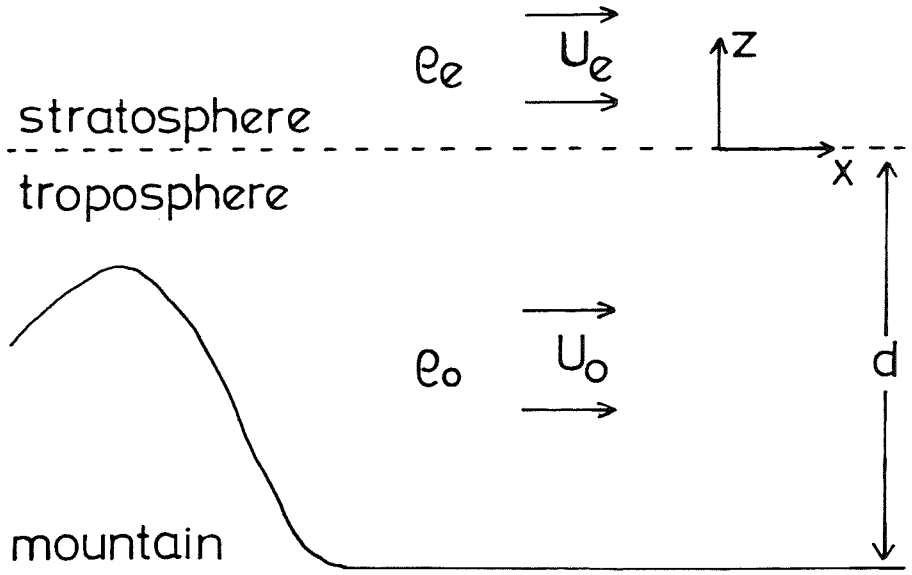

Figure 4.10 The undisturbed ducted fluid situation in the lee of a mountain

undisturbed fluid the densities and horizontal (x) velocities in these layers are ρ_0, ρ_e and U_0, U_e, respectively. By neglecting the vertical (z) variation of ρ_e and ρ_0, for waves satisfying a variation of the form

$$v_z = \hat{v}_z(z)e^{ik_x x}$$

along the layer, Scorer (1949) showed that,

$$\frac{d^2\hat{v}_z}{dz^2} - (k_x^2 - \ell^2)\hat{v}_z = 0, \qquad (4.30)$$

where ℓ^2 is given, for the tropospheric layer, by

$$\ell^2 = \ell_0^2 = \frac{-g^2}{U_0^2 c_0^2} - \frac{U_0''}{U_0}.$$

(A dash denotes differentiation with respect to z.) A similar equation with $\ell = \ell_e$ is satisfied in the stratosphere. These equations are, of course, just the atmospheric wave equivalents of (4.28), with x and z interchanged. Then for velocity solutions which are continuous at the interface $z = 0$, have $v_z = 0$ at $z = -d$, and which decay as $z \to \infty$, the appropriate dispersion relation becomes

$$\sqrt{\ell_0^2 - k_x^2}\, \cot(\sqrt{\ell_0^2 - k_x^2}\, d) = -\sqrt{k_x^2 - \ell_e^2}. \qquad (4.31)$$

This is just the Pekeris equation (2.55). Scorer noted that there are only solutions for $\ell_0 > k_x > \ell_e$ and demonstrated that there were discrete lee waves (that is, waves possessing cut-offs) only if

$$\sqrt{\ell_0^2 - \ell_e^2}\, d \geq (2n + \tfrac{1}{2})\pi, \qquad n = 0,1,2,\ldots . \qquad (4.32)$$

So the criteria for the existence of lee waves is equivalent to there being coronal body waves in *dense* loops only (namely, for $v_{Ae} > \omega/k > v_A$). Unfortunately, neither Scorer (1949) nor Yih (1965) makes reference to Love or Pekeris waves and any connection between atmospheric waves and their seismological counterparts appears to have been missed.

4.6.2 Fibre optics Another area in which equations similar to (4.28) and (4.29) occur is that of optical fibre communications. Over the past two decades glass fibres have been produced which permit the transmission of optical signals for distances of several kilometres (Gloge, 1971 a,b). In general these fibres support many modes, equivalent to the (fast) body waves of Figure 4.2. The numerous modes cause the light signal, which propagates at the group velocity, to become distorted if the signal is transmitted over large distances. One of the aims of optical fibre design is to exploit the fact that the modes have cut-offs (as in Figure 4.2) and so to limit the number which are transmitted and thus prevent signal distortion.

A fibre waveguide consists of a thin central glass core of refractive index n_c surrounded by a glass cladding of slightly lower refractive index, n_e. Snitzer (1961) considered the problem of a homogeneous dielectric cylinder surrounded by an infinitely thick cladding and found that Maxwell's equations for such a problem could be solved. However, the resulting dispersion equation is extremely complicated and difficult to interpret in terms of physical waveguide propagation (Marcuse, 1972; Olshansky, 1979). So usually an assumption of *weakly-guiding* media is made, by which it is assumed that

$$\frac{n_c^2 - n_e^2}{n_c^2} \ll 1. \qquad (4.33)$$

Values of the left-hand ratio usually lie in the range 0.01 to 0.02 so the weak-guidance approximation gives a useful and yet realistic solution.

If the electromagnetic fields

$$\underline{\phi} = \hat{\underline{\phi}} e^{i(kz+\omega t)}$$

are assumed to be either transverse electric (no component of electric field in the z direction, TE modes) or transverse magnetic (no longitudinal magnetic field component, TM modes) then, using (4.33), the governing equations for the transverse amplitudes $\hat{\phi}_t$ reduce to

$$\text{slab :} \qquad \left[\frac{d^2}{dx^2} + (n^2(x)\omega^2\varepsilon_0\mu_0 - k^2)\right]\hat{\phi}_t(x) = 0, \qquad (4.34a)$$

and

$$\text{cylinder :} \qquad \left[\frac{d^2}{dr^2} + \frac{1}{r}\frac{d}{dr} + (n^2(r)\omega^2\varepsilon_0\mu_0 - k^2)\right]\hat{\phi}_t(r) = 0, \qquad (4.34b)$$

for slab and axisymmetric cylindrical waveguides. Here n is the refractive index and ε_0 and μ_0 are, respectively, the dielectric permittivity and magnetic permeability of free space. Equations (4.34) are well-known in the optical fibre literature (e.g., Kirchhoff, 1972, 1973; Marcuse, 1972, 1974; Dil and Blok, 1973; Olshansky, 1979; Keck, 1981), and for uniform dielectrics in which n(x) and

$n(r)$ are constant, are seen to be the same as Equations (4.28) and (4.29), if the refractive index n_c is identified with $(\varepsilon_0\mu_0 v_A^2)^{-\frac{1}{2}}$. ($n_e$, the refractive index in the cladding, is identified with $(\varepsilon_0\mu_0 v_{Ae}^2)^{-\frac{1}{2}}$.) Indeed, the dispersion relation for the so-called LP_{11}, linearly polarized, mode (which corresponds to the lowest order TM_{01} and TE_{01} modes) for a cylindrical waveguide of core radius a surrounded by an infinite cladding, is

$$- u \frac{J_0(u)}{J_1(u)} = w \frac{K_0(w)}{K_1(w)} , \qquad (4.35)$$

where $u = a(\omega^2\varepsilon_0\mu_0 n_c^2 - k^2)^{\frac{1}{2}}$ and $w = a(k^2 - \omega^2\varepsilon_0\mu_0 n_e^2)^{\frac{1}{2}}$. Equation (4.35) is identical to Equation (3.40) describing symmetric mhd body waves in a cold, cylindrically structured plasma.

When a glass fibre is produced the boundary between the core and cladding becomes gradual due to diffusion of the dielectric constituents. Analysis of the refractive index distribution of 'uniform' core fibres reveals that there is no abrupt transition between the core and the cladding. Furthermore such *graded index* glass rods are often manufactured intentionally and so it is of practical interest in optical telecommunications to look at the propagation characteristics of continuously inhomogeneous dielectric waveguides.

In the solar physics context, also, abrupt changes in density or temperature at the bounding surfaces of coronal loops are not envisaged. Cool cores and density variations in loops are suspected

to occur (see Chapter 1). In what follows a gradual density variation across a coronal structure will be examined and compared with the earlier results for a uniform slab or cylinder (which modelled simply a discrete step in density).

4.7 Density Variation in a Coronal Atmosphere

4.7.1 The Slab For a coronal inhomogeneity in the form of a cold slab, across which density varies continuously but the equilibrium magnetic field is uniform ($B_0 = B_e$), the appropriate equation may be written (see Equation (2.12))

$$\frac{d^2\hat{v}_x}{dx^2} + \hat{v}_x\left[\frac{\mu_0\rho_0(x)}{B_0^2}\omega^2 - k^2\right] = 0. \tag{4.36}$$

Consider a density variation that is parabolic within the slab and uniform elsewhere (see Figure 4.11):

$$\rho_0(x) = \begin{cases} \rho_0[1 - (x/x_0)^2(1 - \rho_e/\rho_0)], & |x| < x_0 \\ \rho_e, & |x| > x_0, \end{cases} \tag{4.37}$$

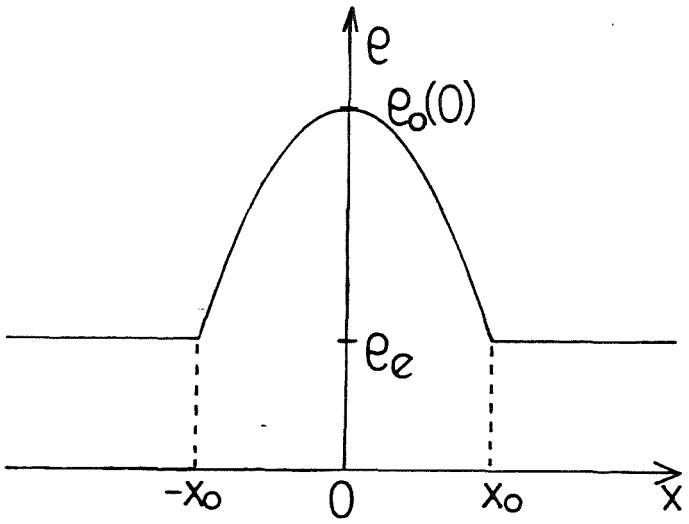

Figure 4.11 The equilibrium parabolic density structure in a cold plasma slab

where $\rho_0 = \rho_0(0) > \rho_e$, $v_A(0) = B_0/(\mu_0\rho_0)^{\frac{1}{2}}$ and x_0 is the slab half-width. Pressure balance in equilibrium (see Equation (2.20)) means that $v_A(0)/v_{Ae} = (\rho_e/\rho_0)^{\frac{1}{2}}$.

The change of variable

$$\xi = \left\{\frac{2\omega(1 - \rho_e/\rho_0)^{\frac{1}{2}}}{v_A(0)x_0}\right\}^{\frac{1}{2}} x \tag{4.38}$$

reduces (4.36) to the parabolic cylinder equation

$$\frac{d^2\hat{v}_x}{d\xi^2} - \left(\frac{\xi^2}{4} - \alpha\right)\hat{v}_x = 0, \tag{4.39}$$

where

$$\alpha = \frac{x_0(\omega^2 - k^2 v_A^2(0))}{2\omega(1 - \rho_e/\rho_0)^{\frac{1}{2}} v_A(0)} . \qquad (4.40)$$

Solutions of (4.39) may be written

$$\hat{v}_x = C_1 e^{-\xi^2/4} M\left(-\frac{\alpha}{2} + \frac{1}{4}, \frac{1}{2}, \frac{\xi^2}{2}\right) + C_2 \xi e^{-\xi^2/4} M\left(-\frac{\alpha}{2} + \frac{3}{4}, \frac{3}{2}, \frac{\xi^2}{2}\right),$$

$$-x_0 < x < x_0, \qquad (4.41)$$

where C_1 and C_2 are constants. Here $M(\hat{a},\hat{b},y)$ is the confluent hypergeometric or Kummer function (Abramowitz and Stegun, 1967) given by

$$M(\hat{a},\hat{b},y) = \sum_{m=0}^{\infty} \frac{(\hat{a})_m}{(\hat{b})_m} \frac{y^m}{m!} \qquad (4.42)$$

where $(\hat{a})_m = \hat{a}(\hat{a}+1)(\hat{a}+2)\ldots(\hat{a}+m-1)$, $(\hat{a})_0 = 1$.

Kirchhoff (1972) has considered a parabolic refractive index distribution for an optical slab waveguide but rather than proceed to match (for his problem) the electromagnetic fields at the boundaries $x = \pm x_0$ of the slab to produce a dispersion relation, he argued (in common with others in the optical fibre field) as follows.

For large positive x, the confluent hypergeometric function in (4.42) behaves as

$$M(\hat{a},\hat{b},x) \propto x^{\hat{a}-\hat{b}} e^{x}. \tag{4.43}$$

So if boundaries are ignored, but yet the wave is *totally guided* in the sense that the amplitude given by (4.41) $\to 0$ as x increases, then $\hat{a}$ in (4.43) must be negative (or zero). Furthermore, if the series in (4.42) is to terminate then $\hat{a}$ must be a negative integer. This means, for example for the symmetric mode in (4.41), that

$$\hat{a} = -\frac{\alpha}{2} + \frac{3}{4} = -q, \quad \text{where} \quad q = 0,1,2,\ldots, \tag{4.44}$$

and the symmetric solution behaves as $\xi e^{-\xi^2/4} M(-q, 3/2, \xi^2/2)$, where

$$M\left(-q, \frac{3}{2}, \frac{\xi^2}{2}\right) = \frac{(-1)^q q!}{(2q+1)!} \frac{\sqrt{2}}{2\xi} H_{2q+1}\left(\frac{\xi}{\sqrt{2}}\right) \tag{4.45}$$

and H denotes a Hermite polynomial (Abramowitz and Stegun, 1967). Substituting for α from (4.40) in (4.44) shows that, for symmetric modes

$$\omega^2 - \frac{(1 - \rho_e/\rho_0)^{\frac{1}{2}} v_A(0)\,(4q+3)}{x_0}\,\omega - k^2 v_A^2(0) = 0. \qquad (4.46)$$

Interpreting Equation (4.46) shows for a wide slab and low orders (small q) that

$$\omega \simeq \pm k v_A(0). \qquad (4.47)$$

This conforms to the intuitive wide slab behaviour of the body waves in Figure 4.2. However, (4.46) has been derived neglecting the exterior entirely and does not determine the cut-offs or describe fully the behaviour of modes in a finite tube.

Equation (4.46) is equivalent to the dispersion relation resulting from a WKB approximation to Equation (4.39). For the latter equation, the turning points ξ_t are given by $\xi_t = \pm 2\sqrt{\alpha}$, and the WKB approximation means that (see Bender and Orszag, 1978)

$$\int_{-2\sqrt{\alpha}}^{2\sqrt{\alpha}} \sqrt{\alpha - \xi^2/4}\; d\xi \simeq (m + \tfrac{1}{2})\pi, \quad m \text{ integer}, \quad m \to \infty. \qquad (4.48)$$

Evaluating the integral in (4.48) by substitution (see Bender and Orszag, 1978) shows that

$$\alpha\pi \simeq (m + \tfrac{1}{2})\pi, \quad m \text{ large integral values}. \qquad (4.49)$$

This equation may be rearranged to give

$$\omega^2 - \frac{(1 - \rho_e/\rho_0)^{\frac{1}{2}} v_A(0)(2m+1)}{x_0}\omega - k^2 v_A^2(0) = 0, \qquad (4.50)$$

the odd integral values of which give Equation (4.46) once more. The even integers and m=0 give the kink modes. As an illustration, the phase and group velocities for the m=0 kink mode (but note the inconsistency with (4.49)) are plotted in Figure 4.12. The expression for the group velocity, obtained by differentiating (4.50), is

$$G = \frac{d\omega}{dk}\Big/ v_{Ae} = \frac{2\rho_e/\rho_0 X}{\{2\hat{W}X - (1 - \rho_e/\rho_0)^{\frac{1}{2}}(\rho_e/\rho_0)^{\frac{1}{2}}\}}, \qquad (4.51)$$

where $X = kx_0$ and $\hat{W} = \omega/kv_{Ae}$. Equation (4.51) differs from its cylindrical counterpart (4.24) in that there are no factors representing modal behaviour in the exterior of the inhomogeneity - the K Bessel functions in (4.24). Indeed Figure 4.12 shows that though the phase-speed has a dispersive behaviour similar to that of the body waves in Figure 4.2, but no cut-off, the group velocity curve bears no resemblance to that of Figure 4.4 and does not have an extremum. So this approximate modal behaviour given by (4.46) or (4.50), for a parabolic density variation, would be an inadequate basis for explaining impulsively generated behaviour, similar to that described earlier in this chapter, for a slab with a step-density profile.

Returning to the problem of describing modes in a slab with density variation (4.37), the velocity amplitude within $|x| < x_0$ is

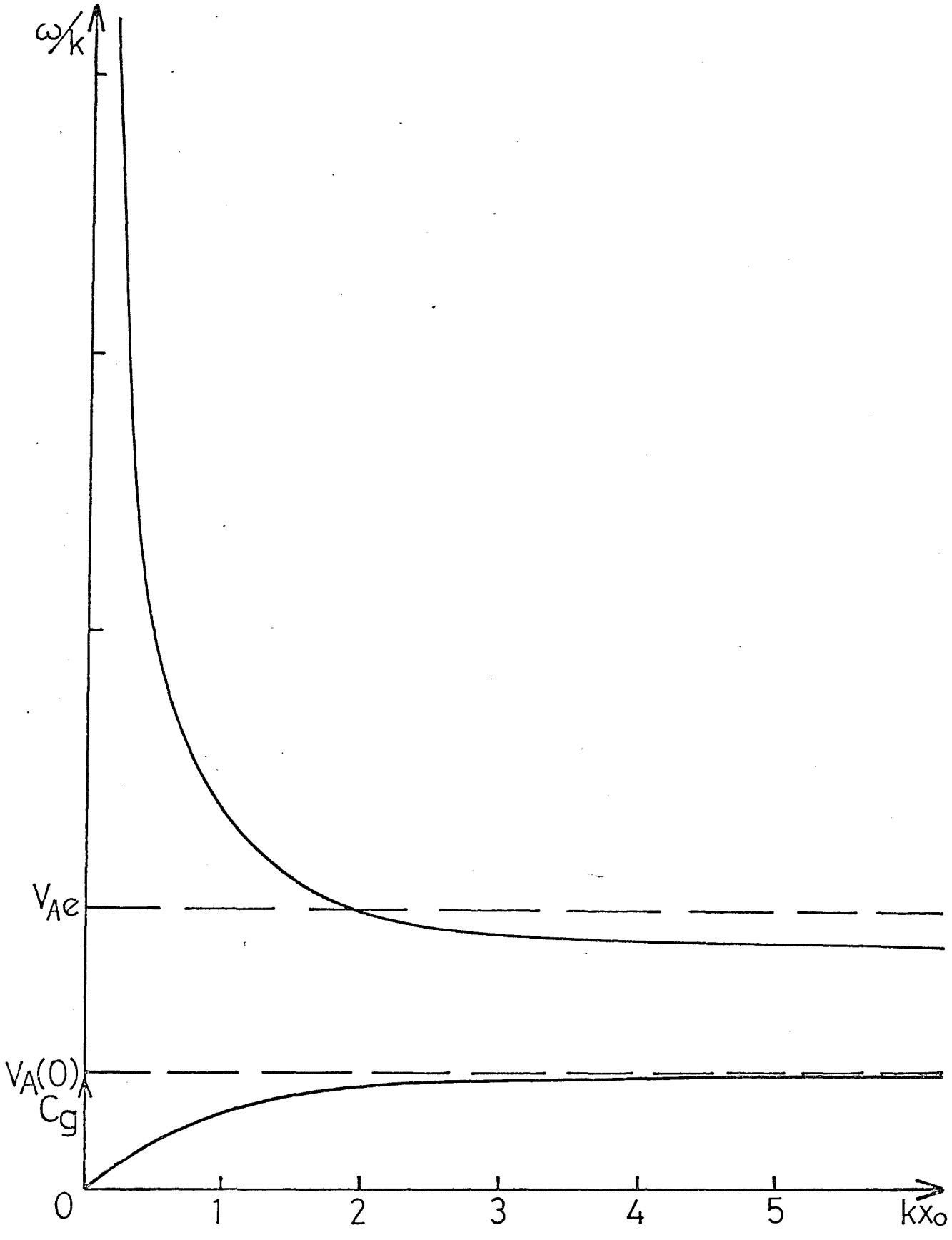

Figure 4.12 The phase-speed ω/k and group velocity $c_g = d\omega/dk$ of the lowest order, totally guided kink mode as functions of kx_0 ($k > 0$) for a slab having parabolic density variation. The totally guided approximation ignores the dispersive effects of the slab's environment.

described by (4.41), whilst in the slab's exterior, where the density is uniform, it is given by (2.25), namely

$$\hat{v}_x = \begin{cases} \alpha_e e^{-m_e(x-x_0)}, & x > x_0, \\ \beta_e e^{m_e(x+x_0)}, & x < -x_0, \end{cases} \tag{4.52}$$

where $m_e^2 = (k^2 v_{Ae}^2 - \omega^2)/v_{Ae}^2$, and α_e and β_e are constants.

Considering sausage (symmetric) modes only and matching velocity and magnetic pressure across the boundaries $x = \pm x_0$ (according to (1.19) and (1.20)) results in the dispersion relation

$$m_e x_0 = \left(\frac{\sigma}{2} - 1\right) - \frac{\sigma\left(-\alpha + \frac{3}{2}\right)}{3} \frac{M\left(-\frac{\alpha}{2} + \frac{7}{4}, \frac{5}{2}, \frac{\sigma}{2}\right)}{M\left(-\frac{\alpha}{2} + \frac{3}{4}, \frac{3}{2}, \frac{\sigma}{2}\right)}, \tag{4.53}$$

where α is given by (4.40) and

$$\sigma = \frac{2\omega x_0 (1 - \rho_e/\rho_0)^{\frac{1}{2}}}{v_A(0)}. \tag{4.54}$$

Now for modes in a cold plasma which are evanescent in the slab's exterior so that $m_e > 0$ and thus $\omega \leq kv_{Ae}$, there will be cut-offs, equivalent to those found for a uniform density slab, where $\omega \to kv_{Ae}$. Then (4.53) yields

$$\frac{M\left(-\frac{\nu}{4}+\frac{7}{4},\ \frac{5}{2},\ \nu\right)}{M\left(-\frac{\nu}{4}+\frac{3}{4},\ \frac{3}{2},\ \nu\right)} = \frac{3(\nu-1)}{\nu(3-\nu)}\ , \tag{4.55}$$

where $\sigma \to 2\nu$, $\alpha \to \nu/2$ and $\nu = X\beta = (kx_0)(\rho_0/\rho_e - 1)^{\frac{1}{2}}$. The cut-off for the lowest order sausage mode in a slab with uniform density was $\pi/2$, but evaluation of (4.55) shows that, instead, for a parabolic density distribution, it is

$$\nu = X\beta \simeq 2.27. \tag{4.56}$$

$\frac{\rho_0(0)}{\rho_e}$	$\frac{v_A(0)}{v_{Ae}} = \left(\frac{\rho_e}{\rho_0(0)}\right)^{\frac{1}{2}}$	Slab cut-offs (kx_0)		Cylinder cut-offs (ka)	
		Uniform density	Parabolic density variation	Uniform density	Parabolic density variation
1.5	.816	2.22	3.21	3.40	4.79
2	.707	1.57	2.27	2.40	3.39
4	.500	0.907	1.31	1.39	1.97
6	.408	0.702	1.02	1.07	1.51
8	.354	0.594	0.858	0.910	1.29
10	.316	0.524	0.757	0.801	1.13
20	.224	0.360	0.521	0.552	0.781
50	.141	0.224	0.324	0.342	0.484
100	.100	0.158	0.228	0.242	0.342

Table 4.2 Comparison of lowest order sausage mode cut-offs in a slab and a cylinder with both uniform and parabolic density profiles.

Table 4.2 (columns 3 and 4) compares the cut-offs (values of $kx_0 = \pi/2.(\rho_0/\rho_e - 1)^{-\frac{1}{2}}$) for a slab of uniform density with those for a parabolic density distribution across the slab, given by (4.56). The cut-offs are larger for a parabolic variation which accords with intuition. The waves only exist in dense loops so as $\rho_0(0) \to \rho_e$ the cut-offs become larger until eventually, for zero density difference, there are no modes. The parabola of density distribution effectively represents a lower overall density difference and so cut-offs are correspondingly increased (area under parabola/area under step function = 2/3). Superficially, Equation (4.53) appears very different in form to the Pekeris equation for symmetric body waves in a cold plasma, uniform density slab. However, changes in density profile from a step function to a parabola do not result in drastic alterations to the behaviour described in Figure 4.2, as the following discussion shows.

The lowest order sausage mode has a cut-off for α (= $\nu/2$) ~ 0(1) suggesting that investigation of (4.53) for small α (a slender slab) would be futile. (Figure 4.2 for a step profile would suggest this too.) However consideration of α large is more illuminating. For a given density profile ρ_e/ρ_0 is fixed and $\omega < kv_{Ae}$ for evanescent modes. Using the behaviour as $\alpha \to \infty$ of the confluent hypergeometric functions (Abramowitz and Stegun, 1967) terms in Equation (4.53) may be simplified according to:

$$M\left(-\frac{\alpha}{2}+\frac{7}{4},\frac{5}{2},\frac{\sigma}{2}\right)\to\frac{\Gamma\left(\frac{5}{2}\right)e^{\sigma/4}\cos(\sqrt{\alpha\sigma}-\pi)}{\frac{\sigma}{2}\left(\frac{\alpha}{2}-\frac{1}{2}\right)\sqrt{\pi}},$$

and

$$M\left(-\frac{\alpha}{2}+\frac{3}{4},\frac{3}{2},\frac{\sigma}{2}\right)\to\frac{\Gamma\left(\frac{3}{2}\right)e^{\sigma/4}\left(\frac{\alpha\sigma}{4}\right)^{-\frac{1}{2}}\cos\left(\sqrt{\alpha\sigma}-\frac{\pi}{2}\right)}{\sqrt{\pi}}.$$

Also, from (4.40) and (4.54),

$$\alpha\sigma=\frac{x_0^2(\omega^2-k^2v_A^2(0))}{v_A^2(0)}=n_0^2x_0^2,$$

so that the dispersion relation (4.53) reduces, in the wide slab ($kx_0 >> 1$) limit to

$$\tan(n_0x_0)=-\frac{n_0}{[m_e-\omega(1-\rho_e/\rho_0)^{\frac{1}{2}}/v_A(0)]}. \qquad (4.57)$$

Provided $\omega^2 \neq k^2v_A^2(0)$, (4.57) describes the modal behaviour of sausage waves in a wide $|kx_0| \to \infty$ slab having a parabolic density variation profile. It is seen that for little density variation, $\rho_0(0) \simeq \rho_e$, that is a shallow, wide profile, the uniform and parabolic density distributions are essentially the same; (4.57) reduces to

$$\tan(n_0x_0)=-n_0/m_e, \qquad (4.58)$$

which is the Pekeris Equation (2.55).

Also, from Equation (4.57), it is seen that for $\omega \to kv_{Ae}$, n_0 tends to $k(\rho_0/\rho_e - 1)^{\frac{1}{2}}$ and m_e tends to zero so that

$$kx_0 \simeq \frac{(2q+1)\pi}{4(\rho_0/\rho_e - 1)^{\frac{1}{2}}} = \frac{(2q+1)\pi}{4\beta}, \qquad (4.59)$$

where q is a positive integer. This result may also be derived from Equation (4.55) by considering ν large. In this limit (4.55) reduces to

$$\tan\nu = 1,$$

which is the same as (4.59), and shows that for large order symmetric modes the cut-offs are $\pi/2$ out of phase with those in a uniform density slab. If β is large (large density variation) then q must also be large to apply (4.59) to a wide slab, but a density ratio of only $\rho_0(0)/\rho_e = 1.5$ and $q = 1$ gives $\nu = 2.36$ and $kx_0 \simeq 3.33$ (cf., first entry of column 4 of Table 4.2).

Figure 4.13 compares plots of the phase-speeds of the lowest order sausage modes in a slab for uniform and parabolic density profiles when $\rho_0(0)/\rho_e = 6$. Apart from the larger cut-off in the parabolic case there is no significant change; the curve is confined to the region $v_A(0) < \omega/k < v_{Ae}$ as anticipated and, as (4.47) also shows, a long wavelength mode travels approximately with the Alfvén speed at the centre of the slab.

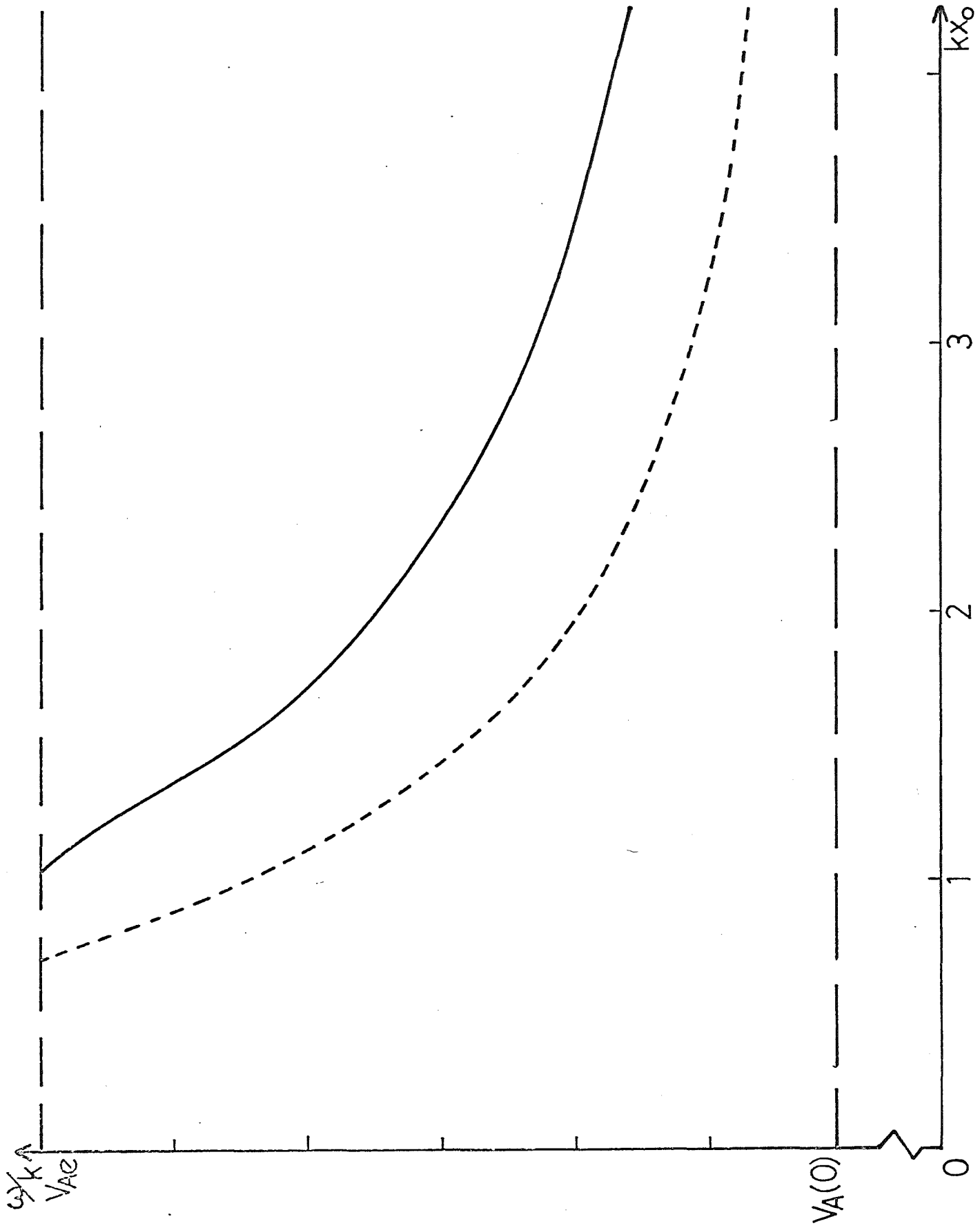

Figure 4.13 The phase-speed ω/k of the lowest order sausage modes in a slab for uniform (---) and parabolic (——) density profiles as functions of kx_0 ($k > 0$). Here $\rho_0(0)/\rho_e = 6$.

How the parabolic density model affects the group velocity for this mode is shown in Figure 4.14, again for a density ratio $\rho_0(0)/\rho_e = 6$. This figure, unlike Figure 4.12 which did not represent a solution of the dispersion relation (4.53), shows that the group velocity curve does possess a minimum value and that this is *lower* and at a *higher* frequency than for the corresponding uniform density model ($G^{min} = 0.239$ as compared to 0.339 for the uniform density slab).

So Figure 4.14 shows that a discrete jump in density across a coronal loop is a valid mathematical simplification of a more realistic varying density and that the theory developed earlier in this chapter may be applied. The step density profile provides an adequate picture in that observable behaviour at height h above an impulsive source is described by Figure 4.5. Since the cut-offs are larger, τ_c given by the uniform slab version of (4.26) is correspondingly larger, but not significantly so. For example, for $\rho_0(0)/\rho_e = 100$, from the last entry of column 4 of Table 4.2, $k_c x_0 \simeq 0.228$ and so

$$\tau_c \simeq \frac{2.76 x_0}{v_A(0)} , \qquad (4.60)$$

giving a similar time scale as for the periodic oscillations in a uniform slab (cylinder). Also the larger value of ω^{min} for a parabolic density distribution means that the time scale of

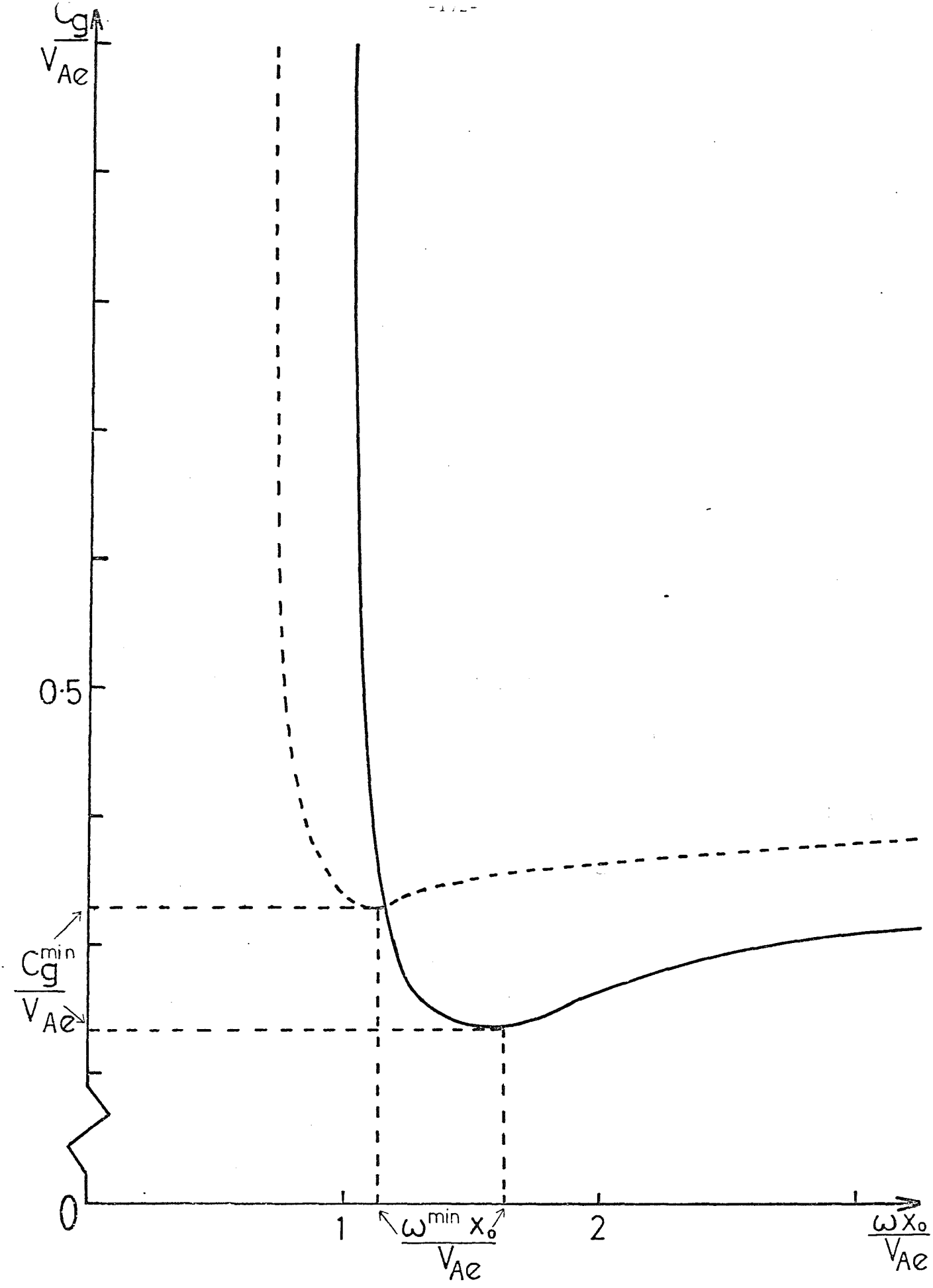

Figure 4.14 The dimensionless group velocity $G = c_g/v_{Ae}$ as a function of dimensionless frequency $\omega x_0/v_{Ae}$ of the lowest order sausage modes for uniform (---) and parabolic (——) density profiles. Here $\rho_0(0)/\rho_e = 6$.

oscillation in the quasi-periodic phase is correspondingly reduced and the lower c_g^{min} value suggests longer duration times (see Figures 4.14 and 4.5). The principles remain the same however and so the suggested explanation for short-period oscillations observed in coronal loops needs little modification to apply to a more realistic continuously varying density distribution.

Most of the work carried out in connection with optical fibres has been concerned with cylindrical dielectric structures. The analogy of ducted mhd plasma waves with TE modes was noted by Pneuman (1965) though it appears not to have been exploited since then. Pneuman examined the symmetric modes in a diffuse linear pinch, a cold plasma with parabolic density variation, surrounded by a vacuum. Thus, in terms of the notation used here, the situation is that of column (ii) of Table 2.2, namely $\rho_e \to 0$ (so v_{Ae} and $c_e \to \infty$) and $c_0 = 0$. The body waves of such a system are similar to those illustrated in Figure 4.2 but their phase-speeds become infinitely large as cut-off values are approached. Since $|m_e| \to |k|$ for this configuration, the group velocity curves are also no longer of the form shown in Figures 4.4 and 4.14. The lowest symmetric mode is illustrated for a cylinder of uniform density in Figure 4.15. For such modes the Pekeris equation becomes

$$\tan(n_0 x_0) = -\frac{n_0}{k} . \qquad (4.61)$$

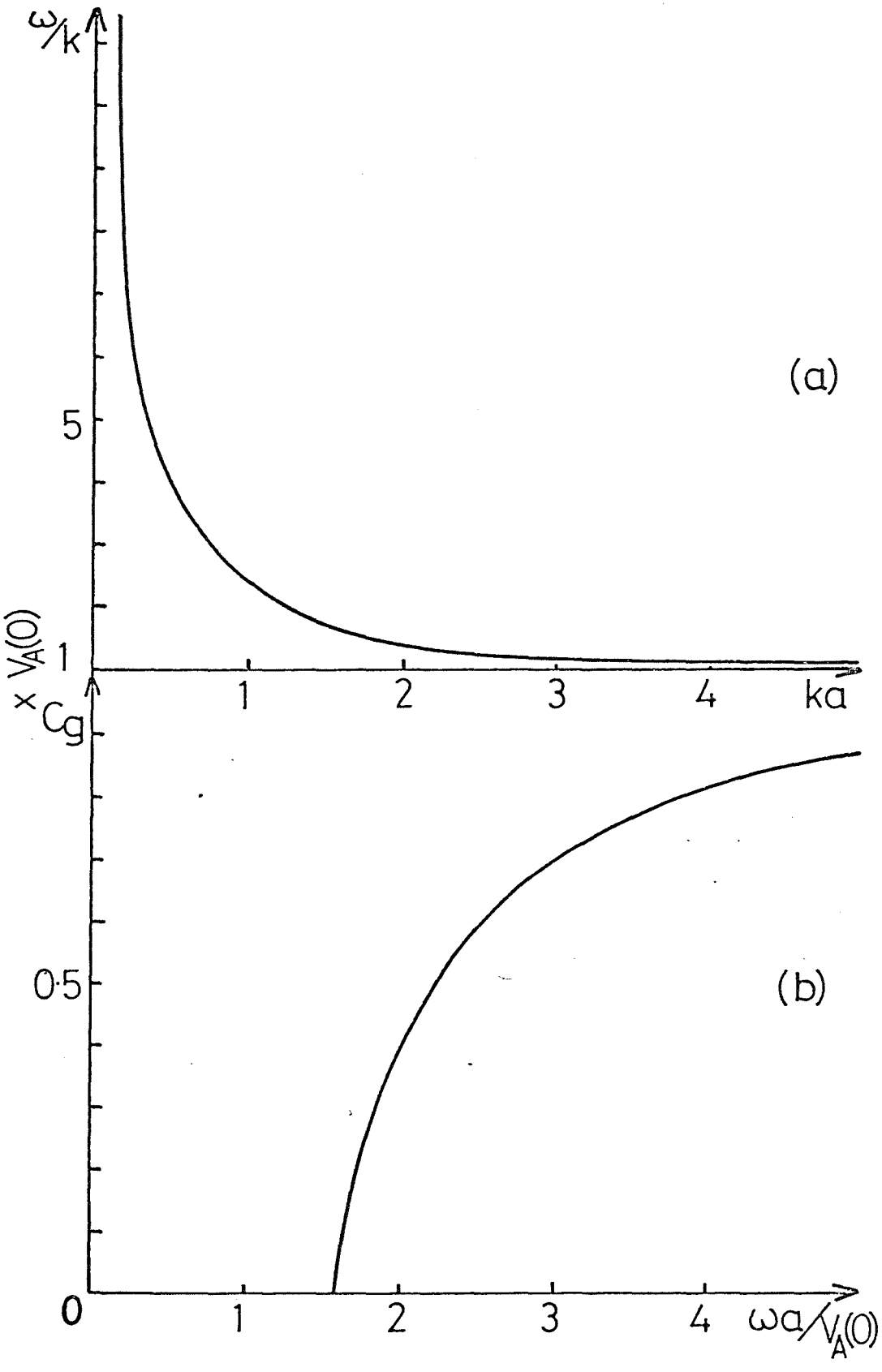

Figure 4.15 (a) The phase-speed ω/k and (b) the group velocity $c_g = d\omega/dk$ as functions of ka ($k > 0$) and $\omega a/v_A(0)$, respectively, for the lowest order symmetric mode in a uniform, cold cylinder surrounded by a vacuum.

Pneuman's Figure 2 (for radial density variation) shows the same characteristic behaviour even though the dispersion relation is somewhat more complicated than (4.61), involving the confluent hypergeometric functions as in the slab case (4.53) discussed earlier: according to Pneuman (1965),

$$-\frac{kaK_0(ka)}{K_1(ka)} = 2 - \frac{\omega a}{v_A(0)} + \frac{M'\left(1 - \frac{\alpha}{2}, 2, \frac{\omega a}{v_A(0)}\right)}{M\left(1 - \frac{\alpha}{2}, 2, \frac{\omega a}{v_A(0)}\right)} .$$

Here α is given by (4.40) with $\rho_e = 0$. Though Pneuman notices that a series of body waves exists, each with its appropriate cut-off, he pursues the problem of 'totally guided' modes along lines of the optical fibre arguments outlined earlier. So impulsively generated waves in Pneuman's configuration would not exhibit the phenomena described in Figure 4.5. Again, it appears that the elastic (dispersive) nature of the environment is an essential ingredient in forming these modes.

4.7.2 Cylindrical geometry Density variations in a cylindrical geometry will now be considered briefly to see how the optical fibre work relates to earlier discussions of cylindrical coronal loops. Attempts to analyse radially inhomogeneous glass fibres have been made by several authors, for example, Dil and Blok (1973), Kirchhoff (1973) and Okoshi and Okamoto (1974). In the last of these papers and also in Unger (1977) there are reviews of the various methods which have been used to examine the problem:

power series expansions, perturbation theory and the use of staircase functions to approximate the variation in refractive index across the cylinder.

The cylindrical fibre has been investigated (see reviews by Unger, 1977; and Olshansky, 1979) subject to the usual optical fibre approximation of ignoring the core's boundary and effectively using the WKB approximation (Gloge, 1975; Arnaud, 1976; Keck, 1981). In the context of a coronal loop, this means that for a parabolic variation the equivalent of Equation (4.29) (for n = 0) may be expressed in the form

$$\frac{d^2\hat{R}}{dr^2} + \frac{1}{r}\frac{d\hat{R}}{dr} + \left[\left(\frac{\omega^2}{v_A^2(0)} - k^2\right) - \frac{4r^2}{\eta^2}\right]\hat{R} = 0, \qquad (4.62)$$

where $\eta = \dfrac{2v_A(0)a}{\omega(1 - \rho_e/\rho_0)^{\frac{1}{2}}}$. Equation (4.62) is a general confluent equation (Abramowitz and Stegun, 1967). When the effect of the cylinder's boundaries are ignored the solutions of (4.62) are again reduced to polynomials, as in the slab case. They have the form

$$e^{-(r^2/\eta)}\, q!\, L_q^{(0)}\left(\frac{2r^2}{\eta}\right), \qquad q = 0,1,2,\ldots; \qquad (4.63)$$

that is, they are Laguerre polynomials multiplied by the Gaussian factor $e^{-r^2/\eta}$. For (4.63) to be a solution of (4.62),

$$4 + 8q = \eta\left(\frac{\omega^2}{v_A^2(0)} - k^2\right). \qquad (4.64)$$

Substituting for η in (4.64) produces the cylindrical equivalent of (4.46):

$$\omega^2 - \frac{(1-\rho_e/\rho_0)^{\frac{1}{2}} v_A(0)(2+4q)\omega}{a} - k^2 v_A^2(0) = 0. \qquad (4.65)$$

As noted before, a dispersion relation such as (4.65) does not reflect the true nature of waves in a finite radius tube, especially the lower order modes.

Okoshi and Okamoto (1974) used a variational method to solve (4.62) (together with the conditions that $\hat{R}$ and $d\hat{R}/dr$ are continuous across $r = a$; see (3.13)). They solved the problem which results from minimizing the functional by the Rayleigh-Ritz method, using a series of trial orthonormal functions of the form $\sqrt{2}\, J_m(j_k^{(m-1)} r/a)/J_m(j_k^{(m-1)})a$, where $j_k^{(m-1)}$ denotes the kth zero of the Bessel function J_{m-1}, with m a non-negative integer and a the radius of the fibre core.

The analogy between the electromagnetic modes of the optical fibre problem and the mhd modes of the coronal loop problem does not hold for all integers m and care must be exercised in drawing comparisons. It was pointed out earlier that the lowest order transverse electric and transverse magnetic modes, using the weak guidance approximation (4.33), are analogous to the mhd modes of a uniform density coronal loop, so that only theory concerning these linearly polarized modes may be used in the analogy. The analogy fails for hybrid electromagnetic modes. Furthermore, for a density

variation across a coronal loop, the Hain-Lüst equation (3.9) governing non-axisymmetric modes no longer has the simple form of (4.34b) and so cannot be compared with the non-axisymmetric optical fibre modes.

With these reservations in mind, one of the cases considered by Okamoto and Okoshi (1976) is relevant to the lowest order sausage mode of the coronal loop problem. Thus, for a μ-power density distribution across the loop, of the form

$$\rho_0(r) = \begin{cases} \rho_0(0)\left[1 - \left(\frac{r}{a}\right)^{\mu}\left(1 - \frac{\rho_e}{\rho_0}\right)\right], & 0 \leqslant r \leqslant a, \\ \rho_e, & r > a, \end{cases} \tag{4.66}$$

the dispersion relation becomes

$$-\frac{wK_0(w)}{K_1(w)} - \frac{\left\{1 - \frac{K_0(w)K_2(w)}{K_1^2(w)}\right\}w^2}{\mu + 2} = \frac{uJ_0(u)}{J_1(u)}, \tag{4.67}$$

where now

$$u^2 = \frac{\mu}{\mu + 2} n_0^2 a^2 \tag{4.68}$$

and, as before,

$$w^2 = m_e^2 a^2. \tag{4.69}$$

Equation (4.67) is to be compared with (4.35). Okamoto and Okoshi (1976) have investigated a generalized version of (4.67) for

several cases, some of which are relevant to the coronal loop problem. It must be noted that for those cases which are relevant, they calculate an approximation to the group delay (reciprocal of the group velocity). This calculation is used extensively in the optical fibre literature (see, for example, Gloge, 1971b; Marcuse, 1974) but it employs the weakly-guiding approximation (4.33) which, for the group velocity calculation, effectively removes the dispersive effects due to the cladding (the coronal loop's environment). Thus the expression for the group velocity is somewhat similar to that resulting from the WKB analysis discussed earlier and does not possess an extremum (cf., Figures 4.12 and 4.15b).

Nevertheless there are several points arising from their discussion which are helpful when considering coronal loops. First, the uniform density profile may be recovered from the μ-power variation one by letting $\mu \to \infty$. Doing this in (4.67) recovers (4.35) as anticipated. For cut-off values, letting $\omega \to kv_{Ae}$ means, from (4.69), that $w \to 0$ and so (4.67) implies that the frequency cut-offs ω_c are given by

$$u_c = j_s^{(0)}, \qquad s = 1,2,\ldots, \tag{4.70}$$

where $j_s^{(0)}$ are the zeros of the Bessel function J_0. Using (4.68) and (4.67), and the non-dimensional notation of the slab case earlier, shows that there are cut-off values X given by

$$ka = X = \frac{j_s^{(0)}}{\beta}\sqrt{1 + \frac{2}{\mu}} = \frac{j_s^{(0)}}{\left(\frac{\rho_0}{\rho_e} - 1\right)^{\frac{1}{2}}}\sqrt{1 + \frac{2}{\mu}}\,. \qquad (4.71)$$

So, for a non-uniform density distribution (specifically, a μ-power one) the cut-offs, instead of being given by the cold plasma versions of (4.5), are now increased by the factor $\sqrt{1 + \frac{2}{\mu}}$; thus, for a parabolic density distribution they are increased by the factor $\sqrt{2}$. This variation in cut-off, compared to that of the cylindrical, uniform density case, is shown in the last two columns of Table 4.2, where it may be compared with the slab cut-offs also. [Several optical fibre papers (e.g., Dil and Blok, 1973; Okoshi and Okamoto, 1974) note that the 'normalised frequency' at cut-off, given by $\nu = X\beta$ in the terminology used here, is $\nu \simeq 3.5$. For a parabolic distribution, this is $\sqrt{2}\, j_s^{(0)}$ (= 3.4), according to (4.71).]

Equation (4.67) may be investigated for a large radius (long wavelength) cylinder, $|k|a \to \infty$. Then, provided $\omega \neq |k|v_A$, both u and $m_e a$ tend to ∞ (from Equations (4.68) and (4.69)). As a result, the ratios of the Bessel functions in (4.67) have the approximate values:

$$\frac{K_0(w)}{K_1(w)} \sim 1, \quad \frac{K_0(w)K_2(w)}{K_1^2(w)} \sim 1 \quad \text{and} \quad \frac{J_0(u)}{J_1(u)} \sim \cot\left(u - \frac{\pi}{4}\right). \qquad (4.72)$$

Thus the dispersion relation (4.67) reduces to the form

$$\tan\left(u - \frac{\pi}{4}\right) = -\frac{u}{w}\,, \qquad (4.73)$$

where

$$u = \frac{\mu}{\mu+2} n_0 a = \frac{\mu}{\mu+2} \frac{(\omega^2 - k^2 v_A^2(0))^{\frac{1}{2}} a}{v_A(0)}, \quad \text{and} \quad w = \frac{(k^2 v_{Ae}^2 - \omega^2)^{\frac{1}{2}} a}{v_{Ae}}.$$

Thus the 'phase-shifted' Pekeris equation (3.48a) appropriate to a large radius cylinder is recovered, though now in a form appropriate for a μ-power density distribution across the coronal loop. Note that to obtain the cut-offs for these waves, setting $\omega = kv_{Ae}$ in (4.73) gives

$$ka \simeq \frac{(2n+1)\pi(\mu+2)}{4\mu(\rho_0/\rho_e - 1)^{\frac{1}{2}}}, \qquad n = 0,1,2,\ldots . \tag{4.74}$$

For $\mu = 2$ (corresponding to a parabolic density profile) this gives a factor of 2 different to the slab case (4.59). For $\mu \to \infty$ (the homogeneous profile) the cut-offs in the two geometries are the same.

4.8 Further Features of the Optical Fibre Analogy

4.8.1 More realistic density distributions

The results of the previous section showed that it is possible to describe the inherent oscillations in a coronal loop which has a continuously varying, non-uniform, density distribution. However the analysis

was limited to at most μ-power density distributions. Most of the discussion concentrated on the parabolic distribution of Figure 4.11.

In the optical fibre field, distributions (of refractive index) other than parabolic have been considered. A cosh type distribution, rather than that of (4.37), has been considered by Kirchhoff (1972) in the optical fibre context. However he did not produce a dispersion relation for this density profile problem, being content instead to apply the usual optical fibre argument of considering totally guided modes and reducing the confluent hypergeometric functions to associated Legendre functions (instead of (4.45)). 'A set of various refractive-index profiles, including the homogeneous core and the quadratic refractive index as two special cases', were investigated by Okoshi and Okamoto (1974) for the cylindrical fibre. Conwell (1973) and Unger (1977) have considered an exponentially decaying distribution for a semi-infinite medium. Kirchhoff (1973), aware that 'uncontrolled diffusion processes' in the manufacture of optical fibres would cause a refractive index profile to tend towards a Gaussian distribution, simulated such a profile, for a cylindrical fibre, by considering power series expansions. He gives a comparison of parabolic and Gaussian profiles. The phase-speed curves are very similar to those shown in Figure 4.13, the Gaussian profile having larger cut-offs.

Coronal loops may be considered as inhomogeneities in which the (higher) density is distributed according to an exponential (Gaussian) law. Using the optical fibre analogy, it may be inferred that there

are possible oscillations, the time signatures of which would be similar to those observed (see Figure 4.1) at radio, hard X-ray and other wavelengths.

4.8.2 Curvature losses At the beginning of this chapter it was assumed, for mathematical simplicity, that coronal loops are straight tubes and curvature effects were neglected. Curvature of the dielectric fibre has important repercussions as regards signal strength and so study of the radiation loss in bends is a topic which has been pursued in some detail in the optical telecommunications field (see Marcatili and Miller, 1969; Gloge, 1972). The analogy between optical fibre modes and mhd modes in dense coronal loops may be exploited to gain some estimate of losses in a curved, coronal loop. The arguments used to interpret the formulae for bending losses in common use for optical fibres (see Olshansky, 1979) are straightforward and will be briefly outlined here as they relate to coronal loops.

Consider the uniform density coronal loop with radius of curvature R_c, shown in Figure 4.16. The stretching of the loop at the outside of the bend leads to an apparent decrease of the wavenumber k so that, in general, k is a function of r (the transverse distance into the loop's exterior measured from its axis) and the wavenumber is now,

$$k(r) = \frac{kR_c}{r + R_c} , \qquad (4.75)$$

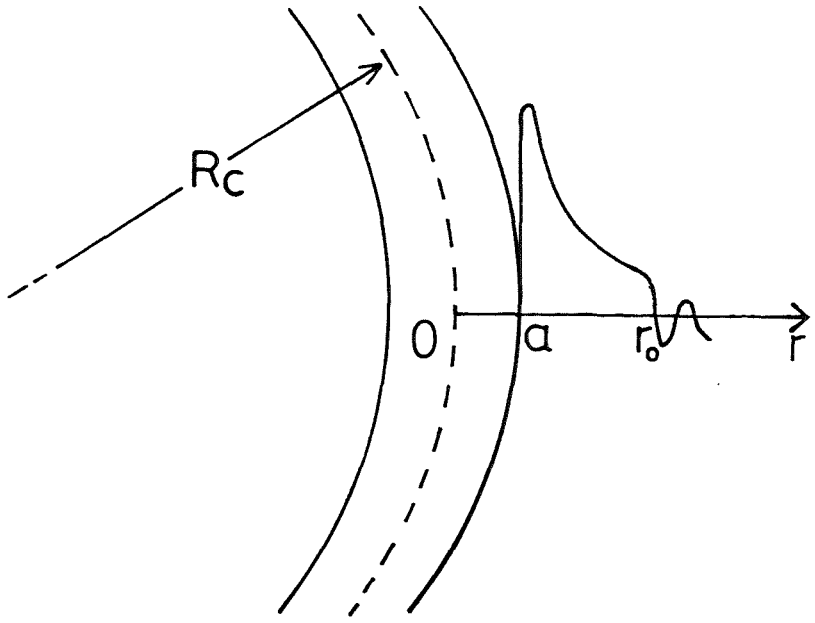

Figure 4.16 Curved coronal loop and its exterior field distribution at the outside of a bend

where $k = k(0)$ is the wavenumber along the loop's axis.

For a straight loop, fields in the exterior of the loop (see expressions (2.25), (3.19) and Section 3.5) decrease as

$$\text{cylinder} : \quad \exp[-m_e(0)(r-a)],$$

or

$$\text{slab} : \quad \exp[-m_e(0)(x-x_0)],$$

where $m_e(0) = m_e$ is independent of r (or x), the value it would have for a straight loop. For curved, cylindrical loops having uniform density profiles, for which k and hence m_e has r dependence, exterior fields decay as

$$\exp\left[- \int_a^r m_e(r)\,dr \right].$$

Now from (2.26) or (3.14), using (4.75), m_e may be approximated as

$$m_e^2 = \left[\frac{R_c^2 k^2}{(r + R_c)^2} - \frac{\omega^2}{v_{Ae}^2} \right] \simeq m_e^2(0) - \frac{2k^2 r}{R_c}. \qquad (4.76)$$

At a point $r = r_0$, $m_e(r_0) = 0$ and wave energy passing this point is radiated away (see Section 3.5) since m_e^2 becomes negative. Thus the resulting loss in energy must be proportional to

$$\exp\left[- 2\int_a^{r_0} m_e(r)\,dr \right]. \qquad (4.77)$$

Evaluating the exponent in (4.77), using $m_e(r_0) = 0$ and (4.76), gives an energy loss, ε, for a uniform density coronal loop with radius of curvature R_c, which is proportional to

$$\exp\left[- \frac{2R_c}{3k^2} \left(k^2 - \frac{\omega^2}{v_{Ae}^2} - \frac{2k^2 a}{R_c} \right)^{3/2} \right]. \qquad (4.78)$$

Approximating ω by kv_A and assuming $ka \simeq 1$, (4.78) may be simplified to

$$\varepsilon \sim \exp\left[- \frac{2R_c}{3a} \left(1 - \frac{v_A^2}{v_{Ae}^2} - \frac{2a}{R_c} \right)^{3/2} \right]. \qquad (4.79)$$

Taking $R_c = 10^5$km, $a = 10^3$km and $v_A/v_{Ae} = \frac{1}{2}$ gives an estimated loss of energy relative to its original value of e^{-41} ($\simeq 10^{-19}$), showing that losses due to curvature of the cylindrical loop are negligible. Curvature losses for both uniform and varying density distributions in both slab and cylinder models have been calculated by various methods. Olshansky (1979) reviews this work in the optical fibre context.

4.9 Summary

In this chapter explanations have been offered for some of the periodic and quasi-periodic oscillatory behaviour observed in the solar corona. It has been shown that the explanation does not depend on the coronal loop having uniform density. Variations in density across the loops would modify the duration of the quasi-periodic phase and the time scale of the periodic phase, but observations and results from radiowave, hard X-ray and other data could still be accounted for.

Whilst it is recognised that the real situation in a coronal loop is unlikely to be that of a single, symmetric mode in a dissipationless, linear system, the theory nevertheless offers an idea which can be tested against further observations, using predicted quantities such as loop width and associated Alfvén speed.

Attention was drawn to the fact that wave modes analogous to those occurring in coronal inhomogeneities feature in other fields such as atmospheric physics and optical telecommunications. The

optical fibre work, in particular, provides a wealth of ideas which may be exploited to further the examination of wave modes in coronal loops. Besides density variations and curvature losses, which were discussed here briefly, the analogy may be exploited in discussing possibilities such as nonlinear behaviour, dissipative effects and varying loop width to further our understanding of coronal features.

Chapter 5 Thermal Dissipation in a Structured Plasma

'... I would thou wert cold or hot.
So then because thou art lukewarm, and neither cold nor hot, ...'

Revelation 3:15

5.1 Dissipative Models

5.1.1 Introduction

The role played by thermal dissipation in a structured medium has up to now been ignored. To some extent this is justified. Using order of magnitude arguments Parker (1979a) has compared the dissipative effects on waves due to uniform-in-space, constant-in-time, non-zero coefficients of kinematic (fluid) viscosity, electrical resistivity and thermal conductivity and has declared that only in the coolest of stellar photospheres is resistivity of importance. Within the solar photosphere, he argues, resistive damping is negligible and viscosity and thermal conductivity are even less important than resistivity effects. However Parker's comments do not refer to detailed calculations or to a structured medium. They are based on order of magnitude arguments involving assumed temperature-dependent forms for the dissipation coefficients. Gordon and Hollweg (1983) also used such coefficients in their examination of viscous and thermal dissipation in a coronal slab. Here only isotropic thermal effects will be discussed; the strongly anisotropic nature of thermal conduction in the solar corona will not be considered.

If, as Parker suggests, thermal conduction is a negligible effect in the non-coronal solar atmosphere then what motivation is

there for considering thermal dissipation in a structured plasma? The controversies regarding the cooling of sunspots were mentioned in Chapter 1. If convective heat transport along magnetic lines of force is suppressed by the magnetic field itself and motion across field lines is also inhibited (by the frozen-in condition) then convection below the sunspot is mainly limited to up-and-down motions along the field lines (see Cowling, 1976). The problem then arises as to whether these oscillatory motions grow in time (overstability), perhaps contributing to the cooling of the sunspot (Parker, 1974a; Roberts, 1976). Furthermore, Parker (1979c) has put forward the idea that umbral dots may be regions where field-free gas (at near normal photospheric temperatures) emerge through the sunspot surface as a result of such vertical motion. To simulate such convective behaviour in sunspots an equation of heat transfer such as (1.6) is employed where Q is considered to be the (uniform) convective heat transfer coefficient (e.g., Roberts, 1976; Spruit, 1977; Parker, 1979a). This equation is often used more generally in the linearized form

$$\rho_0 c_p \frac{\partial T}{\partial t} - \frac{\partial p}{\partial t} = Q \nabla^2 T, \qquad (5.1)$$

where Q is a combined heat transport coefficient which takes into account both conduction, convection and (in some models) radiative heat transport effects (Moore, 1973; Cowling, 1976; Priest, 1982).

A similar model may be applied to the intense flux tube. Parker (1979a) has considered this in some detail, being concerned

with the concentration of magnetic fields into such tubes due to downdrafts and the enhancement of this effect due to superadiabaticity - the suppression of convective heat transport causing the temperature of the gas flowing downwards within the tube to fall below that of the external gas, to be further helped by gravitational effects. Parker (1979a) describes the theory as being 'in an untidy state' and suggests that the physics of flux tubes (and sunspots) in a convective environment warrants further investigation.

It is well-known that the third form of heat transfer, namely radiation, will dissipate wave propagation in the upper photosphere; see, for example, Bray and Loughhead (1974). Parker (1979a) has also drawn attention to the importance of radiative effects in the first thousand or so kilometres below the visible surface of the Sun. He quotes a table from Spruit (1974) showing that in this layer the convective and radiative heat transfer coefficients are of comparable size.

Radiative damping in a structured medium, specifically a flux tube in a non-magnetic environment, has been considered in detail by Webb and Roberts (1980 a,b). In this chapter radiative loss only in a form similar to that considered by Webb and Roberts will be used, mainly as a comparison with other heat transport losses modelled by (5.1). This means that for linear perturbations about the equilibrium, (1.9) and (1.10), the radiative loss term in (1.6) (the rate of heat lost per unit volume due to radiative effects) will be assumed to obey Newton's law of cooling (see Spiegel, 1957, 1964; Souffrin, 1966, 1972; also Webb and Roberts, 1980a) so that

(1.7) reduces to

$$\mathcal{R} = \frac{\rho_0 c_V}{\tau_R} T \tag{5.2}$$

for linear temperature perturbation T. Here τ_R is the radiative decay time, assumed known from tables such as those given by Bray and Loughhead (1974), Spruit (1974) and Giovanelli (1978, 1979). Thus, combining (5.1) and (5.2), the linearized temperature equation will be used in the form

$$\rho_0 c_p \frac{\partial T}{\partial t} - \frac{\partial p}{\partial t} = Q \nabla^2 T - \frac{\rho_0 c_V}{\tau_R} T. \tag{5.3}$$

5.1.2 Thermal time scales As Webb and Roberts (1980a) point out, tabulated values of τ_R show a considerable variation in that part of the solar atmosphere extending from the photosphere to the low chromosphere. So for perturbations with a time-dependence of the form $e^{i\omega t}$ and typical frequencies ω of order $10^{-2}s^{-1}$, both extremes of almost adiabatic ($\omega\tau_R >> 1$) and almost isothermal ($\omega\tau_R << 1$) perturbations are likely to occur.

In this chapter, however, convective and conductive rather than radiative heat transfer effects will be emphasized. An attempt will be made to elucidate the effects of thermal diffusion in a structured medium and to quantify the thermal decay time for a heat transport coefficient Q which represents heat transfer effects as in (5.1), rather than some simplification like (5.2) as in the case of radiative losses.

In the introductory chapter the equation for adiabatic

perturbations was derived by assuming that typical time scales of the system were very much smaller than thermal diffusion time scales, τ_R and τ_κ. Here τ_κ is a typical (convective or conductive) time scale given by

$$\tau_\kappa \propto \frac{\ell^2}{\kappa} = \frac{c\ell^2}{\kappa}, \tag{5.4}$$

where $\kappa = Q/\rho_0 c_p$ is the thermal diffusivity ($m^2 s^{-1}$), ℓ is a length scale and c a constant of proportionality.

In a structured medium the question which naturally arises is what is a 'typical length scale' for the medium. For example, consideration of thermal dissipation in an intense flux tube would suggest using the tube's radius a for ℓ, c remaining undetermined. Parker (1979a), in the argument referred to above (Subsection 5.1.1), supposed that a wave mode of the form e^{ikz} would have a decay factor $\exp(-\alpha\kappa k^2 t)$, where α is a number of order unity. Thus Parker's choice of ℓ ($= 2\pi/k$) as the wavelength of the mode is another obvious possibility.

One may argue, vaguely, that if in some sense heat cannot be transferred across the width of the structure during the time scale of the motion, then the width of the structure has no significance, the radius a is irrelevant and the wavelength $2\pi/k$ is the pertinent length scale of the system. This argument may be expressed in more mathematical terms using the Péclet number P_e (see, e.g., Richardson, 1950; Landau and Lifshitz, 1959) which is defined as

$$P_e = \frac{\ell V}{\kappa}$$

(a "Reynolds number" for thermal dissipation). Here V is a typical velocity. For time dependence of the form $e^{i\omega t}$, a typical phase-speed (V) is ω/k and one way of expressing the Péclet number which will prove useful subsequently is as $\frac{\omega}{k} \cdot \frac{(ka).a}{\kappa}$ or $\frac{a^2\omega}{\kappa}$.

Expressing the above argument symbolically if the Péclet number is large (thermal boundaries can be ignored) then $2\pi/k$, the wavelength, rather than a, the radius, is expected to be the pertinent length scale in τ_κ; that is for

$$P_e = \frac{\omega a^2}{\kappa} > 1, \tag{5.5}$$

a time scale of

$$\tau_\kappa \propto \frac{1}{k^2\kappa} \tag{5.6}$$

is to be expected.

Alternatively, it 'heat can reach the boundaries of the structure' during a typical time scale of the motions, then the thermal properties of the boundaries may be expected to play a part. For example, for perfectly conducting (isothermal) boundaries the temperature perturbation may be expected to have a node on the boundary. The time scale would depend on the width of the structure rather than the wavelength. This would suggest that for

$$P_e < 1 \tag{5.7}$$

a time scale of

$$\tau_\kappa \propto a^2/\kappa \tag{5.8}$$

is anticipated.

In this chapter explicit forms for the time scale τ_κ in (5.4) will be derived, showing how the constant c and the length scale ℓ depend on the size of the Péclet number.

It will be shown that by identifying a particular form of τ_κ with the radiative loss time τ_R, some of the results of Webb and Roberts (1980 a,b) may be exploited to examine thermal dissipative effects in a slender structure as modelled by (5.1) rather than by the (simpler) Newton's law of cooling model investigated by Webb and Roberts.

Heat transfer effects as described by Equation (5.1) will be referred to loosely as 'thermal conduction' or 'conductive effects' in the rest of this thesis. The rate of heat transfer as represented by (1.7) or (5.2) above (the simplified Newton's law of cooling term in (1.6) or (5.3)) will be referred to as 'radiative loss'. To begin with gravitational effects will be ignored.

5.2 Compressible, Gravity-free, Dissipative Modes

The investigations in Chapters 2 and 3 have shown that there

is little to choose mathematically between Cartesian and cylindrical models of a structure especially where symmetric modes are concerned. Here, an attempt to model a cylindrically structured medium, but including thermal conductivity effects, will be made. Most of the previous thermal conduction models have considered a slab geometry (Parker, 1974b, 1979b,c; Roberts 1976) and have been restricted to a Boussinesq (incompressible) fluid (see Section 5.5).

Assuming, then, a variation of the form $e^{i\omega t}$ for the perturbation variables p, ρ, T, v_r, v_z, b_r and b_z (but avoiding its explicit mention) and supposing, for the sake of simplicity, that the system is uniform and axisymmetric, the equations of continuity, motion and induction (Equations (1.16), (1.17) and (1.15)) become:

$$\left.\begin{aligned} i\omega\rho &= -\rho_0\frac{\partial v_z}{\partial z} - \rho_0\frac{\partial v_r}{\partial r} - \rho_0\frac{v_r}{r}, && \text{(a)}\\ \rho_0 i\omega v_r &= -\frac{\partial p}{\partial r} + \frac{B_0}{\mu_0}\left(\frac{\partial b_r}{\partial z} - \frac{\partial b_z}{\partial r}\right), && \text{(b)}\\ \rho_0 i\omega v_z &= -\frac{\partial p}{\partial z}, && \text{(c)}\\ i\omega b_r &= B_0\frac{\partial v_r}{\partial z} && \text{(d)}\\ \text{and}\quad & \\ i\omega b_z &= -B_0\frac{\partial v_r}{\partial r} - B_0\frac{v_r}{r}. && \text{(e)} \end{aligned}\right\} \quad (5.9)$$

Also, the linearized versions of (1.8) (about the equilibrium (1.9)) and (5.3) may be written

$$p = R\rho_0 T + RT_0\rho \qquad (5.10a)$$

and

$$i\omega T = \kappa\left[\frac{\partial^2 T}{\partial r^2} + \frac{1}{r}\frac{\partial T}{\partial r} + \frac{\partial^2 T}{\partial z^2}\right] + \frac{i\omega T_0(\gamma-1)}{\gamma p_0} p - \frac{T}{\gamma \tau_R}, \qquad (5.10b)$$

where κ ($= Q/\rho_0 c_p$) is the constant thermal diffusivity. Equations (5.9) and (5.10) describe the perturbation amplitudes of linear motions in a thermally dissipative plasma.

After Fourier analysing with respect to z (again abusing notation by omitting mention of e^{ikz}), these equations may be expressed in terms of the temperature and pressure perturbations alone:

$$\frac{d^2 p}{dr^2} + \frac{1}{r}\frac{dp}{dr} - m_{0R}^2 p = \alpha_1\left[\frac{d^2 T}{dr^2} + \frac{1}{r}\frac{dT}{dr} - \frac{(k^2 v_A^2 - \omega^2)}{v_A^2} T\right] \qquad (5.11)$$

and

$$\kappa \frac{d^2 T}{dr^2} + \frac{\kappa}{r}\frac{dT}{dr} - \left(k^2\kappa + i\omega + \frac{1}{\gamma\tau_R}\right)T = -\beta_1 p. \qquad (5.12)$$

Here

$$\alpha_1 = \frac{v_A^2 \omega^2 p_0}{T_0(c_0^2/\gamma + v_A^2)(\omega^2 - k^2 c_R^2)}, \quad \beta_1 = \frac{i\omega T_0(\gamma-1)}{\gamma p_0}, \quad m_{0R}^2 = \frac{(k^2 v_A^2 - \omega^2)(k^2 c_0^2/\gamma - \omega^2)}{(c_0^2/\gamma + v_A^2)(k^2 c_R^2 - \omega^2)}, \qquad (5.13)$$

and c_R^2, the 'isothermal equivalent' of c_T^2, is given by

$$c_R^2 = \frac{(c_0^2/\gamma)v_A^2}{(c_0^2/\gamma + v_A^2)} \quad (< c_T^2). \qquad (5.14)$$

The velocity and magnetic fields are related to p and T via the equations,

$$\frac{i\rho_0}{\omega}\,(k^2v_A^2 - \omega^2)v_r = \frac{dp_T}{dr} \tag{5.15}$$

and

$$b_z = \frac{B_0}{\rho_0\omega^2}\,p\left(\frac{\omega^2\gamma}{c_0^2} - k^2\right) - \frac{B_0}{T_0}\,T. \tag{5.16}$$

Equations (5.11) and (5.12) may be combined to yield a fourth-order equation for T, namely

$$\left[\kappa D^4 - \left(\kappa k^2 + i\omega + \frac{1}{\gamma\tau_R}\right)D^2 - \kappa m_{0_R}^2 D^2 + \alpha_1\beta_1 D^2 + \kappa m_{0_R}^2 k^2 + \left(i\omega + \frac{1}{\gamma\tau_R}\right)m_{0_R}^2 - \frac{\alpha_1\beta_1(k^2v_A^2 - \omega^2)}{v_A^2}\right]T = 0, \tag{5.17}$$

where $D^2 \equiv d^2/dr^2 + 1/r\ d/dr$. In general, for finite but non-zero κ, Equation (5.17) has solutions of the form

$$T = A_1 I_0(\lambda_1 r) + A_2\, I_0(\lambda_2 r)\ , \quad (\lambda_1 \neq \lambda_2;\ A_1, A_2 \text{ constants}) \tag{5.18}$$

where I_0 is a modified Bessel function and the possible K_0 solutions have been rejected because the perturbed temperature is required to be finite along the centre of the inhomogeneity. Of course, as in Chapter 3, J_0 type solutions are possible depending on the nature of λ_1 and λ_2. These latter quantities satisfy a quadratic in λ^2, namely,

$$\kappa\lambda^4 - \left(\kappa k^2 + i\omega + \frac{1}{\gamma\tau_R}\right)\lambda^2 - \kappa m_{0_R}^2\lambda^2 + \alpha_1\beta_1\lambda^2 + \kappa m_{0_R}^2 k^2 + \left(i\omega + \frac{1}{\gamma\tau_R}\right)m_{0_R}^2 - \frac{\alpha_1\beta_1(k^2v_A^2 - \omega^2)}{v_A^2} = 0. \tag{5.19}$$

It would be repetitive to carry out a full analysis of (5.17) and (5.19) since Webb and Roberts (1980 a,b) have already considered the effects of radiative damping ($\kappa = 0$) and here the aim is to study conductive effects ($\tau_R \to \infty$, $\kappa \neq 0$). However in order to better appreciate these equations in their entirety a brief discussion of the work of Webb and Roberts will now be given, thus enabling results for the conductive case to be compared and contrasted with those for radiative damping.

5.2.1 Radiative, non-conducting modes When thermal conduction is neglected ($\kappa = 0$) but radiative effects are considered, Equation (5.17) reduces from fourth to second order and becomes

$$\left[\left(i\omega + \frac{1}{\gamma\tau_R}\right)D^2 - \alpha_1\beta_1 D^2 - \left(i\omega + \frac{1}{\gamma\tau_R}\right)m_{0R}^2 + \frac{\alpha_1\beta_1(k^2v_A^2 - \omega^2)}{v_A^2}\right]T = 0, \tag{5.20}$$

which may be rearranged to give

$$(D^2 - \lambda_0^2)T = 0 \tag{5.21}$$

where

$$\lambda_0^2 = \frac{(k^2v_A^2 - \omega^2)(k^2c_0^2\Omega_0 - \omega^2)}{k^2c_0^2v_A^2\Omega_0 - \omega^2(v_A^2 + c_0^2\Omega_0)} \tag{5.22}$$

and

$$\Omega_0 = (i\omega + 1/\gamma\tau_R)/(i\omega + 1/\tau_R). \tag{5.23}$$

In the adiabatic limit, when $\Omega_0 = 1$, Equations (5.21) and (5.22) reduce to Equations (3.11) (in axisymmetric form) and (3.12), which were investigated for a structured medium in Chapter 3.

The effects of radiative damping in a structured medium have been considered by Webb and Roberts (1980a), who discussed Equations (5.21), (5.22) and (5.23) as they relate to both an unbounded medium and to a flux tube.

For a non-conducting ($\kappa = 0$) radiative medium explicit mention of temperature may be removed from Equations (5.9) and (5.10) so that (see Equation (5.12) with $\kappa = 0$) the amplitude of the pressure perturbation, p, or of the divergence of the velocity, $\hat{R}$, satisfies an equation such as (5.21) which has axisymmetric solutions

$$\hat{R}(r) = A_0 I_0(\lambda_0 r), \tag{5.24}$$

where A_0 is constant. Other field variables, v_r, ρ, etc., may be related to $\hat{R}$ by Equations (3.13) with m_0^2 replaced by λ_0^2, given by (5.22) above. Thus, invoking continuity of the transverse velocity and total pressure (see Equations (1.19) and (1.20)), Webb and Roberts showed that the appropriate dispersion relation for a radiative, structured medium (a flux tube with a field-free exterior) is

$$(k^2 v_A^2 - \omega^2)\, \lambda_e \frac{I_0(\lambda_0 a)}{I_1(\lambda_0 a)} = \frac{\rho_e}{\rho_0}\, \omega^2 \lambda_0 \frac{K_0(\lambda_e a)}{K_1(\lambda_e a)}. \tag{5.25}$$

Here $\lambda_e^2 = k^2 - \omega^2/c_e^2\Omega_e$, where Ω_e is the equivalent of (5.23) in the exterior.

Equation (3.20) is seen to be the special case of (5.25) when radiative damping is neglected, so that λ_0 and λ_e then reduce to m_0 and m_e respectively.

Webb and Roberts (1980a) examined the dispersion relation (5.25) for the effects of radiative relaxation on the $\omega^2 \simeq k^2 c_T^2$ mode (see (3.27)) of a slender flux tube $|k|a << 1$. Assuming that $|\lambda_0|a << 1$ in this limit, (5.25) reduces to (see Equation (3.26))

$$\omega^2(v_A^2 + c_0^2\Omega_0) = k^2 c_0^2 v_A^2 \Omega_0, \tag{5.26}$$

which, on using (5.23), becomes

$$(c_0^2 + v_A^2)\omega^3 - \frac{i}{\tau_R}\left(\frac{c_0^2}{\gamma} + v_A^2\right)\omega^2 - k^2 c_0^2 v_A^2 \omega + \frac{ik^2 c_0^2 v_A^2}{\gamma \tau_R} = 0. \tag{5.27}$$

In the adiabatic limit Equation (5.27) is seen to give the tube speed $\omega^2 \simeq k^2 c_T^2$ or $\omega = 0$.

Webb and Roberts (1980a) considered the radiative damping of modes from two viewpoints, namely temporal damping, in which the wavenumber k is considered real and ω, from (5.27), is then complex, and spatial damping, in which ω is prescribed real and the wavenumber is then complex.

If τ_S is a typical sound travel time of the system, equal to $1/kc_0$, say, then for large radiative decay times $\tau_R >> \tau_S$, Webb and Roberts showed that temporally-damped disturbances are described by

$$\omega_{1,2} \simeq \pm kc_T\left[1 + 0\left(\frac{\tau_S}{\tau_R}\right)^2\right] + \frac{i}{2}\left(\frac{\gamma-1}{\gamma}\right)\frac{c_T^2}{c_0^2 \tau_R} \tag{5.28}$$

and

$$\omega_3 \simeq \frac{i}{\gamma} kc_0\left(\frac{\tau_S}{\tau_R}\right), \tag{5.29}$$

so that modes given by (5.28) are reduced from their adiabatic values by a damping factor, the decay rate being greater for a stronger magnetic field. In addition there is a purely thermal mode given by (5.29).

For small radiative decay times, $\tau_R \ll \tau_S$, the almost isothermal slender tube modes are given by

$$\omega_{1,2} \simeq \pm kc_R \left[1 + 0\left(\frac{\tau_R}{\tau_S}\right)^2 \right] + \frac{i}{2}\left(\frac{\gamma-1}{\gamma}\right) \frac{v_A^4}{(c_0^2/\gamma + v_A^2)^2 \tau_S} \left(\frac{\tau_R}{\tau_S}\right) \qquad (5.30)$$

and

$$\omega_3 \simeq -\left(\frac{c_0^2/\gamma + v_A^2}{c_0^2 + v_A^2}\right) kc_0 \left(\frac{\tau_S}{\tau_R}\right), \qquad (5.31)$$

with c_R given by (5.14).

If heat transfer effects near the solar surface are to be considered then the effects of stratification on wave propagation are also important. Roberts and Webb (1978) discussed wave propagation in an intense magnetic flux tube embedded in a stratified, non-magnetic, non-radiative atmosphere. For a stratified atmosphere, equilibrium quantities B_0, ρ_0, p_0, etc. have z-dependence, c_0^2 equals $\gamma p_0(z)/\rho_0(z)$, and certain characteristic variables arise, namely the density scale-height $H_0(z)$, the pressure scale-height $\Lambda_0(z)$ and the Brunt-Väisälä (buoyancy) frequency $N_0(z)$, given by

$$H_0(z) = -\frac{\rho_0(z)}{\rho_0'(z)}, \quad \Lambda_0(z) = \frac{R T_0(z)}{g} \quad \text{and} \quad N_0^2(z) = \frac{g}{H_0(z)} - \frac{g^2}{c_0^2(z)}. \qquad (5.32)$$

Roberts and Webb found that linear pressure perturbations $\hat{p}$ about the equilibrium (1.9) and (1.14), for a dissipationless medium, satisfies

$$(\omega^2 - N_0^2(z))\hat{p}'' + \alpha_0(z;\omega^2)\hat{p}' + \beta_0(z;\omega^2)\hat{p} = 0, \tag{5.33}$$

where

$$\alpha_0(z;\omega^2) = (\omega^2 - N_0^2)\left(\frac{2c_0'}{c_0} - \frac{B_0'}{B_0} + \frac{1}{\Lambda_0}\right) + 2N_0N_0',$$

$$\beta_0(z;\omega^2) = (\omega^2 - N_0^2)\left[\left(\omega^2 - \frac{g}{H_0}\right)\left(\frac{1}{c_0^2} + \frac{1}{v_A^2}\right) + \frac{g^2}{c_0^2v_A^2} + \frac{g}{c_0^2\Lambda_0} - \frac{g\,B_0'}{c_0^2B_0}\right]$$

$$+ 2g\,\frac{N_0N_0'}{c_0^2}, \tag{5.34}$$

and dash ($'$) denotes differentiation with respect to z. Additionally, they showed that the velocity amplitude $\hat{v}_z$ satisfies:

$$\hat{v}_z'' - \frac{1}{2\Lambda_0}\hat{v}_z' + \left[\frac{(\omega^2 - N_0^2)}{c_T^2} + \left(1 - \frac{\gamma}{2}\right)\frac{N_0^2}{c_0^2}\right]\hat{v}_z = 0. \tag{5.35}$$

They also showed that propagation only occurs for frequencies greater than a critical frequency ω_v, where

$$\omega_v^2 = \frac{c_T^2(z)}{\Lambda_0^2(z)}\left\{\frac{3}{4}\Lambda_0'(z) + \frac{9}{16} - \frac{1}{2\gamma} + \frac{1}{\gamma}\left[\frac{\gamma-1}{\gamma} + \Lambda_0'(z)\right]\frac{c_0^2}{v_A^2}\right\}$$

$$= N_0^2 + \frac{c_T^2}{\Lambda_0^2}\left(\frac{3}{4} - \frac{1}{\gamma}\right)\left(\frac{3}{4} - \frac{1}{\gamma} + \Lambda_0'\right). \tag{5.36}$$

Extending the work described above, to consideration of radiative relaxation *and* stratification, Webb and Roberts (1980b) examined the effect of radiative relaxation on the propagation of waves in an intense magnetic flux tube in a stratified, non-magnetic environment. As in their previous paper (1980a) Newton's law of cooling was assumed so that the relatively simple form (5.2) was used for radiative losses. Webb and Roberts found that the amplitude of the velocity $\hat{v}_z$, where $v_z = \hat{v}_z(z)e^{i\omega t}$, satisfies the equation

$$\frac{d^2\hat{v}_z}{dz^2} + \left[\alpha_1 + \left(\frac{1 - i\Omega}{1 + \Omega^2}\right)\alpha_2\right]\frac{d\hat{v}_z}{dz} + \left[\beta_1 + \left(\frac{1 - i\Omega}{1 + \Omega^2}\right)\beta_2\right]\hat{v}_z = 0, \qquad (5.37)$$

where

$$\left.\begin{aligned} \Omega = \gamma\omega\tau_R, \quad \alpha_1 = -\frac{1}{2\Lambda_0}, \quad \alpha_2 = -\frac{\Lambda_0'}{\Lambda_0}, \quad \beta_1 = \frac{\omega^2 - N_0^2}{c_T^2} + \left(1 - \frac{\gamma}{2}\right)\frac{N_0^2}{c_0^2} \\ \text{and} \\ \beta_2 = \left(\frac{\gamma-1}{\gamma}\right)\left[\frac{\omega^2}{g\Lambda_0} + \frac{1}{\Lambda_0^2}\left(\frac{c_0^2}{\gamma v_A^2} + \frac{1}{2}\right)\right] + \frac{\Lambda_0'}{\Lambda_0^2}\left(\frac{c_0^2}{\gamma v_A^2} + 1\right) - \left(\frac{\Lambda_0'}{\Lambda_0}\right)'. \end{aligned}\right\} \qquad (5.38)$$

A full discussion of (5.37) is difficult, but by considering an isothermal atmosphere ($\Lambda_0' \equiv 0$) Webb and Roberts were able to deduce certain general results and compare them with observations. Briefly, by considering spatial damping (damping per scale height, in which ω^2 is real and τ_R finite) they found that for small decay time τ_R, high frequencies suffer a large amount of damping, which is

increased for a stronger magnetic field, and the cut-off frequency for propagation in (5.36) is reduced. Modes which were progressive waves in the absence of dissipation ($\omega > \omega_V$) become damped, whereas those which were evanescent ($\omega < \omega_V$) are able to propagate.

5.2.2 Conducting, non-radiative modes Neglecting terms involving radiative losses by setting $\tau_R \to \infty$, and for large thermal conductivity ($\kappa \to \infty$), the roots of (5.19) become

$$\lambda^2 = k^2 \text{ or } m_{0_R}^2.$$

On the other hand consideration of the dominant terms of (5.19) for $\kappa \to 0$, $\tau_R \to \infty$ shows that a scaling in the form $\lambda = \kappa^{-\frac{1}{2}} q$ converts the equation to the form

$$q^4 - B_1 q^2 = 0, \tag{5.39}$$

where

$$B_1 = \frac{i\omega(k^2 c_0^2 - \omega^2) m_{0_R}^2}{\gamma m_0^2 (k^2 c_0^2/\gamma - \omega^2)}.$$

The four solutions of (5.39) are $q = 0$, 0 and $\pm B_1^{\frac{1}{2}}$ and a perturbation analysis (see, for example, Bender and Orszag, 1978) shows that the corresponding solutions of (5.19) ($\tau_R \to \infty$) are

$$\lambda_1 = q\kappa^{-\frac{1}{2}} = \pm m_0 \left[1 - \frac{(m_0^2 - k^2)(m_0^2 - m_{0_R}^2)\gamma(k^2 c_0^2/\gamma - \omega^2)\kappa}{2i\omega\, m_{0_R}^2 (k^2 c_0^2 - \omega^2)} \right] \tag{5.40a}$$

and

$$\lambda_2 = \kappa^{-\frac{1}{2}}(\pm B_1^{\frac{1}{2}}) = \pm \frac{i^{\frac{1}{2}}\omega^{\frac{1}{2}}(k^2c_0^2 - \omega^2)^{\frac{1}{2}}m_{0_R}}{\gamma^{\frac{1}{2}}m_0(k^2c_0^2/\gamma - \omega^2)^{\frac{1}{2}}\kappa^{\frac{1}{2}}}. \qquad (5.40b)$$

From (5.40a) it is obvious that for the incompressible ($m_0^2 = k^2$) problem, thermal conductivity does not affect the 'original' solutions $I_0(\pm m_0 r)$ to order κ. In fact, as will be shown in the special case (iii) below this is true for all orders of κ.

Using (5.15), (5.16) and (5.18) it may be shown that for continuity of temperature, heat flux, total pressure and radial velocity (conditions (1.19) to (1.22)) the following quantities must be matched across the boundary of the cylinder ($r = a$):

$$\left.\begin{aligned} T &= A_1 I_0(\lambda_1 r) + A_2 I_0(\lambda_2 r), \\ \kappa \frac{\partial T}{\partial r} &= \kappa[\lambda_1 A_1 I_1(\lambda_1 r) + \lambda_2 A_2 I_1(\lambda_1 r)], \\ p + \frac{B_0}{\mu_0} b_z &= A_1 F_1 I_0(\lambda_1 r) + A_2 F_2 I_0(\lambda_2 r) \end{aligned}\right\} \qquad (5.41)$$

and

$$\left.\begin{aligned} v_r = \frac{\omega}{i\rho_0(k^2 v_A^2 - \omega^2)} \; [\lambda_1 F_1 A_1 I_1(\lambda_1 r) + \lambda_2 F_2 A_2 I_1(\lambda_2 r)]. \end{aligned}\right\}$$

In the above,

$$F_j = C_j \frac{(c_0^2/\gamma + v_A^2)(\omega^2 - k^2 c_R^2)}{\omega^2 c_0^2/\gamma} - \frac{B_0^2}{\mu_0 T_0}, \quad C_j = \frac{i\gamma p_0}{(\gamma-1)T_0\omega}(\lambda_j^2\kappa - k^2\kappa - i\omega) \qquad (5.42)$$

and A_j are constants; $j = 1,2$.

In the exterior of the cylinder a similar set of expressions will describe the variables, except that now solutions which do not decay as $r \to \infty$ are ruled out (I_0, J_0 Bessel functions are excluded). Thus the exterior variables may be described by the equations:

$$\left.\begin{aligned} T^e &= a_1 K_0(\lambda_{e_1} r) + a_2 K_0(\lambda_{e_2} r), \quad (\lambda_{e_1} \neq \lambda_{e_2},\ \mathrm{Re}(\lambda_{e_1}) \text{ and } \mathrm{Re}(\lambda_{e_2}) > 0) \\ \kappa_e \frac{\partial T^e}{\partial r} &= -\kappa_e \lambda_{e_1} a_1 K_1(\lambda_{e_1} r) - \kappa_e \lambda_{e_2} a_2 K_1(\lambda_{e_2} r), \\ p^e + \frac{B_e}{\mu_0} b_{e_z} &= a_1 d_1 K_0(\lambda_{e_1} r) + a_2 d_2 K_0(\lambda_{e_2} r) \end{aligned}\right\} \quad (5.43)$$

and

$$v_{e_r} = \frac{\omega}{i\rho_e(k^2 v_{Ae}^2 - \omega^2)} \left[\lambda_{e_1} d_1 a_1 K_1(\lambda_{e_1} r) + \lambda_{e_2} d_2 a_2 K_1(\lambda_{e_2} r)\right],$$

where

$$d_j = \frac{i\gamma p_e(\lambda_{e_j}^2 \kappa_e - k^2 \kappa_e - i\omega)\left[(c_e^2/\gamma + v_{Ae}^2)\omega^2 - k^2 c_e^2 v_{Ae}^2/\gamma\right]}{(\gamma-1) T_e \omega^3 c_e^2/\gamma} - \frac{B_e^2}{\mu_0 T_e} \quad (5.44)$$

and the a_j are constants, with $j = 1,2$.

Matching (5.41) and (5.43) across the boundary $r = a$ of the cylinder results in the dispersion relation for ω, which in determinant form is

$$\begin{vmatrix} 1 & 1 & -1 & -1 \\ \kappa\lambda_1\Phi_1 & \kappa\lambda_2\Phi_2 & \kappa_e\lambda_{e_1}\Psi_1 & \kappa_e\lambda_{e_1}\Psi_2 \\ F_1 & F_2 & -d_1 & -d_2 \\ \dfrac{\lambda_1 F_1\Phi_1}{V_A} & \dfrac{\lambda_2 F_2\Phi_2}{V_A} & \dfrac{-\lambda_{e_1} d_1\Psi_1}{\rho_r V_e} & \dfrac{-\lambda_{e_2} d_2\Psi_2}{\rho_r V_e} \end{vmatrix} = 0, \tag{5.45}$$

where $\Phi_j = \dfrac{I_1(\lambda_j a)}{I_0(\lambda_j a)}$, $\Psi_j = \dfrac{K_1(\lambda_{e_j} a)}{K_0(\lambda_{e_j} a)}$, $\rho_r = \dfrac{\rho_e}{\rho_0}$, $V_A = k^2 v_A^2 - \omega^2$

and $V_e = k^2 v_{Ae}^2 - \omega^2$. (5.46)

Equation (5.45), in principle, solves the problem of the possible modes, but it is rather unwieldy. However, special cases both confirm its validity and eludicate, to some extent, the nature of its rich spectrum of solutions.

(i) Thermal conductivity negligible. With κ and κ_e both $\to$ zero, Equation (5.45) reduces to

$$(\lambda_{e_2} + \lambda_2)\, \frac{\rho_0(c_0^2 + v_A^2)(k^2 c_T^2 - \omega^2)\rho_e(c_e^2 + v_{Ae}^2)(k^2 c_{Te}^2 - \omega^2)}{(\gamma - 1)^2 \omega^4 T_0 T_e} \left[\frac{m_e\Psi_1}{\rho_r V_e} + \frac{m_0\Phi_1}{V_A}\right] = 0, \tag{5.47}$$

where λ_2 is given by (5.40b) and λ_{e_2} is the equivalent expression in the external medium. On examination this equation yields either the degenerate roots $\omega^2 = k^2c_T^2$ and $k^2c_{Te}^2$, or

$$\frac{m_e K_1(m_e a)}{K_0(m_e a)} (k^2 v_A^2 - \omega^2) = - \frac{\rho_e}{\rho_0} m_0 \frac{I_1(m_0 a)}{I_0(m_0 a)} (k^2 v_{Ae}^2 - \omega^2). \qquad (5.48)$$

Hence Equation (3.25), for symmetric surface waves in a cylindrically structured non-conducting medium (see Figs. 3.3 and 3.4 for illustrations of its solutions), is recovered.

(ii) Isothermal disturbances. In the limit of κ and κ_e both tending to infinity the determinantal equation (5.45) reduces to

$$\frac{\rho_0 \rho_e \kappa \kappa_e \gamma^2 \omega^2}{(\gamma-1) T_0 T_e} \left(\frac{\lambda e_2 \Psi_2}{\rho_r V_e} + \frac{\lambda_2 \Phi_2}{V_A} \right) \left(\frac{K_1(ka)}{K_0(ka)} + \frac{I_1(ka)}{I_0(ka)} \right) = 0, \qquad (5.49)$$

where

$$\lambda_2^2 = m_{0_R}^2, \quad \lambda_{e_2}^2 = m_{e_R}^2 = \frac{(k^2 v_{Ae}^2 - \omega^2)(k^2 c_e^2/\gamma - \omega^2)}{(c_e^2/\gamma + v_{Ae}^2)(k^2 c_{Re}^2 - \omega^2)}$$

$$\text{and} \quad c_{Re}^2 = \frac{(c_e^2/\gamma) v_{Ae}^2}{(c_e^2/\gamma + v_{Ae}^2)}.$$

So, excepting $\omega = 0$, the possible modes satisfying (5.49) obey the isothermal equivalent of (5.48), namely

$$m_{e_R} \frac{K_1(m_{e_R} a)}{K_0(m_{e_R} a)} (k^2 v_A^2 - \omega^2) = - \frac{\rho_e}{\rho_0} m_{0_R} \frac{I_1(m_{0_R} a)}{I_0(m_{0_R} a)} (k^2 v_{Ae}^2 - \omega^2). \qquad (5.50)$$

(iii) The incompressible medium. Evaluating the determinantal equation (5.45) for an incompressible medium ($c_0, c_e \to \infty$) results in

$$\left[\frac{\lambda_1\Phi_1}{V_A} + \frac{\lambda_{1e}\Psi_1}{\rho_r V_e}\right]\left[\kappa_e\lambda_{e_2}\Psi_2 + \kappa\lambda_2\Phi_2\right] = 0. \tag{5.51}$$

The first factor of (5.51) gives

$$\frac{\omega^2}{k^2} = \frac{\left(\frac{v_{Ae}^2\rho_e}{\rho_0}\frac{I_1(ka)}{I_0(ka)}\cdot\frac{K_0(ka)}{K_1(ka)} + v_A^2\right)}{\left(\frac{\rho_e}{\rho_0}\frac{I_1(ka)}{I_0(ka)}\cdot\frac{K_0(ka)}{K_1(ka)} + 1\right)}, \tag{5.52}$$

which is just Equation (3.22) for the incompressible sausage modes. The solutions of (5.52) are illustrated in Figure 3.2. In general there are kink modes also but in this chapter discussion is restricted to the axisymmetric case.

The second factor of (5.51) shows that there are possible modes of the form

$$\omega = \frac{ij_n^{(0)2}\kappa}{a^2} + ik^2\kappa \quad (\kappa_e >> \kappa) \quad \text{and} \quad \omega = \frac{ij_n^{(1)2}\kappa}{a^2} + ik^2\kappa \quad (\kappa_e << \kappa), \tag{5.53}$$

where $j_n^{(0)}$ and $j_n^{(1)}$ are the zeros of the Bessel functions J_0 and J_1, respectively. Equations (5.53) may be interpreted for an incompressible, conducting fluid as follows.

For an incompressible fluid the linearized energy equation (5.1) becomes

$$\rho_0 c_p \frac{\partial T}{\partial t} = Q\nabla^2 T, \tag{5.54}$$

since pressure variations are radiated instantaneously (see Roberts, P.H., 1967). Fourier analysing Equation (5.54) gives

$$\frac{d^2T}{dr^2} + \frac{1}{r}\frac{dT}{dr} - \left(k^2 + \frac{i\omega}{\kappa}\right)T = 0. \tag{5.55}$$

The problem separates into the original ($\kappa = 0$) case and one for which

$$T = AI_0(\lambda_0 r),$$

where A is a constant and where only symmetric solutions, finite on $r = 0$, are considered. Here λ_0 satisfies

$$\lambda_0^2 = k^2 + i\omega/\kappa, \tag{5.56}$$

so, as in Chapter 3, J_0 type solutions are also possible.

Similarly, equations like (5.55) and (5.56) are obeyed in the exterior of the tube. For evanescent behaviour in the exterior, symmetric (sausage) modes are described by

$$\frac{I_0(\lambda_0 a)}{I_1(\lambda_0 a)} = -\frac{\kappa\lambda_0 K_0(\lambda_e a)}{\kappa_e \lambda_e K_1(\lambda_e a)}, \tag{5.57}$$

where λ_0 satisfies (5.56) and $\lambda_e^2 = k^2 + i\omega/\kappa_e$ with $\Re e(\lambda_e) > 0$. Setting

the second factor of Equation (5.51) to zero recovers Equation (5.57).

Hence, in addition to the surface modes described in Figure 3.2, there are thermal decay modes, for non-zero κ, described by (5.57). For an incompressible medium these modes are not coupled and so, as Parker (1974b) and Roberts (1976) have pointed out, there are no overstable modes. For isothermal boundaries ($\kappa_e >> \kappa$) expression (5.53) in dimensionless form becomes

$$\frac{\omega}{kv_A} = i\left(\frac{\kappa}{av_A}\right)\left[ka + \frac{j_n^{(0)2}}{ka}\right]. \qquad (5.58)$$

The modes are seen to decay linearly in time with increasing $K \equiv \frac{\kappa}{av_A}$, for fixed tube width. Also, it may be noted that there is an optimal wavenumber k for which the decay in time is minimal, for fixed a and κ.

(iv) <u>A single interface between conducting and highly conducting media</u>. This case is obtained by considering $\kappa/\kappa_e << 1$ and $ka >> 1$. Then the determinantal equation (5.45) simplifies considerably, since $\Phi_j, \Psi_j \to 1$ $(j = 1,2)$, giving

$$F_1\left\{\frac{\lambda_{e_1}\lambda_{e_2}}{\rho_r V_e}(d_2 - d_1) + \frac{\lambda_1}{V_A}(\lambda_{e_1}d_2 - \lambda_{e_1}d_1)\right\} = 0, \qquad (5.59)$$

which results in either the spurious root $\omega^2 = k^2 v_A^2$ or

$$m_{e_R}(k^2v_A^2 - \omega^2)\rho_0 + m_0\rho_e(k^2v_{Ae}^2 - \omega^2) = 0. \qquad (5.60)$$

Equation (5.60) is the equivalent of (3.39), the non-dissipative wide slab/interface result, as expected. Parker (1979b) uses the incompressible version of this equation in modelling the modes at the edge of a sunspot, so effectively the modes in his Equation (40) are just those of Equation (5.60) with $m_0 = m_{e_R} = k$, $v_{Ae} = 0$, $\rho_0 = \rho_e$ and one of the ω's replaced by $\omega + kU$, where U is a superposed velocity representing a downdraft in the basic state. Then (5.60) becomes

$$0 = k^2v_A^2 - \omega^2 - (\omega + kU)^2,$$

and Parker's result follows.

The above special cases ((i) - (iv)) serve to illustrate the generality and complexity of (5.45) but produce very little in the way of new information. Rather, they confirm some of the results derived earlier. As a precursor to a more detailed study of a *slender*, conducting cylindrical inhomogeneity the limit of (5.45) in this special case is now considered.

(v) The slender cylinder. Provided κ_e is not so small as to counteract the effect of slenderness (a statement to be expanded upon in Section 5.3), that is, provided $|\lambda_{e_1}|a$ and $|\lambda_{e_2}|a \to 0$ as $|k|a \to 0$, and velocity and temperature variations in the environment are negligible (so that the K_0 Bessel functions are small) or

equivalently that Ψ_j are the dominant terms in (5.45), the dispersion relation (5.45) in the limit of $|k|a << 1$ reduces to

$$\frac{\kappa_e I_0(\lambda_1 a) I_0(\lambda_2 a)}{\rho_r V_e a^2} (F_1 - F_2)(d_1 - d_2) = 0.$$

(It will be seen shortly that $\kappa_e \to \infty$, i.e. an isothermal environment, is consistent with the results derived here.)

There are four possibilities to discuss:

(1) $d_1 = d_2$, in which case either $\lambda_{e_1} = \lambda_{e_2}$ or $\omega^2 = k^2 c_{R_e}^2$. However both these possibilities can be ruled out, the first because it is the degenerate case of equal roots and the second because it represents a spurious solution;

(2) $F_1 = F_2$. This situation is similar to (1) in that either $\lambda_1 = \lambda_2$ or $\omega^2 = k^2 c_R^2$;

(3) $I_0(\lambda_1 a) = J_0(i\lambda_1 a) = 0$. As an illustration of this possibility, suppose that κ is small so that $\lambda_1 \to m_0$ and $I_0(\lambda_1 a) \to 1$ as $|k|a \to 0$. Thus, for this limiting value of κ, at least, the possibility (3) does not produce roots. Similarly, for $\kappa \to \infty$, $\lambda_1 \to m_{0_R}$ and so again $I_0(\lambda_1 a) \to 1$. In general, since the Bessel function does not have a root for $\lambda_1 a \to 0$, there will be no modes;

(4) There remains the possibility that $J_0(i\lambda_2 a) = I_0(\lambda_2 a) = 0$. For κ small this implies, on using (5.40), that

$$(c_0^2 + v_A^2)\omega^3 - \frac{i\kappa j_n^{(0)^2}\gamma}{a^2}\left(\frac{c_0^2}{\gamma} + v_A^2\right)\omega^2 - k^2 c_0^2 v_A^2 \omega + \frac{i j_n^{(0)^2}}{a^2}\kappa k^2 c_0^2 v_A^2 = 0. \quad (5.61)$$

Equation (5.61), it may be noted, has the same form as found by Webb and Roberts (1980a) - that is, as Equation (5.27) - provided their radiative time scale τ_R is here identified with κ through the correspondence

$$\frac{1}{\tau_R} = \frac{\gamma\kappa j_n^{(0)2}}{a^2} .$$

Webb and Roberts' equation, it will be recalled, described modes in a slender, cylindrical flux tube subject to radiative damping (Newton's law of cooling; see Equation (5.2)) with a constant radiative decay time, τ_R.

For disturbances with typical time scales short compared to τ_R, for example, the solutions of (5.61) are given by (5.28) and (5.29).

In principle it would be possible to solve (5.45) to higher order in κ and thus find corrections to dispersion relations such as (5.48) and (5.60). However this manipulation is extremely cumbersome and yields very little useful information for the effort expended. In the dissipationless case (Chapter 3) the most valuable progress, apart from numerical solutions, came from studying the extreme of the slender inhomogeneity. Thus, the slender, conducting inhomogeneity, representing perhaps a photospheric intense tube, will now be considered.

5.3 The Slender, Conducting Inhomogeneity

Returning to Equations (5.9) and (5.10b) describing linear perturbations about (1.9) to (1.11), the idea of slenderness may be made more rigorous by examination of the comparative sizes of terms in these equations. Radiative effects will now be ignored: $\tau_R^{-1} = 0$. Introducing the variable $\eta = r/a$, these equations become

$$\left.\begin{aligned}
i\omega\rho &= -\frac{\rho_0}{a}\left[a\frac{\partial v_z}{\partial z} + \frac{\partial v_r}{\partial \eta} + \frac{v_r}{\eta}\right], && \text{(a)}\\
i\omega v_r &= -\frac{1}{a\rho_0}\frac{\partial p}{\partial \eta} + \frac{B_0}{\mu_0\rho_0}\left(\frac{\partial b_r}{\partial z} - \frac{1}{a}\frac{\partial b_z}{\partial \eta}\right), && \text{(b)}\\
\rho_0 i\omega v_z &= -\frac{\partial p}{\partial z}, && \text{(c)}\\
i\omega b_r &= B_0\frac{\partial v_r}{\partial z}, && \text{(d)}\\
i\omega b_z &= -\frac{B_0}{a}\left[\frac{\partial v_r}{\partial \eta} + \frac{v_r}{\eta}\right] && \text{(e)}
\end{aligned}\right\} \quad (5.62)$$

and

$$i\omega T = \frac{\kappa}{a^2}\left[\frac{\partial^2 T}{\partial \eta^2} + \frac{1}{\eta}\frac{\partial T}{\partial \eta} + a^2\frac{\partial^2 T}{\partial z^2}\right] + \frac{i\omega p T_0(\gamma-1)}{\gamma p_0}. \qquad \text{(f)}$$

Ignoring magnetic fields for the moment (i.e., ignoring equations (d) and (e) and the last two terms of (b)), Equations (5.62)

and (5.10a) describe the well-known problem of the flow of gas (sound waves) along a rigid cylinder with isothermal walls, and are often described as Kirchhoff's equations (Tidjeman, 1974,1975). The full solution of the basic equations (which additionally may include fluid viscosity but not circulation or turbulence) was derived by Kirchhoff in 1868 in the form of a transcendental complex frequency equation, which does not lend itself to further analytical treatment. Tidjeman (1974) gives a numerical solution of the full equations using a Newton-Raphson procedure and expresses the problem in terms of four dimensionless parameters. He bases his starting values on a commonly used approximation of Kirchhoff's equations, the so-called 'low reduced frequency approximation' in which $\omega a/c_0 << 1$. Applied to Equations (5.10a) and (5.62) the approximation is seen to encompass both the aforementioned fluid mechanical approximation and the slender tube approximation $|k|a << 1$ of Roberts and Webb (1978) since in the mhd case c_0 is replaced for the slow modes by c_T and $\frac{\omega a}{c_T} \simeq |k|a << 1$. In both approximations it may be seen that (5.62b) becomes

$$0 = \frac{\partial}{\partial \eta}\left(\frac{B_0}{\mu_0} b_z + p\right), \tag{5.63}$$

expressing the fact that the total pressure perturbation across the tube is constant. The fluid dynamical argument, in which (for dimensionless $\xi = \frac{\omega a z}{c_0}$, $\tilde{T} = T/T_0$ and $\tilde{p} = p/p_0$ and the fluid viscosity is λ_f) (5.62f) may be written as

$$i\tilde{T} = \left(\frac{\kappa}{\lambda_f}\right)\left(\frac{\lambda_f}{a^2\omega}\right)\left[\frac{\partial^2\tilde{T}}{\partial\eta^2} + \frac{1}{\eta}\frac{\partial\tilde{T}}{\partial\eta} + \left(\frac{\omega^2a^2}{c_0^2}\right)\frac{\partial^2\tilde{T}}{\partial\xi^2}\right] + \frac{i(\gamma-1)\tilde{p}}{\gamma}, \qquad (5.64)$$

neglects the third term of the right-hand side of (5.64) since $\left(\frac{\omega a}{c_0}\right)^2 << 1$ ($k^2a^2 << 1$). (See also Equation (2.5) of Tidjeman.) However, the Prandtl number, λ_f/κ, and the Reynolds or shear wave number, $a^2\omega/\lambda_f$, are both non-dimensional parameters of the fluid dynamical problem which may be varied at will. For the non-viscous mhd problem considered here the role of κ depends on the value of $\kappa/a^2\omega$, the inverse of the Péclet number. As was mentioned in 5.1 this parameter, in some sense, measures the thermal conductivity effects relative to the transverse dimension of the cylindrical structure.

In the following, two approximations of (5.64) will be considered:

(a) $\kappa \gtrsim a^2|\omega|$, the fluid dynamical approximation following Tidjeman, and

(b) $\kappa < a^2|\omega|$, which, since $|k|a < 1$ and $\omega \sim kc_T$ (for slow disturbances) is the approximation considered by Roberts (1976) for a Boussinesq fluid. It might also be argued, heuristically, that conduction is predominantly along the cylindrical tube (as in the coronal/transition region models, though κ is constant here) so that temperatures are isothermal across the structure, and the first two terms on the right-hand side of (5.64) may be neglected.

(a) $\kappa \gtrsim a^2|\omega|$. With this approximation and writing $T = f(z)\,h(y)$, where $y = i^{3/2}\eta\, s$ and $s^2 = a^2\omega/\kappa$, Equation (5.62f) becomes

$$f\left(\frac{d^2h}{dy^2} + \frac{1}{y}\frac{dh}{dy} + h\right) = p\alpha_1 \tag{5.65}$$

where $\alpha_1 = T_0(\gamma-1)/p_0\gamma$. Differentiating this equation twice with respect to z and using Equations (5.10a) and (5.62) produces another equation for f in the form

$$\left(f'' + \frac{\rho_0\omega^2}{p_0} f\right)\left(\frac{d^2h}{dy^2} + \frac{1}{y}\frac{dh}{dy}\right) + \left\{f'' - \frac{\omega^2\rho_0}{p_0}(\rho_0\alpha_1 R - 1)f\right\}h = \frac{B_0}{\mu_0} b_z \frac{\alpha_1\omega^2}{v_A^2}. \tag{5.66}$$

Adding (5.65) and (5.66) and using the special form of (5.63), in which the total pressure perturbation p_T on r = a is *zero*, results in a separation of variables:

$$\frac{\frac{d^2h}{dy^2} + \frac{1}{y}\frac{dh}{dy}}{h} = \frac{-\left\{\frac{v_A^2}{\alpha_1\omega^2}\left[f'' - \frac{\omega^2 f\rho_0}{p_0}(R\rho_0\alpha_1 - 1)\right] + \frac{f}{\alpha_1}\right\}}{\left\{\left(f'' + \frac{\rho_0\omega^2 f}{p_0}\right)\frac{v_A^2}{\alpha_1\omega^2} + \frac{f}{\alpha_1}\right\}} = -\lambda^2, \tag{5.67}$$

where $-\lambda^2$ is the separation constant. For solutions finite along the centre (r = 0) of the inhomogeneity, $h = J_0(\lambda y)$ and so

$$T = (A_1 e^{ikz} + A_2 e^{-ikz}) J_0(\lambda y) e^{i\omega t}, \tag{5.68}$$

where

$$k^2 = \left[\omega^2\left(\frac{1}{v_A^2} + \frac{\gamma}{c_0^2}\right)(\lambda^2 - 1) + \frac{\omega^2}{c_0^2}(\gamma - 1)\right]\Big/(\lambda^2 - 1), \qquad (5.69)$$

and A_1 and A_2 are constants. [The case $\lambda = 0$ gives $T \sim e^{i\omega t}(A_1 e^{ikz} + A_2 e^{-ikz})$ where $\omega^2/k^2 = c_T^2$, as expected. $\lambda^2 = 1$, from (5.67), gives the trivial solution $f = 0$.]

If, further, it is assumed that the temperature perturbation on the boundary is zero, so that the environment is isothermal, then

$$J_0\left(\frac{\lambda i^{3/2} a\omega^{1/2}}{\kappa^{1/2}}\right) = 0$$

and thus $\lambda = \lambda_n$ are given by

$$\lambda_n^2 = \frac{ij_n^{(0)2}\kappa}{a^2\omega}, \qquad n = 1,2,\ldots . \qquad (5.70)$$

Equation (5.69) may be re-expressed as

$$(c_0^2 + v_A^2)\omega^3 - (c_0^2/\gamma + v_A^2)\gamma\omega\lambda_n^2\omega^2 - k^2 v_A^2 c_0^2\omega + \omega\lambda_n^2 k^2 v_A^2 c_0^2 = 0. \qquad (5.71)$$

If the formula for λ_n^2 given by (5.70) is substituted into (5.71) then

$$(c_0^2 + v_A^2)\omega^3 - \frac{i\kappa j_n^{(0)2}\gamma}{a^2}\left(\frac{c_0^2}{\gamma} + v_A^2\right)\omega^2 - k^2 v_A^2 c_0^2\omega + \frac{ij_n^{(0)2}\kappa}{a^2} k^2 c_0^2 v_A^2 = 0, \qquad (5.72)$$

which is just Equation (5.27) with $\tau_R^{-1} \equiv \gamma\kappa j_n^{(0)2}/a^2$ (or Equation (5.61)). However, though the corresponding modes given by (5.28) and (5.29) for κ small result, the analysis here does not restrict κ other than $\kappa \gtrsim a^2|\omega|$.

Almost isothermal perturbations $\left(\frac{a^2}{\gamma j_n^{(0)2}\kappa} << \mathfrak{T}\right)$, where $\mathfrak{T}$ is a typical time scale of the system, may be described by (5.30) and (5.31); in this case, there are solutions $\omega^2 \simeq \pm k c_R$, and a thermal mode. This behaviour explains the (not-unexpected) spurious solution, $\omega^2 = k^2 c_R^2$, of the slender cylinder case (v) (2) in Section 5.2 above, when the whole structure is virtually isothermal.

It is clear that, since pressure and temperature perturbations on the tube's boundary have been neglected, (5.72) describes the effect of damping due to thermal conduction on the *body* waves of the structure.

Expressions for the pressure, velocity, density and magnetic fields follow from (5.62). For example, the normal component of velocity v_r varies according to

$$v_r \sim \frac{\omega a c_p}{i j_n^{(0)} v_A^2}\left(1 - \frac{i j_n^{(0)2}\kappa}{a^2\omega}\right) J_1\left(\frac{j_n^{(0)} r}{a}\right) e^{ikz} e^{i\omega t}. \qquad (5.73)$$

(b) $\underline{\kappa < a^2|\omega|}$. Returning to Equations (5.10a), (5.62) and (5.63), and Fourier analysing them in the form $e^{i(kz+\omega t)}$, it may be shown, for a slender, conducting tube, with zero total pressure

variation resulting from its environment, that temperature perturbations may be expressed in the form:

$$\frac{\kappa}{a^2\omega}\left[\frac{\partial^2 T}{\partial\eta^2} + \frac{1}{\eta}\frac{\partial T}{\partial\eta}\right] = \left[\frac{\kappa k^2}{\omega} + i - \frac{i\ (\gamma - 1)}{\gamma\left(1 + \frac{RT_0}{v_A^2} - \frac{RT_0 k^2}{\omega^2}\right)}\right] T. \qquad (5.74)$$

Thus if it is assumed that $\kappa < a^2|\omega|$ (or simply, but less rigorously, that the temperature does not vary across the cylindrical structure), then the left-hand side of Equation (5.74) may be neglected and for a non-trivial solution ω must satisfy

$$\omega^3(c_0^2 + v_A^2) - i\omega^2 k^2 \kappa\gamma(c_0^2/\gamma + v_A^2) - k^2 c_0^2 v_A^2 \omega + ik^2\kappa k^2 c_0^2 v_A^2 = 0. \qquad (5.75)$$

So once again a cubic equation, of similar form to (5.27), (5.61) and (5.72), results; τ_R of Webb and Roberts' (1980a) radiative regime may here be identified with $1/k^2\kappa\gamma$. The roots of (5.75) for small κ (i.e., conductive time scales longer than typical time scales of the system, or $\tau_\kappa = \frac{1}{k^2\gamma\kappa} >> \mathfrak{T}$), may be written as (see (5.28) and (5.29)):

$$\omega_{1,2} \simeq \pm kc_T\left[1 + 0\left(\frac{\mathfrak{T}}{\tau_\kappa}\right)^2\right] + \frac{i(\gamma-1)c_T^2 k^2 \kappa}{2\ c_0^2}$$

and (5.76)

$$\omega_3 \simeq ik^2\kappa,$$

where ω_3 is a thermal decay mode.

In summary, as a result of considering cases (a) $\kappa \gtrsim a^2|\omega|$ and (b) $\kappa < a^2|\omega|$, there are several points to note. First, neglect of the η derivative terms in (5.74) reduces the order of the system (from fourth to second order). So T does not appear explicitly in the equations (it may be removed using (5.10a)) and only two boundary conditions for the continuity of transverse velocity and total pressure are needed to determine the solution. Effectively, the velocity/pressure problem and the temperature problem decouple as in the incompressible case.

Secondly, comparison of (5.61) and (5.75) with (5.27) shows that if "conduction is large", so that thermal effects have time to propagate across the width of the slender structure, i.e. the Péclet number is < 1, then

$$\tau_\kappa = \frac{a^2}{\gamma\kappa j_n^{(0)2}} \tag{5.77}$$

is the appropriate time scale for the heat dissipation in the structure. This was the prediction in (5.7) and (5.8) of Section 5.1 but now (5.77) gives a definite form for τ_κ (for a slender structure having isothermal boundaries) in which the constant of proportionality is determined. However, if thermal boundaries can be ignored (i.e. thermal effects vary only axially) so that heat conduction is small compared with transverse dimensions ($\kappa < |\omega|a^2$), the Péclet number is large, and then the appropriate thermal time scale is

$$\tau_\kappa = \frac{1}{k^2\gamma\kappa}, \tag{5.78}$$

which is the explicit form anticipated in (5.5) and (5.6) of Section 5.1.

Also it must be pointed out that this second case does not describe an empty set of modes. The restrictions for axial conduction in a slender inhomogeneity are $|k|a << 1$ and $\kappa < a^2|\omega|$. Since it has been shown that the slow body wave is damped, for κ small, according to (5.76) these expressions mean that $\kappa < (|k|a)ac_T < ac_T$. As will be seen in Chapter 7 this is not too severe a restriction on κ, especially when it is remembered that 'slender' is only relative to wavelength.

5.4 Gravitational Effects in a Slender, Conducting Inhomogeneity

The model of a conducting, compressible, slender inhomogeneity for which $\kappa \gtrsim a^2|\omega|$ need not be confined to a gravity-free one. Including the gravitational body force in the basic equations [(1.1), (1.4), (1.5), (1.8) and (1.6) with $\mathcal{R} = 0$] and linearizing them by considering small perturbations about the equilibrium (1.9), (1.10), (1.13) and (1.14) gives, with $\kappa \gtrsim a^2|\omega|$, instead of (5.10a) and (5.62), the governing equations:

$$
\left.
\begin{aligned}
i\omega\rho &= -\rho_0' v_z - \rho_0/a\left[a\frac{\partial v_z}{\partial z} + \frac{\partial v_r}{\partial \eta} + \frac{v_r}{\eta}\right], && \text{(a)}\\
0 &= \frac{\partial}{\partial \eta}\left(\frac{B_0}{\mu_0} b_z + p\right), && \text{(b)}\\
i\omega\rho_0 v_z &= -\frac{\partial p}{\partial z} - \rho g, && \text{(c)}\\
i\omega b_r &= B_0 \frac{\partial v_r}{\partial z}, && \text{(d)}\\
i\omega b_z &= -v_z B_0' - \frac{B_0}{a}\left[\frac{\partial v_r}{\partial \eta} + \frac{v_r}{\eta}\right], && \text{(e)}\\
iT &= \frac{1}{s}\left[\frac{\partial^2 T}{\partial \eta^2} + \frac{1}{\eta}\frac{\partial T}{\partial \eta}\right] + \frac{ipT_0}{p_0}\left(\frac{\gamma-1}{\gamma}\right) + \frac{v_z}{\omega}\left[\frac{T_0(\gamma-1)p_0'}{p_0\gamma} - T_0'\right] && \text{(f)}
\end{aligned}
\right\} \quad (5.79)
$$

and

$$
p = R[\rho_0 T + \rho T_0], \qquad \text{(g)}
$$

where $\eta = r/a$, $s = \omega a^2/\kappa$ and $'$ denotes differentiation with respect to z. Assuming that there is zero total pressure perturbation on the boundary of the cylinder ($r = a$), Equation (5.79b) is interpreted as

$$
p + b_z B_0/\mu_0 = 0,
$$

and an analysis very similar to that for the gravity-free case given above, reduces (5.79) to an equation for $T = f(z)h(y)$ in the form

$$f\left[\frac{d^2h}{dy^2} + \frac{1}{y}\frac{dh}{dy} + h\right] = \alpha_1 p + \alpha_2 \frac{\partial p}{\partial z}, \qquad (5.80)$$

where

$$y = i^{3/2}\eta m, \quad m^2 = \frac{(\omega^2 - N_0^2)a^2}{\omega\kappa}, \quad \alpha_1 = \frac{T_0}{p_0(\omega^2 - N_0^2)}\left[\frac{(\gamma-1)\omega^2}{\gamma} - N_0^2\right],$$

$$\alpha_2 = -\frac{T_0 N_0^2}{\rho_0 g(\omega^2 - N_0^2)},$$

and $N_0(z)$ and $H_0(z)$ are given by (5.32). Solving for T by a procedure similar to that following (5.65) produces a solution, finite on $r = 0$, given by

$$T = \text{const. } f(z)\, J_0\left\{\frac{\lambda i^{3/2}(\omega^2 - N_0^2)^{1/2} r}{\omega^{1/2}\kappa^{1/2}}\right\} e^{i\omega t} \qquad (5.81)$$

where f(z) satisfies a second order ordinary differential equation whose coefficients depend on λ^2 (cf., (5.67)). Alternatively, the pressure perturbation, p, may be determined from

$$d_1(\omega^2 - \lambda^2 d_1)p'' + \left[\omega^2\alpha_0(z,\omega^2) + d_1^2\lambda^2\left(\frac{B_0'}{B_0} - \frac{1}{\Lambda_0}\right)\right]p'$$

$$+ \left[\omega^2\beta_0(z,\omega^2) - \lambda^2 d_1\left(\frac{\omega^2}{g\Lambda_0} + \frac{\omega^2}{v_A^2} - \frac{1}{\Lambda_0}\left(\frac{B_0'}{B_0} + \frac{\Lambda_0'}{\Lambda_0}\right)\right)\right]p = 0, \qquad (5.82)$$

where $d_1 = \omega^2 - N_0^2$. The coefficients $\alpha_0(z,\omega^2)$, $\beta_0(z,\omega^2)$ are given by (5.34) and are precisely those given by Roberts and Webb (1978, Eqn.

(29)) in their adiabatic analysis based upon the slender flux tube approximation.

It is also possible to find the equation governing the axial velocity, which may be compared to Equation (5.37), i.e. that of Webb and Roberts (1980b, Eqn (9)) for motion in a stratified medium with radiative relaxation. The velocity equation is

$$\left[\frac{\partial}{\partial z} + \frac{(\gamma\mu^2-1)}{(\mu-1)}\frac{g}{c_0^2}\right]\left\{\frac{\frac{\partial v_z}{\partial z} - \left[\frac{B_0'}{B_0} - \frac{\rho_0'}{\rho_0} + \frac{N_0^2}{g(\mu^2-1)}\right]v_z}{\frac{i\omega}{c_0^2\rho_0}\left[\frac{(\gamma\mu^2-1)}{(\mu^2-1)} + \frac{c_0^2}{v_A^2}\right]}\right\}$$

$$+ \frac{\rho_0}{i\omega}\left(\omega^2 + \frac{N_0^2}{(\mu^2-1)}\right)v_z = 0, \qquad (5.83)$$

where $\mu^2 = \dfrac{\lambda^2(\omega^2 - N_0^2)}{\omega^2}$.

Of course Equations (5.81) to (5.83) depend on λ^2, but as in the gravity-free case, λ^2 may be determined by making some assumptions about the temperature or heat flux on the cylinder's boundary. Assuming that the environment is infinitely heat conducting so that it is isothermal, temperature perturbations on $r = a$ will be zero (see (5.81)). In this case λ are determined from $\lambda = \lambda_n$, where

$$\lambda_n^2 = \frac{ij_n^{(0)^2}\omega\kappa}{a^2(\omega^2 - N_0^2)}, \qquad (5.84)$$

and $j_n^{(0)}$ are the zeros of J_0. Equation (5.81) then becomes

$$T \sim f(z)\, J_0\left(\frac{j_n^{(0)} r}{a}\right) e^{i\omega t},$$

with similar expressions for the other variables. Even the non-conducting $\kappa \to 0$ limits of (5.82) and (5.83), which are Equations (5.33) and (5.35), respectively, are complicated enough, but it can be seen from the analysis given in Roberts and Webb (1978) that, in general, the slow body modes in a compressible slender structure including gravitational and small thermal conductivity effects, but neglecting the effects of the environment, will be those of Roberts and Webb (1978), namely,

$$\omega^2 \simeq k^2 c_T^2 + \omega_v^2 \tag{5.85}$$

where ω_v^2, given by (5.36), is the cut-off frequency. However, these modes will be modified for $\kappa \neq 0$, as described for corresponding radiative effects in Webb and Roberts (1980b). To see this most easily it must be noted that substitution of (5.84) into (5.83) produces an identical equation to (5.37), that is Webb and Roberts (1980b, Eqn. (10)), namely:

$$\frac{d^2 v_z}{dz^2} + \left[\alpha_1 + \left(\frac{1 - i\Omega}{1 + \Omega^2}\right)\alpha_2\right]\frac{dv_z}{dz} + \left[\beta_1 + \left(\frac{1 - i\Omega}{1 + \Omega^2}\right)\beta_2\right] v_z = 0, \tag{5.86}$$

where α_1, α_2, β_1 and β_2 are given by (5.38). To make the comparison, Ω, given for the radiative loss case by (5.38), is here

$$\Omega = \frac{\omega a^2}{j_n^{(0)2}\kappa}. \qquad (5.87)$$

So the equivalence of Webb and Roberts' (5.37) and (5.86) may be exploited if their decay time τ_R is set equal to $a^2/(\gamma\kappa j_n^{(0)2})$, as suggested earlier (case (v)(4) of Section 5.2 and Section 5.3). Webb and Roberts' findings were summarized briefly in Section 5.1. The significance as regards photospheric waves in a stratified, conductive atmosphere will be discussed in Chapter 7.

5.5 Structuring in a Thermally Dissipative, Boussinesq Fluid

The picture obtained so far as regards thermal conduction is rather patchy. A full analysis as in Section 5.2, even for the gravity-free structure, seems virtually intractable and results only possible for special cases such as slender inhomogeneities, disregarding their environments, though it was seen in Section 5.4 that even gravitational effects can be included in this particular case. To try to draw together the previous results, this chapter will end with an analysis of a thermally dissipative, Boussinesq fluid in a cylindrical geometry. In the context of magnetic structuring, modelled by a slab of field in a field-free environment, such a fluid has been studied in some detail by

Roberts (1976) and Parker (1979b,c). According to the results presented in Chapters 2 and 3 the geometry makes little difference to modelling the slow symmetric modes of a structured medium so it should be possible to verify some of the previous results as well as extending them.

5.5.1 The Boussinesq approximation The governing equations are the (non-slender) ones of the previous section, Equations (5.79), to which the Boussinesq approximation is now made (see, e.g., Chandrasekhar, 1961; Roberts, P.H., 1967; Proctor and Weiss, 1982). This approximation means that

(i) the continuity equation (5.79a) is simplified because $\rho/\rho_0 = -\alpha T << 1$, where α is the coefficient of volume (thermal) expansion and ρ_0 is constant,

(ii) in the z (vertical) equation of motion (5.79c), $\rho/\rho_0 = -\alpha T$, which cannot be neglected as a product with g,

and (iii) the energy equation, instead of being (5.79f), is the linearized Fourier form of Equation (1.6) with $\mathcal{R} = 0$, in which

$$G_0 = -T_0' = -\frac{dT_0}{dz} \text{ and } \frac{d\bar{p}}{dt} = 0,$$

since pressure changes occur instantaneously.

Also, for a non-slender tube, the r-component of the equation of motion is (5.9b) rather than (5.79b). The appropriate equations for a thermally dissipative medium in the Boussinesq approximation are therefore:

$$\left.\begin{aligned}
&\frac{\partial v_z}{\partial z} + \frac{\partial v_r}{\partial r} + \frac{v_r}{r} = 0, && \text{(a)}\\
&\rho_0 i\omega v_r = -\frac{\partial p}{\partial r} + \frac{B_0}{\mu_0}\left(\frac{\partial b_r}{\partial z} - \frac{\partial b_z}{\partial r}\right), && \text{(b)}\\
&\rho_0 i\omega v_z = -\frac{\partial p}{\partial z} + \rho_0 \alpha g T, && \text{(c)}\\
&i\omega T = \kappa\left[\frac{\partial^2 T}{\partial r^2} + \frac{1}{r}\frac{\partial T}{\partial r} + \frac{\partial^2 T}{\partial z^2}\right] + v_z G_0, && \text{(d)}\\
&i\omega b_r = B_0 \frac{\partial v_r}{\partial z} && \text{(e)}
\end{aligned}\right\} \quad (5.88)$$

and

$$i\omega b_z = -B_0 \frac{\partial v_r}{\partial r} - B_0 \frac{v_r}{r}. \qquad \text{(f)}$$

The Boussinesq approximation is well-known and has been used extensively in the study of the thermal stability of liquids, notably by Chandrasekhar (1961). Following Chandrasekhar, Cowling (1976) discussed the stability of a layer of incompressible fluid bounded by horizontal planes at $z = 0$ and L, including electrical resistivity and kinematic fluid viscosity as well as thermal dissipation. Since thermal effects are of chief concern here, the non-thermal dissipative mechanisms in Cowling's Equation 4.22 may be neglected so that his equation simplifies to:

$$\omega^3 - i\kappa(k_\perp^2 + k^2)\omega^2 + \left[\alpha G_0 g\left(1 - \frac{k^2}{k_\perp^2 + k^2}\right) - k^2 v_A^2\right]\omega + i\kappa k^2 (k_\perp^2 + k^2) v_A^2 = 0, \quad (5.89)$$

where $k_\perp$ is the wavenumber in the transverse (r) direction. The layer is assumed to have infinite extent in the horizontal direction so there is no structuring of the medium other than the horizontal bounding planes, which, for the periodic form of solution assumed by Cowling, determine the vertical wavenumber k to be π/L.

When $k_\perp >> k$ Equation (5.89) reduces to

$$\omega^3 - i\kappa k_\perp^2\omega^2 + (\alpha g G_0 - k^2 v_A^2)\omega + i\kappa k^2 k_\perp^2 v_A^2 = 0. \qquad (5.90)$$

For an unbounded, dissipationless ($\kappa = 0$), Boussinesq fluid the condition for marginal stability ($\omega = 0$) is obtained from (5.90) as:

$$k^2 v_A^2 = \alpha g G_0,$$

that is

$$\pi^2 B_0^2 = \mu_0 \rho_0 \alpha g G_0 L^2. \qquad (5.91)$$

This is Cowling's Equation 4.26, the condition for onset of instability in a dissipationless fluid. The significance of (5.91) as regards a structured medium will be made apparent in the next subsection.

It may be noted in passing that Equation (5.90) with $v_A = 0$ and $\kappa = 0$ has the roots $\omega^2 = -\alpha g G_0$ and $\omega = 0$. The Boussinesq limits of Equation (5.32) and (5.36) give $N_0^2 \to -\alpha g G_0$ and $\omega_v^2 = N_0^2$. So in the absence of magnetic field gravity waves only exist if the stratification is stable, i.e. $N_0^2 > 0$ or $G_0 < 0$ (Schwarzschild's criterion). However for $v_A \neq 0$, $\kappa = 0$ the roots of (5.90) are $\omega = 0$ or $\omega^2 = k^2 v_A^2 - \alpha g G_0$, so stable oscillations with

$$G_0 > 0 \quad \text{and} \quad k^2 v_A^2 > \alpha g G_0 \tag{5.92}$$

are possible.

Cowling further discusses marginal stability in a dissipative medium ($\kappa \neq 0$ and including resistivity and viscosity) but Equation (5.89) with $\omega = 0$ shows that the discussion is redundant if only thermal effects are included. Indeed Cowling points out that for thermal dissipation dominating over resistive and viscous dissipation, overstability sets in before ordinary instability. Overstability in a slenderly-structured, Boussinesq medium is discussed a little further in Subsection 5.5.4.

In order to examine the role of thermal conductivity in the solutions of (5.88) a brief discussion of the dissipationless, Boussinesq fluid will be given first.

5.5.2 Thermal conductivity negligible For $\kappa = 0$ and by Fourier analysing with respect to z, Equations (5.88c) and (5.88d) imply that

$$v_z = - \frac{k\omega p}{\rho_0(\omega^2 + \alpha g G_0)},$$

so that substituting for variables other than v_r in (5.88) results in

$$\frac{d^2 v_r}{dr^2} + \frac{1}{r}\frac{dv_r}{dr} - \frac{k^2(k^2 v_A^2 - \omega^2)v_r}{(k^2 v_A^2 - \alpha g G_0 - \omega^2)} - \frac{v_r}{r^2} = 0. \tag{5.93}$$

This is the equation equivalent to (3.10) for axisymmetric perturbations of a uniform cylinder of inhomogeneity. Equation (5.93) shows that, in the Boussinesq approximation, m_0^2 of Equation (3.12) is replaced by

$$\frac{k^2(k^2v_A^2 - \omega^2)}{(k^2v_A^2 - \alpha g G_0 - \omega^2)}.$$

A similar equation to (5.93) will of course hold in the exterior of the inhomogeneity, and matching the transverse velocity amplitude v_r and the total pressure perturbation p_T across the cylinder's boundary ($r = a$) results in, formally, the same dispersion relations as (3.20) and (3.21):

$$\rho_0(k^2v_A^2 - \omega^2)\, m_e \frac{K_0'(m_e a)}{K_0(m_e a)} = \rho_e(k^2v_{Ae}^2 - \omega^2)\, m_0 \frac{I_0'(m_0 a)}{I_0(m_0 a)} \qquad (5.94)$$

and

$$\rho_0(k^2v_A^2 - \omega^2)\, m_e \frac{K_0'(m_e a)}{K_0(m_e a)} = \rho_e(k^2v_{Ae}^2 - \omega^2)\, n_0 \frac{J_0'(n_0 a)}{J_0(n_0 a)}, \qquad (5.95)$$

where now m_0 and m_e are given by

$$m_0^2 = \frac{k^2(k^2v_A^2 - \omega^2)}{(k^2v_A^2 - \alpha g G_0 - \omega^2)} \quad \text{and} \quad m_e^2 = \frac{k^2(k^2v_{Ae}^2 - \omega^2)}{(k^2v_{Ae}^2 - \alpha_e g G_{0e} - \omega^2)}, \qquad (5.96)$$

with obvious notation.

It is noted in passing that the equivalent dispersion relations to (5.94) and (5.95) for a *slab* inhomogeneity in a Boussinesq fluid have also been obtained. They are obviously similar to (2.27) and (2.43):

$$\rho_e(k^2v_{Ae}^2 - \omega^2)m_0\begin{Bmatrix}\tanh\\ \coth\end{Bmatrix}(m_0x_0) + \rho_0(k^2v_A^2 - \omega^2)m_e = 0 \quad (m_0^2 > 0) \qquad (5.97)$$

and

$$\rho_e(k^2v_{Ae}^2 - \omega^2)n_0\begin{Bmatrix}-\tan\\ \cot\end{Bmatrix}(n_0x_0) + \rho_0(k^2v_A^2 - \omega^2)m_e = 0 \quad (n_0^2 = -m_0^2 > 0), \qquad (5.98)$$

with m_0 and m_e given by (5.96). Roberts (1976) obtained (5.98) when considering the non-thermally conducting modes for a slab in a field-free atmosphere ($v_{Ae} = 0$).

Returning to the cylindrical geometry, setting $g = 0$ in Equation (5.96) shows that $m_0^2 = m_e^2 = k^2$ and the solutions of (5.94) are the incompressible modes (3.22) illustrated in Figure 3.2.

To discuss the general case of $g \neq 0$ suppose, for simplicity, that α and G_0 have the same value inside the tube as in the environment (i.e. $\alpha = \alpha_e$, $G_0 = G_{0e}$) and that $\rho_0 = \rho_e$. It is also convenient to introduce

$$k_g^2 = \frac{\alpha g G_0}{v_A^2}, \qquad (5.99)$$

where k_g^2 is assumed positive using (5.92). Then Equations (5.96)

may be rewritten

$$m_0^2 = \frac{k^2(k^2 - \omega^2/v_A^2)}{(k^2 - k_g^2 - \omega^2/v_A^2)} = k^2 + \frac{k_g^2 k^2}{(k^2 - k_g^2 - \omega^2/v_A^2)}$$

$$\text{and} \quad m_e^2 = \frac{k^2(k^2 - \omega^2/v_{Ae}^2)}{(k^2 - k_g^2 V^2 - \omega^2/v_{Ae}^2)}, \tag{5.100}$$

where $V = v_A/v_{Ae}$. It can be seen from (5.100) that consideration of evanescent modes ($m_e > 0$) alone no longer means that stability is guaranteed. Modes will be unstable and evanescent in the exterior if, for real $k > 0$,

$$\omega^2 < 0 \quad \text{and} \quad |\omega^2| + k^2 v_{Ae}^2 > k_g^2 v_A^2. \tag{5.101}$$

The condition for marginal (neutral) stability may be obtained by setting $\omega^2 = 0$ in (5.94) (or (5.97)) and (5.100). For the cylindrical inhomogeneity it is

$$v_A^2(k^2 - k_g^2)^{\frac{1}{2}} \frac{K_0'(m_e a)}{K_0(m_e a)} = v_{Ae}^2(k^2 - k_g^2 V^2)^{\frac{1}{2}} \frac{I_0'(m_0 a)}{I_0(m_0 a)}, \tag{5.102}$$

where $m_0^2 = \frac{k^4}{(k^2 - k_g^2)}$ and $m_e^2 = \frac{k^4}{(k^2 - k_g^2 V^2)}$.

For $V = v_A/v_{Ae} \gg 1$, this condition becomes

$$k^2 = k_g^2, \tag{5.103}$$

and for $V = v_A/v_{Ae} \ll 1$ it is

$$k^2 = k_g^2 V^2 \simeq 0. \tag{5.104}$$

Combining Equations (5.103) and (5.99) , comparison with (5.91) shows that the condition for the onset of instability in a finite structure with a field-free exterior is equivalent to that given by Cowling (1976) when the horizontal wavenumber is large, $k_\perp \gg k$. If there is a magnetic environment to the structure, however, it has a stabilising influence as (5.104) shows.

In order to investigate the effects of thermal dissipation on the modes it will be assumed that $k > k_g$ (> 0 for simplicity) so that only stable modes will be considered. This is in keeping with Parker's (1979c) assumption of strong magnetic field so that $M \equiv \dfrac{\alpha g G_0}{k^2 v_A^2} < 1$. Parker (1979b,c) calls M a 'Rayleigh number'.

If only evanescent modes are permitted in the cylinder's exterior then m_e, given by (5.100), must be positive. There are three possibilities:

(i) $V^2 < k^2/k_g^2$ and either (a) $V > 1$ or (b) $V < 1$;

(ii) $V^2 = k^2/k_g^2$ and $m_e > 0$ only if $\omega > k v_{Ae}$;

(iii) $V^2 > k^2/k_g^2 > 1$.

Modes which are evanescent in the exterior of the inhomogeneity will be surface waves ($m_0^2 > 0$) if

$$0 < \omega^2/v_A^2 < k^2-k_g^2 \tag{5.105}$$

and body waves ($m_0^2 < 0$) if

$$k^2-k_g^2 < \omega^2/v_A^2 < k^2. \tag{5.106}$$

So, considering only stable modes $k > k_g$ and a magnetic field inhomogeneity v_A, $v_{Ae} \neq 0$, $\rho_e = \rho_0$, the dispersion relations (5.94) and (5.95) yield, for slender $|k|a << 1$, axisymmetric solutions;

$$\text{surface modes} : \frac{\omega^2}{v_A^2} \simeq (k^2 - k_g^2)\left[1 + \frac{1}{4v_A^2}\left(v_A^2 - \frac{k^2 v_{Ae}^2}{(k^2 - k_g^2)}\right)(ka)^2 \ell n(k^2a^2)\right], \tag{5.107}$$

and

$$\text{body modes} : \frac{\omega^2}{v_A^2} \simeq (k^2 - k_g^2) + \frac{k_g^2 (ka)^2 v_A^2}{j_n^{(1)2}}, \quad n = 1,2,3,\ldots \tag{5.108}$$

where $j_n^{(1)}$ is the nth root of the Bessel function J_1. For $k_g = 0$ (zero gravity) Equation (5.107) is seen to give the incompressible surface mode (3.23a). There is a similar expression for the kink modes. For $k_g = 0$ the body waves do not exist (see (5.106)). The body waves are present as a result of the competing effects of magnetic and gravitational forces in the duct formed by the inhomogeneity. Body waves feature in all of the evanescent ($m_e > 0$)

cases (i) to (iii) listed above but in cases (i)(b) and (iii) surface waves are also present. Thus for the case (i)(b) of, say, an umbral dot (a relatively field-free region encased in a sunspot, $V < 1$) and case (iii), say, a photospheric flux tube (a magnetic structure in a field-free exterior, $V > 1$) both types of wave mode are possible.

For a wide inhomogeneity (an interface) again it is Equation (3.39), with m_0 and m_e given here by (5.96), which expresses the phase-speed behaviour. In the case of $\rho_e = \rho_0$ this reduces to

$$\frac{\omega^2}{k^2} \simeq \frac{v_A^2 + v_{Ae}^2 - v_A^2 k_g^2/k^2}{2} . \qquad (5.109)$$

Also, as noted in Chapter 3, Equation (5.109) gives the slender kink mode behaviour. Expression (5.109) has also been given by Roberts (1976) and Parker (1979b), for $v_{Ae} = 0$. For $k_g = 0$ (5.109) is just the incompressible result for $\rho_e = \rho_0$, namely,

$$\frac{\omega^2}{k^2} \simeq \frac{v_A^2 + v_{Ae}^2}{2} \left(= c_k^2 \Big|_{\rho_0 = \rho_e} \right) . \qquad (5.110)$$

Thus in a slender tube the sausage and kink incompressible surface wave frequencies, kv_A and kc_k, respectively, become $v_A(k^2 - k_g^2)^{\frac{1}{2}}$ and $(k^2 c_k^2 - k_g^2 v_A^2/2)^{\frac{1}{2}}$ as a result of including the gravitational effects of a Boussinesq fluid.

5.5.3 Dissipative effects The analysis of Section 5.2 carries over to Equations (5.88) so a full derivation of the dispersion relation for the Boussinesq fluid will not be repeated. Also, as before, the notation is abused so that in what follows v_r, b_z, etc. are in fact perturbation amplitudes (functions of r) and require multiplicative factors $e^{i(kz+\omega t)}$.

As in the gravity-free case, there are solutions, finite along $r = 0$, of the form

$$T = A_1 I_0(\lambda_1 r) + A_2 I_0(\lambda_2 r) \qquad (\lambda_1 \neq \lambda_2,\ A_i \text{ constants}) \qquad (5.111)$$

(or J_0 type solutions), where λ_1 and λ_2 satisfy the quadratic

$$\kappa\lambda^4 + \kappa(-2k^2)\lambda^2 - i\omega\lambda^2 + \frac{i\omega G_0 \alpha g}{V_A}\lambda^2 + i\omega k^2 + \kappa k^4 = 0, \qquad (5.112)$$

and $V_A = k^2 v_A^2 - \omega^2$.

For large thermal conductivity, $\kappa \to \infty$,

$$\lambda^2 = k^2 \pm \frac{k(i^{3/2}\omega G_0 \alpha g)^{1/2}}{V_A^{1/2}\,\kappa^{1/2}}, \qquad (5.113)$$

but for $\kappa \to 0$ there is a reduction in the order of the system.

If $\kappa = 0$ then the equation to be satisfied by T is

$$\left[D^2 - \frac{k^2 V_A}{(V_A - G_0 \alpha g)}\right] T = 0, \qquad (5.114)$$

where D is the operator $d^2/dr^2 + 1/r\ d/dr$. For this second order system explicit dependence on T may be removed, using (5.88c), so there are only two boundary conditions to be satisfied ((1.19) and (1.20)) and the problem with $\kappa = 0$ is that of the previous subsection. Thus for κ small, but non-zero, the roots of (5.112) are given by

$$\lambda^2 = \frac{k^2 V_A}{(V_A - G_0\alpha g)}\left[1 - \frac{i\kappa k^2 (G_0\alpha g)^2}{2\omega(V_A - G_0\alpha g)^2}\right]^2, \text{ and } \lambda^2 = \frac{i\omega(V_A - G_0\alpha g)}{\kappa V_A}. \quad (5.115)$$

The determinant of coefficients A_i is exactly the same as in (5.45) though of course F_1, F_2, d_1 and d_2 are simpler for the Boussinesq case. They are given by

$$F_j = \frac{1}{\omega^2}\left\{\frac{\alpha g \rho_0 k v_A^2}{i} + \frac{V_A i\rho_0}{G_0 k}\left[i\omega\kappa(\lambda_j^2 - k^2) + (G_0\alpha g + \omega^2)\right]\right\}$$

and (5.116)

$$d_j = \frac{1}{\omega^2}\left\{\frac{\alpha_e g \rho_e k v_{Ae}^2}{i} + \frac{V_e i\rho_e}{G_0 k}\left[i\omega\kappa_e(\lambda_{ej}^2 - k^2) + (G_0\alpha_e g + \omega^2)\right]\right\}, \quad (j = 1,2),$$

where λ_{e_j} are the equivalents of (5.115) in the exterior with α replaced by α_e, V_A replaced by $V_e = k^2 v_{Ae}^2 - \omega^2$, and $G_0 = G_{0_e}$.

If the determinantal equation (5.45) is evaluated assuming κ and κ_e 'small', for a finite tube it may be reduced to

$$\omega^4(1 - \mathcal{F}^2) + \omega^2(2k^2 v_{Ae}^2 \mathcal{F}^2 + G_0\alpha g - 2k^2 v_A^2 - \mathcal{F}^2\alpha_e g G_0) + k^2 v_A^2(k^2 v_A^2 - G_0\alpha g)$$

$$- k^2 v_{Ae}^2 \mathcal{F}^2(k^2 v_{Ae}^2 - G_0\alpha_e g) = 0, \quad (5.117)$$

where $\mathcal{F}(\omega) = \dfrac{K_0(\lambda_{e_1} a) I_1(\lambda_1 a) \rho_e}{K_1(\lambda_{e_1} a) I_0(\lambda_1 a) \rho_0}$, λ_j are given by (5.115) and λ_{e_j} are the equivalent roots in the external medium. Unfortunately little headway can be made with this expression except to confirm the dissipationless results of Subsection 5.5.2, namely that for a *wide* tube/interface (with $\alpha = \alpha_e$, $\rho_0 = \rho_e$) $\mathcal{F} \to 1$ and (5.117) results in

$$\omega^2 = \frac{k^2}{2} (v_A^2 + v_{Ae}^2) - \frac{\alpha g G_0}{2} \tag{5.118}$$

which is Equation (5.109); whilst for a *slender* tube, $\mathcal{F} \to 0$ (which removes any external influence) and the phase-speeds are given by

$$\omega^2 = v_A^2 (k^2 - k_g^2), \tag{5.119}$$

as in Equation (5.107). (There is also a spurious root $\omega^2 = k^2 v_A^2$.) These are results neglecting terms of order $\kappa/ka^2 v_A$ and have been derived previously for small conductivity by Roberts (1976) in considering a finite slab in a field-free environment and by Parker (1979 b,c) in two specialized Cartesian regimes, an interface at the edge of a sunspot (i.e., between magnetic and non-magnetic regions), and a field-free region within a sunspot. These results will be discussed further in Chapter 7.

It is clear that for small conductivity in a slender inhomogeneity there is a wave with frequency $\mathrm{Re}(\omega) \simeq \pm v_A (k^2 - k_g^2)^{\frac{1}{2}}$, $k > k_g$. The fact that the medium is thermally conducting makes very little difference as regards the environmental (dispersive)

effects on this wave. (Roberts (1976) gives numerical results and shows that a small amount of overstability exists.) The conductive effects do appear to be significant as far as the internal structure (body waves) are concerned. It is of interest then to look at waves with frequency $\mathrm{Re}(\omega) = v_A(k^2 - k_g^2)^{\frac{1}{2}}$ in a slender inhomogeneity and apply the results of Section 5.3 to the Boussinesq case.

For $\kappa \gtrsim a^2|\omega|$, an analysis as in Section 5.3(a) shows that for zero total pressure perturbation on the boundary $r = a$ of the inhomogeneity, the temperature can be described by

$$T \sim f(z)\, J_0\left\{\frac{\lambda\, i^{3/2}(\omega^2 + G_0\alpha g)^{1/2} r}{\kappa^{1/2}\ \omega^{1/2}}\right\}, \tag{5.120}$$

where f satisfies

$$f'' - k^2 f = 0$$

and

$$k^2 = \frac{(1 - \lambda^2)(\omega^2 + G_0\alpha g)\omega^2}{v_A^2\{\omega^2 - \lambda^2(\omega^2 + G_0\alpha g)\}}. \tag{5.121}$$

If, further, the external medium is assumed to be isothermal so that there are no temperature perturbations on the boundary and the slender inhomogeneity is therefore not influenced by its environment, then

$$T \sim e^{ikz} J_0 \left(\frac{j_n^{(0)} r}{a} \right), \tag{5.122}$$

and

$$\lambda^2 = \lambda_n^2 = \frac{j_n^{(0)^2} \omega \kappa}{i^3 a^2 (\omega^2 + G_0 \alpha g)} . \tag{5.123}$$

Substituting (5.123) into (5.121) results in a cubic equation for ω:

$$\omega^3 - \frac{i}{\tau_\kappa} \omega^2 + \omega(G_0 \alpha g - k^2 v_A^2) + \frac{i}{\tau_\kappa} k^2 v_A^2 = 0, \tag{5.124}$$

where

$$\tau_\kappa = \frac{a^2}{j_n^{(0)^2} \kappa} . \tag{5.125}$$

[$\kappa = 0$ just recovers (5.119) above, viz, $\omega^2 = v_A^2(k^2 - k_g^2)$.]

However, in Section 5.3, it was also seen that for $\kappa < a^2|\omega|$ there is another time scale associated with the problem and, in the Boussinesq case, this leads to the same equation as (5.124) but with τ_κ replaced by τ_{κ_2}, where

$$\tau_{\kappa_2} = \frac{1}{k^2 \kappa} . \tag{5.126}$$

Equations (5.125) and (5.126) give the appropriate time scales in a *structured*, stratified, incompressible, thermally dissipative

fluid. It is interesting to compare these results with those for an infinite medium.

Moore (1973) and Cowling (1976) give the equivalent of (5.124) in a medium unbounded in the transverse direction. In fact Equation (5.124) is seen to be identical to Moore's and Cowling's equation (see Equation (5.90)) for large horizontal wavenumber $k_\perp >> k$ and if τ_κ is identified by

$$\tau_\kappa^{-1} = \kappa k_\perp^2 . \tag{5.127}$$

Equations (5.125) and (5.127) imply that

$$k_\perp^2 = j_n^{(0)2}/a^2$$

so that the restriction of $k_\perp$ to $k_\perp >> k$ means that the theory is valid if

$$ka << j_n^{(0)} .$$

Since only slender flux tubes are being considered here, this criterion is easily satisfied.

The idea of relating the results for slender structures to those for an unbounded medium is pursued further in Chapter 7. Though (5.125) appears to be the appropriate time scale in this relationship, it has been shown here that, depending on the Péclet number, there are two decay times for slender structures given by either (5.125) or (5.126).

5.5.4 Slender structures Equation (5.124) may be expressed in dimensionless form as

$$s^3 + \left(\frac{\tau_V}{\tau}\right)s^2 + (1 - k_g^2/k^2)s + \left(\frac{\tau_V}{\tau}\right) = 0, \qquad (5.128)$$

where $\tau_V = 1/kv_A$, $s = i\omega\tau_V$ and τ is given either by (5.125) or (5.126) according as $\kappa \gtrsim a^2|\omega|$ or $\kappa < a^2|\omega|$.

So for the stable situation $k > k_g$ all the coefficients of (5.128) are real and positive and it can be shown that either there is one real root and a pair of complex conjugate roots, or all roots are real and at least two are equal. So in terms of ω there is always an imaginary root giving non-oscillatory behaviour in time.

Examination of (5.128) in the limit $\left(\frac{\tau_V}{\tau}\right) \ll 1$ $\left(\text{i.e. } \frac{\kappa k}{v_A} \ll 1\right)$, appropriate for $\tau = \tau_{\kappa_2}$, since $\kappa \leqslant a^2 k v_A \ll a v_A$, shows that there are roots given by

$$\frac{\omega}{v_A} \simeq \pm(k^2 - k_g^2)^{\frac{1}{2}}\left[1 + \frac{k_g^2(4 - k_g^2/k^2)\kappa^2}{8(1 - k_g^2/k^2)^3 v_A^2}\right] - \frac{k_g^2\, i\kappa}{2(1 - k_g^2/k^2)v_A}, \qquad (5.129)$$

and

$$\frac{\omega}{v_A} \simeq \frac{ik^2\kappa}{(1 - k_g^2/k^2)v_A}. \qquad (5.130)$$

Equation (5.130) is simply thermal relaxation, but (5.129) shows that the amplitude of the wave grows in time as it oscillates; that is, there is overstability for $0 < k_g < k$ with growth factor

$$\mathrm{Im}\left(\frac{\omega}{kv_A}\right) = \frac{k_g^2 K}{2(k^2 - k_g^2)} = \frac{MK}{2(1-M)}, \tag{5.131}$$

where $K = \frac{\kappa k}{v_A}$ and $M = \frac{\alpha g G_0}{k^2 v_A^2}$.

Similarly, for $\left(\frac{\tau_v}{\tau}\right) >> 1$ $\left[\text{i.e., } \frac{j_n^{(0)2}\kappa}{a^2 k v_A} >> 1\right]$, appropriate for $\tau = \tau_\kappa$, the roots of (5.128) are, approximately,

$$\frac{\omega}{v_A} \simeq \frac{i\, j_n^{(0)2}\kappa k}{a^2} \tag{5.132}$$

and

$$\frac{\omega}{v_A} \simeq \pm k - \frac{ia^2 k_g^2 k}{2j_n^{(0)2}K} \pm \left(\frac{a^2}{j_n^{(0)2}K}\right)^2 k\left(\frac{k_g^4}{4} - \frac{k_g^2 k^2}{2}\right)$$

$$= \pm k - \frac{ia^2 k^2 v_A M}{2j_n^{(0)2}\kappa}. \tag{5.133}$$

So again there is a thermal decay mode given by (5.132), and overstability for $0 < k_g < k$ having a growth factor

$$\mathrm{Im}\left(\frac{\omega}{kv_A}\right) = \frac{X^2 k_g^2}{2j_n^{(0)2}k^2 K} = \frac{X^2 M}{2j_n^{(0)2}K}, \tag{5.134}$$

where $X = ka$ and $K = \frac{\kappa k}{v_A}$. In both cases the growth rates go to zero in the extremes of K as is expected for overstability.

Parker (1979c) has given growth rates similar to those in (5.131) and (5.134) by considering the approximation to the Boussinesq case (in a Cartesian geometry) resulting from perturbations about the incompressible solutions for M small. For a slender slab he gives a growth rate of

$$\mathrm{Im}\left(\frac{\omega}{kv_A}\right) = \frac{k_g^2}{2k^2K} + \ldots = \frac{M}{2K}\,[1 + 0(ka \text{ or } kx_0)], \qquad (5.135)$$

which, he notes, remains finite as $ka \to 0$. However Parker gives no qualification on K for this rate. Numerical values calculated are for K small (typically 0.15 to 0.92) but the rate in (5.135) is inappropriate as $K \to 0$.

Further, Parker gives a rate for small $K \ll ka$ but ka (kx_0) of the order of one, equal to

$$\mathrm{Im}\left(\frac{\omega}{kv_A}\right) \simeq \frac{1}{2}MK\left[\coth ka + 0\left(\frac{kv_AK}{\omega}\right)^{\frac{1}{2}}\right]. \qquad (5.136)$$

Expression (5.136) only holds for $ka \sim 0(1)$ so that it cannot be applied to a slender slab for finite conductivity. The difficulty in providing appropriate expressions for small conductivity in a slender slab via Parker's method probably arises because an expansion has been performed about the incompressible limit of the Boussinesq case i.e. M or $k_g \to 0$. In this case (5.105) and (5.106) show that

only surface waves exist whereas it would appear from the foregoing discussion to be the body waves which are more readily affected by the inclusion of thermal dissipation.

Parker points out that the growth factor in (5.136) (he takes ka = 1) is similar to that used by Savage (1969) and Moore (1973), being

$$\mathrm{Im}\left(\frac{\omega}{kv_A}\right) = \mathcal{B}MK, \tag{5.137}$$

where $\mathcal{B}$ is a number between 0.5 and 1 and which depends on the geometry of the situation. (He makes no mention of the growth factor in (5.135).) Equation (5.131) exhibits a growth factor of this form (5.137), too, but that in Equation (5.134) is more like Parker's in Equation (5.135). These ideas will be discussed further in Chapter 7. Suffice it to say here that it has been shown that there is a growth rate of the form (5.137) which depends on the geometry of the situation, but that it appears to be appropriate only for large Péclet number situations. For smaller Péclet number (5.134) describes the growth factor in a slender tube.

To conclude the discussion of a Boussinesq fluid, with conduction, it must be noted that an analysis similar to that including gravity in Section 5.4 (or alternatively the Boussinesq limit $c_0^2 \to \infty$, $N_0^2 \to -\alpha g G_0$, $\frac{1}{\lambda_0} \to 0$ of Equation (5.83)) yields a velocity equation of the form

$$\frac{\partial^2 v_z}{\partial z^2} + \frac{\omega(1-\lambda^2)(\omega^2 + \alpha g G_0) v_z}{v_A^2[\omega^2(1-\lambda^2) - G_0 \alpha g \lambda^2]} = 0. \tag{5.138}$$

For $\lambda = 0$ this is just the Boussinesq limit of Equation (5.35) (Roberts and Webb, 1978, Eqn (31)),

$$\frac{\partial^2 v_z}{\partial z^2} + \frac{(\omega^2 + \alpha g G_0) v_z}{v_A^2} = 0, \qquad (5.139)$$

which describes the behaviour in a flux tube having 'no width' and disregarding its environment. For variation in the z-direction of the form e^{ikz} Equation (5.139) gives $\omega^2 = v_A^2 (k^2 - k_g^2)$, which is just the 'tube' wave in the Boussinesq approximation discussed in Subsection 5.5.2. Discussion of Equation (5.138) for $\lambda \neq 0$ ($\kappa \neq 0$), but given instead by (5.123), just repeats the above discussion concerning growth rates.

5.6 Summary

The inclusion of non-adiabatic effects in the otherwise ideal mhd equations leads to mathematical complications because the system of equations is no longer second order. This complication is usually side-stepped in models of the lower solar atmosphere by assuming heat dissipation in the form of radiative losses which obey Newton's law of cooling. Estimates of the damping effects on wave propagation due to radiative relaxation are then possible via tabulated values of the radiative relaxation time τ_R calculated from properties (such

as opacity) of the solar atmosphere (see, e.g., Spruit, 1974; Bray and Loughhead, 1974; Giovanelli, 1978).

In this chapter it was shown that a full solution of a thermally dissipative system is in principle possible for an unstratified, structured medium and some special cases were given. Another case considered was that of a slender inhomogeneity in a stratified medium.

The dissipative time scales of a slender structure were found to be analogous to the radiative time τ_R with, however, a dependence on the Péclet number, $P_e = a^2\omega/\kappa$:

$$\text{for } P_e < 1, \quad \tau_{\kappa_1} = \frac{a^2}{\gamma\kappa j_n^{(0)2}}$$

and (5.140)

$$\text{for } P_e > 1, \quad \tau_{\kappa_2} = \frac{1}{k^2\gamma\kappa} \cdot$$

An extension of investigations such as those in Webb and Roberts (1980 a,b) to a thermally dissipative atmosphere, using the appropriate pseudo-radiative time scales of (5.140), is thus possible.

In an attempt to give an overall picture incorporating the effects of stratification, thermal dissipation and structuring in a single model, inhomogeneities in a thermally conducting, Boussinesq fluid were discussed and growth factors, appropriate to the time scales in (5.140), were produced. There is further discussion of the results derived here in Chapter 7 where they are applied to specific structures in the solar atmosphere.

Chapter 6 Nonlinear Effects : Slender Structures and Solitons

'A line is length without breadth.'

Euclid c.300 B.C.

6.1 The Nonlinear Slender Tube Equations

Up to now the structured medium has taken the form of a slab or cylindrical intrusion in an otherwise homogeneous medium. Only linear wave motions have been examined, though non-adiabatic behaviour has also been considered. In this chapter the previous assumptions still hold, except that now the discussion will encompass nonlinear motions. However, in achieving this greater generalization it has proved necessary to consider inhomogeneities that are 'slender', that is the discussion is restricted to waves of long (relative to the width of the inhomogeneity) wavelength.

Thus the basic set of nonlinear equations will be (1.1), (1.4), (1.5) (with $\underline{g} = \underline{0}$), (1.6) and (1.8). With the assumption of slenderness, so that the magnetic field and flow are essentially axial and have the form

$$\underline{\bar{B}} = (0,0,\bar{B}(z,t)), \quad \underline{v} = (0,0,v_z(z,t)), \tag{6.1}$$

these equations become (Roberts and Webb, 1978):

$$\frac{\partial \bar{B}}{\partial t} = -(\mathrm{div}\ \underline{v})_{\mathrm{axis}}\, \bar{B} + \bar{B}\,\frac{\partial v_z}{\partial z} - v_z\,\frac{\partial \bar{B}}{\partial z}, \tag{6.2}$$

$$\frac{\partial \bar{\rho}}{\partial t} + \bar{\rho}(\text{div } \underline{v})_{\text{axis}} + v_z \frac{\partial \bar{\rho}}{\partial z} = 0, \tag{6.3}$$

$$\bar{\rho}\left(\frac{\partial v_z}{\partial t} + v_z \frac{\partial v_z}{\partial z}\right) = - \frac{\partial \bar{p}}{\partial z} \tag{6.4}$$

and

$$\bar{p} = R\bar{\rho}\bar{T}. \tag{6.5}$$

It will also be assumed that conduction (see Section 5.2) and radiation losses are also essentially axial (the Péclet number is large) so that the energy equation (1.6) becomes

$$\bar{\rho} c_p \left(\frac{\partial \bar{T}}{\partial t} + v_z \frac{\partial \bar{T}}{\partial z}\right) - \left(\frac{\partial \bar{p}}{\partial t} + v_z \frac{\partial \bar{p}}{\partial z}\right) = Q \frac{\partial^2 \bar{T}}{\partial z^2} - \frac{\bar{\rho} c_v}{\tau_R} (\bar{T} - T_0). \tag{6.6}$$

Also (6.1) means that symmetric rather than kink modes are being considered, since, as noted in Chapter 2, transverse modes have $|v_x| >> |v_z|$. Transverse modes will be considered later.

If the inhomogeneity (slab or cylinder) has cross-sectional area $\bar{A}(z,t)$, then Equation (1.3) becomes

$$\bar{B}\bar{A} = \text{constant } (= C). \tag{6.7}$$

Using (6.7), and eliminating the term $(\text{div } \underline{v})_{\text{axis}}$ between (6.2) and (6.3), shows that explicit mention of the magnetic field $\bar{B}(z,t)$ can be avoided. The nonlinear, slender tube equations are

$$\frac{\partial}{\partial t} (\bar{\rho} \bar{A}) + \frac{\partial}{\partial z} (\bar{\rho} \bar{v}_z \bar{A}) = 0 \tag{6.8}$$

together with Equations (6.4), (6.5) and (6.6).

In equilibrium ($\underline{v} = 0$, $\partial/\partial t \equiv 0$) the system satisfies equations

$$(1.9) \quad : \quad p_0 = R\rho_0 T_0, \tag{6.9a}$$

$$(1.3) \quad : \quad B_0 A_0 = C, \tag{6.9b}$$

and

$$(1.13) \quad : \quad p_0 + B_0^2/2\mu_0 = \Gamma_0. \tag{6.9c}$$

Here Γ_0 is the total equilibrium pressure ($= p_e + B_e^2/2\mu_0$) in the tube's exterior, evaluated on the boundary of the tube; A_0 is the equilibrium cross-section and C is the (constant) magnetic flux.

Equations (6.4) and (6.8) apply quite generally to longitudinal waves in an elastic tube (see Lighthill, 1978), modelling, for example, pulsating blood flow. To provide the relationship between pressure $\bar{p}(z,t)$ and $\bar{A}(z,t)$ relevant to slender, structured mhd flows the transverse component of the equation of motion (1.5) must be used. For a slender tube in which pressure varies only weakly across its width and for a magnetic field assumed to have the form in (6.1) this transverse component may be written

$$\bar{p} + \frac{1}{2}\frac{\bar{B}^2}{\mu_0} = \bar{\Gamma}_T, \tag{6.10}$$

where $\bar{\Gamma}_T(z,t) = \bar{p}_{T_e}(x_{bdy},z,t)$ is the total pressure in the exterior evaluated on the boundary of the tube ($x_{bdy} = x_0$ in a slab, $x_{bdy} = a$ for a cylinder).

Using (6.9b) and (6.7), Equation (6.10) may be re-expressed as

$$\bar{p} + \rho_0 \frac{v_A^2}{2} \left(\frac{A_0}{\bar{A}}\right)^2 = \bar{\Gamma}_T. \tag{6.11}$$

6.2 Linearized Equations

To verify that Equations (6.4) to (6.11) are a faithful model, in the slender regime, of the analysis of preceding chapters, and in order to explain the motivation behind the nonlinear considerations, the linearized versions of these equations in a Cartesian geometry, infinite in the y-direction, will be discussed briefly.

Considering small perturbations about the equilibrium described in (6.9) of the form $\bar{p} = p_0 + p$, $\bar{B} = B_0 + b_z$, etc., the linearized, slender equations become

$$\left.\begin{aligned}
&\frac{1}{A_0}\frac{\partial A}{\partial t} + \frac{1}{\rho_0}\frac{\partial \rho}{\partial t} + \frac{\partial v_z}{\partial z} = 0, && \text{(a)}\\
&\rho_0 \frac{\partial v_z}{\partial t} = -\frac{\partial p}{\partial z}, && \text{(b)}\\
&\rho_0 c_p \frac{\partial T}{\partial t} = \frac{\partial p}{\partial t} + Q\frac{\partial^2 T}{\partial z^2} - \frac{\rho_0 c_v T}{\tau_R}, && \text{(c)}\\
&p = R[\rho_0 T + \rho T_0] && \text{(d)}
\end{aligned}\right\} \tag{6.12}$$

and

$$\left.\begin{aligned}
&p + \frac{B_0}{\mu_0} b_z = \Gamma_T, && \text{(e)}
\end{aligned}\right\}$$

where $\Gamma_T(z,t)$ is the value of the perturbed external pressure field p_{T_e} evaluated at the tube boundary. The linearized forms of (6.3) and (6.7) together with (6.12a) imply that

$$\frac{1}{A_0}\frac{\partial A}{\partial t} = -\frac{1}{B_0}\frac{\partial b_z}{\partial t} = \left.\frac{\partial v_x}{\partial x}\right|_{x=0}. \tag{6.13}$$

If the perturbations are expressed in Fourier form,

$$v_z(z,t) \sim \hat{v}_z\, e^{i(\omega t - kz)}, \text{ etc.}, \tag{6.14}$$

and p, ρ, A and T are eliminated between Equations (6.12b) to (6.13) then

$$\frac{\hat{v}_z}{kc_0^2(i\omega + D)}\left[\omega(\omega^2 - k^2c_0^2) + iD(k^2c_0^2 - \gamma\omega^2)\right] = \left.\frac{d\hat{v}_x}{dx}\right|_{x=0} \tag{6.15}$$

and

$$\frac{i\rho_0\hat{v}_z}{kc_0^2\omega(i\omega + D)}\left[\omega^3(v_A^2 + c_0^2) - iD\omega^2(\gamma v_A^2 + c_0^2) - \omega k^2 v_A^2 c_0^2 + iDk^2 v_A^2 c_0^2\right] = \Gamma_T, \tag{6.16}$$

where $D = \kappa k^2 + \frac{1}{\gamma\tau_R}$.

In order to link (6.15) and (6.16) the coupling between the slab and its environment must be considered in more detail. Across the boundary $|x| = x_0$ of the slab (1.19) is satisfied so

$$\hat{v}_x\Big|_{x=x_0} = \hat{v}_{e_x}\Big|_{x=x_0}, \tag{6.17}$$

where $\hat{v}_{e_x}$ is the amplitude of the transverse component in the slab's environment. For the symmetric behaviour being considered here, $\hat{v}_x$ will vary approximately linearly from zero at the slab's centre to $\hat{v}_x\Big|_{x=x_0}$ at the boundary, so that

$$\hat{v}_x\Big|_{x=x_0} \simeq x_0 \left.\frac{d\hat{v}_x}{dx}\right|_{x=0}. \tag{6.18}$$

In the slab's environment, where the 'slender' approximation is not appropriate, the linearized x-components of the momentum and induction Equations, (1.17) and (1.15), are

$$\rho_e \frac{\partial v_{e_x}}{\partial t} = - \frac{\partial p_{T_e}}{\partial x} + \frac{1}{\mu_0} B_e \frac{\partial b_{e_x}}{\partial z}$$

and

$$\frac{\partial b_{e_x}}{\partial t} = B_e \frac{\partial v_{e_x}}{\partial z},$$

which, when Fourier analysed, result in

$$\hat{v}_{e_x} = - i\omega \frac{dp_{T_e}}{dx} \Big/ \rho_e (k^2 v_{Ae}^2 - \omega^2). \tag{6.19}$$

Combining Equations (6.15) through (6.19) the dispersion relation for long wavelength, symmetric disturbances results as

$$\frac{[\omega^3(v_A^2+c_0^2) - iD\omega^2(\gamma v_A^2+c_0^2) - \omega k^2 v_A^2 c_0^2 + iDk^2 v_A^2 c_0^2]}{[\omega(\omega^2-k^2c_0^2) + iD(k^2c_0^2-\gamma\omega^2)]\ (k^2v_{Ae}^2-\omega^2)} = \frac{\rho_e}{\rho_0} K_E, \quad (6.20)$$

where $K_E = x_0 p_{T_e}(x_0) \Big/ \left.\frac{dp_{T_e}}{dx}\right|_{x=x_0}$ depends upon the width of the slender slab and the assumed form of the pressure variations in the environment. To demonstrate the significance of K_E, some special cases will be considered.

(i) $\underline{K_E = 0 \text{ - the rigid tube.}}$ In this case (6.20) becomes

$$\omega^3(v_A^2+c_0^2) - i\left(\kappa k^2 + \frac{1}{\gamma\tau_R}\right)\omega^3(\gamma v_A^2+c_0^2) - \omega k^2 v_A^2 c_0^2 + i\left(\kappa k^2 + \frac{1}{\gamma\tau_R}\right)k^2 v_A^2 c_0^2 = 0. \quad (6.21)$$

For $\kappa = 0$ this is just Equation (5.27) or Webb and Roberts (1980a, Eqn.(34)), expressing the possible modes in a slender, rigid tube subject to constant radiative decay. When this decay time (τ_R) is very large but $\kappa \neq 0$ then (6.21) is Equation (5.75) describing the modes in a slender, conducting medium. So neglecting dispersive effects due to the tube's surroundings, but including dissipation due to thermal conduction and radiative decay, solutions of (6.20) may be expressed as

$$\omega \simeq \pm kc_T + \frac{i}{2}\left(\frac{\gamma-1}{\gamma}\right)\frac{c_T^2}{c_0^2\tau_R} + \frac{i}{2}\frac{(\gamma-1)c_T^2 k^2 \kappa}{c_0^2}, \quad (6.22)$$

where $\frac{k\gamma\kappa}{c_T} << 1$, $\frac{1}{kc_T\tau_R} << 1$, i.e., conductive and radiative time scales are long compared to a typical time scale $\frac{1}{kc_T}$ of the system.

(ii) $K_E \neq 0$, $D = 0$. Here dissipation is ignored but the effects of the tube's environment are included in the form of (2.25); that is, there is evanescent behaviour away from the inhomogeneity so that in $x > x_0$

$$p_{T_e} \sim e^{-m_e(x-x_0)} e^{i(\omega t - kz)},$$

where

$$m_e = \frac{(k^2 v_{Ae}^2 - \omega^2)^{\frac{1}{2}}(k^2 c_e^2 - \omega^2)^{\frac{1}{2}}}{(c_e^2 + v_{Ae}^2)^{\frac{1}{2}}(k^2 c_{Te}^2 - \omega^2)^{\frac{1}{2}}} > 0.$$

Then $K_E = -(x_0/m_e)$ and (6.20) reduces to

$$\rho_0(k^2 v_A^2 - \omega^2)m_e + \rho_e(k^2 v_{Ae}^2 - \omega^2)m_0^2 x_0 = 0, \qquad (6.23)$$

which is just Equation (2.34) governing long wavelength symmetric disturbances again, derived here by a much simpler argument, namely, assuming the slender flux tube equations *ab initio*. From the discussion in Chapter 2 it is seen that slow, symmetric, surface waves can be described by, for example, (see (2.35c))

$$\omega^2 \simeq k^2 c_T^2 \left\{1 - \left(\frac{\rho_e}{\rho_0}\right) \frac{(c_0^2 - c_T^2)(c_T^2 - v_{Ae}^2)^{\frac{1}{2}}(c_e^2 + v_{Ae}^2)^{\frac{1}{2}}(c_T^2 - c_{Te}^2)^{\frac{1}{2}}|k|x_0}{(c_e^2 - c_T^2)^{\frac{1}{2}}(c_0^2 + v_A^2)c_T^2}\right\}$$

$$c_e > c_T > v_{Ae}. \qquad (6.24)$$

Equations (6.22) and (6.24) suggest that a dissipative, dispersive, slender slab inhomogeneity will support symmetric modes of the form

$$\omega = kc_T - \alpha k|k| + i\mu k^2 + i\mu', \tag{6.25}$$

where

$$\alpha = \frac{\rho_e}{\rho_0}\,\frac{(c_0^2 - c_T^2)(c_T^2 - v_{Ae}^2)^{\frac{1}{2}}(c_e^2 + v_{Ae}^2)^{\frac{1}{2}}(c_T^2 - c_{Te}^2)^{\frac{1}{2}}x_0}{2(c_e^2 - c_T^2)^{\frac{1}{2}}(c_0^2 + v_A^2)c_T}, \quad \mu = \frac{(\gamma-1)c_T^2\kappa}{2c_0^2},$$

$$\mu' = \frac{1}{2}\left(\frac{\gamma-1}{\gamma}\right)\frac{c_T^2}{c_0^2\tau_R}.$$

(iii) $K_E \neq 0$, $D = \frac{1}{\gamma\tau_R}$, $v_{Ae} = 0$. A similar analysis to that of Chapter 2 for the derivation of the appropriate dispersion relation for a non-slender, radiative slab in a field-free, radiative environment has been carried out. In the slender slab limit it has the form

$$(k^2c_e^2\Omega_e - \omega^2)^{\frac{1}{2}}\left\{k^2v_A^2c_0^2\Omega_0 - \omega^2(v_A^2 + c_0^2\Omega_0)\right\} = \left(\frac{\rho_e}{\rho_0}\right)c_e\Omega_e^{\frac{1}{2}}\omega^2x_0(k^2c_0^2\Omega_0 - \omega^2) \tag{6.26}$$

where

$$\Omega_e = \frac{i\omega + \frac{1}{\gamma\tau_{Re}}}{i\omega + \frac{1}{\tau_{Re}}}, \quad \Omega_0 = \frac{i\omega + \frac{1}{\gamma\tau_R}}{i\omega + \frac{1}{\tau_R}},$$

and τ_{R_e} is the radiative decay time in the slab's exterior. (Equation (6.26) may also be derived in the $|ka| \ll 1$ limit from Equation (5.25) or Webb and Roberts (1980a, Eqn. (31)); only the $K_E = 0$ case was considered there.) Alternatively, it can be shown that (6.20) is reduced to (6.26) in the appropriate dispersive $\left(K_E = -\frac{x_0}{\lambda_e}\right)$, non-conducting but radiative $\left(\kappa = 0,\ D = \frac{1}{\gamma \tau_R}\right)$, field-free ($v_{Ae} = 0$) limit. The slender, symmetric modes of Equation (6.26) have been investigated. They have the form

$$\omega = kc_T + i\mu' - \frac{\rho_e (c_0^2 - c_T^2) c_e\, c_T |k| k x_0}{\rho_0{}^2 (v_A^2 + c_0^2)(c_e^2 - c_T^2)^{\frac{1}{2}}}, \qquad (6.27)$$

further supporting the more general suggested expression (6.25).

6.3 Solitons

The importance, in the solar physics context, of a dispersion formula such as (6.25), with $\mu = \mu' = 0$, was first noticed by Roberts and Mangeney (1982); see also Roberts (1983a, 1984). A similar expression arises in the study of water waves whenever an internal density inhomogeneity occurs in the fluid, forming a waveguide. Roberts and Mangeney were able to exploit the extensive work in the fluid dynamical context (Benjamin, 1967; Davis and Acrivos, 1967; Ono, 1975) to produce similar equations appropriate to structured mhd.

Equation (6.25) shows that the wave is dispersive. So as the wave propagates the dispersive effects tend to spread the wave. Whitham (1974) suggests that for such a dispersion relation the equation of longitudinal motion for the velocity $v(z,t)$ ($\equiv v_z(z,t)$) along the slab will be an integro-differential equation of the form

$$\frac{\partial v}{\partial t} + \frac{\partial}{\partial z} \int_{-\infty}^{\infty} v(z',t)\, G(z' - z)\, dz' = 0 \qquad (6.28)$$

where

$$G(z) = \frac{1}{2\pi} \int_{-\infty}^{\infty} \frac{\omega}{k} \exp(-ikz)\, dk, \qquad (6.29)$$

is the generalized Fourier transform of the phase-speed ω/k, which in this case is given by (6.25). Then (6.29) becomes (see Lighthill, 1958; Table 1)

$$G(z) = c_T \delta(z) + \frac{\alpha}{\pi} \left(\frac{1}{z^2}\right) - \mu \delta'(z) + \frac{\mu'}{2} \operatorname{sgn} z, \qquad (6.30)$$

where $\delta(z)$ is the Dirac delta function and δ' is its derivative.

Substituting (6.30) into (6.28) gives

$$\frac{\partial v}{\partial t} + c_T \frac{\partial v}{\partial z} - \mu \frac{\partial^2 v}{\partial z^2} + \mu' v + \alpha \frac{\partial^2}{\partial z^2} \mathcal{H}[v(z,t)] = 0, \qquad (6.31)$$

where $\mathcal{H}(v)$ is the Hilbert transform of v,

$$\mathcal{H}[v(z,t)] = \frac{1}{\pi} \int_{-\infty}^{\infty} \frac{v(z',t)dz'}{z' - z}, \qquad (6.32)$$

the integral being a Cauchy principal value.

Linear theory assumes that the wave amplitude is small. If nonlinear effects are included then, as many texts illustrate (e.g., Whitham, 1974; Lighthill, 1978) the wave amplitude can grow and steepen and a shock wave results. However, if the system is dispersive, as here, the two competing effects of nonlinearity and dispersion can result in a soliton. Roberts and Mangeney (1982) and Roberts (1983a) showed that the soliton corresponding to the slow, symmetric, linear mode ($\omega/k \simeq c_T$) in a magnetic slab in a field-free environment, is the solution of the *Benjamin-Ono Equation* (see reviews by Ablowitz and Segur, 1981; Miles, 1981)

$$\frac{\partial v}{\partial t} + c_T \frac{\partial v}{\partial z} + \beta v \frac{\partial v}{\partial z} + \alpha \frac{\partial^2}{\partial z^2} \mathcal{H}[v(z,t)] = 0, \qquad (6.33)$$

where β, the coefficient of the nonlinear term, is given by

$$\beta = \frac{1}{2} v_A^2 [3c_0^2 + (\gamma+1)v_A^2]/(c_0^2 + v_A^2)^2. \qquad (6.34)$$

One solution of (6.33), first found by Benjamin (1967), is the soliton

$$v(z,t) = \frac{N}{1 + \left(\frac{z-st}{L}\right)^2} \qquad (6.35)$$

with amplitude N, speed s and scale L related by

$$s = c_T + \frac{1}{4}\beta N, \qquad L = \frac{4\alpha}{N\beta}. \tag{6.36}$$

This solution is illustrated in Figure 6.1.

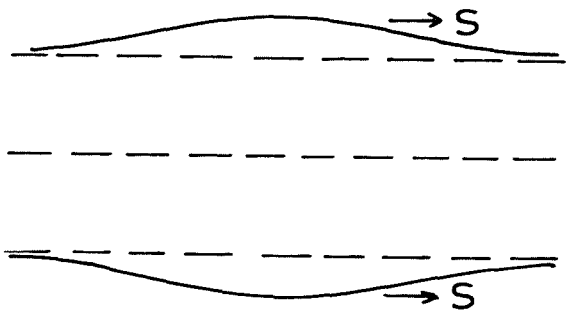

Figure 6.1 The soliton propagating on a slab

Ott and Sudan (1969, 1970) have shown that if a third contributory effect, namely dissipation, is included the appropriate governing nonlinear equation - in their case a Korteweg-de Vries equation with dissipation - represents a balance between nonlinearity, dispersion and dissipation and has slowly decaying 'soliton' solutions. The following sections show that motions in a weakly nonlinear, weakly dissipative, slender inhomogeneity and which are described by (6.31) also are 'solitons' of slowly decaying amplitude. In common with other authors (e.g., Watanabe, 1978; Tanaka, 1979) the term 'soliton' will be used throughout to mean a solution of either the dissipationless or the weakly-damped system. The solution of the latter is actually

a soliton plus a 'tail' due to dissipation, but only the soliton-like properties will be considered here.

Such a dispersion/dissipation balance has already been considered by Su and Gardner (1969) for solitons satisfying the Korteweg-de Vries equation in a wide class of long wavelength systems arising from a variety of physical situations (gas dynamics, hydromagnetic and ion-acoustic waves in cold plasmas, and waves in shallow water). In fact long wavelength motions in a stratified fluid of finite depth have been shown to obey an equation representing a balance between nonlinearity and dispersion which reduces to the Korteweg-de Vries equation for shallow water and the Benjamin-Ono equation for fluid of great depth (Kubota *et al.*, 1978). Nor are examples of solitary waves confined to fluids. Bataille and Lund (1982) have recently shown that nonlinear waves in elastic media satisfy a modified Korteweg-de Vries equation (see Jeffrey and Kakutani, 1972) as a result of the nonlinearity/dispersion balance.

6.3.1 A structured, dissipative plasma The work of Roberts (1984) is extended in two ways: (i) a non-zero magnetic field exterior to the slender slab is considered so that, more generally, the results are pertinent to a plasma structured by a slender intrusion of magnetic field, density or temperature (Figure 2.2), and (ii) weak dissipation in the form of thermal conduction or radiative decay is included. In the interior of the slab the appropriate nonlinear equations are (6.4), (6.5), (6.6), (6.8) and

(6.11), from which bars (-) and suffices z will be removed to simplify the notation. To solve these equations a multiple scale analysis similar to that employed by Ono (1975) is used. The linear dispersion law (6.25) suggests a variable transformation of the form

$$\xi = \varepsilon(z - c_T t), \quad \tau = \varepsilon^2 t. \tag{6.37}$$

Here ε is a small parameter representing the effect of weak dispersion and weak nonlinearity. It is effectively the dimensionless wave number kx_0 so that the long wavelength (slender slab) approximation is being assumed; also it is the amplitude of the velocity perturbation, say, see Equation (6.38) below. Thermal conduction effects are assumed weak too (Equation (6.25)); also, to ensure that radiative decay effects of the same order are being considered, it will be assumed that

$$\frac{1}{\tau_R} = \frac{\varepsilon^2}{\hat{\tau}_R}.$$

(See also the paragraph following Equation (1.11).)

Expanding all variables in a regular series in ε gives:

$$\begin{aligned}
v &= \varepsilon v_1 + \varepsilon^2 v_2 + \ldots \\
p &= p_0 + \varepsilon p_1 + \varepsilon^2 p_2 + \ldots \\
\rho &= \rho_0 + \varepsilon \rho_1 + \varepsilon^2 \rho_2 + \ldots \\
A &= A_0 + \varepsilon A_1 + \varepsilon^2 A_2 + \ldots \\
T &= T_0 + \varepsilon T_1 + \varepsilon^2 T_2 + \ldots \\
\Gamma_T &= \Gamma_0 + \varepsilon \Gamma_1 + \varepsilon^2 \Gamma_2 + \ldots
\end{aligned} \tag{6.38}$$

Transforming variables according to (6.37) and substituting the expansions (6.38) into Equations (6.4) to (6.8) and (6.11) results in a sequence of equations to be satisfied to each order in ε.

The zeroth order equations are just restatements of the equilibrium conditions (6.9):

$$p_0 + \frac{1}{2}\rho_0 v_A^2 = \Gamma_0 = p_e + \frac{1}{2}\frac{B_e^2}{\mu_0}, \qquad p_0 = R\rho_0 T_0.$$

The first order equations are:

$$\left.\begin{aligned} &\rho_0 A_0 \frac{\partial v_1}{\partial \xi} = c_T \frac{\partial}{\partial \xi}(\rho_1 A_0 + \rho_0 A_1), \qquad p_1 = \Gamma_1 + \rho_0 v_A^2 \frac{A_1}{A_0}, \\ &\rho_0 c_T \frac{\partial v_1}{\partial \xi} = \frac{\partial p_1}{\partial \xi}, \qquad\qquad c_p \rho_0 \frac{\partial T_1}{\partial \xi} = \frac{\partial p_1}{\partial \xi}, \\ &p_1 = R(\rho_0 T_1 + T_0 \rho_1). \end{aligned}\right\} \quad (6.39)$$

Equations (6.39) may be integrated subject to the conditions that all variables $\to 0$ as $|\xi| \to \infty$, giving:

$$\left.\begin{aligned} &A_1 = A_0\left(\frac{c_T}{v_A^2}\right)v_1, \qquad\qquad T_1 = \frac{c_T}{c_p} v_1, \\ &\rho_1 = \rho_0 \frac{c_T}{c_0^2} v_1, \qquad p_1 = \rho_0 c_T v_1, \qquad \Gamma_1 = 0. \end{aligned}\right\} \quad (6.40)$$

Proceeding to the next order in ε and eliminating v_2, p_2, A_2 and T_2 it can be shown, after some lengthy manipulation, that

$$\frac{\partial v_1}{\partial \tau} + \beta v_1 \frac{\partial v_1}{\partial \xi} - \mu \frac{\partial^2 v_1}{\partial \xi^2} + \mu' v_1 + \frac{c_T^2}{2 v_A^2 \rho_0} \frac{\partial \Gamma_2}{\partial \xi} = 0, \qquad (6.41)$$

where

$$\beta = \frac{v_A^2[(\gamma+1)v_A^2 + 3c_0^2]}{2(c_0^2 + v_A^2)^2}, \qquad \mu = \frac{c_T^2(\gamma-1)Q}{2c_0^2\rho_0 c_p}, \qquad \mu' = \frac{c_T^2(\gamma-1)}{2c_0^2\gamma\hat{\tau}_R}.$$

In the above Equation (6.41) the non-stationary motions $v_1(\xi,t)$ are determined by the nonlinearity (2nd term), the dissipation (3rd and 4th terms) and the dispersion (final term), this dispersion being caused by the total pressure variations in the slab's environment on the slab itself (cf., K_E in (6.20)). In order to describe $v_1(\xi,t)$, Γ_2 must be determined by considering the appropriate equations in the region exterior to the inhomogeneity. In this latter region the simplification of slenderness is inappropriate and the governing nonlinear equations are fourth order if thermal conduction effects are included. Thus dissipation in the slab's exterior will be restricted to radiative decay.

The appropriate equations are (1.1), (1.4), (1.5) (with $\underline{g} = \underline{0}$), (1.6) (with $Q = 0$), (1.7) and (1.8). If the velocity, magnetic, density, pressure and temperature fields are $\underline{u}$, $\underline{B}^e$, ρ^e, p^e and T^e respectively, these equations may be written:

$$
\left.
\begin{aligned}
&\frac{\partial \rho^e}{\partial t} + \operatorname{div}(\rho^e \underline{u}) = 0 && \text{(a)}\\
&\rho^e\left(\frac{\partial u_x}{\partial t} + u_x\frac{\partial u_x}{\partial x} + u_z\frac{\partial u_x}{\partial z}\right) = -\frac{\partial}{\partial x}\left(p^e + \frac{B_z^{e2}}{2\mu_0}\right) + \frac{B_z^e}{\mu_0}\frac{\partial B_x^e}{\partial z} && \text{(b)}\\
&\rho^e\left(\frac{\partial u_z}{\partial t} + u_x\frac{\partial u_z}{\partial x} + u_z\frac{\partial u_z}{\partial z}\right) = -\frac{\partial}{\partial z}\left(p^e + \frac{B_x^{e2}}{2\mu_0}\right) + \frac{B_x^e}{\mu_0}\frac{\partial B_z^e}{\partial x} && \text{(c)}\\
&\frac{\partial B_x^e}{\partial t} = B_z^e\frac{\partial u_x}{\partial z} - u_x\frac{\partial B_x^e}{\partial x} - u_z\frac{\partial B_x^e}{\partial z} - B_x^e\frac{\partial u_z}{\partial z} && \text{(d)}\\
&\frac{\partial B_z^e}{\partial t} = B_x^e\frac{\partial u_z}{\partial x} - u_x\frac{\partial B_z^e}{\partial x} - u_z\frac{\partial B_z^e}{\partial z} - B_z^e\frac{\partial u_x}{\partial x} && \text{(e)}\\
&\frac{\partial p^e}{\partial t} + (\underline{u}.\nabla)p^e = \frac{\gamma p^e}{\rho^e}\left(\frac{\partial p^e}{\partial t} + (\underline{u}.\nabla)\rho^e\right) - \frac{p^e}{T^e \tau_{Re}}(T^e - T_e), && \text{(f)}
\end{aligned}
\right\} \quad (6.42)
$$

where, in (6.42f), Equations (1.6) (with $Q = 0$), (1.7) and (1.8) have been combined. Here T_e is the equilibrium temperature, and it will be assumed that radiative decay in the exterior is of the same order as in the slab itself $\left(\text{i.e., } \frac{1}{\tau_{Re}} = \frac{\varepsilon^2}{\hat{\tau}_{Re}}\right)$.

For the exterior region the length scaling introduced in (6.37) is inappropriate since there is no longer any distinction between the x- and z-directions (Benjamin, 1967; Ono, 1975); motions in the exterior are excited only by those in the slab. Following Ono (1975), the scaling which will be used is

$$\tau = \varepsilon^2 t, \quad Z = z - c_T t, \quad X = x, \tag{6.43}$$

and the transverse component of velocity u_x will be assumed to be of the same order in ε as v_x (and thus of order ε^2).

Variables are expanded in powers of ε, as before, according to:

$$\left.\begin{aligned} u_x &= \varepsilon^2 u_x^{(2)} + \ldots & T^e &= T_e + \varepsilon T_1^e + \varepsilon^2 T_2^e + \ldots \\ u_z &= \varepsilon^2 u_z^{(2)} + \ldots & B_x^e &= \varepsilon^2 B_x^{e(2)} + \ldots \\ p^e &= p_e + \varepsilon p_1^e + \varepsilon^2 p_2^e + \ldots & B_z^e &= B_e + \varepsilon^2 B_z^{e(2)} + \ldots \\ \rho^e &= \rho_e + \varepsilon \rho_1^e + \varepsilon^2 \rho_2^e + \ldots \end{aligned}\right\} \tag{6.44}$$

First order equations show ρ_1^e, $B^{e(1)}$ and p_1^e to be zero because $\Gamma_1 = 0$. (p_e, ρ_e, T_e and B_e are the equilibrium values of pressure, density, temperature and z-component of magnetic field, respectively.) Transforming Equations (6.42) according to (6.43) and expanding them using (6.44) the $0(\varepsilon)$ equations become:

$$
\left.
\begin{aligned}
&- c_T \frac{\partial \rho_2^e}{\partial Z} + \frac{\partial}{\partial X}\left(\rho_e u_x^{(2)}\right) + \frac{\partial}{\partial Z}\left(\rho_e u_z^{(2)}\right) = 0 \\
&\rho_e c_T \frac{\partial u_x^{(2)}}{\partial Z} = \frac{\partial}{\partial X}\left(p_2^e + \frac{B_e}{\mu_0} B_z^{e(2)}\right) - \frac{B_e}{\mu_0}\frac{\partial B_x^{e(2)}}{\partial Z} \\
&\rho_e c_T \frac{\partial u_z^{(2)}}{\partial Z} = \frac{\partial p_2^e}{\partial Z} \\
&-c_T \frac{\partial B_x^{e(2)}}{\partial Z} = B_e \frac{\partial u_x^{(2)}}{\partial Z} \\
&c_T \frac{\partial B_z^{e(2)}}{\partial Z} = B_e \frac{\partial u_x^{(2)}}{\partial X} \\
&\frac{\partial p_2^e}{\partial Z} = c_e^2 \frac{\partial \rho_2^e}{\partial Z},
\end{aligned}
\right\} \quad (6.45)
$$

where $c_e^2 = \dfrac{\gamma p_e}{\rho_e}$.

It may be noted that, to this order, dissipation does not feature in the problem. So for $\frac{1}{\tau_R} \sim 0(\varepsilon^2)$, and implicitly $\frac{1}{\tau_K} \sim 0(\varepsilon^2)$, radiative damping and thermal conduction do not affect the argument and the problem is 'almost adiabatic'.

Using the fact that if

$$
p_{T_e} = p^e + \frac{(B^e)^2}{2\mu_0} = p_0^T + p_1^T \varepsilon + p_2^T \varepsilon^2 + \ldots
$$

then $p_0^T = p_e + \frac{B_e^2}{2\mu_0}$, $p_1^T = 0$ and $p_2^T = p_2^e + \frac{B_e}{\mu_0} B_z^{e(2)}$, and assuming that variables $\to 0$ as $X \to \infty$, Equations (6.45) may be combined and rewritten to give

$$\rho_e c_T \left(1 - \frac{v_{Ae}^2}{c_T^2}\right) \frac{\partial u_x^{(2)}}{\partial Z} = \frac{\partial p_2^T}{\partial X}, \tag{6.46}$$

and

$$\left(1 - \frac{c_T^2}{c_e^2}\right) \frac{\partial p_2^T}{\partial Z} = \left\{\left(1 - \frac{c_T^2}{c_e^2}\right) \frac{v_{Ae}^2}{c_T^2} - 1\right\} \rho_e c_T \frac{\partial u_x^{(2)}}{\partial X}. \tag{6.47}$$

Differentiating and combining Equations (6.46) and (6.47) shows that the total pressure p_2^T satisfies the boundary value problem:

$$\left.\begin{aligned} &\frac{\partial^2 p_2^T}{\partial X^2} + \frac{\partial^2 p_2^T}{\partial \bar{Z}^2} = 0 \\ &\text{where} \\ &p_2^T = p_2^T(X, \bar{Z}, \tau) \text{ subject to } p_2^T = \Gamma_2(\bar{Z}, \tau) \text{ on } X = x_0 \text{ and } p_2^T \to 0 \text{ as } X \to \infty. \end{aligned}\right\} \tag{6.48}$$

Here $\bar{Z} = \nu Z$, where $\frac{1}{\nu^2} = \frac{(c_e^2 - c_T^2)(v_{Ae}^2 - c_T^2)}{(c_e^2 + v_{Ae}^2)(c_{Te}^2 - c_T^2)}$. (From Table 2.2, $\nu^2 > 0$ for the slender (symmetric) c_T modes being considered here; if both v_{Ae} and $c_e < c_T$ no slow c_T mode arises.) The boundary conditions in (6.48) ensure that the solution matches with that inside the slab and is zero at infinity.

Problem (6.48) is the Dirichlet problem on the infinite half-plane and it has the Poisson integral solution

$$p_2^T(X,\bar{Z},\tau) = \frac{1}{\pi} \int_{-\infty}^{\infty} \frac{\Gamma_2(s,\tau)(X - x_0)}{(X - x_0)^2 + (s - \bar{Z})^2}\, ds, \quad (X > x_0). \quad (6.49)$$

Differentiating (6.49) with respect to X and noticing that

$$\frac{\partial}{\partial \bar{Z}} \mathcal{H}[\Gamma_2(\bar{Z},\tau)] = \frac{1}{\pi} \int_{-\infty}^{\infty} \frac{\Gamma_2(s,\tau)}{(s - \bar{Z})^2}\, ds$$

(Erdélyi, 1954) means that (6.46) may be rewritten as

$$\rho_e c_T \left(1 - \frac{v_{Ae}^2}{c_T^2}\right) \nu\, u_x^{(2)}(x_0) = \mathcal{H}[\Gamma_2(\bar{Z},\tau)]. \quad (6.50)$$

In order to match $u_x^{(2)}$ in the above with the normal component of velocity inside the slab, boundary condition (1.19) must be used. From the first term in its Taylor expansion about $x = 0$, the slab velocity v_x may be written

$$v_x\Big|_{x=x_0} = x_0 \left(\frac{\partial v_x}{\partial x}\right)_{x=0}. \quad (6.51)$$

Also, since $v_x = 0(\varepsilon^2)$ a linearized form of the continuity equation (6.3) may be used:

$$\left(\frac{\partial v_x}{\partial x}\right)_{x=0} = -\left(\frac{1}{\rho_0}\frac{\partial \rho}{\partial t} + \frac{\partial v}{\partial z}\right). \tag{6.52}$$

Recalling the transformation (6.37) and expansions (6.38) then gives

$$v_x\Big|_{x=x_0} = -\varepsilon^2 x_0 \frac{\partial}{\partial \xi}\left(v_1 - \frac{c_T}{\rho_0}\rho_1\right) + O(\varepsilon^3). \tag{6.53}$$

The fact that the inverse of $\mathcal{H}$ is $-\mathcal{H}$ means that (6.53) and (6.50) may be combined via (1.19) and (6.40) to give an expression for the total pressure on the boundary:

$$\Gamma_2 = (c_0^2 - c_T^2)(c_T^2 - v_{Ae}^2)\frac{\rho_e c_T \nu}{c_0^2\, c_T^2} x_0 \frac{\partial}{\partial \xi}[\mathcal{H}(v_1)]. \tag{6.54}$$

Substituting (6.54) into (6.41) establishes the equation for weakly nonlinear, weakly damped, symmetric motions in a slender inhomogeneity:

$$\frac{\partial v_1}{\partial \tau} + \beta v_1 \frac{\partial v_1}{\partial \xi} - \frac{c_T^2(\gamma-1)Q}{2c_0^2\rho_0 c_p}\frac{\partial^2 v_1}{\partial \xi^2} + \frac{c_T^2(\gamma-1)}{2c_0^2\gamma\hat{\tau}_R} v_1$$

$$+ \frac{(c_0^2 - c_T^2)(c_T^2 - v_{Ae}^2)\rho_e \nu c_T x_0}{c_0^2\, 2\rho_0\, v_A^2}\frac{\partial^2}{\partial \xi^2}[\mathcal{H}(v_1)] = 0. \tag{6.55}$$

Reverting to original variables this can be written

$$\frac{\partial v}{\partial t} + c_T \frac{\partial v}{\partial z} + \beta v \frac{\partial v}{\partial z} - \mu \frac{\partial^2 v}{\partial z^2} + \mu' v + \alpha \frac{\partial^2}{\partial z^2} [H(v)] = 0, \quad (6.56)$$

where

$$\beta = \frac{v_A^2[(\gamma+1)v_A^2 + 3c_0^2]}{2(c_0^2 + v_A^2)^2}, \quad \mu = \frac{c_T^2(\gamma-1)\kappa}{2c_0^2} = \frac{c_T^2(\gamma-1)Q}{2c_0^2\rho_0 c_p}, \quad \mu' = \frac{c_T^2(\gamma-1)}{2c_0^2\gamma\hat{\tau}_R},$$

and

$$\alpha = \frac{\rho_e(c_0^2 - c_T^2)(c_T^2 - v_{Ae}^2)^{\frac{1}{2}}(c_e^2 + v_{Ae}^2)^{\frac{1}{2}}(c_T^2 - c_{Te}^2)^{\frac{1}{2}}x_0}{\rho_0(c_e^2 - c_T^2)^{\frac{1}{2}}(c_0^2 + v_A^2)c_T}.$$

The coefficient α of the dispersion term can be identified as that multiplying $|k|k$ in Equation (6.24), the dispersion relation (2.35c), just as Whitham's generalized theory predicts.

6.3.2 Discussion of the nonlinear, dispersive, dissipative equation Some idea of the solutions of (6.56) may be gained by considering special cases.

(i) $\mu = \mu' = 0$, $v_{Ae} = 0$. In this case (6.56) reduces to the Benjamin-Ono equation considered by Roberts and Mangeney (1982) and having soliton solutions given by (6.35) and (6.36). Note also that from Table 2.2 it can be seen that the slow, sausage, surface, c_T mode does not exist if $v_{Ae} > c_e$. So the Benjamin-Ono equation will also be appropriate in the $\mu = \mu' = 0$, $v_{Ae} \neq 0$ regime provided $v_{Ae} < c_T < c_e$. However, coronal solitons, if they exist, will not

be described by this equation. This point is taken up later, and again in Chapter 7.

(ii) $\underline{\alpha = 0,\ \mu' = 0}$. Equation (6.56) reduces to Burgers equation (see Karpman, 1975; Whitham, 1974). In this case solutions are not affected by the tube's environment (dispersion is negligible) and the nonlinearity causes the waves to steepen and eventually shock. In this simplified form (6.55) has a solution given by the Cole-Hopf transformation (Whitham, 1974) of

$$v_1 = \frac{\int_{-\infty}^{\infty} \frac{\xi-\eta}{\tau} e^{-G/2\mu}\, d\eta}{\beta \int_{-\infty}^{\infty} e^{-G/2\mu}\, d\eta},$$

where

$$G(\eta,\xi,\tau) = \frac{(\xi-\eta)^2}{2\tau} + \int_0^{\eta} v_0(\eta')\, d\eta'$$

and $v(\xi) = v_0(\xi)$ at $\tau = 0$. Whitham discusses how and where the shock forms. Since structuring is the main theme of this thesis the effects of the environment of the slab are thus of primary importance and this dispersionless, nonlinear case will not be pursued further, save for a brief discussion in Chapter 7.

(iii) $\underline{\mu' \neq 0}$. Ott and Sudan (1970) consider a damping term of this form in conjunction with the Korteweg-de Vries equation in order to model ion-acoustic waves being damped by ion-neutral

collisions. They show that the Korteweg-de Vries soliton amplitude N_k decays exponentially according to

$$N_k = N_{0_k} \exp(-4\mu'\tau/3),$$

where N_{0_k} is the initial amplitude. In the next section it is shown that the attenuation term $\mu'v$ of Equation (6.56) also produces exponential decay of the Benjamin-Ono soliton.

6.3.3 Compatability with linear, incompressible, dissipationless theory Since the term involving β is the nonlinear contribution to (6.56) setting $\beta = 0$ should recover the earlier linear description (Chapter 2). Certainly (6.56) then becomes Equation (6.31), as predicted by Whitham's theory for a dispersion relation of the form (6.25), but it can hardly be identified with a linear description such as (6.20) because of the Fourier form in which the latter is cast. That the equations are in fact equivalent descriptions for linear perturbations is most easily shown by considering an incompressible, dissipationless medium structured by a magnetic slab lying in a field-free medium. In this case Equations (6.12) and (6.13) reduce to

$$\frac{\partial^2 v_z}{\partial t^2} - v_A^2 \frac{\partial^2 v_z}{\partial z^2} = -\frac{1}{\rho_0} \frac{\partial^2 \Gamma_T}{\partial t \partial z}, \qquad (6.57)$$

and the equivalents of (6.17) and (6.18) combine to give

$$u_x(x=x_0,z,t) = - x_0 \frac{\partial v_z}{\partial z}(z,t). \tag{6.58}$$

This relates the solution in the slab to that in its environment. Outside the slab, in the field-free region, linearized Equations (6.42) with $\underline{B}^e = \underline{0}$ show that the pressure satisfies Laplace's equation,

$$\frac{\partial^2 p^e}{\partial x^2} + \frac{\partial^2 p^e}{\partial z^2} = 0, \tag{6.59}$$

which is to be solved subject to $p^e = \Gamma_T(z,t)$ on $x = x_0$ and $p^e \to 0$ as $x \to \infty$ (in $x > x_0$). Again, this is the Dirichlet problem with solution, in Fourier form, of

$$p^e(x,z) = \int_{-\infty}^{\infty} f(s,t)\, e^{-isz-|s|(x-x_0)}\, ds, \quad x > x_0, \tag{6.60}$$

where

$$\Gamma_T(z,t) = \int_{-\infty}^{\infty} f(s,t) e^{-isz} ds, \quad f(s,t) = \frac{1}{2\pi} \int_{-\infty}^{\infty} \Gamma_T(z,t) e^{isz} dz. \tag{6.61}$$

The linearized x-component of the momentum equation (6.42b) ($\underline{B}^e = \underline{0}$) is

$$\rho_e \frac{\partial u_x}{\partial t} = - \frac{\partial p^e}{\partial x}, \tag{6.62}$$

which, using (6.60) gives

$$\rho_e \left.\frac{\partial u_x}{\partial t}\right|_{x=x_0} = \int_{-\infty}^{\infty} |s| f(s,t) e^{-isz} ds. \qquad (6.63)$$

Thus, from (6.58), and using (6.61) and the convolution theorem, variables are related by

$$- x_0 \rho_e \frac{\partial^2 v_z(x_0,z,t)}{\partial t \partial z} = \int_{-\infty}^{\infty} |s| f(s,t) e^{-isz} ds = - \frac{1}{\pi} \int_{-\infty}^{\infty} \frac{\Gamma_T(s,t)}{(z-s)^2} ds, \qquad (6.64)$$

where the table of transforms in Lighthill (1958) has been used. Since

$$\frac{\partial}{\partial z} [\mathcal{H}(\Gamma_T(z,t))] = \frac{1}{\pi} \int_{-\infty}^{\infty} \frac{\Gamma_T(s,t)}{(z-s)^2} ds, \qquad (6.65)$$

Equations (6.64) and (6.57) mean that the equation for linear motions of a slender slab in an incompressible medium (field-free environment) is

$$\frac{\partial^2 v_z}{\partial t^2} - v_A^2 \frac{\partial^2 v_z}{\partial z^2} = - \frac{1}{\rho_0} \frac{\partial^2}{\partial t \partial z} \left[\mathcal{H}^{-1} \left(\rho_e x_0 \frac{\partial v_z}{\partial t} \right) \right]. \qquad (6.66)$$

The Hilbert transform has inverse $\mathcal{H}^{-1} = -\mathcal{H}$, so (6.66) may be written as

$$\frac{\partial^2 v_z}{\partial t^2} - v_A^2 \frac{\partial^2 v_z}{\partial z^2} - \left(\frac{\rho_e}{\rho_0} x_0 \right) \frac{\partial^3 [\mathcal{H}(v)]}{\partial t^2 \partial z} = 0. \qquad (6.67)$$

This is the linear equivalent of (6.56) for the special case of dissipationless, incompressible waves in a field-free environment ($c_0 \to \infty$, so $c_T \simeq v_A$), save Equation (6.67) gives the waves in both directions ($\simeq \pm v_A$) whereas (6.56) is restricted to the waves in one direction. If v_z varies as $e^{i\omega t - ikz}$ (see (6.14)) then, using a table of Hilbert transforms (Erdélyi, 1954), (6.67) yields

$$(k^2 v_A^2 - \omega^2) - \omega^2 \left(\frac{\rho_e}{\rho_0} x_0\right) k \operatorname{sgn} k = 0.$$

This dispersion relation may be rearranged to give

$$\omega \simeq \pm k v_A \left[1 - \frac{\rho_e}{2\rho_0} |k| x_0\right],$$

which is in agreement with (2.32a) ($v_{Ae} = 0$) for a symmetric disturbance in an incompressible, slender slab.

Returning to Equation (6.56), the special cases of Subsections 6.3.2 and 6.3.3 show that this equation reduces to the Benjamin-Ono equation or Burgers equation depending on whether the system is dispersion or dissipation dominated. Equation (6.56), for $\mu' = 0$, may thus be called the *Benjamin-Ono-Burgers equation*.

6.4 Solutions of the Benjamin-Ono-Burgers and Related Equations

Investigations into the behaviour of solitons in dissipative media have concentrated mainly on the soliton solutions of the Korteweg-de Vries equation (e.g., Su and Gardner, 1969; Kadomtsev and Karpman, 1970; Ott, 1971; Karpman, 1975; Miles, 1976; Watanabe, 1978; Nagashima and Amagishi, 1979; Tanaka, 1979; Karpman *et al*, 1980; Yagi, 1981) though Nicholson and Goldman (1976) have considered the damped nonlinear Schrödinger equation. However, the so-called 'algebraic' solitons of the Benjamin-Ono equation (Ono, 1975) are well-known and describe behaviour in a fluid of great depth (Benjamin, 1967; Kubota *et al*, 1978) as well as the nonlinear waves in a stratified plasma as described here. In the following the techniques due to Ott and Sudan (1969, 1970) for investigating the effect of weak dissipation on a nonlinear, dispersive system will be applied to the soliton solution (6.35) of the Benjamin-Ono equation. As far as the writer is aware this has not been treated elsewhere in the literature.

Consider Equation (6.56) with $\mu' = 0$. By a transformation of the form

$$\hat{z} = (z - c_T t)/x_0, \qquad \tau = \left(\frac{c_T}{x_0}\right) t, \qquad v = c_T u$$

it may be expressed in the dimensionless form

$$\frac{\partial u}{\partial \tau} + \hat{\beta} u \frac{\partial u}{\partial \hat{z}} + \hat{\alpha} \frac{\partial^2 H(u)}{\partial \hat{z}^2} - \hat{\mu} \frac{\partial^2 u}{\partial \hat{z}^2} = 0, \tag{6.68}$$

where $\hat{\beta} = \beta \sim 0(1)$, $\hat{\alpha} = \frac{\alpha}{x_0} \sim 0(1)$ and $\hat{\mu} = \frac{\mu}{c_T x_0}$. Only weak dissipation in the form of thermal conductivity of magnitude $\hat{\mu} << 1$ (that is $\kappa << c_T x_0$, consistent with conduction being essentially axial i.e. the Péclet number being large) will be considered. If

$$y = \left(\frac{N\hat{\beta}}{4\hat{\alpha}}\right) \left[\hat{z} - \frac{\hat{\beta}}{4} \int_0^\tau N d\tau\right]$$

is used as a new space coordinate in a frame moving with the solitary wave and normalized to its length, and if it is assumed that N varies slowly with time, then, using (6.35) as a guide, anticipated solutions of (6.68) are:

$$u(\hat{z},\tau) = \frac{N}{y^2 + 1}. \tag{6.69}$$

Since $\hat{\mu}$ is small, it is expected that there will be both fast and slow time scales involved,

$$\eta_0 = \tau, \qquad \eta_1 = \hat{\mu}\tau, \tag{6.70}$$

and by supposing that $N = N(\hat{\mu}\tau)$, and that u has the form

$$\begin{aligned} u(y,\tau,\hat{\mu}) &= u_0(y,\eta_0,\eta_1) + 0(\hat{\mu}) \\ &= u_0(y,\eta_0,\eta_1) + \hat{\mu} u_1(y,\eta_0) + 0(\hat{\mu}^2), \end{aligned} \tag{6.71}$$

a solution of (6.68) may be sought.

To do this it is necessary to perform the transformation (6.70) and substitute (6.71) into (6.68) giving, after some algebra,

$$\left[-\sigma \frac{\partial u_0}{\partial y} + \frac{\partial u_0}{\partial \eta_0} + \frac{4\sigma u_0}{N} \frac{\partial u_0}{\partial y} + \sigma \frac{\partial^2}{\partial y^2} \mathcal{H}[u_0(y,\eta_0,\eta_1)]\right]$$

$$+ \hat{\mu}\left\{\frac{y}{N} \frac{\partial N}{\partial \eta_1} \frac{\partial u_0}{\partial y} - \sigma \frac{\partial u_1}{\partial y} + \frac{\partial u_1}{\partial \eta_0} + \frac{\partial u_0}{\partial \eta_1} - \frac{\sigma}{\hat{\alpha}} \frac{\partial^2 u_0}{\partial y^2} + \frac{4\sigma u_0}{N} \frac{\partial u_1}{\partial y} + \frac{4\sigma u_1}{N} \frac{\partial u_0}{\partial y}\right.$$

$$\left. + \sigma \frac{\partial^2}{\partial y^2} \mathcal{H}[u_1(y,\eta_0)]\right\} = 0, \tag{6.72}$$

where $\sigma = \frac{N^2\hat{\beta}^2}{16\hat{\alpha}}$. The zeroth order ($\hat{\mu} = 0$) equation is just a Benjamin-Ono equation with a solution

$$u_0 = \frac{N(\eta_1)}{1+y^2}, \quad N(0) = N_0, \tag{6.73}$$

satisfying the conditions

$$u_0(y,0,\hat{\mu}) = \frac{N_0}{1+y^2} \quad \text{and} \quad u_0(\pm\infty,\tau,\hat{\mu}) = 0.$$

(Note that u_0 is independent of η_0.)

To first order in $\hat{\mu}$ it is seen that

$$\frac{\partial u_1}{\partial \eta_0} + L[u_1] = M[u_0], \tag{6.74}$$

where

$$L[u_1] = \sigma\left\{\frac{\partial^2}{\partial y^2}\,\mathcal{H}[u_1(y,\eta_0)] + \frac{4}{N}\frac{\partial}{\partial y}(u_0u_1) - \frac{\partial u_1}{\partial y}\right\},$$

$$-M[u_0] = \frac{\partial u_0}{\partial \eta_1} + \frac{y}{N}\frac{\partial N}{\partial \eta_1}\frac{\partial u_0}{\partial y} - \frac{\sigma}{\hat{\alpha}}\frac{\partial^2 u_0}{\partial y^2},$$

and $u_1(\pm\infty, \eta_0) = 0$ and $u_1(y,0) = 0$.

In order that u_1 does not exhibit secular behaviour on a time scale $\tau \sim O\left(\frac{x_0}{c_T}\right)$, the condition that $M[u_0]$ be orthogonal to the solution, ϕ, of the time-independent, homogeneous equation adjoint to (6.74) is imposed. This means that

$$\int_{-\infty}^{\infty} \phi M[u_0]\,dy = 0, \tag{6.75}$$

where $L^*(\phi) = 0$, $\phi(\pm\infty) = 0$ and, by the definition of the adjoint, L^*,

$$\int_{-\infty}^{\infty} \psi(y)L[\phi(y)]\,dy = \int_{-\infty}^{\infty} \phi(y)L^*[\psi(y)]\,dy, \tag{6.76}$$

and $\psi(\pm\infty) = 0$. Integrating the left-hand side of (6.76) by parts and using the boundary conditions on ϕ and ψ results in the above criteria being satisfied if $\phi = 1/(1+y^2)$. Equation (6.75) then becomes

$$\int_{-\infty}^{\infty} \frac{1}{(1+y^2)}\left[\frac{\partial u_0}{\partial \eta_1} + \frac{y}{N}\frac{\partial N}{\partial \eta_1}\frac{\partial u_0}{\partial y} - \frac{\sigma}{\hat{\alpha}}\frac{\partial^2 u_0}{\partial y^2}\right] dy = 0. \tag{6.77}$$

Substituting solution (6.73) for u_0 in (6.77) and evaluating the integrals involved shows that, in the notation of Equation (6.68), the soliton amplitude N satisfies

$$N = N_0\left[1 + \frac{\hat{\beta}^2 N_0^2 \hat{\mu}\tau}{8\hat{\alpha}^2}\right]^{-\frac{1}{2}}. \tag{6.78}$$

The combination of Equations (6.78), (6.35) and (6.36) provides the desired solution of the Benjamin-Ono-Burgers equation for weak damping. Thus a small amount of dissipation by thermal conduction causes a slow decrease in the amplitude of the solitary wave. From the expressions (6.36) there is also a slowing down of the propagation speed s and a lengthening of the pulse width.

A similar analysis may be carried out for Equation (6.56) with $\mu = 0$, $\mu' \neq 0$. The principles are the same so it will not be repeated in full. In dimensionless form (6.56) becomes

$$\frac{\partial u}{\partial \tau} + \hat{\beta} u \frac{\partial u}{\partial \hat{z}} + \hat{\alpha} \frac{\partial^2 \mathcal{H}(u)}{\partial \hat{z}^2} + \hat{\mu}' u = 0, \tag{6.79}$$

where $\hat{\mu}' = x_0 \mu'/c_T$, and $\hat{\beta}$ and $\hat{\alpha}$ are as before (and are $0(1)$). In this case weak dissipation by radiative relaxation means $\hat{\mu}' << 1$, which implies $\frac{x_0}{c_T} << \tau_R$. The foregoing equations remain unchanged, save for (6.72), and the operator M in (6.74) is now given by

$$-M[u_0] = \frac{\partial u_0}{\partial \eta_1} + \frac{y}{N}\frac{\partial N}{\partial \eta_1}\frac{\partial u_0}{\partial y} + u_0. \tag{6.80}$$

For (6.75) to be satisfied by M of the form (6.80) the soliton amplitude varies exponentially as

$$N = N_0 e^{-2\hat{\mu}'\tau}. \tag{6.81}$$

Therefore the soliton solution for weak radiative damping of (6.56) (with $\mu = 0$);

$$\frac{\partial v}{\partial t} + c_T \frac{\partial v}{\partial z} + \beta v \frac{\partial v}{\partial z} + \mu' v + \alpha \frac{\partial^2}{\partial z^2} [\mathcal{H}(v)] = 0, \tag{6.82}$$

is

$$v(z,t) = \frac{N_0 e^{-2\mu' t}}{1 + \left(\frac{N_0 e^{-2\mu' t}\beta}{4\alpha}\right)^2 \left(z - \frac{\beta N_0}{4} \int_0^t e^{-2\mu' t} dt - c_T t\right)}. \tag{6.83}$$

(As a check (6.83) was differentiated and shown to satisfy (6.82) to $0(\mu')$.) The significance of these results will be discussed in Chapter 7.

6.5 Modes in Slender Structures

The investigation has so far concentrated on the slow, symmetric mode in a slender slab, but the discussion of Chapters 2 (see Table 2.2) and 3 (see Summary, Section 3.6) shows that for a Cartesian geometry there are typically two symmetric modes ($\omega/k \sim c_T$, c_e) and two kink modes ($\omega/k \sim v_{Ae}$, c_{Te}) and that though in a cylindrical

geometry the symmetric modes are basically similar, the kink modes can have $\omega/k \sim v_{Ae}$, c_k or even c_T.

Several questions present themselves. Does the assumption of slenderness, *ab initio*, yield these modes (as it did in Section 6.2 for the c_T mode); are there corresponding solitons in a nonlinear analysis and, if so, what forms do the nonlinear equations take in the slab and cylindrical geometries?

To deal first with the symmetric solutions and thus conclude the discussion of the c_T mode, Roberts (1984) has analysed the c_T mode in a slender cylindrical geometry and shown that it satisfies an equation allied to the Benjamin-Ono equation, namely

$$\frac{\partial v}{\partial t} + c_T \frac{\partial v}{\partial z} + \beta v \frac{\partial v}{\partial z} + \alpha' \frac{\partial^3}{\partial z^3} \int_{-\infty}^{\infty} \frac{v(s,t)ds}{[\lambda^2 + (s-z)^2]^{\frac{1}{2}}} = 0$$

where β is given as in (6.56) and α' and λ are constants. The dispersive behaviour is given by the slender, symmetric approximation of (3.25), retaining the Bessel function rather than its approximation (as in (3.27)).

As regards the other symmetric mode, $\omega/k \sim c_e$, this results from slenderness assumptions via Equation (6.23), but attempts to find a corresponding soliton satisfying an appropriate nonlinear equation have proved elusive. However, as Roberts and Mangeney (1982) have pointed out, the forms of dispersion for both the fast, symmetric ($\omega/k \sim c_e$) mode and the kink ($\omega/k \sim c_{Te}$, v_{Ae}) modes

(Equations (2.35a), (2.37) and (2.38)), namely,

$$\frac{\omega^2}{k^2} \simeq c^2[1 - \alpha k^2], \qquad (\alpha > 0), \tag{6.84}$$

where c equals c_e, c_{Te} or v_{Ae}, suggest (Whitham's theory, Equations (6.28) and (6.29)) that corresponding nonlinear waves will satisfy a Korteweg-de Vries equation for these non-c_T modes.

Similarly, in a cylindrical geometry dispersive corrections to (3.31) have been calculated (Edwin and Roberts, 1983) so that (3.31) may be expressed more accurately as

$$\frac{\omega}{k} = c_k\left\{1 - \frac{1}{2}\frac{\rho_0\rho_e(v_{Ae}^2 - v_A^2)}{(\rho_0 + \rho_e)^2 c_k^2}\lambda^2(ka)^2 K_0(\lambda|k|a)\right\},$$

where

$$\lambda = \frac{(c_e^2 - c_k^2)^{\frac{1}{2}}(v_{Ae}^2 - c_k^2)^{\frac{1}{2}}}{(c_e^2 + v_{Ae}^2)^{\frac{1}{2}}(c_{Te}^2 - c_k^2)^{\frac{1}{2}}} > 0.$$

This result holds for $c_k < c_e$. Again this phase-speed is of the general form discussed by Roberts (1984) and suggests that the c_k kink wave may propagate nonlinearly as a solitary wave.

Until a full analysis can be performed the form of the nonlinear term for these non-c_T modes remains unknown. However, the one remaining question of those posed above which can be answered is whether the linear dispersion relations can be derived directly by assuming a slender inhomogeneity *ab initio*. For the symmetric (sausage) modes this was achieved in Section 6.2 to obtain

relation (6.23). For kink modes the derivations for both a cylindrical and a slab structure follow. The derivations for a slender slab were published in Edwin and Roberts (1982). Roberts (1981b) derived the result for a slab in a field-free environment.

6.5.1 Kink modes in a slender inhomogeneity

(a) The slab. The dispersion relation for a kink mode follows by applying the argument of Parker (1979a) first to a slender slab. Parker considered an incompressible fluid in a field-free exterior. Here the result is generalized to allow for compressibility and structuring.

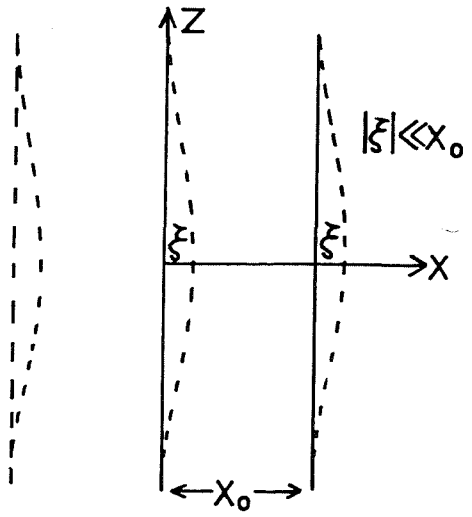

Figure 6.2 The slender slab

Consider the transverse motions of an element of slab of width $2x_0$ and unit lengths in the y- and z-directions (Figure 6.2). The equation of motion for small disturbances ξ in the x-direction is

$$\rho_0 2x_0 \frac{\partial^2 \xi}{\partial t^2} = \frac{2x_0 \hat{\mathfrak{T}}}{R_c} - [p_{T_e}(x_0) - p_{T_e}(-x_0)], \qquad (6.85)$$

where $\hat{\mathfrak{T}}$ is the tension in the magnetic field and R_c is the radius of curvature ($= \partial^2\xi/\partial z^2$ to linear order). Here it has been assumed that for small disturbances ($|\xi| << x_0$) the total pressure at the disturbed boundary, $p_{T_e}(x_0 + \xi)$ equals $p_{T_e}(x_0)$ to linear order, with a similar assumption for the boundary $x = -x_0$. As in the derivation of the symmetric slender dispersion relation (6.23) there is a dispersive term representing the effects of the surrounding medium. Here it is the term in brackets on the right of (6.85). It can be evaluated in the slab's exterior using (2.23), which applies quite generally for linear motions in an unbounded medium. Equation (6.85) then becomes

$$\rho_0 2x_0 \frac{\partial^2 \xi}{\partial t^2} = 2x_0 \rho_0 v_A^2 \frac{\partial^2 \xi}{\partial z^2} - \frac{i\rho_e (c_e^2 + v_{Ae}^2)(k^2 c_{Te}^2 - \omega^2)}{\omega(k^2 c_e^2 - \omega^2)} \left[\frac{d\hat{v}_{e_x}}{dx}\bigg|_{x=x_0} - \frac{d\hat{v}_{e_x}}{dx}\bigg|_{x=-x_0} \right]. \qquad (6.86)$$

For evanescent behaviour in the form

$$\hat{v}_{e_x}(x) = \begin{cases} \alpha_e e^{-m_e(x-x_0)}, & x > x_0, \\ \beta_e e^{m_e(x+x_0)}, & x < -x_0, \end{cases}$$

(cf., Equation (2.25)), Equation (6.86) reduces to

$$\rho_0 2x_0 \frac{\partial^2 \xi}{\partial t^2} = 2x_0 \rho_0 v_A^2 \frac{\partial^2 \xi}{\partial z^2} + \frac{i\rho_e (k^2 v_{Ae}^2 - \omega^2)}{\omega m_e} (\alpha_e + \beta_e). \qquad (6.87)$$

(m_e is defined in Equation (2.26)). Noting that $v_x = \partial\xi/\partial t = i\omega\xi$, with $\xi = \hat{\xi}(x)e^{i(\omega t - kz)}$, and supposing that both sides of the slab are displaced by equal amounts, ξ_0, say, continuity of the normal component of velocity across the slab boundaries implies that

$$\alpha_e + \beta_e = 2i\omega\hat{\xi}. \qquad (6.88)$$

Finally, expressing (6.87) in Fourier form and substituting in (6.88) recovers the dispersion relation (2.36) for the kink mode of oscillation in a slender slab.

(b) The cylinder. Similarly, for a cylindrical inhomogeneity of radius a (Figures 6.3a,b) the equation of motion for a portion of cylinder of unit depth is

$$2\rho_0 a \sin\theta dx \frac{\partial^2 \xi}{\partial t^2} = 2a\rho_0 v_A^2 \sin\theta dx \frac{\partial^2 \xi}{\partial z^2} - p_{Te}(a,\theta,t)dx + p_{Te}(a,-\theta,t)dx. \qquad (6.89)$$

Now again calculating the dispersive effect due to the cylinder's environment from Equations (3.13), the total perturbed pressure p_{Te} is given by

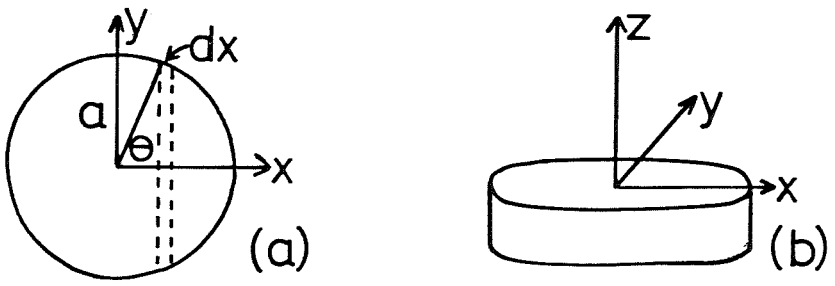

Figure 6.3 (a) Plan view and (b) unit depth section of a slender cylinder

$$p_{Te} = p^e + B_e \frac{b_{ez}}{\mu_0}$$

$$= \frac{\rho_e(c_e^2 + v_{Ae}^2)(k^2 c_{Te}^2 - \omega^2) e^{i(\omega t + n\theta + kz)}}{i\omega^3} \hat{R}(r), \qquad (6.90)$$

where $\hat{R}(r) = A_2 K_n(m_e r)$, with A_2 a constant, for evanescent behaviour exterior to the cylinder (see Equation (3.19)). Also $v_r = \sin\theta \frac{\partial \xi}{\partial t}$ and continuity of normal velocity on $r = a$, using (3.13) again, means that

$$v_r = - \frac{(c_e^2 + v_{Ae}^2)(k^2 c_{Te}^2 - \omega^2)}{\omega^2(k^2 v_{Ae}^2 - \omega^2)} \left.\frac{d\hat{R}}{dr}\right|_{r=a} e^{i(\omega t + n\theta + kz)}. \qquad (6.91)$$

Substituting (6.90) and (6.91) into (6.89) and cancelling common factors shows that

$$\rho_0 a(k^2 v_A^2 - \omega^2) \left.\frac{d\hat{R}}{dr}\right|_{r=a} = (k^2 v_{Ae}^2 - \omega^2)\rho_e \hat{R}(a). \qquad (6.92)$$

For $n = 1$, on substitution for $\hat{R}$ this results in the dispersion relation

$$(k^2 v_A^2 - \omega^2) m_e a \frac{K_1'(m_e a)\rho_0}{K_1(m_e a)} = \rho_e (k^2 v_{Ae}^2 - \omega^2). \qquad (6.93)$$

Equation (6.93) is consistent with Equation (3.29) for the kink mode in a slender cylindrical structure *only in the limit* $\frac{m_0 a I_1'(m_0 a)}{I_1(m_0 a)} \to 1$. Thus the slender kink modes with phase-speeds given by

$$\frac{\omega^2}{k^2} \simeq \frac{\rho_e v_{Ae}^2 + \rho_0 v_A^2}{\rho_e + \rho_0} = c_k^2 \quad \text{and} \quad \frac{\omega^2}{k^2} \simeq c_{Te}^2 \left[1 - \frac{c_{Te}^2 (ka)^2}{(c_e^2 + v_{Ae}^2)\mu^2} \right]$$

(μ given by Equation (3.33)) are recovered (see Equations (3.31) and (3.34)) but not the $\omega^2 \simeq k^2 c_T^2$ mode. Since this latter case was found to occur only when the inhomogeneity was particularly strong and so had a dominant effect (see Section 3.6) presumably treating the inhomogeneity as a uniform 'vibrating string' is no longer valid in this case.

6.6 Summary

The work in this chapter can be summarized as follows. If the inhomogeneity is slender (kx_0, $ka \ll 1$), so that long wavelengths

relative to the transverse dimension are being considered, then for a linear analysis it is sufficient to treat the inhomogeneity as having essentially no width and simplified one-dimensional equations may be used *ab initio* to determine the dispersive behaviour (except for the slow kink mode under photospheric conditions, say, mentioned above).

The dispersive nature of the waves is important in deciding if the structure can support solitons and an effective balance between dispersion, nonlinearity and dissipation was found to exist for the slow, symmetric wave. This balance, for a slender inhomogeneity, was established in the form of the Benjamin-Ono-Burgers equation. The nature of solutions of this equation was considered and it was shown that, for weakly damped systems, the solutions are slowly decaying solitary waves, that is slowly decaying forms of the soliton solutions of the Benjamin-Ono equation. A dispersion/nonlinearity balance in the form of the Korteweg-de Vries equation is suspected to exist for other modes but was not proved.

Dispersion was shown to be a manifestation of the environment on the inhomogeneity. Its importance in the context of group velocity, for non-slender structures in the corona was discussed in Chapter 4. Its relevance here, in the context of solitons, will be discussed in the next chapter.

Chapter 7 Further Applications and Conclusions

'Il n'existe pas de sciences appliquées, mais seulement des applications de la science.'

Louis Pasteur 1872

Chapter 4 concentrated on coronal applications so most of the discussion here will deal with other parts of the Sun's atmosphere, namely the photosphere and chromosphere. Examples of other structured plasmas, specifically the Earth's magnetosphere and, briefly, laboratory plasmas, will also be considered.

7.1 The Photosphere

The theory developed in Chapters 2 and 3 was an extension of the work of Roberts (1981 a,b) to include a magnetic field in the environment of a magnetic inhomogeneity. As far as the isolated intense magnetic tubes of the photosphere are concerned, therefore, the work here superficially contributes little by way of new information, since an appropriate model is the one discussed by Roberts, namely a magnetic inhomogeneity (representing the approximately kilogauss field) surrounded by a virtually field-free environment. Indeed, Figure 2.6 (see also Fig. 3 of Edwin and Roberts, 1982) confirms Roberts' picture (see Fig. 1a of Roberts, 1981b) of the possible wave modes due to the magnetic field structuring of the isolated tube when modelled as a slab. The only

difference is the identification and inclusion of a fast surface kink mode. This was overlooked in Roberts' work because it does not exist as a surface mode in the long wavelength approximation. It is only when the inhomogeneity is modelled as a cylinder (see Figure 3.3) that this weakly dispersive fast kink mode is apparent (Chapter 3).

The modes of oscillation under conditions expected in photospheric flux tubes (Figures 2.6 and 3.3) can be summarized then as comprising:

(i) a longitudinal wave consisting of expansions and contractions along the tube (the slow sausage wave) having speed $c_T = c_0 v_A / (c_0^2 + v_A^2)^{\frac{1}{2}}$;

(ii) a transverse wave (the fast kink wave) consisting of bends in the tube which acts like a rope of magnetic flux moving in its relatively field-free environment with speed $c_k = ((\rho_0 v_A^2 + \rho_e v_{Ae}^2)/(\rho_0 + \rho_e))^{\frac{1}{2}}$;

(iii) an 'external' longitudinal wave (the fast sausage wave) consisting of pulsations along the tube due to the environmental gas pressure changes and having speed c_e in a slender tube;

(iv) a transverse slow kink wave having speed c_T (modified when an extremely slender infinite slab of field has to displace so much more of the environment than in the cylindrical case), and

(v) an infinite set of both sausage and kink body waves oscillating with phase-speed approximately c_T, regardless of the flux tube's environment.

It is thus the 'tube speed' c_T which is the predominant feature of an intense photospheric flux tube, serving as the approximate phase-speed description for (i), (iv) and (v) above. Though the slow, pulsating mode in (i), often described as the 'tube wave' (c_T) has received much attention in this thesis, Spruit (1981b, 1983) has argued in favour of the fast kink wave (c_k) in (ii), being the easier to excite and has suggested its identification with the swaying motion of Hα mottles (Bray and Loughhead, 1974) and the Hα fibrils (Giovanelli and Beckers, 1983).

The typical photospheric waves described in (i) were investigated further by including weakly nonlinear, weakly dissipative effects in the model of their propagation in slender, isolated flux tubes. It was shown in the previous chapter that it is possible for such tubes to support solitons of decaying amplitude. Roberts and Mangeney (1982) have speculated that solitons may be manifest as spicules, the elongated jets of cool, dense gas described in Chapter 1 and thought likely to correspond cospatially with photospheric flux tubes.

As an example of the results in Chapter 6, for a magnetic flux tube in the upper photosphere with equal sound and Alfvén speeds, say, $c_0 = v_A = 7.5\,\mathrm{km\,s^{-1}}$, and a typical radiative decay time of 350 s (Bray and Loughhead, 1974), ignoring thermal conduction, the soliton amplitude would decay by a factor of e in $\left(\frac{1}{2\mu'}\right)$ seconds, that is, in a time of $5\tau_R = 1750$s. The initial soliton speed is given by (6.35) and for the values here is therefore $5.3 + 0.17N_0\,\mathrm{km\,s^{-1}}$. Velocity

amplitudes at photospheric levels are unlikely to exceed those generated by granules so that N_0 is probably of the order of 1-3 $km\,s^{-1}$ (Athay, 1981a). This gives an initial soliton speed of at most 6 $km\,s^{-1}$ and so such a solitary wave could travel through the whole of the solar photosphere and chromosphere without suffering significant attenuation from radiative losses.

Of course, the glaringly obvious omission of these models is that of gravity, and though an attempt to include gravitational effects was made by including (in Chapter 5) a discussion of the Boussinesq fluid, as (i)-(v) above show (see also Spruit, 1981b, 1983), many features of these photospheric waves are due to compressibility effects, which the Boussinesq model does not reveal. Attempts have been made to include gravitational effects in the extremes of a slender flux tube (e.g., Roberts and Webb, 1978; Spruit and Zweibel, 1979; Roberts, 1983b) and an infinitely wide medium (e.g., Antia and Chitre, 1979; Zhughda, 1979), but it is the photospheric structure of finite width, the sunspot, which still awaits detailed explanation.

One way of reconciling the ideas and analyses developed for slender photospheric tubes and those for an infinite photospheric atmosphere is to invoke the result noted by Webb (1980), namely, that by taking the limit $k_x \to \infty$, where k_x is the horizontal wave number (see Equation (2.15)) in the infinite medium equations, one recovers the behaviour in a slender flux tube (Figure 7.1).

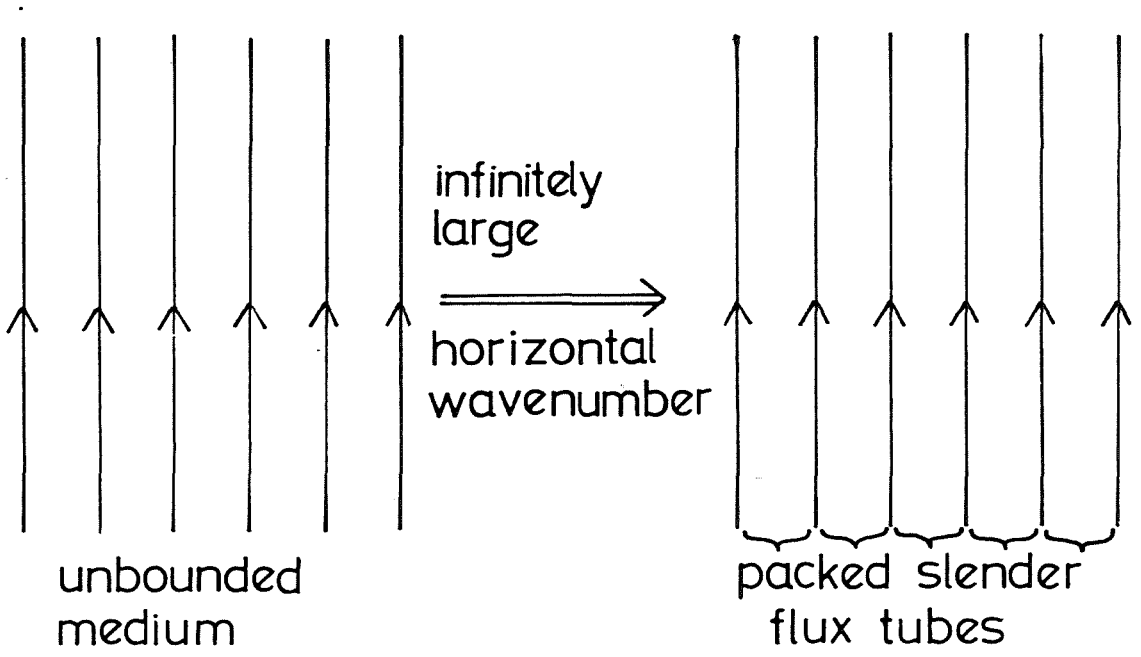

Figure 7.1 Schematic illustration of the slender tube behaviour resulting from the limit $k_x \to \infty$ in the infinite medium equations

So, for example, the investigation carried out by Adam (1975) into the nonlinear behaviour of a compressible, isothermal, viscous but unstratified fluid, permeated by a magnetic field, produced Burgers equation and he calculated the effects of the viscous damping on the fast and slow modes. By taking an infinite limit of the horizontal wavenumber in his Equation (38) it can be shown that the coefficient of the nonlinear term is exactly the same as that in the slender, nonlinear regime.

Adhering as far as possible to the notation of Chapter 6, Adam's Equation (38) may be written

$$\frac{\partial v}{\partial \tau} + \frac{a\omega}{k_y^2} v \frac{\partial v}{\partial z} - \frac{b}{k_y^2} \frac{\partial^2 v}{\partial z^2} = 0, \tag{7.1}$$

where

$$a = \frac{\omega\{2k_x^2 + 3s(k_y^2/\omega^2 - 1)^2 (k_x^2 + k_y^2)\}}{\{k_x^2(1 + k_y^2/\omega^2) + (k_y^2/\omega^2 - 1)^2(\omega^2 + s(k_x^2 + k_y^2))\}}, \tag{7.2}$$

$s = v_A^2/c_0^2$, $\omega/k_y = c_T/c_0$ and b is a coefficient representing the viscous damping of the fluid. In the limit of infinitely large horizontal wavenumber, $k_y/k_x << 1$, Equation (7.2) gives

$$a = \frac{\{2 + 3s(k_y^2/\omega^2 - 1)^2\}}{(1 + k_y^2/\omega^2) + (k_y^2/\omega^2 - 1)^2 s},$$

so that, after some manipulation, the coefficient of the nonlinear term, $v \frac{\partial v}{\partial z}$, in (7.1) becomes

$$\frac{a\omega}{k_y^2} = \frac{(2v_A^2 + 3c_0^2)v_A^2}{2(c_0^2 + v_A^2)^2}$$

which is just β of Equation (6.56) for the isothermal ($\gamma = 1$) case which Adam (1975) considered. Of course the dispersive effects due to the tube's environment are not apparent in such a limit since the infinite medium is essentially composed of packed, parallel slender tubes each oblivious of the others' existence. The idea

may prove useful however in linking results established in the narrow and wide photospheric tube limits.

Another example of this small horizontal wavelength approximation is that obtained by considering Zhugzhda's (1979) paper on magnetogravity waves in an infinite, isothermal, conductive atmosphere. He assumes that the heat exchange obeys Newton's law of cooling so that radiative relaxation with a characteristic time τ_R is being modelled. By taking the infinite horizontal wavenumber limit of his Equation (12), the equivalent of Equation (5.86) (but for the transverse velocity v_x in an isothermal atmosphere) results. Simplifying still further by considering an unstratified ($\underline{g} = \underline{0}$) atmosphere, his equation reduces to

$$\frac{d^2 v_x}{dz^2} + \omega^2 \left[\frac{(i\Omega + \gamma)}{c_0^2 (i\Omega + 1)} + \frac{1}{v_A^2} \right] v_x = 0, \tag{7.3}$$

which, for e^{ikz} variation, results in

$$\omega^2 \{ (i\Omega + \gamma) v_A^2 + c_0^2 (i\Omega + 1) \} = v_A^2 c_0^2 (i\Omega + 1) k^2, \tag{7.4}$$

where $\Omega = \gamma \omega \tau_R$. Equation (7.4) may be rewritten as

$$\omega^3 (c_0^2 + v_A^2) - \frac{i}{\tau_R} \left(\frac{c_0^2}{\gamma} + v_A^2 \right) - k^2 c_0^2 v_A^2 \omega + \frac{i k^2 c_0^2 v_A^2}{\gamma \tau_R} = 0, \tag{7.5}$$

which is just Equation (5.61) or (5.75) with the appropriate τ_R (or, equivalently, Equation (34) in Webb and Roberts, 1980a). So

here again the small horizontal wavelength limit for the infinite medium produces the same results as for close-packed slender tubes. As Figure 7.1 shows this mathematical result may be represented by a picture not unlike the physical 'spaghetti' model of a sunspot (Parker, 1979b) described in Chapter 1. Sunspots are the photospheric structures considered next.

There has been much debate about the formation and structure of sunspots (see, for example, summaries by Priest, 1982; Spruit and Roberts, 1983) which still continues. If the sunspot is modelled as a single, large flux tube then the theory developed in this thesis cannot further the analysis; though the modes in a finite photospheric structure have been considered in great detail, this was done by excluding gravitational effects, and though thermal conductivity effects have been included, even for a stratified medium, these could only be interpreted for slender structures.

Parker (1979a,b,c) and Spruit (1981a), however, have both put forward several ideas connected with a sunspot model composed of a group of flux tubes held together at the solar surface by magnetic buoyancy and a downdraft beneath the sunspot. Some of the ways of applying this 'spaghetti' model to explain sunspot behaviour are taken up and discussed further.

The simplest idea has been described in detail in Chapter 1. Parker (1979a) envisages a process whereby knots and pores accumulate until a spot of perhaps 3000 G and 4000 km diameter is formed. Mathematically, if this is interpreted as a set of closely-packed

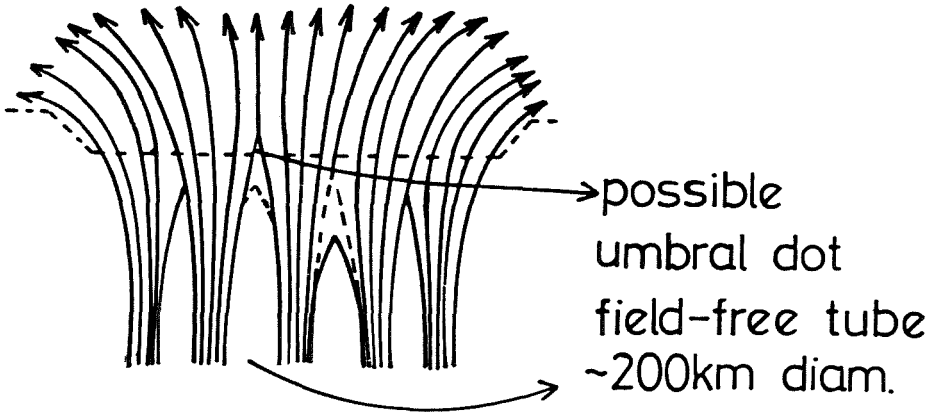

Figure 7.2 Sketch of the vertical profile of a sunspot (after Parker, 1979c)

photospheric flux tubes, as shown in Figures 7.1 and 7.2, then (i) - (v) above indicate that possible candidates for consideration are the waves with phase-speed c_T, but modified by gravity. Roberts and Webb (1978) and Roberts (1983b) have considered such modes, as given by (5.85),

$$\omega^2 \simeq k^2 c_T^2 + \omega_v^2,$$

for tubes of zero width. Roberts found that the observations of Giovanelli *et al.* (1978), showing a discrepancy in duration time for waves propagating inside and outside flux tubes, could be explained in terms of such modes propagating in a non-adiabatic medium. However, once the individual flux tubes are assumed to have finite width, and thermal conductivity is taken into account, the problem

requires an analysis of something like Equation (5.86). Though this has been carried out by Webb and Roberts (1980b) and would suitably describe the effects of thermal conductivity in the photosphere (by replacing their radiative decay time by $\tau_\kappa = a^2/\gamma\kappa j_n^{(0)^2}$) it would be less appropriate for a sunspot model because of their assumption of an isothermal atmosphere.

Some headway can be made by considering the Boussinesq fluid model of a sunspot, though this removes consideration of compressibility effects, which contribute to forming the c_T mode, since $c_T \to v_A(1 - k_g^2/k^2)^{\frac{1}{2}}$ in this limit, as noted in Subsection 5.5.2. Such a model accepts that the basic modes are the c_T ones, modified by gravity, and concentrates on the overstability aspects introduced by allowing for non-zero thermal conduction effects.

Some criticism of Parker's (1979c) estimates of growth rates of these overstable modes was expressed in Chapter 5, since they appeared to become infinitely large in certain limits. He was attempting to explain the appearance of umbral dots (Figure 7.2) in sunspots as being the consequence of individual columns of field-free gas punching through the surface and remaining there for an hour or so "as islands of photosphere". He obtained growth times of ~ 1-3 hrs. which he argued were comparable to the lifetimes of umbral dots. This is quite a large discrepancy compared to the lifetimes of ~ 1500 s (Beckers, 1981) quoted in Chapter 1.

The removal of compressibility effects via the Boussinesq approximation must be treated with caution. If umbral dots are to be explained in terms of oscillatory behaviour then presumably they

must relate to body waves which oscillate back and forth within the structure (see Figure 2.3) as opposed to surface waves. However as Figures 2.5 and 3.2 show, the incompressible plasma supports only *surface* modes. Boussinesq body waves arise from including gravity in the system. Physically this explains the mathematical dilemma of Parker's (1979c) attempted explanation of umbral dots referred to in Chapter 5. Since he regards the Boussinesq approximation as a 'small gravity' (M small) expansion about the incompressible case, the limits of zero thermal conductivity and tube width do not produce well-behaved expressions. It was shown in Subsection 5.2.2 (iii) that consideration of non-zero thermal conductivity in the incompressible case reveals the original surface modes and decoupled thermal decay modes. Body waves do not exist in this situation.

According to Chapter 5 there are two estimates of the growth factor, depending upon whether the Péclet number P_e is > or < 1. For example, in the former case the growth factor is given by Equation (5.131) which for a tube of width 200km (Figure 7.2), $M = 0.5$, a dimensionless tube width ka of 0.3 and a value of $\kappa = 400\ km^2 s^{-1}$ (consistent with Parker, 1979c) gives a growth time of $\simeq$ 37 mins. A second calculation but using a value of $\kappa = 10^3 km^2 s^{-1}$ (consistent with Roberts, 1976) means that the $P_e < 1$ regime must be considered and the growth rate is therefore given by (5.134). Substitution of the above values yields a growth time of $\simeq$ 42 mins. These growth times are shorter than those given by

Parker (1979c) but they still appear to be rather long to explain either overstable oscillations or the umbral dot behaviour. The period of oscillation of the gas beneath the sunspot is ~ 100s for Parker's figures. For the two cases cited here the periods are 592s (10 min) and 418s (7 mins), respectively, so in the most favourable case it would take three periods for the oscillation to e-fold, which is not unreasonable. However, periods of 100s and growth rates of 1-3 hrs (which Parker argues are comparable to the 1500s lifetime of the dots) seem to ask too much of a linear analysis. Parker's explanation is indeed that the observed umbral dots represent fluid in which vertical oscillations have increased into a nonlinear regime. Knobloch and Weiss (1984) have recently considered nonlinear umbral oscillations. Their model is restricted to a Boussinesq fluid and rather than a spaghetti model they consider convective motions in a monolithic, single tube of flux. They estimate umbral oscillation periods of around 6 hrs. but umbral dot lifetimes of ~ $\frac{1}{8}$ of this period, that is ~ 45 mins.

The periods given here of 592s and 418s (using $\omega \sim kv_A$ and $\omega \sim v_A(k^2 - k_g^2)^{\frac{1}{2}}$ from Equations (5.133) and (5.129)) are also long compared with observed periods of 300s and 180s, though Moore (1981a) quotes periods in the range 2-8 mins for umbral oscillations. It must be remembered that the Boussinesq approximation is being used here. Taking $\omega/k \sim c_T$ gives periods on the order of 300s

(295s) which is more acceptable. Also it is important to realize that there are other possible photospheric modes as listed in the summary at the beginning of this section. It may be possible that the whole structure is moving predominantly in kink-like fashion with higher c_k-like frequencies.

There are of course many uncertainties and omissions in this simple sunspot model. It has been assumed that the flux tubes are vertically orientated, that the regime is linear and Boussinesq, and no attempt has been made to model any reflection or transmission of the waves at horizontal boundaries/interfaces. No bulk flows, by way of superposed velocities representing observed strong downdrafts ($\sim 1\,\mathrm{km\,s^{-1}}$), have been included. As a matter of detail, the values of κ, v_A and a are also uncertain. The possibility remains, however, of being able to link these slender tube models to those for an infinite medium to help to produce a comprehensive picture of a sunspot.

7.2 The Chromosphere : Waves in Fibrils

The possible link between photospheric flux tubes and spicules has already been mentioned. Another feature of the chromosphere described in the introductory chapter is the bright and dark elongated fine-scale mottling, fibrils, which according to Athay (1981b) have the appearance of flux tubes and in which the

brightness fluctuates on a time scale of minutes. Giovanelli (1975) has described in detail the propagation of waves as observed in chromospheric fibrils. To quote from Giovanelli's paper, '... typical value (of drift velocity) is around 70 $km\,s^{-1}$. This is obviously a wave system, the direction of propagation being horizontal ... in directions parallel to fibrils ... it is not certain whether the wave motion is approximately periodic; the best estimates ... of the period are in the range 150s to 190s, with a mean of about 170s. At 70 $km\,s^{-1}$ the corresponding wavelength is 1.2×10^4km ... the wavefront appears to cover only the width of a single fibril'.

Giovanelli points out that the disturbances, with amplitudes ~ 5 $km\,s^{-1}$, though transverse to the fibrils, involve intensity fluctuations and so are *not* Alfvén waves. His remark, that the wavefronts are confined to the fibril rather than spreading outwards, is consistent with the model of trapped waves (which are laterally evanescent outside the structure; see comments in Section 3.5).

Wentzel (1979c) has suggested that fibril waves are likely to be flux tube modes, the tube having an internal Alfvén speed that is lower than that in the surroundings. Spruit (1983), too, in his discussion of transversal (kink) tube waves comments that the expected wave amplitudes and periods agree well with the observations of wave motions in the Hα fibrils.

In the terminology used here, the fibril wave would be an example of the fast kink mode of Figure 3.4, *a magnetic Love wave propagating in a density enhancement* (for which $v_{Ae} > v_A\ (> c_e, c_0)$).

If it is assumed that the chromosphere is more or less magnetically dominated then these fibril waves can only occur where there are density enhancements, corresponding to regions of lower Alfvén speed.

For example, Giovanelli (1975) estimated a magnetic field of 10G and used a density, which was higher inside the fibril, of 10^{11} particles cm^{-3}. So using these values in Equation (4.12), an observed period of 170s would mean a wavelength of 8.3×10^3km which is entirely consistent with the observed fibril lengths of 10-15 arc sec (see Chapter 1 and Giovanelli's remarks above).

7.3 Structuring in the Magnetosphere

7.3.1 The plasma sheet Having set up a general Cartesian structure in Chapter 2 and looked at an initial value problem in connection with the Sun's corona in Chapter 4, applications to the plasma sheet of the magnetosphere follow straightforwardly. The plasma sheet (see Figure 7.3a; also Figures 1.3 and 1.5) is modelled as an infinite, hot, plasma slab of thickness $2x_0 = 4Re \simeq 2.4 \times 10^4$km. Since this represents the narrow field-free region between the antiparallel magnetic field of the magnetotail, it will be assumed that $v_A = 0$ (in keeping with McKenzie, 1970; Tamao, 1973). The sound speed within the sheet will be taken as $300\ km\,s^{-1}$ and the external Alfven speed as $v_{Ae} = 600\ km\,s^{-1}$. Since the plasma in the surrounding magnetotail is considered cold, with sound speed

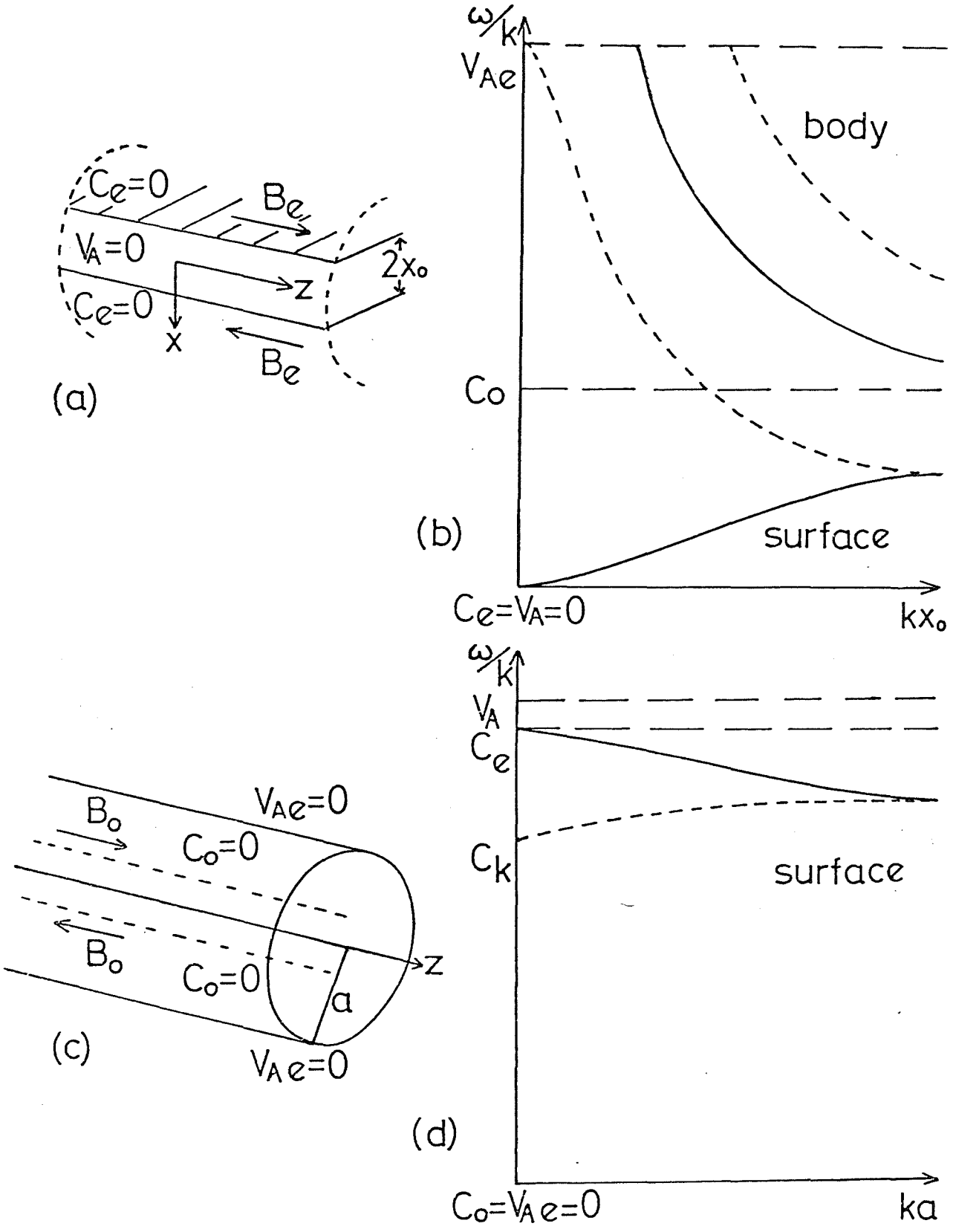

Figure 7.3 (a) The plasma sheet and (b) the modes which it can support sketched as a function of kx_0 ($k > 0$).

(c) The cylindrical magnetotail and (d) the modes which it can support sketched as a function of ka ($k > 0$).

—— : sausage; --- : kink

~ 80 km s^{-1} (Patel, 1968a), c_e will be considered negligible compared to v_{Ae}. The fact that the exterior magnetic field is oppositely directed outside the sheet (slab) does not affect the arguments in Chapter 2 since it is the magnetic field squared which appears in the expression for v_{Ae} (or v_A).

Thus with $v_A = c_e = 0$ the dispersion relations (2.27) and (2.43) of Chapter 2 become

$$\frac{2c_0^2}{\gamma v_{Ae}^2}\,(k^2 v_{Ae}^2 - \omega^2)\, m_0 \begin{Bmatrix}\tanh\\ \coth\end{Bmatrix} m_0 x_0 = \omega^2 m_e \qquad (7.6)$$

and

$$\frac{2c_0^2}{\gamma v_{Ae}^2}\,(k^2 v_{Ae}^2 - \omega^2)\, n_0 \begin{Bmatrix}-\tan\\ \cot\end{Bmatrix} n_0 x_0 = \omega^2 m_e, \qquad (7.7)$$

where $m_e^2 = (k^2 v_{Ae}^2 - \omega^2)/v_{Ae}^2$, $m_0^2 = (k^2 c_0^2 - \omega^2)/c_0^2 = -n_0^2$. As was noted earlier (Chapter 2), these agree with the dispersion relations of McKenzie (1970). The mhd waves which the plasma sheet can support are shown in Figure 2.7, with $v_A = c_e = 0$. This special case of the figure is sketched as Figure 7.3b for easier reference. There is a sausage surface wave given by (2.52), that has

$$\omega^2 \simeq k^2 \frac{2c_0^2}{\gamma}\,.\,kx_0, \qquad (k > 0), \qquad (7.8)$$

for kx_0 not too large, a result also found by McKenzie (1970). Taking $kx_0 = \frac{1}{2}$ yields, in agreement with McKenzie, a result of

10.8 mins for the period of this sausage mode.

Table 7.1 summarizes some time periods observed in the magnetosphere, or thought to originate from the magnetosphere. Geomagnetic pulsations are usually classified by their pc names (see, for example, Lanzerotti and Southwood, 1979) which refer to quite broad temporal ranges. For example, pc4 corresponds to a period of 45-150 s, so it is difficult to be precise. However though the sausage mode cited above gives a time period in agreement with some observations, there appear to be much shorter time periods requiring explanation. As with the coronal pulsation problem, it is the body waves (McKenzie called them 'bouncing waves') of Figure 7.3b which have these characteristically shorter periods. The appropriate dispersion relation is Equation (7.7) above.

For wavelengths that are long compared to the width of the plasma sheet the phase-speed of the kink mode is (see Equation (2.38))

$$\frac{\omega^2}{k^2} \simeq v_{Ae}^2 \left\{ 1 - \frac{\gamma^2 v_{Ae}^4}{4c_0^4} (kx_0)^2 \right\}, \qquad (7.9)$$

which results in a period of ~ 4 minutes (for $kx_0 = \frac{1}{2}$). It may be noted in passing that had the plasma sheet been modelled as a cylindrical structure, rather than a slab, with radius ~ $4R_e$ the appropriate long wavelength kink mode is given by (3.43) rather than (7.9). The appropriate period is then more like 3.4 minutes.

Reference	Time periods			Observations
	< 3 mins	3 → 10 mins	> 10 mins	
Cummings *et al.* (1969)	50 → 300s 102s, 190s dominant			ATS 1
Siscoe (1969)	?	3 → 6 mins	12 → 20 mins	OGO 1
Mihalov *et al.* (1970)	≤ 2 → 10 mins			EXPLORERS 33 and 35 (plasma sheet)
Lanzerotti *et al.* (1973)		200 s		EXPLORERS ground based
Arthur *et al.* (1977)	10 → 45s, pc3 30s dominant			ATS 6
Lepping and Burlaga (1979)		170 ± 60s		VOYAGER 1 (magnetopause)
Williams (1979)	≥ 140s			ISEE 1 (magnetopause)
Williams *et al.* (1979)	90 → 150s	8 → 10 min	30 min	ISEE 1, ISEE 2 (magnetopause)
Williams (1980)	150 → 400 ± 50s superimposed 9 min - period			ISEE 1 (magnetopause)
Greenwald *et al.* (1981)	150 → 600s, pc5			GEOS2, STARE
Hones *et al.* (1983)	150 → 600s, pc5			ISEE 1, ISEE 2 (plasma sheet)
Observations exhibiting wave-packet behaviour:				
Herron (1966)	40 → 150s 20s, 70s, 400s			ground based
Hughes *et al.* (1978)	24 → 40s, 40 → 80s 80 → 200s, 150s dominant			ATS 6, SMS 1, SMS 2 (dayside magnetosphere)
Walker *et al.* (1978, 1979)	150 → 600s, pc5			STARE ground based
Mier-Jedrzejowicz and Hughes (1980)	45 → 150s, pc4			SMS 2, ATS 6 ground based
Yumota and Saito (1982)	10 → 45s, pc3			ground based

Table 7.1 Examples of oscillatory data observed in, or thought to originate from, the magnetosphere. Last column indicates how data obtained and, in parentheses, from where in magnetosphere, if known. pc numbers explained in the text.

? : period < 3 mins suspected; STARE : Scandanavian twin auroral radar experiment; VOYAGER 1 : outer planet flyby spacecraft.

ATS, EXPLORER, GEOS, ISEE, OGO and SMS refer to satellite series.

The uncertainty about the source of magnetospheric oscillations was discussed in Chapter 1. Whatever the mechanism, impulsive sources are not ruled out. Indeed, Mier-Jedrzejowicz and Hughes (1980) note in their analysis of geostationary satellite and ground-based data that "some impulsive excitation" starts an oscillation; see also Southwood and Hughes (1983). It seems appropriate therefore to apply the initial-value theory of Chapter 4 to these magnetospheric waves.

Differentiating (7.7) with respect to k yields, for both sets of modes, an expression for the dimensionless group velocity, $G = d\omega/dk/v_{Ae}$:

$$G = \frac{(V^2 D_1 + W^2 D_2)}{W(D_1 + D_2)}, \qquad (7.10)$$

where $V = c_0/v_{Ae}$, $W = \omega/kv_{Ae}$, $D_1 = [(W^2 - V^2)(1 - W^2) + \gamma^2 W^4/4V^2]2X(1 - W^2)^{\frac{1}{2}}$, $D_2 = \gamma[W^2(1 + V^2) - 2V^2]$ and $X = kx_0$. A plot of G against WX looks very similar to Figure 4.4. Since in this magnetospheric case the group velocity curve again possesses a minimum, the behaviour in time of an oscillation at a position along the magnetotail is very similar to that shown in Figure 4.5. This is remarkably similar to the observed wave-packet behaviour described in the papers comprising the last five entries of Table 7.1.

Consider the lowest order, symmetric, fast body wave shown in Figure 7.3b. It has a cut-off, for the parameters given here, of $k_c x_0 = 0.907$. Thus the (largest) time scale of the periodic

disturbance illustrated in Figure 4.5 is given by

$$\tau_c = 2\pi/k_c v_{Ae} \simeq 138 \text{ s}.$$

Reading off the minimum from the group velocity curve (constructed for the parameters v_{Ae}, c_0 considered so far in this section) shows that

$$\frac{\omega^{min} x_0}{v_{Ae}} = 1.406,$$

which results in a period at the onset of the Airy phase of $\tau^{min} \simeq$ 89 s. Thus considering that the observed behaviour is likely to be a combination of various modes, the theory presented above provides a possible explanation of the differing periods (perhaps three bands) occurring in Table 7.1, especially the shorter period Love waves. It also suggests why there is wave-packet behaviour, which, as both Herron (1966) and Mier-Jedrzejowicz and Hughes (1980) have pointed out, is *not* a beating phenomena, though Yumoto and Saito (1982) refer to it as such. Sometimes the termination of oscillations has been interpreted as a dissipative (damping) effect (see, for example, Tamao, 1973).

It must also be noted that though the analysis has been carried out for $v_A = c_e = 0$, the basic pattern of modes, for non-zero values, is very similar, as a comparison of Figure 2.7 with Figure 7.3b shows. Other variations, such as increasing the Alfvén velocity outside the sheet to 1000 km s^{-1}, are possible. This yields a period of 100s, as given by Mier-Jedrzejowicz and Hughes (1980).

On the other hand, increasing the sound/Alfvén speed ratio slightly results in periods more on the order of those given by Arthur *et al.* (1977) (entry 5 of Table 7.1) which were explained in that paper by their consistency with Chen and Hasegawa's (1974a) and Southwood's (1974) models.

7.3.2 The cylindrical magnetotail Attention so far has concentrated on a slab model of the plasma sheet. It is possible, instead, to model the magnetotail as a cylindrical whole (see Figure 7.3c), ignoring the plasma sheet (Patel, 1968a,b). Considering then the magnetotail as being the basic cylindrical inhomogeneity of Chapter 3, the dispersion relations are given by Equations (3.25) and (3.29). McKenzie (1970), too, produced such a model. He made the following two assumptions.

The plasma inside the cylinder is cold so that $c_0 = 0$. This is a reasonable assumption, consistent with those of Subsection 7.3.1 above, except in the plasma sheet. Note that c_e in Subsection 7.3.1 is c_0 here (cf., Figures 7.3a and 7.3c).

The second assumption is that the magnetic pressure in the magnetosheath, that is outside the cylinder, is negligible compared to the gas pressure, so that $v_{Ae} = 0$.

The relevant regime is thus a special case of Figure 3.3 and it is sketched as Figure 7.3d for easier reference. From that figure, and as McKenzie also points out, it is clear that the above assumptions simplify the discussion without removing any essential

physics from the problem. (The low frequency c_T modes are ignored; these give rise to longer periods.) Several points arise:

1. From Figure 7.3d it is seen that unless radiative modes in the exterior of the cylinder (magnetotail) are considered, that is, as long as it is insisted that there are only evanescent modes in the magnetosheath, only fast *surface* waves are possible. As a result small time periods (associated with fast body waves) are not obviously explained by this model.

2. A more realistic model may be used which includes a bulk flow (solar wind) in the exterior of the cylinder. McKenzie (1970) in fact does this and then his model is very similar to that of Parker's (1979b) paper which models a sunspot in a downdraft. The interface becomes Kelvin-Helmholtz unstable if the shear velocity exceeds the velocity in the tail (see, e.g., Chen and Hasegawa, 1974b; Southwood, 1974).

3. McKenzie's analysis ends with a brief calculation which is easily deduced from Figure 7.3d. Since both kink and sausage modes are not greatly dispersive a rough estimate of the time periods associated with these modes may be gained by putting $\omega/k \simeq c_e = 100\ \mathrm{km\,s^{-1}}$, say. Then if the radius of the tail, a, is approximately 20Re (see Chapter 1), for $ka \simeq 2\pi$ the period of oscillations is 20 mins. McKenzie also gives a slightly lower time period (13 minutes) by using a slightly higher speed in the magnetosheath. Even the rough calculation just given yields time

periods of ~ 10 mins and ~ 6 mins for sound speeds of 200 $km\,s^{-1}$ and 300 $km\,s^{-1}$, respectively. These values, for *surface waves*, are in agreement with those quoted by Williams *et al.* (1979) (entry 8 of Table 7.1) of 9 ~ 10 mins for oscillations at the magnetopause. However they are slightly longer than those calculated by Lepping and Bulaga (1979) using Voyager I (spacecraft) data.

7.3.3 Comparisons In an effort to produce a similar model of the whole magnetotail Tamao (1981) used modified versions of (7.7). However the boundary conditions which he imposes are rather artificial; they are similar to those used by Rosenberg (1970) and Meerson *et al.* (1978) in the coronal radio wave case. Solutions correspond to radiative, not free, modes and ignore the effect on the interface due to the surrounding magnetosheath. In an earlier paper, Tamao (1973) used a slab model for a combined magnetotail and plasma sheet. He recognised the importance of the group velocity in his calculation and by using a regime similar to that shown in Figure 2.10 ($v_{Ae} >> v_A \simeq c_0$) produced two time scales, of ~ 5 mins and ~ 15 mins, for the plasma sheet oscillations. However, the above discussion in Subsection 7.3.2, for the magnetotail, has shown that if artificial boundary conditions (as in his 1981 paper) are not imposed then only mildly dispersive surface waves feature (Figure 7.3d). They do not yield group velocity curves of the form shown in Figure 4.4 and hence the structure does not support waves of very short time scales.

In order to test the plasma sheet model of Subsection 7.3.1 it would be nice to correlate the predicted duration time T_{dur} of

the bursts (cf., Equation 4.27),

$$T_{dur} = h\left[\frac{1}{c_{g_{min}}} - \frac{1}{c_0}\right], \qquad (7.11)$$

where h (km) is the distance from the impulsive source, with the observed duration times. For example, a sound speed of 300 $km\,s^{-1}$ in the sheet and an Alfvén speed of 600 $km\,s^{-1}$ in the surrounding tail gives $T_{dur} = 0.001\,h$ secs. Taking $h = 50R_e$ therefore yields a duration time of approximately 5 mins. Observed duration times vary considerably. Herron's (1966) data seem to indicate ~ 2½ mins, Yumota and Saito's (1980) data ~ 2~3 mins, and Mier-Jedrzejowicz and Hughes' (1980) data ~ 10 mins. It should be noted, however, that the first two of these references refer to ground-based data, the latter to satellite observations. The difference may arise, as noted in the introductory chapter, because of the effect of the Earth's ionosphere, and it is possible that two completely different features are being observed here. Unfortunately, unless the source of excitation is positively identified, so that h in (7.11) is known, the duration times cannot at present be compared.

It has been assumed in these models that, once generated, these fast and slow surface and body waves can propagate in the magnetosphere. Some speculation has occurred in the past (for example, Belcher and Davies, 1971; Burlaga and Turner, 1976; Hollweg, 1978; Greenwald *et al.* 1981) as to the type of mhd waves moving in

the outer corona, solar wind and interplanetary medium in general. In support of the suggestions made here it must be pointed out, however, that Burlaga and Turner did claim evidence of fast mhd waves rather than pure Alfvén modes. Also, most discussions expressing doubts on the inability of fast mhd modes to propagate are based on the results for infinite media; it is argued here that it is the very structuring of the medium, the ducting, which allows these waves to exist.

7.4 Laboratory Plasmas

It would be inappropriate here to attempt a detailed explanation of wave behaviour in that most obvious of structured plasmas, the laboratory magnetoplasma column; it is a specialist subject in its own right. Indeed, some of the main equations used here were established in forms specific to laboratory applications long before solar physics applications were attempted; the dispersion relations for the slab (Axford, 1960) and cylinder (Kruskal and Schwarzschild, 1954; Hain and Lüst, 1958), Equations (2.31) and (3.20), and the idea of density gradients in a linear pinch (Pneuman, 1965) arose in attempts to model physical behaviour, with confinement of plasmas for controlled thermonuclear reactions (CTR) in mind. More recently, however, two phenomena have been observed in plasma columns for which the properties of waves in structured plasmas established here could offer explanations.

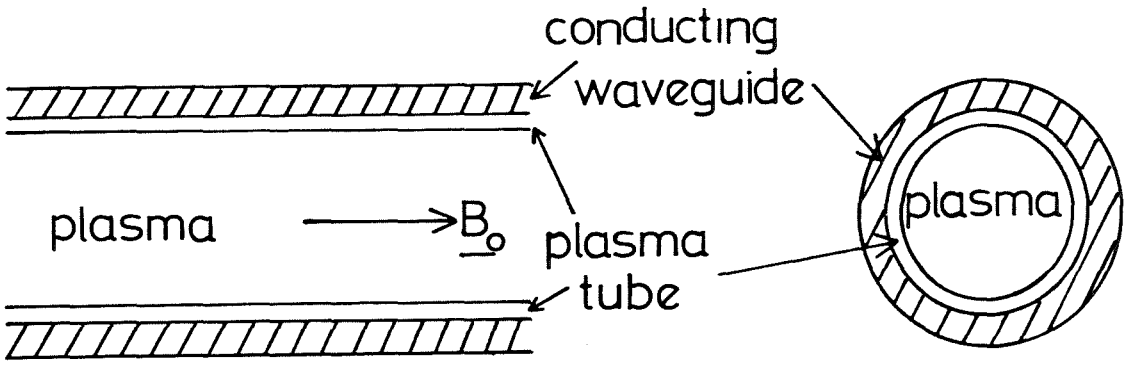

Figure 7.4 Schematic illustration of experimental plasma column and its cross-section

Kunhardt and Cheo (1976, 1979) report observations achieved with an experimental apparatus shown schematically in Figure 7.4. For an axial magnetic field of 200G they report impulsively generated wave-packet behaviour at a given point along the column very similar to that illustrated in Figure 4.5. They suspect that such packets result from the nonlinear, dispersive nature of the waves and offer an explanation (without supportive theory) for a long wavelength, cold plasma, model. However, such wave-packet behaviour could be explained in similar terms to the coronal model of Chapter 4. Indeed, Kunhardt and Cheo invoke the relationship between arrival time, which depends on group velocity, and which in turn is related to amplitude (see Equation (4.20)), to explain the difference in arrival times of the wave-packet when the amplitude of the oscillations is varied. However, the relative values of the

magnetic field and density inside the column and the waveguide are not given and it is not clear whether other, non-mhd, effects are more pertinent.

A second feature of wave behaviour in a low pressure magneto-plasma column has been reported by Ventrice (1979). Ventrice notes that the spontaneous generation of acoustic waves in weakly ionized plasmas has been observed many times and explained theoretically by Ingard (1966) and Ingard and Schultz (1967). Waves are more easily generated the higher the gas pressure and it was accepted that acoustic wave generation seemed impossible for pressures less than 0.1 Torr (13.3 Pa). However, by applying an axial magnetic field of ~ 10G, Ventrice found that he observed acoustic waves for gas pressures less than 0.1 Torr, and by increasing this axial field he found that acoustic wave generation was possible for fields as large as 100G. But once the gas pressure was reduced below 0.04 Torr no oscillations were observed, even for large magnetic fields.

Uberoi and Somasundaram (1982b) offered an explanation of this phenomenon by modelling an ideal incompressible, cylindrical plasma column surrounded by a non-conducting, compressible gas. The appropriate dispersion relation, in the terminology used here, is then not (3.20) but

$$\frac{\omega^2}{k^2 v_A^2}\left[1 - \frac{\rho_e}{\rho_0}\frac{I_n'(ka)K_n(m_e a)k}{I_n(ka)K_n'(m_e a)m_e}\right] + \frac{B_e^2}{B_0^2}\frac{I_n'(ka)K_n(ka)}{I_n(ka)K_n'(ka)} = 1, \qquad (7.12)$$

where $m_e = (k^2 c_e^2 - \omega^2)^{\frac{1}{2}}/c_e$. However, their explanation is unsatisfactory

in several ways. They used pressures in the range >> 0.1 Torr, which was not the range in the experiments, and considered the *wide* tube limit ka >> 1, whereas Ventrice had specifically stated that the radius a was much smaller than the tube length (typical lengths are 0.5 - 1.5 m; internal diameters 10 ~ 20 mm). They also considered just the sausage mode (n = 0 in (7.12)) and took $B_e = B_0$. In fact, their explanation is altogether confused: for example, they refer to a cold gas blanket for the plasma when they have $c_e \neq 0$; and other statements of similar type appear to be in contradiction to Ventrice's paper.

If any sort of explanation is to be offered, the configuration which is to be modelled, and the appropriate boundary conditions, must be understood. As Moisan *et al.* (1982) have pointed out in their review, there are several possible magnetoplasma column configurations, a cylindrical or rectangular plasma column being surrounded by one or some of glass tubes (dielectrics), metallic cylinders (conductors) and air (or vacuum), in varying order. If it is supposed that the plasma column is modelled as shown in Figure 7.4 then the interpretation outlined below, in terms of the theory of Chapters 2 and 3, seems to offer a partial explanation. This is consistent with many laboratory plasma models. For example, the dispersion relation quoted by Moisan *et al.* (1982) for a cold plasma is (in the notation used here)

$$\frac{m_0}{\varepsilon_0}\frac{I_0(m_0 a)}{I_1(m_0 a)} + m_e \frac{K_0(m_e a)}{K_1(m_e a)} = 0, \qquad (7.13)$$

which is just (3.25) when the permittivity ε_0 of the plasma is set equal to 1. Granatstein and Schlesinger (1965) have given both experimental and theoretical phase-speed and group velocity curves for an afterglow plasma column in argon at 4 Torr, surrounded by a thin glass tube in a vacuum (i.e., in Figure 7.4 no metallic waveguide is present). Their theoretical curves are just those of Figures 4.2 (fast body waves) and 4.4 with $v_{Ae} \to \infty$, since $\rho_e \to 0$ in the vacuum surrounding the tube. It is a fairly common approximation to neglect the thickness and permittivity of the glass tube and model a plasma column surrounded by a vacuum.

Returning to Ventrice's experiment, initially there is no magnetic field (so $v_A = v_{Ae} = 0$) and presumably the external pressure modes, for example those of Figure 2.8, are the ones being observed, though why these should cease to exist for $c_0 \to 0$ cannot be explained in terms of ideal mhd theory. If an axial field is applied, then for $c_0 \to 0$, Table 2.2 (columns (ii) and (iv)) is relevant. If the medium exterior to the plasma column has $c_e > v_{Ae}$, then initially there will be fast acoustic waves (col. (ii), $v_A > c_e > v_{Ae} > c_0$); but as the magnetic field increases and dominates the acoustic effects in the external medium then $v_{Ae} > c_e$ and column (iv) shows that there are no acoustic modes. Such an explanation of Ventrice's result is of course very speculative. However, according to Moisan *et al.'s* (1982) review, theoretical support for observed experimental behaviour is no more advanced than this. The analogy with wave propagation in dielectrics (Chapter 4) has been recognized but not

exploited though density variation across the column was suspected by Granatstein *et al.* (1967) to account for the differences between their experimental and theoretical (for a homogeneous plasma cylinder) results. Moisan *et al.* (1982) identify and discuss the many discrepancies and unresolved issues.

7.5 The Corona Revisited

The idea of modelling the ubiquitous loop structures of the corona by inhomogeneity structures (ducts), and thence explaining the observed short period oscillatory behaviour, was considered at length in Chapter 4. It was shown that if the ducts were considered to be density inhomogeneities these need not necessarily be modelled as abrupt structures; density variations across the loops could be considered without significant changes to the explanations of oscillatory behaviour offered earlier.

It may be possible to explain radio pulsations and related behaviour observed in the corona by an alternative ducted model, that of the helmet streamer proposed by Carmichael (1964) and Sturrock (1966) and shown in Figure 7.5. Several authors (e.g., Forbes and Priest, 1982) since Sturrock have observed that this helmet streamer model is analogous to that of the magnetospheric tail, and the effect of ducting caused by an antiparallel magnetic field in the corona could be considered in the same way as in Section 7.3, using Figure 7.3a. Here the parameters are slightly

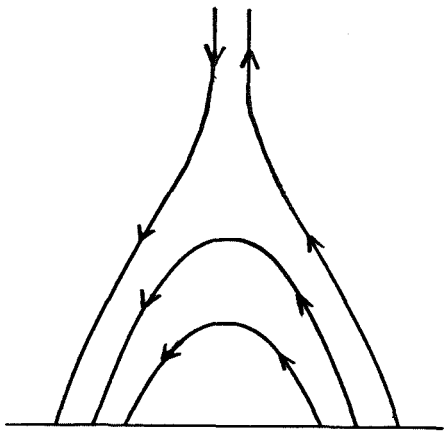

Figure 7.5 The helmet streamer model

different. Typical Alfvén speeds, v_{Ae}, in the corona are 10^3 km s^{-1} and sound speeds c_0 are ~ 200 km s^{-1}. Substituting these values in Equation (7.11), together with the appropriate value of c_g^{min}, calculated to be 0.13 v_{Ae} km s^{-1}, results in a duration time, T_{dur}, of 0.0026 h sec (h in km). For emission observed at a height of ~ 5×10^4km above the impulsive source (Krüger, 1979; Wagner *et al.*, 1981) this gives a duration time of ~ 2 mins. The shortest 'periodicity' τ^{min} may also be calculated from the group velocity curve (c.f., Figure 4.4) and is given by $\tau^{min} = 0.013x_0$ sec. The equivalents of expressions (4.5), (4.23) and (4.26) for the wave-number, frequency and period at cut-off in the situation under consideration here are given by

$$k_c = \frac{\pi}{2x_0}\left(\frac{c_0^2}{v_{Ae}^2 - c_0^2}\right)^{\frac{1}{2}}, \qquad \omega_c = k_c v_{Ae}$$

and

$$\tau_c = \frac{2\pi}{\omega_c} .$$

These combine to give a cut-off period of $\tau_c = 0.02x_0$sec. For an inhomogeneity of total width $2x_0$ = 1000 km this results in time scales of τ^{min} = 6.5s and τ_c = 10s, which are comparable to several entries in Table 4.1 or those reported by, for example, Trottet *et al.* (1979). Though Trottet *et al.* report emission which exhibits a strong modulation on a time scale of 1 min (Chapter 4), they also calculate short scales ~ 7s and report several events of duration 25 - 32s though exactly what is being measured here is not clear. For an observed height of h = 10^4km, say, above the source the values presented here are compatible with those reported by Trottet *et al.* However the width of the sheet is uncertain; it is thought to be possibly a dense and much narrower region E.R. Priest (private communication 1984). If this were so, extremely short, millisecond, time scales could be explained by either this, or the alternative model in Chapter 4, but in either case the ducting of the waves due to the inhomogeneity is essential to the explanation.

Most of the coronal discussion has concentrated on ideas involving the fast body waves of Figures 2.10, 3.4 and 4.2. Indeed this is most appropriate for the low β situation of the corona. But it must be remembered that all these ideas involve only linear theories. The solar corona is probably far more complicated. Do coronal solitons exist, for example?

In Section 6.5 the dispersion correction to the c_k mode was developed. For a cold plasma, as illustrated by Figure 3.4, it is shown to have the form

$$\frac{\omega}{k} \simeq c_k\{1 - \alpha k^2 K_0(\sigma|k|a)\},$$

where $\sigma = \dfrac{(v_{Ae}^2 - c_k^2)^{\frac{1}{2}}}{v_{Ae}}$, and $\alpha = \dfrac{1}{2}\dfrac{\rho_0\rho_e(v_{Ae}^2 - v_A^2)\sigma^2 a^2}{(\rho_0 + \rho_e)^2 c_k^2}$.

This phase-speed is of the general form discussed by Roberts (1984) and suggests that for a cylindrical inhomogeneity the kink mode may propagate nonlinearly as a solitary wave according to an integro-differential equation allied to the Benjamin-Ono equation. So coronal solitons are a possibility, though a detailed, self-consistent derivation has yet to be given.

The applications and ideas expressed here concerning waves in structured plasmas cannot be exhaustive. Many theoretical aspects, such as stability, twist, turbulence, viscosity, shocks, etc., have been omitted and it is virtually impossible to include all the important features into any one problem. As more observations of the solar atmosphere, the Earth's magnetosphere and, indeed, in the laboratory are performed, detailed physical information about these systems will increase and more faithful mathematical representations can then perhaps be attempted, the knowledge gained in one field hopefully supplementing the other. Indeed it may be other physical

fields, as diverse as fibre optics and oceanography, which may offer the necessary inspiration. Whatever mechanisms and explanations are involved, the fact remains that waves have been observed on the Sun, and in interplanetary space, and it can only be supposed that oscillatory behaviour is governed by the structured situation in which it is found, just as happens here on Earth.

'Alio relinquente fluctu, alius excepit.'
(When one wave recedes, another follows.)

Erasmus 'Adagia'

References

Ablowitz, M.J. & Segur, H., Solitons and the Inverse Scattering Transform, Siam, Philadelphia, 1981.

Abrami, A., Solar Phys., 11, 104, 1970.

Abrami, A., Nature, 238, 25, 1972.

Abramowitz, M. & Stegun, I.A., Handbook of Mathematical Functions, Dover, New York, 1967.

Achong, A., Solar Phys., 37, 477, 1974.

Adam, J.A., Astrophys. Space Sci., 36, 479, 1975.

Antia, H.M. & Chitre, S.M., Solar Phys., 63, 67, 1979.

Anzer, U. & Galloway, D.J., Mon. Not. Roy. Astron. Soc., 203, 637, 1983.

Appert, K., Gruber, R. & Vaclavik, J., Phys. Fluids, 17, 1471, 1974.

Arnaud, J.A., Beam and Fiber Optics, Academic Press, New York, 1976.

Arthur, C.W., McPherron, R.L. & Hughes, W.J., J. Geophys. Res., 82, 1149, 1977.

Athay, R.G., Observations of Mass Motions in Active Regions, in Solar Active Regions, ed. Orrall, F.Q., Colo. Assoc. Univ. Press, Boulder, 1981a.

Athay, R.G., The Chromosphere and Transition Region, in The Sun as a Star, ed. Jordan, S., NASA SP-450, 1981b.

Athay, R.G. & White, O.R., Astrophys. J. Supp., 39, 333, 1979.

Axford, W.I., Quart. J. Mech. Appl. Math., 13, 314, 1960.

Bataille, K. & Lund, F., Physica D, 6, 95, 1982.

Beckers, J.M., Ann. Rev. Astron. Astrophys., 10, 73, 1972.

Beckers, J.M., Magnetic Fields in the Solar Atmosphere, in Physics of Solar Planetary Environments, I, ed. Williams, D.J., Proc. Int. Symp. on Solar-Terrestrial Physics, Am. Geo. Union, 1976.

Beckers, J.M., Dynamics of the Solar Photosphere, in The Sun as a Star, ed. Jordan, S., NASA SP-450, 1981.

Beckers, J.M. & Artzner, G., Solar Phys., 37, 309, 1974.

Belcher, J.W. & Davis, L., Jnr., J. Geophys. Res., 76, 3534, 1971.

Bender, C.M. & Orszag, S.A., Advanced Methods for Scientists and Engineers, McGraw Hill, Tokyo, 1978.

Benjamin, T.B., J. Fluid Mech., 29, 559, 1967.

Benz, A.O. & Tarnstrom, G.L., Astrophys. J., 204, 597, 1976.

Bray, R.J. & Loughhead, R.E., The Solar Chromosphere, Chapman & Hall, London, 1974.

Brekhovskikh, L.M., Waves in Layered Media, Academic Press, New York, 1960.

Browning, P.K. & Priest, E.R., Astron. Astrophys., 131, 283, 1984.

Burlaga, L.F. & Turner, J.M., J. Geophys. Res., 81, 73, 1976.

Carmichael, H., A Process for Flares, in The Physics of Solar Flares, ed. Hess, W.N., NASA SP-50, 1964.

Chakraborty, B.B., Prog. Theo. Phys., 40, 210, 1968.

Chandrasekhar, S., Hydrodynamic and Hydromagnetic Stability, Oxford Univ. Press, 1961.

Chen, L. & Hasegawa, A., J. Geophys. Res., 79, 1024, 1974a.

Chen, L. & Hasegawa, A., J. Geophys. Res., 79, 1033, 1974b.

Cliver, E.W., Hurst, M.D., Wefer, F.L. & Bleiweiss, M.P., Solar Phys., 48, 307, 1976.

Conwell, E.M., Appl. Phys. Lett., 23, 328, 1973.

Cowling, T.G., Magnetohydrodynamics, Adam Hilger, Bristol, 1976.

Cram, L.E. & Wilson, P.R., Solar Phys., 41, 313, 1975.

Cribbens, A.H. & Matthews, P.A., Nature, 222, 158, 1969.

Cummings, W.D., O'Sullivan, R.J. & Coleman, P.J., Jnr., J. Geophys. Res., 74, 778, 1969.

Davis, R.E. & Acrivos, A., J. Fluid Mech., 29, 593, 1967.

Defouw, R.J., Astrophys. J., 209, 266, 1976.

Dennis, B.R., Frost, K.J. & Orwig, L.E., Astrophys. J., 244, L167, 1981.

Dil, J.G. & Blok, H., Opto-electronics, 5, 415, 1973.

Dunn, R.B. & Zirker, J.B., Solar Phys., 33, 281, 1973.

Edwin, P.M. & Roberts, B., Solar Phys., 76, 239, 1982.

Edwin, P.M. & Roberts, B., Solar Phys., 88, 179, 1983.

Emslie, A.G., Astrophys. Lett., 22, 41, 1981.

Erdélyi, A., Tables of Integral Transforms, II, McGraw Hill, New York, 1954.

Ewing, W.M., Jardetzky, W.S. & Press, F., Elastic Waves in Layered Media, McGraw Hill, New York, 1957.

Forbes, T.G. & Priest, E.R., Planet. Space Sci., 30, 1183, 1982.

Foukal, P.V., Solar Phys., 43, 327, 1975.

Foukal, P.V., Astrophys. J., 210, 575, 1976.

Frazier, E.N., Phil. Trans. Roy. Soc., A281, 295, 1976.

Gaizauskas, V. & Tapping, K.F., Astrophys. J., 241, 804, 1980.

Galeev, A.A., Magnetospheric Tail Dynamics, in Magnetospheric Plasma Physics, ed. Nishida, A., Center for Academic Publications Japan, Tokyo, 1982.

Gerwin, R., Phys. Fluids, 10, 2164, 1967.

Giovanelli, R.G., Solar Phys., 44, 299, 1975.

Giovanelli, R.G., Solar Phys., 59, 293, 1978.

Giovanelli, R.G., Solar Phys., 62, 253, 1979.

Giovanelli, R.G., Solar Phys., 68, 49, 1980.

Giovanelli, R.G. & Beckers, J., in Solar and Magnetic Fields: Origins and Coronal Effects, ed. Stenflo, J.O., IAU Symp., 102, 407, 1983.

Giovanelli, R.G. & Brown, N., Solar Phys., 52, 27, 1977.

Giovanelli, R.G. & Jones, H.P., Solar Phys., 79, 267, 1982.

Giovanelli, R.G., Livingston, W.C. & Harvey, J.W., Solar Phys., 59, 49, 1978.

Gloge, D., Appl. Optics, 10, 2252, 1971a.

Gloge, D., Appl. Optics, 10, 2442, 1971b.

Gloge, D., Appl. Optics, 11, 2506, 1972.

Gloge, D., IEEE Trans. Microwave Theory Tech., MTT23, 106, 1975.

Goedbloed, J.P., Physica, 53, 412, 1971.

Goedbloed, J.P., Phys. Fluids, 18, 1258, 1975.

Goedbloed, J.P., Lecture Notes on Ideal Magnetohydrodynamics, Rijnhuizen Report 83-145, Nieuwegein, The Netherlands, 1983.

Gordon, B.E. & Hollweg, J.V., Astrophys. J., 266, 373, 1983.

Gotwols, B.L., Solar Phys., 25, 232, 1972.

Granatstein, V.L. & Schlesinger, S.P., J. Appl. Phys., 36, 3503, 1965.

Granatstein, V.L., Korn, P., Ojo, A. & Schlesinger, S.P., J. Appl. Phys., 38, 1969, 1967.

Greenwald, R.A., Walker, A.D.M. & Candidi, M., J. Geophys. Res., 86, 11, 251, 1981.

Habbal, S.R. & Leer, E., Astrophys. J., 253, 318, 1982.

Habbal, S.R., Leer, E. & Holzer, T.E., Solar Phys., 64, 287, 1979.

Hain, V.K. & Lüst, R., Z. Naturforsch., 13a, 936, 1958.

Hale, G.E., Astrophys. J., 28, 315, 1908.

Harvey, J., Observations of Small-Scale Photospheric Magnetic Fields, in Highlights of Astronomy 4 (II), ed. Müller, E.A., 1977.

Hasegawa, A. & Chen, L., Phys. Rev. Lett., 32, 454, 1974.

Hasegawa, A. & Chen, L., Phys. Fluids, 19, 1924, 1976.

Herron, T.J., J. Geophys. Res., 71, 871, 1966.

Heyvaerts, J. & Priest, E.R., Astron. Astrophys., 117, 220, 1983.

Hollweg, J.V., Geophys. Res. Lett., 5, 731, 1978.

Hollweg, J.V., Mechanisms of Energy Supply, in Solar Active Regions, ed. Orrall, F.Q., Colo. Assoc. Univ. Press, Boulder, 1981.

Hollweg, J.V., Astrophys. J., 257, 345, 1982.

Hollweg, J.V., Coronal Heating by Waves, in Solar Wind V, ed. Neugebauer, M., 1983.

Hollweg, J.V., Astrophys. J., 227, 392, 1984.

Hones, E.W., Jnr., Baker, D.N., Bame, S.J., Feldman, W.C., Gosling, J.T., McComas, D.J., Zwickl, R.D., Slavin, J., Smith, E.J. & Tsurutani, B.T., Geophys. Res. Lett., 11, 5, 1984.

Hones, E.W., Jnr., Birn, J., Bame, S.J. & Russell, C.T., Geophys. Res. Lett., 10, 674, 1983.

Hughes, W.J., Hydromagnetic Waves in the Magnetosphere, in Solar-Terrestrial Physics, eds. Carovillano, R.L. & Forbes, J.M., D. Reidel & Co., Dordrecht, 1983.

Hughes, W.J., McPherron, R.L. & Barfield, J.N., J. Geophys. Res., 83, 1109, 1978.

Ingard, U., Phys. Rev., 145, 41, 1966.

Ingard, U. & Schultz, M., Phys. Rev., 158, 106, 1967.

Ionson, J.A., Astrophys. J., 226, 650, 1978.

Jansenns, T.J. & White, K.P. III, Astrophys. J., 158, L127, 1969.

Jansenns, T.J., White, K.P. III & Broussard, R.M., Solar Phys., 31, 207, 1973.

Jeffrey, A. & Kakutani, T., SIAM Rev., 14, 582, 1972.

Jensen, E., Astrophys. Norvegica V, 289, 1957.

Jordan, C., in Solar Gamma-, X- and EUV Radiation, ed. Kane, S.R., IAU Symp., 68, 109, 1975.

Jordan, S., The Sun as a Star, NASA SP-450, 1981.

Kadomtsev, B.B. & Karpman, V.I., Sov. Phys. J.E.T.P., 14, 40, 1970.

Kai, K. & Takayanagi, A., Solar Phys., 29, 461, 1973.

Kane, S.R., Kai, K., Kosugi, T., Enome, S., Landecker, P.B. & McKenzie, D.L., Astrophys. J., 271, 376, 1983.

Karpman, V.I., Non-linear Waves in Dispersive Media, Pergamon Press, Oxford, 1975.

Karpman, V.I., Lynov, J.P., Michelsen, P., Pécseli, H.L., Rasmussen, J.J. & Turikov, V.A., Phys. Fluids, 23, 1782, 1980.

Kaufmann, P., Rizzo Piazza, L. & Raffaelli, J.C., Solar Phys., 54, 179, 1977.

Keck, D.B., Optical Fiber Waveguides, in Fundamentals of Optical Fiber Communications, ed. Barnoski, M.K., Academic Press, New York, 1981.

Kennett, B.L.N., Seismic Wave Propagation in Stratified Media, C.U.P., Cambridge, 1983.

Kiplinger, A.L., Dennis, B.R., Emslie, A.G., Frost, K.J. & Orwig, L.E., Astrophys. J., 265, L99, 1983a.

Kiplinger, A.L., Dennis, B.R., Frost, K.J. & Orwig, L.E., Astrophys. J., 273, 783, 1983b.

Kirchhoff, H., Arch. Elektron. & Übertrangungstech, 26, 537, 1972.

Kirchhoff, H., Arch. Elektron. & Übertrangungstech, 27, 13, 1973.

Knobloch, E. & Weiss, N.O., Mon. Not. Roy. Astron. Soc., 207, 203, 1984.

Koutchmy, S., Zhugzhda, Y.D. & Locans, V., Astron. Astrophys., 120, 185, 1983.

Krüger, A., Introduction to Solar Radio Astronomy and Radio Physics, D. Reidel & Co., Dordrecht, 1979.

Kruskal, M. & Schwarzschild, M., Proc. Roy. Soc. Lond., A223, 348, 1954.

Kubota, T., Ko, D.R.S. & Dobbs, L.D., J. Hydronautics, 12, 157, 1978.

Kuijpers, J., Solar Phys., 36, 157, 1974.

Kunhardt, E.E. & Cheo, B.R., Phys. Rev. Lett., 37, 1688, 1976.

Kunhardt, E.E. & Cheo, B.R., Plasma Phys., 21, 237, 1979.

Kuperus, M., Ionson, J.A. & Spicer, D.S., Ann. Rev. Astron. Astrophys., 19, 7, 1981.

Landau, L.D. & Lifshitz, E.M., Fluid Mechanics, Pergamon Press, London, 1959.

Landau, L.D. & Lifshitz, E.M., Electrodynamics of Continuous Media, Pergamon Press, Oxford, 1960.

Lanzerotti, L.J., Fukunishi, H., Hasegawa, A. & Chen, L., Phys. Rev. Lett., 31, 624, 1973.

Lanzerotti, L.J. & Southwood, D.J., Hydromagnetic Waves, in Solar System Plasma Physics Vol. III, eds. Lanzerotti, L.T., Kennel, C.F. & Parker, E.N., North-Holland Publ. Co., Amsterdam, 1979.

Lee, M.A., Astrophys. J., 240, 693, 1980.

Leibacher, J.W. & Stein, R.F., Oscillations and Pulsations, in The Sun as a Star, ed. Jordan, S., NASA SP-450, 1981.

Lepping, R.P. & Burlaga, L.F., J. Geophys. Res., 84, 7099, 1979.

Levine, R.H., Future Active Region Observations, in Solar Active Regions, ed. Orrall, F.Q., Colo. Assoc. Univ. Press, Boulder, 1981.

Lighthill, M.J. Sir, Introduction to Fourier Analysis and Generalised Functions, C.U.P., Cambridge, 1958.

Lighthill, M.J. Sir, Phil. Trans. Roy. Soc., A252, 397, 1960.

Lighthill, M.J. Sir, Waves in Fluids, C.U.P., Cambridge, 1978.

Lites, B.W., White, O.R. & Packman, D., Astrophys. J., 253, 386, 1982.

Liu, S-Y., Astrophys. J., 189, 359, 1974.

Love, A.E.H., Some Problems of Geodynamics, C.U.P., London, 1911.

McKenzie, J.F., J. Geophys. Res., 75, 5331, 1970.

McKenzie, J.F., J. Geophys. Res., 76, 2958, 1971.

McLean, D.J. & Sheridan, K.V., Solar Phys., 32, 485, 1973.

McLean, D.J., Sheridan, K.V., Stewart, R.T. & Wild, J.P., Nature, 234, 140, 1971.

Marcatili, E.A.J. & Miller, S.E., Bell System Tech. J., 48, 2161, 1969.

Marcuse, D., Light Transmission Optics, Van Nostrand Reinhold, New York, 1972.

Marcuse, D., Theory of Dielectric Optical Waveguides, Academic Press, New York, 1974.

Marsh, K.A., Solar Phys., 50, 37, 1976.

Maxwell, A. & Fitzwilliam, J., Astrophys. Lett., 13, 237, 1973.

Meerson, B.I., Sasorov, P.V. & Stepanov, A.V., Solar Phys., 58, 165, 1978.

Mier-Jedrzejowicz, W.A.C. & Hughes, W.J., J. Geophys. Res., 85, 6888, 1980.

Mihalov, J.D., Sonett, C.P. & Colburn, D.S., Cosmic Electrodynamics, 1, 178, 1970.

Miles, J.W., Phys. Fluids, 19, 1063, 1976.

Miles, J.W., J. Fluid Mech., 106, 131, 1981.

Moisan, M., Shivarova, A. & Trivelpiece, A.W., Plasma Phys., 24, 1331, 1982.

Moore, R.L., Solar Phys., 30, 403, 1973.

Moore, R.L., Space Sci. Rev., 28, 387, 1981a.

Moore, R.L., Dynamic Phenomena in Sunspots, in The Physics of Sunspots, eds. Cram, L.E. & Thomas, J.H., Proc. Sac. Peak Obs., Summer Workshop, Sunspot, New Mexico, 1981b.

Nagashima, H. & Amagishi, Y., J. Phys. Soc. Japan, 47, 2021, 1979.

Nicholson, D.R. & Goldman, M.V., Phys. Fluids, 19, 1621, 1976.

Nocera, L., Leroy, B. & Priest, E.R., Astron. Astrophys., 133, 387, 1984.

Noyes, R.W., The Sun, Our Star, Harvard Univ. Press, Cambridge, Mass., 1982.

Okamoto, K. & Okoshi, T., IEEE Trans. Microwave Theory Tech., MTT24, 416, 1976.

Okoshi, T. & Okamoto, K., IEEE Trans. Microwave Theory Tech., MTT22, 938, 1974.

Olshansky, R., Rev. Mod. Phys., 51, 341, 1979.

Ono, H., J. Phys. Soc. Japan, 39, 1082, 1975.

Orrall, F.Q., Solar Active Regions, A Monograph from Skylab Solar Workshop III, Colo. Assoc. Univ. Press, Boulder, 1981.

Orwig, L.E., Frost, K.J. & Dennis, B.R., Astrophys. J., 244, L163, 1981.

Ott, E., Phys. Fluids, 14, 748, 1971.

Ott, E. & Sudan, R.N., Phys. Fluids, 12, 2388, 1969.

Ott, E. & Sudan, R.N., Phys. Fluids, 13, 1432, 1970.

Parker, E.N., Solar Phys., 36, 249, 1974a.

Parker, E.N., Solar Phys., 37, 127, 1974b.

Parker, E.N., Astrophys. J., 190, 429, 1974c.

Parker, E.N., Cosmical Magnetic Fields Their Origin and their Activity, Oxford, New York, 1979a.

Parker, E.N., Astrophys. J., 233, 1005, 1979b.

Parker, E.N., Astrophys. J., 234, 333, 1979c.

Parks, G.K. & Winckler, J.R., Astrophys. J., 155, L117, 1969.

Pasachoff, J.M. & Landman, D.A., Solar Phys., 90, 325, 1984.

Patel, V.L., Nature, 218, 857, 1968a.

Patel, V.L., Phys. Lett., 26A, 596, 1968b.

Pekeris, C.L., Theory of Propagation of Explosive Sound in Shallow Water, in Propagation of Sound in the Ocean, Geol. Soc. Am. Memoir, 27, 1948.

Pick, M. & Trottet, G., Solar Phys., 60, 353, 1978.

Pick, M., Trottet, G. & MacQueen, R.M., Solar Phys., 63, 369, 1979.

Pneuman, C.W., Phys. Fluids, 8, 507, 1965.

Pračka, M. & Karlický, M., Bull. Astron. Inst. Czechosl., 30, 257, 1979.

Priest, E.R., Solar Magnetohydrodynamics, D. Reidel & Co., Dordrecht, 1982.

Proctor, M.R.E. & Weiss, N.O., Rep. Prog. Phys., 45, 1317, 1982.

Rae, I.C. & Roberts, B., Geophys. Astrophys. Fluid Dynamics, 18, 197, 1981.

Rae, I.C. & Roberts, B., Mon. Not. Roy. Astron. Soc., 201, 1171, 1982.

Ramsey, H.E., Schoolman, S.A. & Title, A.M., Astrophys. J., 215, L41, 1977.

Richardson, E.G., Dynamics of Real Fluids, Edward Arnold Ltd., London, 1950.

Roberts, B., Astrophys. J., 204, 268, 1976.

Roberts, B., Solar Phys., 61, 23, 1979.

Roberts, B., Solar Phys., 69, 27, 1981a.

Roberts, B., Solar Phys., 69, 39, 1981b.

Roberts, B., in Solar and Magnetic Fields: Origins and Coronal Effects, ed. Stenflo, J.O., IAU Symp., 102, 61, 1983a.

Roberts, B., Solar Phys., 87, 77, 1983b.

Roberts, B., to appear in Phys. Fluids, 1984.

Roberts, B., Edwin, P.M. & Benz, A.O., Nature, 305, 688, 1983.

Roberts, B., Edwin, P.M. & Benz, A.O., Astrophys. J., 279, 857, 1984.

Roberts, B. & Mangeney, A., Mon. Not. Roy. Astron. Soc., 198, 7P, 1982.

Roberts, B. & Webb, A.R., Solar Phys., 56, 5, 1978.

Roberts, B. & Webb, A.R., Solar Phys., 64, 77, 1979.

Roberts, P.H., An Introduction to Magnetohydrodynamics, Longmans, London, 1967.

Rosenberg, H., Astron. Astrophys., 9, 159, 1970.

Rosenberg, H., Solar Phys., 25, 188, 1972.

Rosenberg, H., Phil. Trans. Roy. Soc., A281, 461, 1976.

Savage, B.D., Astrophys. J., 156, 707, 1969.

Scorer, R.S., Quart. J. Roy. Met. Soc., 75, 41, 1949.

Sedláček, Z., J. Plasma Phys., 5, 239, 1971.

Shawhan, S.D., Magnetospheric Plasma Waves, in Solar System Plasma Physics Vol. III, eds. Lanzerotti, L.T., Kennel, C.F. & Parker, E.N., North-Holland Publ. Co., Amsterdam, 1979.

Sheeley, N.R., Jnr., The Overall Structure and Evolution of Active Regions, in Solar Active Regions, ed. Orrall, F.Q., Colo. Assoc. Univ. Press, Boulder, 1981.

Siscoe, G.L., J. Geophys. Res., 74, 6482, 1969.

Snitzer, E., J. Opt. Soc. Am., 51, 491, 1961.

Souffrin, P., Ann. d'Astrophys., 29, 55, 1966.

Souffrin, P., Astron. Astrophys., 17, 458, 1972.

Southwood, D.J., Planet. Space Sci., 22, 483, 1974.

Southwood, D.J. & Hughes, W.J., Space Sci. Rev., 35, 301, 1983.

Southwood, D.J. & Kivelson, M.G., J. Geophys. Res., 86, 5643, 1981.

Spicer, D.S. & Brown, J.C., Solar Flare Theory, in The Sun as a Star, ed. Jordan, S., NASA SP-450, 1981.

Spiegel, E.A., Astrophys. J., 126, 202, 1957.

Spiegel, E.A., Astrophys. J., 139, 959, 1964.

Spruit, H.C., Solar Phys., 34, 277, 1974.

Spruit, H.C., Solar Phys., 55, 3, 1977.

Spruit, H.C., Magnetic Flux Tubes, in The Sun as a Star, ed. Jordan, S., NASA SP-450, 1981a.

Spruit, H.C., Astron. Astrophys., 98, 155, 1981b.

Spruit, H.C., Solar Phys., 75, 3, 1982.

Spruit, H.C., in Solar and Magnetic Fields: Origins and Coronal Effects, ed. Stenflo, J.O., IAU Symp., 102, 41, 1983.

Spruit, H.C. & Roberts, B., Nature, 304, 401, 1983.

Spruit, H.C. & Zwiebel, E.G., Solar Phys., 62, 15, 1979.

Stenflo, J.O., in Energy Balance and Hydrodynamics of the Solar Chromosphere and Corona, eds. Bonnet, R.-M. & Delache, Ph., IAU Coll., 36, 143, 1976.

Strauss, F.M., Kaufmann, P. & Opher, R., Solar Phys., 67, 83, 1980.

Sturrock, P.A., Nature, 211, 695, 1966.

Su, C.H. & Gardner, C.S., J. Math. Phys., 10, 536, 1969.

Summerfield, W., Phil. Trans. Roy. Soc., A272, 361, 1972.

Švestka, Z., Space Sci. Rev., 35, 259, 1983.

Švestka, Z., Dennis, B.R., Pick, M., Raoult, A., Rapley, C.G., Stewart, R.T. & Woodgate, B.E., Solar Phys., 80, 143, 1982.

Takakura, T., Kaufmann, P., Costa, J.E.R., Degaonkar, S.S., Ohki, K. & Nitta, N., Nature, 302, 317, 1983.

Tamao, T., J. Plasma Phys., 9, 429, 1973.

Tamao, T., J. Geophys. Res., 86, 11, 258, 1981.

Tanaka, M., J. Phys. Soc. Japan, 47, 2013, 1979.

Tapping, K.F., Solar Phys., 59, 145, 1978.

Tidjeman, H., On the Propagation of Sound Waves in Cylindrical Tubes, NLR MP 74004 U, National Aerospace Laboratory NLR, The Netherlands, 1974.

Tidjeman, H., J. Sound Vib., 39, 1, 1975.

Tolstoy, I., Wave Propagation, McGraw Hill, New York, 1973.

Trehan, S.K. & Singh, M., Astrophys. Space Sci., 53, 165, 1978.

Trottet, G., Kerdraon, A., Benz, A.O. & Treumann, R., Astron. Astrophys., 93, 129, 1981.

Trottet, G., Pick, M. & Heyvaerts, J., Astron. Astrophys., 79, 164, 1979.

Tsubaki, T., Solar Phys., 51, 121, 1977.

Uberoi, C. & Somasundaram, K., Plasma Phys., 22, 747, 1980.

Uberoi, C. & Somasundaram, K., Plasma Phys., 24, 465, 1982a.

Uberoi, C. & Somasundaram, K., Phys. Rev., 25, 2414, 1982b.

Unger, H.G., Planar Optical Waveguides and Fibres, Oxford Univ. Press, 1977.

Vaiana, G.S. & Rosner, R., Ann. Rev. Astron. Astrophys., 16, 393, 1978.

Vasyliunas, V.M., Comparative Magnetospheres, in Solar-Terrestrial Physics, eds. Carovillano, R.L. & Forbes, J.M., D. Reidel & Co., Dordrecht, 1983.

Ventrice, C.A., Phys. Rev., 20, 2625, 1979.

Vorpahl, J.A., Astrophys. J., 205, 868, 1976.

Wagner, W.J., Hildner, E., House, L.L., Sawyer, C., Sheridan, K.V. & Dulk, G.A., Astrophys. J., 244, L123, 1981.

Walker, A.D.M., Greenwald, R.A., Stuart, W.F. & Green, C.A., Nature, 273, 646, 1978.

Walker, A.D.M., Greenwald, R.A., Stuart, W.F. & Green, C.A., J. Geophys. Res., 84, 3373, 1979.

Watanabe, S., J. Phys. Soc. Japan, 45, 276, 1978.

Webb, A.R., Ph.D. Thesis, St Andrews University, 1980.

Webb, A.R. & Roberts, B., Solar Phys., 68, 71, 1980a.

Webb, A.R. & Roberts, B., Solar Phys., 68, 87, 1980b.

Webb, D.F., Active Region Structures in the Transition Region and Corona, in Solar Active Regions, ed. Orrall, F.Q., Colo. Assoc. Univ. Press, Boulder, 1981.

Wentzel, D.G., Astrophys. J., 227, 319, 1979a.

Wentzel, D.G., Astrophys. J., 233, 756, 1979b.

Wentzel, D.G., Astron. Astrophys., 76, 20, 1979c.

Wentzel, D.G., Coronal Heating, in The Sun as a Star, ed. Jordan, S., NASA SP-450, 1981.

White, O.R. & Athay, R.G., Astrophys. J. Supp., 39, 317, 1979.

Whitham, G.B., Linear and Nonlinear Waves, Wiley & Sons, New York, 1974.

Williams, D.J., J. Geophys. Res., 84, 101, 1979.

Williams, D.J., J. Geophys. Res., 85, 3387, 1980.

Williams, D.J., Fritz, T.A., Wilken, B. & Keppler, E., J. Geophys. Res., 84, 6385, 1979.

Wilson, P.R., Astrophys. J., 221, 672, 1978.

Wilson, P.R., Astron. Astrophys., 71, 9, 1979.

Wilson, P.R., Astron. Astrophys., 87, 121, 1980.

Wilson, P.R., Astrophys. J., 251, 756, 1981.

Withbroe, G.L. & Noyes, R.W., Ann. Rev. Astron. Astrophys., 15, 363, 1977.

Yagi, T., J. Phys. Soc. Japan, 50, 2737, 1981.

Yih, C.-S., Dynamics of Nonhomogeneous Fluids, Macmillan, New York, 1965.

Yumoto, K. & Saito, T., J. Geophys. Res., 87, 5159, 1982.

Zhugzhda, Y.D., Sov. Astron., 23, 42, 1979.

Zirker, J.B., The Solar Corona and the Solar Wind, in The Sun as a Star, ed. Jordan, S., NASA SP-450, 1981.

Zodi, A.M. & Kaufmann, P., preprint, 1984.

Zwaan, C., Solar Magnetic Structure and the Solar Activity Cycle Review of Observational Data, in The Sun as a Star, ed. Jordan, S., NASA SP-450, 1981.